

***Sensitivity of Land-Atmosphere Coupling Strength
in Dependence of Land Cover and Atmospheric
Thermodynamics over Europe***

**Dissertation to obtain the doctoral degree of
Natural Sciences (Dr. rer. nat.)**

**Faculty of Natural Sciences
University of Hohenheim**

Institute of Physics und Meteorology

submitted by
Lisa Lea Jach

from Frechen, Germany

2022

Dekan: Prof. Dr. rer. nat. Uwe Beifuß

1. berichtende Person: Prof. Dr. rer. nat. Volker Wulfmeyer
2. berichtende Person: Assistant-Prof. Dr. Chiel van Heerwaarden
3. berichtende Person: Dr. rer. nat. Marcus Breil

Eingereicht am: 28.09.2022

Mündliche Prüfung am: 10.02.2023

Die vorliegende Arbeit wurde am 04.10.2022 von der Fakultät Naturwissenschaften der Universität Hohenheim als “Dissertation zur Erlangung des Doktorgrades der Naturwissenschaften” angenommen.

Abstract

Biogeophysical feedbacks between the land surface and the atmosphere have been identified to heavily control the climate system. Land-atmosphere (L-A) coupling strength is a concept to quantify the feedback processes. However, the quantification is still subject to uncertainties, in particular, in the context of land surface influences on local convective precipitation. On the one hand, feedback processes are the result of a chain of complex interactions between various components in the L-A system all exhibiting spatiotemporal variability. On the other hand, L-A coupling strength is not a directly measurable quantity. It can be assessed with different scientific approaches, which makes the quantification dependent on the methodology and the availability of suitable data sets.

The aim of this doctoral thesis is to investigate the impact of changes in the vegetation cover and the atmospheric thermodynamic conditions on the long-term coupling signal between the land surface and the triggering of deep moist convection during the European summer. The ‘convective triggering potential – low-level humidity index’ framework, which is a commonly used L-A coupling metric, classifies a day in favor for L-A coupling or not, based on the prevailing thermodynamic conditions in the atmosphere. . The daily classifications are used to measure the frequency of days with favorable conditions during the study period, and to identify regions with high frequencies of favorable conditions as coupling hot spots. The framework is applied to model output from regional climate model (RCM) simulations with WRF-NoahMP with diverging land cover conducted over the historical period 1986-2015 for the Euro-CORDEX domain. Impacts of changes in vegetation cover are analyzed by comparing the L-A coupling strength from two sensitivity experiments with idealized extreme land use and land cover changes (LULCCs) against a simulation with realistic land cover. A posteriori modifications to the temperature and moisture output fields of the simulation with realistic land cover were implemented to analyze impacts of systematic changes in the atmospheric thermodynamic conditions.

A potential coupling hot spot with predominantly positive feedbacks was identified over Eastern Europe. In Southern Europe and Europe’s coastal areas, the coupling is regularly inhibited by very dry, very wet or stable conditions in the atmosphere. The location of the hot spot appeared insensitive to LULCCs and changes in the thermodynamic conditions. None of the sensitivity tests within a realistic range of temperature and moisture modifications for a recent climate period, led to a disappearance of the hot spot or to overcome the causes for inhibiting coupling in the respective areas

in summer. Nevertheless, the experiments demonstrated also considerable variance of the coupling strength within the hot spot region. LULCCs changed the turbulent heat fluxes from the land surface, and thus the atmospheric boundary layer (ABL) heating and moistening. This impacted the boundary layer development of each day. It also caused changes in the average thermodynamic characteristics during the study period, which changed the frequency of favorable pre-conditioning for convection triggering and enhanced the variance in the coupling strength in the hot spot. Both effects were identified to influence the land surface control on the occurrence of convective precipitation. Furthermore, the sensitivity tests with a posteriori modifications revealed uncertainties in the predominant atmospheric response to differently wet surfaces around the Black Sea, shown by a disagreement in the predominant coupling pathway between the modification cases. The findings further indicate uncertainty in whether the hot spot expands over Central Europe, as the feedback signal was sensitive to changes in temperature and moisture. Additionally, the model has a warm and dry bias in this area, which suggests an overestimation of the humidity deficit. The large humidity deficit, in turn, was the inhibiting factor for a high frequency of occurrence of favorable pre-conditions for deep moist convection. The analyses reveal a sensitivity of the L-A coupling strength and atmospheric response to the prevailing land surface and atmospheric conditions in the hot spot. This highlights the need to consider both the land surface state and its impact on L-A coupling strength with respect to predictions of convective precipitation events in strongly coupled regions (and periods). Given that L-A coupling provides predictive skill for climate projections and seasonal forecasts, improved understanding about causes of variability in L-A coupling strength is crucial for improvements therein.

Zusammenfassung

Biogeophysikalische Rückkopplungsprozesse zwischen Landoberfläche und Atmosphäre haben einen großen Einfluss auf das Klimasystem. Allerdings unterliegt ihre Quantifizierung, allen voran des Einflusses der Landoberflächen auf die Auslösung konvektiver Niederschläge, weiterhin großen Unsicherheiten. Ursachen dafür sind die Komplexität der Interaktionen im Land-Atmosphären (L-A)-System unter Beteiligung vieler verschiedener Komponenten, die alle unterschiedlich starker räumlich-zeitlicher Variabilität unterliegen. Zudem ist die L-A Kopplungsstärke keine direkt messbare, sondern eine diagnostische Größe, die noch dazu mit verschiedenen wissenschaftlichen Ansätzen untersucht wird, sodass Ergebnisse sowohl von der Wahl der Metrik, als auch von der Qualität und dem Zugang zu geeigneten Datensätzen abhängt.

Das Ziel dieser Doktorarbeit ist die Untersuchung, ob und wie sich Änderungen in der Landnutzung und den thermodynamischen Bedingungen der Atmosphäre auf die potentielle Kopplungsstärke zwischen Landoberflächenfeuchte und dem Auslösen von hochreichender Konvektion in den europäischen Sommermonaten auswirken. Dafür wurden drei Klimasimulationen mit dem regionalen Klimamodel WRF-NoahMP für den historischen Zeitraum 1986-2015 für die Euro-CORDEX Domain durchgeführt, die sich in der Landbedeckung unterscheiden. Die Kopplungsstärke wurde mit Hilfe der L-A-Kopplungsmetrik ‚Convective triggering potential – low-level humidity index Framework‘ analysiert, welche die Häufigkeit von förderlichen Bedingungen für lokal ausgelöste Konvektion in der Atmosphäre quantifiziert. Durch den Vergleich der Ergebnisse der Kopplungsmetrik für die Simulationen mit verschiedener Landbedeckung konnten die Einflüsse von Änderungen in der Vegetation analysiert werden. Weitere systematische Änderungen in den thermodynamischen Bedingungen und deren Auswirkungen auf die Kopplungsstärke konnten mit Hilfe von nachträglichen Modifikationen der Temperatur- und Feuchtefelder der Simulation mit realistischer Landbedeckung erfasst werden.

Sämtliche Analysen zeigten einen Kopplungshotspot über Ost- und Nordosteuropa, wo vorwiegend positive Rückkopplungen zwischen Landoberfläche und konvektiven Niederschlägen auftreten. Die Lage des Hotspots wird nicht durch Änderungen der Landbedeckung oder der Atmosphärenstruktur beeinflusst. Keine der Temperatur- und Feuchteänderungen, deren Spektrum einen realistischen Rahmen für das gegenwärtige Klima abdecken, konnten ein Verschwinden des Hotspots herbeiführen oder die Ursachen für die Unterdrückung von Rückkopplungen (zu starke Trockenheit,

Feuchte oder Stabilität in der Atmosphäre) über Südeuropa und in Küstennähe beseitigen. Allerdings zeigen die Experimente und Sensitivitätstests eine deutliche Varianz in der Kopplungsstärke in der Hotspotregion. Landnutzungsänderungen modifizieren die Aufteilung der Wärmeflüsse an der Landoberfläche und beeinflussen, ob die Grenzschicht vorwiegend feuchter oder aufgeheizt wird. Dadurch wird die Grenzschichtentwicklung jedes Tages beeinflusst, aber auch die mittleren thermodynamischen Eigenschaften der Atmosphäre, welche direkt mit förderlichen Vorbedingungen für das Auslösen von hochreichender Konvektion in Verbindung stehen und diese verändern. Beides wirkt sich auf den Einfluss der Landoberfläche auf das Auftreten konvektiver Niederschläge aus. Zusätzlich zeigten die Sensitivitätstests Unsicherheiten in der Reaktion der Atmosphäre auf die Variabilität der Landoberflächenfeuchte um das Schwarze Meer, und der Ausdehnung des Hotspots über Zentraleuropa. Die Ausdehnung wird von den Temperatur- und Feuchtemodifikationen beeinflusst, und im Modell wird das Feuchtedefizit in dieser Region überschätzt. Das regelmäßig hohe Feuchtedefizit ist die Hauptursache für das Verhindern von Rückkopplungen in dieser Region. Sämtliche Analysen zeigen eine Sensitivität der L-A Kopplungsstärke und der Reaktion der Atmosphäre auf die Landoberflächen- und Atmosphärenbedingungen im Hotspot. Daher ist es notwendig, sowohl die Landoberflächenbedingungen selber, als auch deren Einfluss auf die Kopplungsstärke zu berücksichtigen, um konvektiven Niederschlag akkurat vorhersagen zu können, vor allem in stark gekoppelten Regionen bzw. Zeiträumen. Da L-A Kopplung auch einen prognostischen Wert für Klimaprojektionen und saisonale Vorhersagen hat, trägt ein erhöhtes Verständnis über Ursachen für Variabilität in L-A Kopplungsstärke zu deren Verbesserung bei.

Candidate's contribution to the articles

Publication I: Jach, L., K. Warrach-Sagi, J. Ingwersen, E. Kaas, and V. Wulfmeyer, 2020: Land cover impacts on land-atmosphere coupling strength in climate simulations with WRF over Europe. *J. Geophys. Res-Atmos.* 125(18), 1-21 DOI: 10.1029/2019JD031989.


Contribution: I designed and realized the research in regular consultation with all co-authors, and under consideration of the FPS LUCAS' design for the land use and land cover change experiments. Specific tasks included:

- Conducting the three regional climate model simulations with varying land cover using WRF3.8.1 coupled to NoahMP.
- Research design of the coupling strength analyses.
- Post-processing of the model data primarily using climate data operators (CDOs) and the NCAR command language (NCL). Conduction of the final coupling strength analyses using MATLAB.
- Visualization of the research results using MATLAB.
- Drafting the manuscript, and its final editing after discussion with the coauthors.

Publication II: Jach, L.L., T. Schwitalla, O. Branch, K. Warrach-Sagi, V. Wulfmeyer, 2022: Sensitivity of land-atmosphere coupling strength to changing temperature and moisture over Europe. *Earth Syst. Dynam.*, 13, 109-132, DOI: 10.5194/esd-13-109-2022.

Contribution: I developed the modification approach, and designed and realized the research presented in this publication. The development of the methodology as well as the realization of the research included regular meetings and discussions with the coauthors. Specific tasks I conducted include:

- Development and testing of the a posteriori modifications strategy as well as the measures examining the resemblance of the cases and uncertainty in the coupling strength.
- Post-processing of the model data, applying the modification factors and analyzing the coupling strength of each modification case under the use of CDOs and NCL. This also included the investigation of variability in the coupling strength and thus an evaluation of the uncertainty in the coupling strength signal. The final analysis steps were realized in MATLAB again.
- Visualization of the research results using MATLAB.
- Drafting the manuscript, and its final editing in collaboration with all coauthors.



Signature, Supervisor

Contents

1	Introduction	1
1.1	State of the Art	1
1.2	Motivation and Objectives of the Doctoral Thesis	5
2	Land-Atmosphere Coupling Strength	9
2.1	Definition	10
2.2	Coupling Hotspots	12
2.2.1	Global Coupling Hotspots	12
2.2.2	Strong Coupling over Europe	13
2.3	Physical Influences on Land-Atmosphere Coupling Strength	15
2.3.1	Land State	15
2.3.2	Atmospheric large-scale circulations	16
2.4	Convection Triggering	18
2.4.1	Surface Influence on Convection Triggering	19
2.5	LoCo Working Group and its Process Chain	21
2.6	Quantification of L-A Coupling Strength	23
2.6.1	Process-Level Coupling Metrics	23
2.6.2	CTP-HI _{low} Framework	24
2.6.3	Statistical Coupling Metrics	27
3	Flagship Pilot Study on “Land Use and Climate Across Scales”	29
3.1	Experiments	29
3.2	Outcome of sensitivity experiments	29
4	Impacts of large-scale land cover changes on L-A coupling strength	33

4.1	Overview	33
4.2	Publication	34
5	Impacts of changing atmospheric temperature and moisture on L-A coupling strength	57
5.1	Overview	57
5.2	Publication	58
6	Summary	85
7	Outlook	93
A	Excursus: Potential Coupling Strength and Modeled Precipitation Frequency	95
A.1	Wet-day frequency	96
A.2	Implications of Precipitation Occurrence on Feedback Representation	100
A.3	Discussion	103
B	Annual Cycle of Land-Convection Coupling Strength	105
C	Supplementary Material Publication I	111
D	Supplementary Material Publication II	117
	Bibliography	123
	Acknowledgements	143

List of Tables

3.1	Overview about participating models in LUCAS Phase I. JLU – Justus-Liebig-University Gießen; BTU – "Brandenburgische Technische Universität"; CMCC – Euro-Mediterranean Center on Climate Change; KIT – Karlsruhe Institute of Technology; ETH – "Eidgenössische Technische Hochschule" Zürich; ICTP – International Centre for Theoretical Physics; GERICS – Climate Service Center Germany; IDL – "Instituto Dom Luiz" University of Lisbon; UHOH – University of Hohenheim; AUTH – Aristotle University of Thessaloniki; BCCR – Bjerknes Center for Climate Research; SMHI – Swedish Meteorological and Hydrological Institute	30
3.2	Atmospheric physics parameterizations of the LUCAS WRF model configurations.	31

List of Figures

2.1	Schematic about L-A interactions (by Michael Ek, Santanello et al., 2018)	9
2.2	LoCo process chain (Santanello et al., 2018)	21
2.4	Data base for studies applying the CTP-HI _{low} framework	25
A.1	Fraction of summer days under high-pressure conditions with low pressure gradients in the WRF-NoahMP simulation.	97
A.2	Wet-day frequency per season from a) E-OBS over the period 1986-2015 and b) the bias in wet-day frequency of the WRF-NoahMP evaluation simulation.	98
A.3	Wet-day frequency per season from a) the Kain-Fritsch cumulus parameterization and b) the fraction of total precipitation originating from the cumulus scheme. c) and d) show the same for the high-pressure area (HPA) precipitation.	99
A.4	Frequency of precipitation occurrence per evaporative fraction (EF)-pre-conditioning bin for a) the total precipitation b) the cumulus scheme precipitation, and c) high pressure area precipitation. The rows indicate the EF-bins, while the columns depict the different coupling classes. The lowest row contains the frequency of occurrence for each coupling class without considering differences in the EF. The right-most column shows the frequency of occurrence of precipitation for nAC-days, which is the sum of the columns for wet soil advantage, dry soil advantage and transition zones days.	100
A.5	Difference of precipitation occurrence between the wet soil advantage (WSA) and the dry soil advantage (DSA) for all ranges of the evaporative fraction (EF) and all precipitation types.	102

B.1	Monthly long-term coupling signals based on the ‘Convective Triggering Potential – low-level Humidity Index’ framework (a-c) for the winter months December, January, and February between 1986-2015. Subplots d-f show the fraction of non-atmospherically controlled (nAC) days per month, subplots g-i show the difference in the fraction of nAC-days when realistic land cover (from 2006) is changed to forest over the entire European continent (FOREST-CORINE), and subplots j-l show the differences in the fraction of nAC-days when the land cover is changed to grassland over the entire European continent (GRASS-CORINE).	107
B.2	As Appendix Figure B.1 but for March, April and May.	108
B.3	As Appendix Figure B.1 but for June, July and August.	109
B.4	As Appendix Figure B.1 but for September, October and November.	110

List of Abbreviations

ABL	A tmospheric B oundary L ayer
AC	A tmospherically C ontrolled
AGCM	A tmospheric G eneral C irculation M odel
CAPE	C onvective A vailable P otential E nergy
CDO	C limate D ata O perators
CIN	C onvective I Nhibition
CTP-HI_{low}	C onvective T riggering P otential - low-level H umidity- I ndex
DSA	D ry S oil A dvantage
ECMWF	E uropean C entre for M edium- R ange W eather F orecasts
EF	E vaporative F raction
ET	E vapo T ranspiration
Euro-CORDEX	E uropean B ranch of the C Oordinated R egional C limate D ownscaling E xperiment
FPS LUCAS	F lagship P ilot S tudy on L and- U se and C limate A cross S cales
GEWEX	G lobal E nergy and W ater E Xchanges
GLACE	G lobal L and A tmosphere C oupling E xperiment
GLASS	G lobal L and/ A tmosphere S ystem S tudy
HPA	H igh P ressure A rea
IPCC	I ntergovernmental P anel on C limate C hange
KF	K ain- F ritsch cumulus scheme
L-A	L and- A tmosphere
LAI	L eaf A rea I ndex
LCL	L ifted C ondensation L evel
LEM	L arge- E ddy M odel
LH	L atent H eat F lux

LoCo	Local land-atmosphere Coupling
LULCC	Land Use and Land Cover Change
nAC	non-Atmospherically Controlled
NDVI	Normalized Differences Vegetation Index
Noah-MP	Noah with MultiParameterization land surface model
RH	Relative Humidity
RCM	Regional Climate Model
SH	Sensible Heat Flux
SM	Soil Moisture
SGP ARM	Southern Great Plains Atmospheric Radiation Measurement site
TZ	Transition Zone
UTC	Coordinated Universal Time
WCRP	World Climate Research Program
WRF	Weather Research and Forecasting Model
WSA	Wet Soil Advantage

Chapter 1

Introduction

1.1 State of the Art

In the light of recognizing climate change as one of the major threats to human kind in the 21st century, reliable climate projections became essential to develop efficient adaptation and mitigation measures (IPCC, 2021). Although on ensemble base, the models resemble with the observed changes in the historical period (Tebaldi et al., 2021) with few outliers, the projected climate change signals of some variables vary significantly among models, which is shown by large ensemble spreads in both global model ensembles (Tebaldi et al., 2021; IPCC, 2021 -Technical Summary 1.2.2) and regional ensembles (e.g. Hübener et al., 2017; Vautard et al., 2020). Especially, summer precipitation still faces great uncertainties. The model projections presented in Hübener et al. (2017) disagree both in the sign and in the magnitude of changes until 2100 under the RCP8.5 scenario over Europe.

Generally, reasons for model spread (in both global and regional model ensembles) are manifold and can reach from differences in the parameterization of physical processes (Chen and Dirmeyer, 2017), the grid increment (Coppola et al., 2018; Hohenegger et al., 2009), initialization (e.g. Santanello Jr. et al., 2019) to internal model variability (Lavín-Gullón et al., 2021). In regional climate models (RCMs), the lateral boundary forcing causes uncertainty, as well (Ebell et al., 2008). An additional source of uncertainty is the incomplete understanding of biogeophysical interactions and feedback loops in the land-atmosphere (L-A) system and their representation in models. In models, L-A feedback usually evolves from interactions between the parameterization schemes rather than being directly calculated (Koster et al., 2006), wherefore the strength of interactions may be under-

or overestimated. The effect of considering L-A feedback in regional climate simulations was shown e.g. by Seneviratne et al. (2006). Besides their influence on climate change signals, the consideration of accurate land initialization and a more physically based linkage between land surface and atmosphere was shown to improve seasonal forecasts (Dirmeyer et al., 2018b), and especially predictions of extreme events including heatwaves, droughts (Roundy et al., 2014; Roundy and Wood, 2015) such as the European drought 2018 (Dirmeyer et al., 2021), and heavy precipitation events (Song et al., 2016).

In particular, L-A feedback processes related to convection triggering and local summer precipitation lack sufficient understanding and quantification of their frequency of occurrence, which are necessary for improving the processes' representation in models. Deep moist convection evolves from complex interactions between land surface and atmosphere, as well as among atmospheric variables. The surface influence on convection triggering happens through two main coupling pathways (Dirmeyer et al., 2014), which predominate in different areas of the Earth (e.g. Findell and Eltahir, 2003b). The hydrological pathway refers to convection triggering by moistening the atmospheric boundary layer (ABL) to reach saturation and enable cloud formation, wherefore wet surfaces support convection triggering better than dry ones (Dirmeyer, 2006). In contrast, within the thermal pathway, convection triggering is supported by surface heating from preferably dry soils, which enhances ABL growth (Taylor et al., 2012; Dirmeyer et al., 2014). This raises the ABL top to higher altitudes with cooler conditions and enables reaching saturation and cloud formation by that. Whether or not convection is triggered depends on both the land state and the atmospheric conditions in each individual case. The land state determines a preference for surface moistening or heating the ABL, thus promoting either the hydrological or thermal pathway. In addition, spatial heterogeneity in the land characteristics can support convection triggering owing to differential heating. The ratio of surface moistening and heating is determined by the energy balance at the land surface, which depicts how net radiation is partitioning into the latent, sensible and ground heat fluxes. The flux partitioning depends on the availability of moisture in the first place, but also on the land cover and its biophysical properties. The vegetation albedo determines the amount of incoming radiation which is reflected by the land surface and thus the available energy to partitioning in latent and sensible heat. Leaf area and stomatal conductance influence the evapotranspiration (ET) rate, and thus the latent heat flux, and rooting depths influence water limitations for ET as deeper roots enable the

plants to reach deeper moisture reservoirs. The roughness length impacts aerodynamic resistance. The individual combinations of these properties lead to a characteristic footprint of each vegetation type on the energy balance at the land surface (Duveiller et al., 2018b), and thus on whether the surface is rather moistening or heating the ABL, which is not necessarily well represented in models (Duveiller et al., 2018a).

Consequently, any land use and land cover change (LULCC) modifies this footprint, which has minor to major implications for the climate system depending on the type of vegetation change, its location, timing and the background climate (Duveiller et al., 2018b). Biogeophysical impacts of LULCC on the climate are not fully understood, yet, as changes in the radiative (albedo) and non-radiative properties (ET and roughness, Breil et al., 2021) can cause opposing climate responses. The net impact depends on which effect dominates (Davin and Noblet-Ducoudré, 2010), and the dominant control, in turn, varies across different regions of the globe (Chen et al., 2020; Laguë et al., 2019). By changing the degree of surface moistening and heating as well as their ratio to each other, LULCCs also have the potential to change convection triggering and land-convection coupling. An analysis of whether and how LULCCs impact convection triggering and land-convection coupling over Europe remains lacking, though.

The importance of considering biogeophysical feedback from LULCC was underlined by Noblet-Ducoudré et al. (2012), who demonstrated that biogeophysical feedback from the land surface can regionally overcome the impacts from increases in the greenhouse gas concentration. However, assessments of the mitigation potential of biogeophysical feedback for climate change was largely limited to albedo changes in the big IPCC assessment reports, so far. Only recently, the full potential of biogeophysical feedback gained importance in climate sciences underlined by the publication of the IPCC special report on climate change and land (IPCC, 2019). Additionally, the flagship pilot study (FPS) 'land-use and climate across scales' (LUCAS) was endorsed by the world climate research program (WCRP) within the Euro-CORDEX community (Rechid et al., 2017). As the land cover is typically a static field in RCM simulations, the FPS strives to test the implementation of LULCC in a coordinated RCM ensemble and investigates the impact of idealized and realistic LULCCs on the European climate. The simulations analyzed within this dissertation also contribute to the LUCAS phase I ensemble with focus on idealized large-scale LULCCs.

The atmospheric conditions influencing the potential for deep convection triggering comprise of

both, the thermodynamic and dynamic characteristics of the atmosphere. The thermodynamic structure refers to how humid and stable the atmosphere is. Initial moisture content and atmospheric stratification before ABL development impact the likelihood to reach saturation from mixing surface air upward, with intermediately humid and conditionally unstable conditions being most favorable for local surface triggered deep convection (Findell and Eltahir, 2003b). Uncertainties arising e.g. from model biases in temperature and specific humidity profiles influence the estimated potential for triggering deep convection. This introduces also uncertainty in the coupling strength signals from model ensemble studies. A verification remains challenging due to the lack of spatially comprehensive observations of thermodynamic profiles with a horizontal resolution typically higher than $1^\circ \times 1^\circ$, which substantially limits a detailed representation of the land surface. In addition, changes in the atmospheric temperature and moisture content evolve in consequence of global warming, which is hypothesized to impact the frequency of occurrence of favorable conditions for convection triggering. A trend of increasing importance of land surface processes for the atmosphere along with climate change was identified by Dirmeyer et al. (2013b). The most relevant dynamic conditions for long-term coupling signals are horizontal wind speeds, which can dampen local interactions during periods with moderate to strong wind speeds (Taylor, 2015).

There exist several approaches to study and quantify the land surface influence on the atmospheric state and here specifically local convection triggering. Analyzing individual synoptic cases yields process understanding by identifying underlying mechanisms (e.g. Kottmeier et al., 2008; Wulfmeyer et al., 2011), but do not allow for a quantification of their frequency of occurrence. Sensitivity experiments with models are used to quantify model responses e.g. in precipitation to perturbations of soil moisture (Hohenegger et al., 2009; Leutwyler et al., 2021; Baur et al., 2018; Baur et al., 2022) or the vegetation cover (e.g. McDermid et al., 2019). Finally, L-A coupling metrics relate instantaneous states in the L-A system to infer on coupling or assess co-variability between land and atmospheric variables (e.g. Findell and Eltahir, 2003b; Findell and Eltahir, 2003c; Dirmeyer, 2011). The analyses in this dissertation make use of a process-based coupling metric, which assesses the coupling strength based on classifying the atmospheric structure into favorable vs unfavorable pre-conditioning for local convection triggering and then quantifying the frequency of occurrence of favorable conditions. Impacts of LULCCs on the coupling strength were investigated by conducting sensitivity experiments changing a realistic vegetation distribution to a fully afforested land cover

and a land surface fully covered by grassland. Impacts of different average thermodynamic conditions were investigated by implementing a posteriori modifications of the temperature and moisture fields from the simulation with realistic land cover. The implemented modifications were designed to approximate a realistic spread in the mean atmospheric conditions suggesting a probable range for the coupling strength. The spread in coupling strength depicts the uncertainty in the expansion of a land-convection coupling hot spot and confined areas prone to uncertainties in the predominant coupling pathway.

1.2 Motivation and Objectives of the Doctoral Thesis

To summarize, the occurrence of local convective precipitation events depends on the prevailing land surface and atmospheric conditions as well as on interactions between them. The conditions and consequently their interactions vary on different spatiotemporal scales, wherefore also the role of the land surface for triggering convective precipitation varies regionally and over time. Whether, where and to which extent changes at the land surface and in the atmospheric thermodynamic conditions impact the coupling on the long-term was barely investigated and quantified, yet.

From this follows the general aim of this dissertation, which is the investigation of how changes in the L-A system in form of LULCCs and large-scale variations in the thermodynamic structure influence the potential strength of interactions between the land surface and the atmosphere. The analyses focus on the investigation of changes in the long-term mean coupling signals between surface wetness represented by the evaporative fraction (EF) and the thermodynamic pre-conditioning for deep moist convection triggering over the period 1986-2015 for Europe. A combination of sensitivity model experiments and a process-level L-A coupling metric was applied to understand and quantify impacts of the changes on the convection triggering potential over Europe. The coupling metric of choice is the 'convective triggering potential - low-level humidity index' (CTP-HI_{low}) - framework, which provides the advantage of considering the instantaneous state of the atmosphere and can be used to compute spatially comprehensive maps of potential coupling strength. Differences in the long-term coupling signals resulting from extreme LULCCs are analyzed on the basis of sensitivity experiments with the RCM WRF. The investigations resulted in two publications: Jach et al. (2020) analyzed the impact of land cover changes on land-convection triggering coupling, and

Jach et al. (2022) examined how variations in the thermodynamic conditions affect the coupling. Objectives of Jach et al. (2020) were:

1. Locate coupling hot spot(s) between surface wetness and convective triggering by assessing the frequency of favorable atmospheric preconditions for locally triggered convection in the European summer.
2. Investigate how wide-spread afforestation and the transition of the vegetation to grassland change the coupling between the land surface and convection triggering by comparing L-A coupling strength estimates from regional climate simulations with different vegetation cover.
3. Assess the relationship between surface fluxes and cloud and precipitation statistically in dependence of the land cover.

The publication of Jach et al. (2022) is dedicated to analyze where and in which sense large-scale changes in the atmospheric thermodynamic structure modify the pre-conditioning for deep convection. Modifications of the atmosphere are implemented a posteriori on the model output of the regional climate simulation with realistic land cover, which is already used in the first publication. The analyses aimed at fulfilling following objectives:

1. Quantify the impacts of modifying the mean atmospheric temperature and moisture as well as their vertical gradients for L-A coupling strength during the European summer months to approximate a spread in L-A coupling strength.
2. Analyze regional differences in the sign and magnitude of impacts on L-A coupling strength from changing the temperature and moisture profiles, and identify whether changes in temperature or moisture dominate differences in the coupling strength signals.
3. Identify regions with low sensitivity in the frequency of potential coupling days and the predominant coupling sign, which thus can be considered reliable L-A coupling hot spots.

The following literature review provides an overview about the current state of the art of research on L-A feedback with focus on Europe, which is followed by an overview about LUCAS phase I. As the simulations analyzed within this dissertation contribute to the LUCAS phase I RCM ensemble, the chapter also provides a summary of the model intercomparison studies, whose analyses made

use of the simulations. Section 4 contains the publication dealing with the LULCC impact on coupling between surface wetness and convection triggering, while section 5 presents the publication on sensitivity of land-convection coupling to modifications of the thermodynamic characteristics in the ABL. The final sections contain the general discussion of the findings and an outlook.

Chapter 2

Land-Atmosphere Coupling Strength

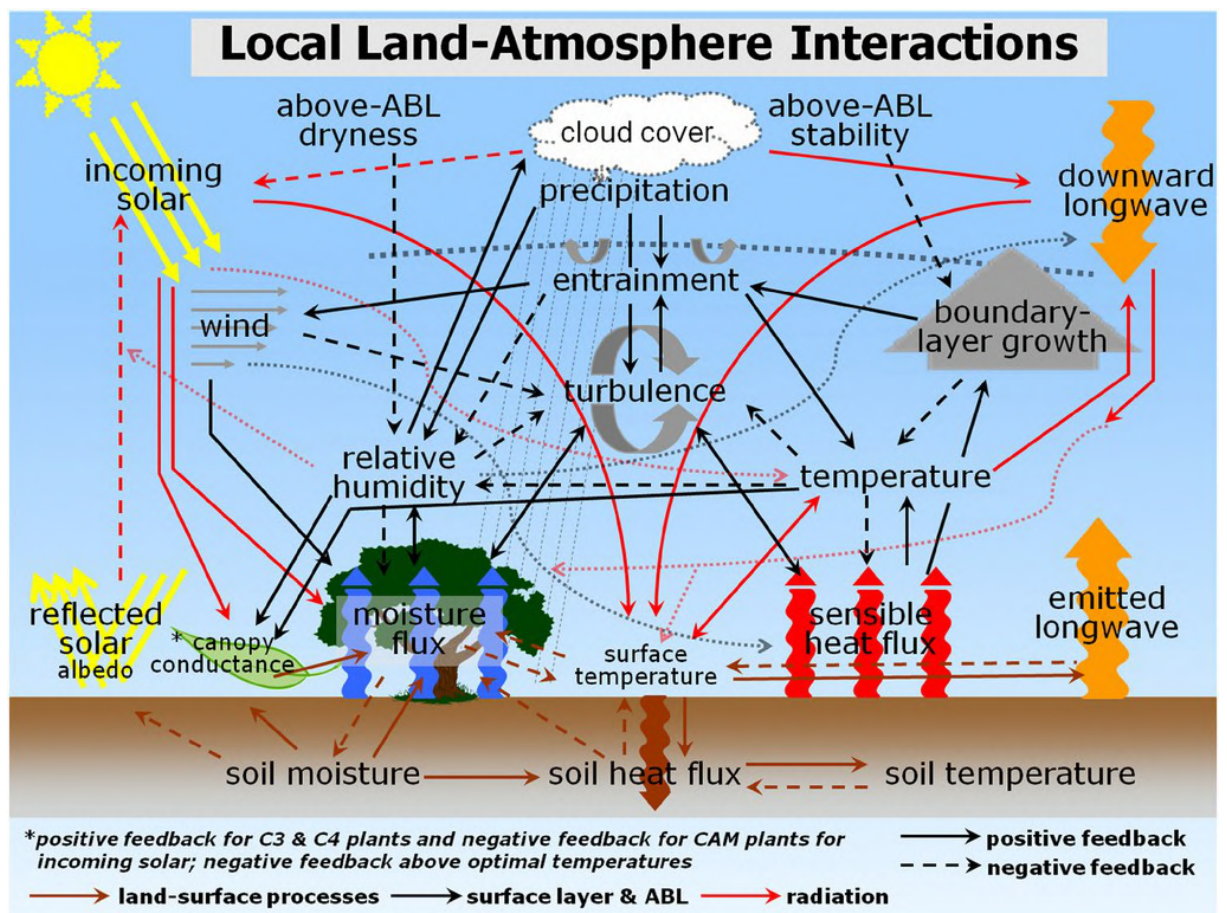


FIGURE 2.1: Schematic about L-A interactions (by Michael Ek, Santanello et al., 2018)

2.1 Definition

L-A coupling strength is not clearly and uniquely defined in literature. The term is used for a variety of relationships in the climate system which are exemplary depicted in Figure 2.1. Definitions in individual studies are usually tailored to the studies' respective purpose such as:

- Koster et al. (2004) define: “*Coupling strength in this report refers to the general ability of land surface moisture anomalies – either local or remote – to affect precipitation in a given region. Inferences regarding soil moisture measurement in the indicated hot spots require an assumption of local influence.*” Koster et al. (2006) add that “[...] *coupling strength is not an explicitly defined quantity in the AGCMs; it is rather a complex product of many interacting model parameterizations.*” (Note: AGCM stands for atmospheric general circulation model)
- The Local Land Atmosphere Coupling (LoCo) working group defines its scope as: “*The realm of LoCo has been defined by GLASS as “the temporal and spatial scale of all land-surface related processes that have a direct influence on the state of the PBL.”*” (<https://www.gewex.org/loco/>; accessed 09.02.2022)
- Wakefield et al. (2021) broadly refer to it as “*The sensitivity of the atmosphere to changes in land surface conditions ...*” and “*...how the atmosphere and land surface covary, also referred to as land-atmosphere coupling (LA coupling), ...*”.
- Leutwyler et al. (2021) assess soil moisture-precipitation coupling as “*the sensitivity of summertime precipitation to continental-scale spring SM perturbations.*” “*The soil moisture–precipitation feedback is then assessed based on the precipitation difference emerging from that perturbation.*”

The land surface is typically represented by the soil texture, soil wetness and the vegetation cover. Surface wetness is typically represented by soil moisture (Knist et al., 2017; Roundy et al., 2013; Seneviratne et al., 2010), but also the EF (latent heat flux / latent+sensible heat flux) can be used (Berg et al., 2013; Findell et al., 2011). The vegetation cover is usually characterized by the leaf area index (LAI, Hong et al., 2007; McDermid et al., 2019; Chen and Dirmeyer, 2020b) or the Normalized Difference Vegetation Index (NDVI, Wang et al., 2006). Further important vegetation variables are the roughness, albedo and rooting depths. Beside temperature (e.g. Lorenz et al., 2015;

Seneviratne et al., 2013) and precipitation (e.g. Koster et al., 2004; Findell et al., 2011), the diverse possibilities on the atmospheric side include the ABL height (Dirmeyer et al., 2014)), convective available potential energy (CAPE), or the lifted condensation level (LCL) deficit (Santanello et al., 2011; Yin et al., 2015). In the context of L-A coupling studies, biogeophysical processes can be connected in process chains such as the local coupling (LoCo) process chain (see section 2.5, which have a terrestrial leg connecting soil moisture or vegetation characteristics with the turbulent heat fluxes at the land surface and an atmospheric leg connecting the heat fluxes with an ABL quantity. Hence, L-A coupling strength can be considered an umbrella term, and as different studies examine different relationships under the umbrella of L-A coupling strength, their comparability can be challenging (Knist et al., 2017). Besides the choice of the variable, also the choice of the coupling metric (measure to quantify L-A coupling strength; see section 2.6) influences the coupling strength estimate (Lorenz et al., 2015).

Generally speaking, L-A coupling strength is defined here as the degree of communication between the land surface and the atmosphere mostly shown in a co-variability of a land surface and an atmospheric variable. The role of the land surface for local weather and climate is the result of the prevailing land surface conditions and their (detectable) communication with the atmosphere and vice versa. In the analyses (sections 4 and 5), L-A coupling strength refers more specifically to the coupling between surface wetness and the potential to trigger convection during the subsequent day which can lead to the development of convective precipitation.

2.2 Coupling Hotspots

L-A coupling strength varies spatially and temporally. Temporal variability, e.g., arises from variability in the large-scale circulation, which allows for strong coupling mainly during the summer months and suppresses strong feedback in winter (see also B). The investigation of so called L-A coupling hot spots targets the evaluation and understanding of spatial variability. Similar to the L-A coupling strength, there is no unique definition of coupling hot spots. Guo et al. (2006) for instance refer to “[...] *robust regions [across models] of significant soil moisture impact on precipitation and near-surface air temperature; [...]*” which is similar to Lorenz et al. (2015) who call “[...] *regions of strong land-atmosphere coupling [...]*” hot spots. Paul Dirmeyer considers regions a hot spot, where the complete coupling pathway is in effect (soil moisture linked to the boundary layer via turbulent heat flux partitioning; Dirmeyer et al. (2014)), but others investigate the terrestrial or the atmospheric legs separately and define strong coupling regions rather relative to the rest of the study domain.

Findell and Eltahir (2003b) consider regions as high potential for feedback, when more than 20 % of the days in a study period have the potential for a surface influence on convection triggering. In this dissertation, the definition of coupling hot spot follows the rationale of Findell and Eltahir (2003b) but resets this threshold. A region is considered a strong coupling region or hot spot when more than 10 % of the days have a high potential coupling strength between the land surface and subsequent convection triggering. The decrease of the threshold builds on the fact that Germany experiences large-scale weather patterns associated with convective conditions in about 10% of the summer days (Lang, 2010). Convective summer precipitation events are considered socio-economically relevant and lowering the threshold aims at ensuring that also the dominant coupling signal of these events can be captured by the analyses. The practice does not effect the frequency of favorable preconditioning for convection triggering.

2.2.1 Global Coupling Hotspots

In a global model intercomparison effort, the "Global Land Atmosphere Coupling Experiment" (GLACE), found that hot spots for both temperature and precipitation coupling with soil moisture usually resemble in transition regions between wet and dry climates under semi-arid conditions (Koster et al., 2004; Koster et al., 2006; Guo et al., 2006). The most intense coupling was identified

over the central Great Plains of North America, the Sahel, equatorial Africa and India. Regions identified as less intense hot spots or only concerning either temperature or precipitation coupling are China, central Asia and South America.

Lorenz et al. (2015) confirmed the hot spots for soil moisture-temperature coupling using a suite of different coupling metrics which agree on the location of very strongly coupled regions but found disagreement in less intensely coupled regions. Further they showed that the Northern and the Southern Hemisphere diverge in their coupling behaviors. While in the Northern Hemisphere, strong coupling occurred in the transition regions between wet and dry climates as reported before, in the Southern Hemisphere strongest coupling was shown rather in the tropics and mid-latitudes.

The US Southern Great Plains (SGP) evolved to be one of best-studied hot spot regions globally (e.g. Phillips et al., 2017). The SGP atmospheric radiation measurement (ARM) site is heavily equipped with remote sensing devices to measure the various reservoir and flux variables involved in the LoCo process chain. These data form a valuable basis for improving the understanding of L-A feedback and understand the complex weather phenomena in this region.

2.2.2 Strong Coupling over Europe

In the global hot spot identifications, Europe has a weak soil moisture-precipitation and soil moisture-temperature coupling hot spot over Northeastern Europe (Koster et al., 2004). Taylor (2015) explained two physical causes for weaker coupling over Europe than e.g. over the Sahel. Firstly, Europe experiences stronger synoptic forcing which suppresses the development of daytime circulations. Additionally, strong winds move convective cells downwind potentially causing the development of precipitation in downwind direction (Froidevaux et al., 2014). Secondly, the dependence of ET on soil moisture availability is weaker than in semi-arid regions due to higher soil moisture availability and denser vegetation cover. Though not identified as very strong coupling hot spot relative to other regions globally, L-A coupling processes came to the fore of climate researchers also over Europe.

Most L-A coupling studies over Europe focused on the influence of soil moisture on the turbulent flux partitioning and their connection to near-surface temperature. This is of particular interest under extreme conditions such as droughts, heat waves or their compound occurrence (Dirmeyer et al., 2021), as depleted soil moisture reservoirs were shown to exacerbate heat and drought conditions.

Jaeger and Seneviratne (2011) as well as Vogel et al. (2017) have shown that soil moisture variability impacts temperature extremes stronger than mean temperatures over Europe. Merrifield et al. (2019) added that the effect of dry surfaces on the climate is a composite of short-term influences of the flux partitioning and long-term impacts changing the atmospheric circulation. These large-scale impacts possibly cause remote amplifications of heat waves, e.g. due to reduced cloud cover.

Though the impact of soil moisture variability on mean temperature was shown to be smaller than for extremes (Lorenz et al., 2012), Knist et al. (2017) found coupling of soil moisture with the latent heat flux, as well as the latent heat flux with temperature also on the decadal timescale for Southern Europe. Soil moisture availability is limiting ET under Mediterranean climate and thus controls the turbulent heat flux partitioning, while energy (radiation) availability predominantly limits ET in the high latitudes (Seneviratne et al., 2010). Beside moisture and energy availability, also the vegetation properties themselves control ET. The land cover acts as an interface between the soil and the atmosphere, which influences L-A interactions through various mechanisms as long as the soil is not severely dry (more on the role of the land cover interface for L-A coupling is presented in section 2.3.1). Seneviratne et al. (2006) have shown the evolution and expansion of a coupling hot spot in Central and Eastern Europe along with climate change. They attribute this evolution to increasing greenhouse gas concentrations and increasing temperature variability in future projections, which enhances the atmospheric moisture demand and causes higher latent heat fluxes. This in turn indicates a higher dependence on soil moisture variability, and finally suggests increasing importance of the land surface for the weather and climate in the future.

2.3 Physical Influences on Land-Atmosphere Coupling Strength

Up to now, characterization and quantification of L-A coupling relationships are subject to uncertainties. On the one hand, L-A coupling is highly dynamic, resulting from the dynamic, turbulent nature of the atmosphere and spatiotemporal variability existing at the land surface. On the other hand, L-A coupling relationships need to be estimated with measures tailored for their quantification (see section 2.6) or using models to conduct sensitivity studies (Seneviratne et al., 2006; Hohenegger et al., 2009; Tuttle and Salvucci, 2016; Lawrence et al., 2016; McDermid et al., 2019). They cannot be observed directly, and spatially comprehensive observational data covering periods of at least a decade for verifying model based estimates remain lacking. This chapter aims at providing an overview about the existing literature on how land state and atmosphere impact L-A coupling strength estimates.

2.3.1 Land State

The land state and its changes include availability of moisture in the soil, vegetation cover and orography (e.g. Knist et al., 2020). Noblet-Ducoudré et al. (2012) showed that biogeophysical forcing from the land surface (mostly soil moisture and vegetation) can compensate radiative forcing from greenhouse gases in some regions. This highlights the importance of biogeophysical L-A feedbacks for the climate system, and the importance of the land state to control the climate is likely to increase under global warming (Dirmeyer et al., 2013b).

Since most identified hot spot regions are located in semi-arid regions, soil moisture availability is one of the key factors to determine spatial variability in L-A coupling strength. Additionally, moisture availability introduces also temporal variability e.g. on the interannual timescale (Guo and Dirmeyer, 2013) and during hydrological extremes (droughts e.g. Dirmeyer et al., 2021; floods e.g. Lo et al., 2021). However, apart from soil moisture, the vegetation cover and its spatial distribution strongly controls the coupling, as the vegetation properties determine the ET rate (e.g. Breil et al., 2021). The vegetation influence makes soil moisture-surface flux coupling highly nonlinear in regions, where soil moisture is not severely limiting ET. In consequence, a correlation with soil moisture can suggest weak L-A coupling strength, despite a strong vegetation -and thus land surface- influence on the turbulent flux partitioning (Williams and Torn, 2015). Therefore, the EF will be used for the analyses of this dissertation, as it includes the effects of soil moisture and vegetation. It

informs whether the land surface is predominantly moistening (high fraction of LH suggesting wet surface conditions) or heating (low fraction of LH suggesting dry surface conditions) the ABL.

Each vegetation type has characteristic radiative and non-radiative properties which considerably influence the energy balance at the land surface. Changes in the land use, land cover or land management modify the vegetation properties (Duveiller et al., 2018b), which can lead to changes in the local climate (e.g. Chen and Dirmeyer, 2020a; Devanand et al., 2020; Findell et al., 2017). The exact climate impact depends of the specific LULCC, the location and its evaporative regime, and the background climate (Duveiller et al., 2018b; McDermid et al., 2019). The impacts of non-radiative processes are typically dominant under moisture-limited conditions, whereas those from radiative processes mostly occur under energy-limitation (Davin and Noblet-Ducoudré, 2010). Chen et al. (2020) added that the temperature response to increases in the vegetation cover is dominated by changes in the aerodynamic resistance over most regions around the globe including Europe, which is linked to the surface roughness. Laguë et al. (2019) showed that the net climate responses to LULCC are greatly defined by atmospheric feedback which modify temperature, cloud cover and the circulation. Consequently, atmospheric feedback amplifies the direct impacts, and changes in the circulation additionally drive remote effects.

Nevertheless, uncertainties exist in modeled responses to LULCC arising from different model parameterizations or the way vegetation phenology is represented (Pitman et al., 2009). In consequence, the models do not agree in the sign of the response to various vegetation transitions (Duveiller et al., 2018a), which is largely attributable to disagreements in models' approaches to compute ET (Davin et al., 2020). However, models show less disagreement among each other and more agreement with observations of the temperature response to afforestation, when analyzing the skin temperature, which is a prognostic variable, rather than the diagnostically derived 2-meter temperature (Breil et al., 2020).

2.3.2 Atmospheric large-scale circulations

Synoptic conditions crucially shape L-A interactions on various temporal scales. Differences in the distribution of moisture in the atmosphere (Baur et al., 2018; Leutwyler et al., 2021), inversion strength, and wind speed (Froidevaux et al., 2014) greatly determine, whether a local feedback is likely to occur during a day or not. On the seasonal to multi-decadal time-scale, the frequency

of occurrence of predominantly favorable versus inhibiting synoptic conditions affects whether a region is a soil moisture-precipitation coupling hot spot or only weakly coupled. Findell and Eltahir (2003c) describe atmospheric controls with relatively extreme humidity (very dry, very wet) or the initial inversion strength of the early-morning ABL. Taylor (2015) e.g. concluded that coupling is weaker in the mid-latitudes than in tropical semi-arid regions, because the mid-latitudes face stronger surface winds, than in their case the Sahel, and ET is usually less dependent in soil moisture availability.

Global warming and the amplification of the hydrological cycle will influence the occurrence and persistence of different synoptic conditions, which likely increases the role of the land surface to shape climate (Dirmeyer et al., 2013b). Seneviratne et al. (2006) projected increasing soil moisture-temperature and soil moisture-precipitation coupling over Europe until the end of the century, which they attributed to warming of the atmosphere from rising greenhouse gas concentrations.

2.4 Convection Triggering

Generally speaking, convection means the vertical transport of heat and moisture in the atmosphere via updrafts and downdrafts under unstable atmospheric conditions (NOAA Glossary, <https://forecast.weather.gov/glossary.php?word=CONVECTION>). One can distinguish shallow convection (vertical motion capped below 500hPa) and deep convection. Further, distinguishable are dry convection which is usually invisible as opposed to moist convection, where the upward motion becomes visible as clouds. In this dissertation, convection usually refers to deep moist convection, and convection initiation and convection triggering - meaning that convection occurs - are used as equivalent terms.

Triggering deep moist convection is complex and involves a variety of quantities and processes (Markowski and Richardson, 2010). Initially, upward motion from the surface can be induced by the occurrence of fronts, along orography or by thermals evolving from differential heating at the land surface. In the process of lifting, the air parcel first rises dry adiabatically up to the LCL, where it reaches saturation. Further lifting of the air parcel initiates condensation as it cools, and cloud formation can start. Condensation implies that latent heat is released, which slows down the cooling rate of the air parcel in comparison to the environment. At the level of free convection, the parcel gets warmer than its surroundings, creating positive buoyancy. The parcel further rises moist adiabatically without external force up to the equilibrium level.

One necessary condition for triggering deep moist and potentially precipitating convection is the availability of enough integrated positive buoyant force depicted by the CAPE (Markowski and Richardson, 2010), which is the area between environmental temperature and the moist adiabat integrated between the level of free convection and equilibrium level. Additionally, the air parcel needs to reach the level of free convection to experience positive buoyancy in the first place. The strength to which an initial upward motion is inhibited or in other words the amount of energy necessary to reach the level of free convection is depicted by the convective inhibition (CIN). Convection can be triggered through various mechanisms in the ABL and in connection with different ABL features (Weckwerth and Parsons, 2006; Kottmeier et al., 2008). In the absence of an external lifting force (e.g. a mountain range or a frontal system), the initial lifting from the land surface needs to be thermally induced, which can be inhibited e.g. by temperature inversions or subsidence.

Both conditions depend on the synoptic-scale conditions as they i.a. influence the environmental temperature gradient (Weckwerth and Parsons, 2006), and therefore the instability of the atmosphere. Further, the synoptic scale conditions can determine predominant convergence or divergence (support or dampen upward motion), horizontal wind speed (strong surface wind speed dampens dominant local upward motion), low-level humidity and advection (influences at which height saturation is reached), as well as entrainment (cooling and drying of ABL top, Heerwaarden et al., 2009). Additionally, the land surface plays a key role in triggering convection by moistening and heating the ABL through turbulent heat fluxes (e.g. Ek and Mahrt, 1994). Heterogeneity in the land surface conditions can initiate differential heating, and thus cause thermals to rise from the surface.

2.4.1 Surface Influence on Convection Triggering

This section gives an overview about knowledge on surface influences on convection triggering and convective precipitation focusing on Europe. Convective precipitation occurs most frequently over Central and Eastern Europe (Rüdisühli et al., 2020), and the majority of surface impacts on precipitation are attributable to the average moisture availability and its spatial distribution.

Guillod et al. (2015) showed that more precipitation occurs during wet periods (positive temporal coupling) but over dry patches in relation to surrounding areas (negative spatial coupling), which is enhanced by heterogeneous surface conditions as they initiate differential heating. Air moistens over wet patches, and converges at the upwind border of a wet patch over the abut dry patch, where surface heating initiates lifting of the air masses, and finally can cause the formation of convective precipitation (Baur et al., 2018; Taylor, 2015). However, the results of Baur et al. (2018) also indicated a dependence of the predictability of convective cells on the scale of a soil moisture anomaly. Implementing artificial dry and wet patches of different size in a checkerboard pattern showed that the above described behavior occurred most prominently with patches between 40-80 km. When the patch size was smaller, convective cells collided and diminished before convective precipitation formed, while precipitation occurred more arbitrarily over the wet patch, when the patch size was larger than 80 km. This shows the importance of spatial scales e.g. of soil moisture anomalies in L-A coupling studies.

Several studies also highlighted that the synoptic forcing influences the strength of the soil moisture influence on precipitation (Froidevaux et al., 2014; Keil et al., 2019). Moderate to strong synoptic

forcing dampen or even diminish local feedback, while under weak synoptic forcing, local processes can trigger deep moist convection in orographically complex terrain, despite initially considerable CIN (Barthlott et al., 2011). Koukoula et al. (2019) additionally showed that beside the synoptic forcing itself also the persistence of a synoptic weather situation influences the soil moisture impact on convective precipitation. They showed that differences in the soil moisture initialization impact convective precipitation only in case the weather system persisted long enough.

Beside the physical processes, model based coupling studies have to deal with uncertainties e.g. from the need to parameterize physical processes, and the models' grid increment. Hohenegger et al. (2009) performed two sets of one-month sensitivity simulations on convection resolving and on convection parameterizing resolution. They found not only differences in the coupling strength, but also a switch in the sign of soil moisture-precipitation feedback over Central Europe and the Alpine Region. Leutwyler et al. (2021) examined similar sensitivity tests, but for a domain covering Europe entirely, and for 10 summers. They found a positive feedback sign for both the convection resolving and the convection parameterizing simulations. However, disentangling the precipitation characteristics (intensity, frequency, amount) showed that when convection is resolved, wetter soils predominantly increased precipitation intensity, while they predominantly increased the precipitation frequency in simulations with parameterized convection. Both initiated a higher precipitation amount over wet than over dry soils. Finally, the representation of feedback with precipitation in models depends on the respective cumulus parameterization, and specifically on how the convective mass-flux closure is implemented in the parameterization scheme (CAPE- vs CIN-based convective mass-flux closure, Williams, 2019). Chen et al. (2017) also showed improvements in precipitation patterns of a global climate model, when they added a triggering criterion based on the thermodynamic preconditioning to a purely CAPE-based mechanism.

2.5 LoCo Working Group and its Process Chain

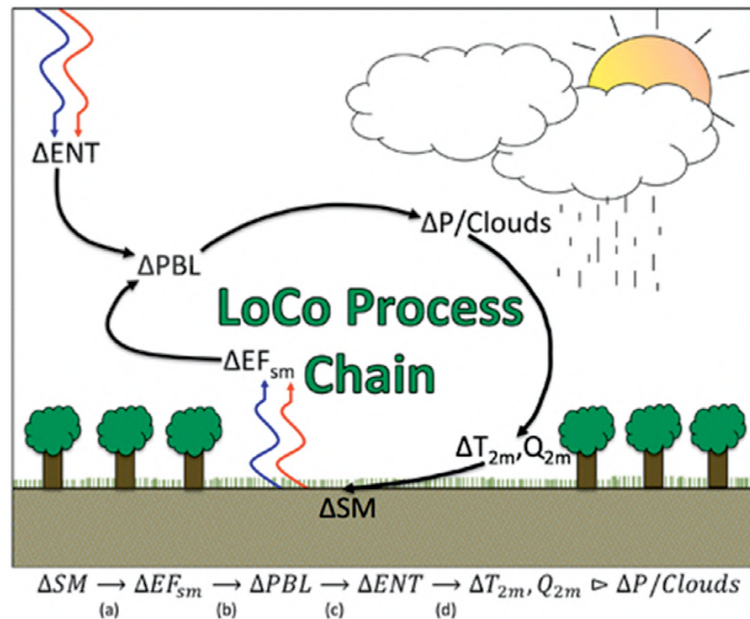


FIGURE 2.2: LoCo process chain (Santanello et al., 2018)

The LoCo working group (<https://www.gewex.org/loco/>) is an initiative under the Global Energy and Water Exchanges (GEWEX) project which was established in the mid-2000s to promote the coordination of research on L-A coupling with the aim to improve the understanding and quantification of local L-A coupling on process-level (Santanello et al., 2018). A schematic depiction of various L-A interactions is shown in figure 2.1.

Its main focus resembles around the investigation of physical processes in the LoCo process chain (Figure 2.2, Santanello et al., 2009; Santanello et al., 2011; Santanello et al., 2018), which connects the impact of soil moisture anomalies with subsequent cloud formation and precipitation development through a chain of physical processes. This process chain covers a terrestrial component, which is the link between soil moisture and the surface fluxes usually referred to as the terrestrial leg (Dirmeyer, 2011; Feldman et al., 2019; Knist et al., 2017; Berg and Sheffield, 2018). The atmospheric component considers the sensitivity of the boundary layer evolution to the surface fluxes. The two components are amended by the influence of entrainment fluxes at the ABL-top to the ABL evolution and effects of the ABL on near-surface temperature and humidity.

Unlike the studies inferring on soil moisture-precipitation feedback by the means of sensitivity experiments with models or based on case studies as introduced in subsection 2.4.1, the LoCo working

group uses process-based or statistical measures to quantify isolated or combined relationships between different variables. This approach bears the potential to disentangle the role of individual processes determining the coupling and investigating impacts of e.g. changes in the land cover on the process chain. Further details on the coupling metrics are noted in subsection 2.6. The LoCo working group's research builds on four pillars covering studies on 1) the local-scale offline, 2) the large-scale offline, 3) the local-scale coupled and 4) the large-scale coupled studies using model simulations and increasingly multi-sensor synergies to target the various and complex relationships in the climate system. The recent focus of the group and its parent the Global Land/Atmosphere System Study (GLASS) panel is the development and improvement of ABL observations and the continuation of implementing LoCo components in field campaigns to improve the verification basis for LoCo process studies.

2.6 Quantification of L-A Coupling Strength

The LoCo working group developed and gathered a suite of different metrics to quantify L-A coupling strength during the last two decades (Santanello et al., 2018). The coupling metrics are generally distinguishable in statistical and process-based approaches. While physical metrics are based directly on physical processes and are primarily used to understand the nature of feedback processes or to evaluate their representation in models, statistical metrics usually target the quantification of relationships on longer time scales, which are already known to be causally related, and thus imply physical relationships. The L-A coupling metric cheat sheets (<https://www.pauldirmeyer.com/coupling-metrics>) provide an overview about the coupling metrics gathered by the community.

2.6.1 Process-Level Coupling Metrics

Process-level coupling metrics infer on L-A coupling strength based on the instantaneous state or the evolution of a variable in the L-A system. This means that a metric e.g. uses the thermodynamic conditions in the ABL to deduce on whether the land surface crucially influences the ABL structure and convection triggering during a subsequent day. Most of the process-level coupling metrics target the land surface influence on hydro-meteorological relationships in the L-A system up to a potential influence of soil moisture and surface flux partitioning on precipitation.

Coupling metrics targeting soil moisture and its influence on the surface fluxes, include the memory decomposition (Koster and Suarez, 2001; Seneviratne and Koster, 2012), the vegetated coupling little omega (e.g. Ek, 2016), and the latent heating tendency (Heerwaarden et al., 2010; Stap et al., 2014). The memory decomposition metric is used to disentangle four to five distinct controlling factors for determining soil moisture persistence in the climate system. The vegetated coupling little omega relates a change in root zone soil moisture to a change in the EF while considering soil and canopy properties. Another metric investigating the turbulent heat fluxes at the land surface is the latent heating tendency. It can be used to analyze the diurnal cycle of ET using a budget equation for ET.

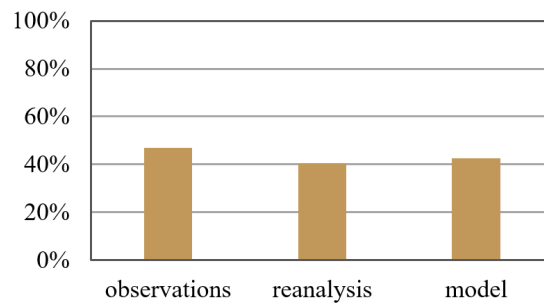
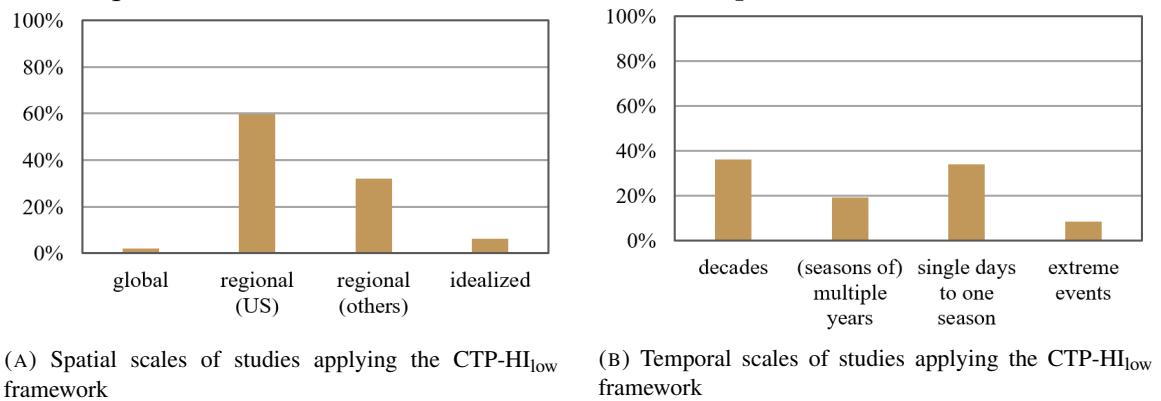
Mixing diagrams are kind of at the border between the terrestrial and atmospheric coupling legs. They assess the co-evolution of the surface temperature and humidity, which is used to infer on the influence of the surface fluxes versus entrainment of dry air from the free troposphere on ABL

evolution during daytime (Santanello et al., 2009). An advection term can be added in case these information are available. Santanello et al. (2011) combined the mixing diagram approach with an evaluation of the atmosphere's tendency toward saturation at the ABL top by quantifying the LCL deficit, which refers to the difference between the ABL height and the LCL height. Recall, that the LCL is the height at which an air parcel reaches saturation, and reaching saturation within the ABL is a necessary condition for local cloud and precipitation formation. This condition, and the fact that the LCL is directly linked to the low-level temperature and humidity, make a combined analysis of mixing diagrams and the LCL deficit a valuable pairing for analyzing L-A coupling. Another metric investigating relative humidity at the ABL top is the relative humidity tendency metric by Ek and Mahrt (1994) and Ek and Holtslag (2004). This metric disentangles the influences of surfaces moistening and heating as well as entrainment of cold and dry on the relative humidity at ABL top, and quantifies their respective contributions under different ABL conditions.

The final two process-level coupling metrics mentioned here inform about the surface influence on the potential for locally triggered convection based on 3D atmospheric temperature and moisture data. The heated condensation framework (Tawfik and Dirmeyer, 2014; Tawfik et al., 2015a; Tawfik et al., 2015b) and the CTP-HI_{low} framework (Findell and Eltahir, 2003b; Findell and Eltahir, 2003c; Findell and Eltahir, 2003a) rely on ABL properties in order to quantify a pre-conditioning for convection triggering without directly including information about the surface wetness. However, several approaches have been published which add soil moisture or EF as a third dimension to the CTP-HI_{low} framework and thus combine pre-conditioning with moisture availability (see subsection 2.6.2).

2.6.2 CTP-HI_{low} Framework

This section gives an overview about applications, modifications and extensions of the CTP-HI_{low} framework, which was the coupling metric mainly used for the analyses of this dissertation. Detailed descriptions of the CTP-HI_{low} framework are included in both publications and won't be repeated here. There is a total of 47 studies including the ones presented in this dissertation (status: 15.2.2022) using at least parts of the CTP-HI_{low} framework in evaluations or applications for different temporal and spatial scales, and based on various datasets (observational, reanalysis, model). An overview is presented in Figures 3 and 4.

FIGURE 2.4: Data base for studies applying the CTP- HI_{low} framework

The framework was originally developed with data from radiosondes over Illinois (Findell and Eltahir, 2003b), and tested over the entire US (Findell and Eltahir, 2003c). In 2015, Findell et al. identified the minimum data length required to provide a robust estimate of the long-term coupling signal using various coupling metrics including the CTP- HI_{low} framework. They found that due to the atmospheric component of the metric, one requires at least 1104 data points corresponding to 12 summers of data, to establish a coupling estimate, which covers the full variability. As the spatial coverage of vertical profiles in the atmosphere is sparse and thus, the application of the framework limited by data availability, Wakefield et al. (2021) evaluate the uncertainty of using data with lower vertical resolution against high resolution radiosonde profiles and show that lower resolution data still provide reasonable estimates of the framework variables. They further showed that profiles are comparable within ± 1 UTC time step, but the comparability decreases for profiles from regions further apart due to the rapid early-morning boundary layer evolution.

By far most studies use the framework, its measures or modifications and extensions on the regional scale to domains covering the US or parts of it. A smaller proportion covers other regions such as India (Tuinenburg et al., 2011; Kar et al., 2014; Huggannavar and Indu, 2020), Afrika (Dione

et al., 2014; Hurk and Meijgaard, 2010), the Arabian Peninsula (Branch and Wulfmeyer, 2019), South America (Doyle et al., 2013; Ghate and Kollias, 2016), and Asia (Li et al., 2019; Zhang et al., 2019; Ma et al., 2021; Zhao et al., 2022). The studies presented in this dissertation provide the first studies applying the framework specifically over Europe. Tuinenburg et al. (2011) showed that not all threshold values as identified by Findell and Eltahir (2003b) for Illinois fit optimally to detect the pre-conditioning for triggering deep convection over other regions such as India in their case. Ferguson and Wood (2011) performed a nearly global investigation and modified the framework based on the climatology of CTP and HI_{low} to ensure its applicability to different regions. The similar reasoning led to the study of Wakefield et al. (2019).

Over the US, the framework measures were used and extended by soil moisture as a third dimension to analyze and improve drought prediction. Roundy et al. (2013) developed the Coupling Drought Index for drought detection and prediction, and in order to understand the influence of L-A coupling on drought development. The coupling drought index was tested both based on a forecasting system (Roundy et al., 2014; Roundy and Wood, 2015) and on satellite remote sensing data (Roundy and Santanello, 2017). Basara et al. (2019) and Gerken et al. (2018) used the framework variables to investigate the evolution and convective suppression of the flash droughts of 2012 and 2017, respectively, over the Central US. Also in China, the framework was used in the context of drought detection (Li et al., 2019).

Berg et al. (2013) and Findell et al. (2011) complemented the atmospheric variables CTP and HI_{low} with the surface fluxes for deriving the triggering feedback strength and the amplification feedback strength. They assessed the influence of the morning surface flux partitioning on triggering or amplifying afternoon convection precipitation. Frye and Mote (2010) combined a reformulated version of the CTP to information about soil moisture and the low-level jet over the Central US to investigate relationships between soil moisture and the occurrence and severity of thunderstorms. Findell and Eltahir (2003a) themselves added low-level wind as a third dimension to the original formulation and found that low-level backing or unidirectional winds with great wind shear can suppress convection. Another approach to combine CTP and HI_{low} with wind was presented by Branch and Wulfmeyer (2019), who derived a Global Feedback Index to detect arid regions in which desert plantations have maximum impacts on convection initiation through L-A feedback processes.

2.6.3 Statistical Coupling Metrics

The range of complexity of statistical coupling metrics spans from simple correlations (Pearson, 1895; Spearman, 1907) and linear regression measures such as the terrestrial and atmospheric coupling indices (Dirmeyer, 2011; Dirmeyer et al., 2014) over conditional probit models (Granger, 1969; Salvucci et al., 2002; Tuttle and Salvucci, 2016), to using singular value decomposition to detect cross-influences of land surface and atmospheric fields (Navarra and Tribbia, 2005; Alessandri and Navarra, 2008; Catalano et al., 2016). As feedback processes are usually highly non-linear, recent research also evolved in the direction of using neural networks (DelSole and Tippet, 2007; Ruddell and Kumar, 2009a; Ruddell and Kumar, 2009b; Goodwell and Kumar, 2017), and non-linear feedback metrics (Hsu and Dirmeyer, 2021).

Statistical coupling metrics do not necessarily establish causality, which is why they should be mainly used to quantify relationships between variables, where a physical relationship was already determined. Especially in case of soil moisture-precipitation or surface flux-precipitation feedback, it is difficult to establish causality. Tuttle and Salvucci (2017) determined and investigated several ‘confounding factors’ which may falsely lead to the detection of a statistically significant relationship between soil moisture and precipitation using statistical metrics. Thus, they need to be accounted for in the investigation of causal feedback: seasonal to interannual variability, precipitation persistence, and endogeneity. The most commonly used statistical coupling metric are the terrestrial coupling index and the two-legged coupling metric by Dirmeyer (2011). It has been applied to a range of variables in global and regional studies to detect mean L-A coupling strengths (Dirmeyer et al., 2013a; Dirmeyer et al., 2014; Warrach-Sagi et al., 2022) and temporal variability (Dirmeyer et al., 2012; Dirmeyer et al., 2013b; Guo and Dirmeyer, 2013; Lorenz et al., 2015).

Chapter 3

Flagship Pilot Study on ‘Land Use and Climate Across Scales’

3.1 Experiments

All simulations analyzed within this dissertation were conducted in the context of the WCRP FPS LUCAS. LUCAS is a model intercomparison effort hosted by the Euro-CORDEX (Jacob et al., 2020) and since 2021 also the CORDEX-North America (Asselin et al., 2022) communities, which was endorsed in 2017 with the aim to investigate and quantify the impact of implementing land cover changes in regional climate simulations. The experiments of phase I were conducted with the aim of testing the sensitivity of different climate parameters (temperature, snow, precipitation) to land cover changes in commonly used regional climate models (RCMs) within Euro-CORDEX. Thus, beside an evaluation run with realistic land cover initialization, two sensitivity runs were conducted – one with Europe fully covered with forests and one with Europe fully covered with grasslands for the historical period 1986-2015 and forced with ECMWF ERA-Interim reanalysis data.

3.2 Outcome of sensitivity experiments

The LUCAS ensemble currently comprises of 11 different RCM configurations (table 3.1), which partly share the same atmospheric or land surface set-up. This allows for an objective determination of the origin of uncertainties in the simulated responses to the implemented LULCCs (Davin et al., 2020). Table 3.2 adds an overview about the atmospheric physics parameterizations used in the three

Model Label	RCM	LSM	Institute
CCLM-TERRA	COSMO_5.0_clm9	TERRA-ML	JLU/BTU/CMCC
CCLM-VEG3D	COSMO_5.0_clm9	VEG3D	KIT
CCLM-CLM4.5	COSMO_5.0_clm9	CLM4.5	ETH
CCLM-CLM5.0	COSMO_5.0_clm9	CLM5.0	ETH
RegCM-CLM4.5	COSMO_5.0_clm9	CLM4.5	ICTP
REMO-iMove	REMO2009	iMOVE	GERICS
WRFa-NoahMP	WRF3.8.1	NoahMP	IDL
WRFb-NoahMP	WRF3.8.1	NoahMP	UHOH
WRFb-CLM4.0	WRF3.8.1	CLM4.0	AUTH
WRFc-NoahMP	WRF3.8.1	NoahMP	BCCR
RCA	RCA4		SMHI

TABLE 3.1: Overview about participating models in LUCAS Phase I. JLU – Justus-Liebig-University Gießen; BTU – "Brandenburgische Technische Universität"; CMCC – Euro-Mediterranean Center on Climate Change; KIT – Karlsruhe Institute of Technology; ETH – "Eidgenössische Technische Hochschule" Zürich; ICTP – International Centre for Theoretical Physics; GERICS – Climate Service Center Germany; IDL – "Instituto Dom Luiz" University of Lisbon; UHOH – University of Hohenheim; AUTH – Aristotle University of Thessaloniki; BCCR – Bjerknes Center for Climate Research; SMHI – Swedish Meteorological and Hydrological Institute

WRF configurations. The model configuration of the runs used in the thesis is marked in bold in both tables. Several intercomparison studies were already published from this effort which mainly target differences the temperature response to LULCC in different RCMs (Davin et al., 2020; Breil et al., 2020; Daloz et al., 2022; Mooney et al., 2022; Sofiadis et al., 2022). The key outcomes of the publications using also the simulations examined in this dissertation will be summarized in the following paragraphs.

Davin et al. (2020) analyzed the LUCAS ensemble with regard to differences in the 2m-temperature as well as daily maximum and minimum temperatures between the two sensitivity runs. They found that in winter and spring, the models agree in the sign of the temperature response to afforestation showing warmer temperatures in the forest than in the grass run. Conversely, in summer and autumn, the models disagree in the direction of changes, which they attribute largely to differences in the simulated evaporative fraction coming from disagreement in simulated evapotranspiration changes. Hence, land processes primarily determine the simulated summer temperature responses, while they found that the atmospheric processes play a dominant role e.g. for winter precipitation. Breil et al. (2020) investigated LULCC impacts on the diurnal cycle of skin temperature, 2-meter temperature and temperature in the lowest atmospheric model layer. They found opposing responses

	WRFa	WRFb	WRFc
Planetary Boundary Layer scheme	MYNN Level 2.5 PBL (Nakanishi and Niino, 2009)	MYNN Level 2.5 PBL	YSU scheme (Hong et al., 2006)
Shortwave and Long-wave Radiation schemes	Rapid Radiative Transfer Model (RRTMG)scheme (Iacono et al., 2008)	RRTMG scheme	RRTMG scheme
Convection scheme	Grell-Freitas scheme (Grell and Freitas, 2014)	Kain-Fritsch scheme	Kain-Fritsch scheme (Kain, 2004)
Shallow Convection scheme	GRIMs scheme (Hong et al., 2013)	none	none
Microphysics scheme	WRF double moment 6-class scheme (Lim and Hong, 2010)	New Thompson scheme	New Thompson scheme (Thompson et al., 2004)

TABLE 3.2: Atmospheric physics parameterizations of the LUCAS WRF model configurations.

in the diurnal cycles of skin temperature and the temperature of the lowest model layer to afforestation, and showed that the skin temperature response of the models agrees with that of observation-based studies for the mid-latitudes. Further, they disentangled the impact of these findings for the modeled 2-meter temperature. The 2-meter temperature is a diagnostic quantity in the models which is derived from the prognostic skin temperature and the temperature of the lowest model layer. They found that analyzing modeled 2m-temperatures can be misleading in the context of LULCC studies, as it does not solely reflect the land processes in summer due to the additional influence of the lowest atmospheric model layer, which exhibited another behavior.

Sofiadis et al. (2022) round up the analyses of different temperatures on the phase I model ensemble by analyzing the response to afforestation in the seasonal cycle of soil temperature in connection with ground heat fluxes and soil moisture. They found that forest-covered grounds tend to be dryer and cooler than grassland-covered grounds and the majority of models agrees in the sign of the soil temperature signals. The same signal was found in in-situ observations from paired FLUXNET stations over grasslands and forests. Soil temperature and moisture are crucially influencing biochemical processes such as soil carbon sequestration, and thus need to be investigated when discussing

afforestation as a mitigation measure for climate change in the mid-latitudes.

The findings up to now highlight the importance of accurately depicting the land cover in regional climate simulations in order to reduce biases originating from a misrepresentation of land processes or ‘misparameterization’ of the vegetation in models. Further analyses are currently in preparation for publication. They cover the evaluations of precipitation and cyclones, soil moisture - extreme temperature feedback during compound events, as well as changes in the snow-albedo feedback in northern Europe.

Chapter 4

Impacts of large-scale land cover changes on L-A coupling strength

Publication I: Jach, L., K. Warrach-Sagi, J. Ingwersen, E. Kaas, and V. Wulfmeyer, 2020: Land cover impacts on land-atmosphere coupling strength in climate simulations with WRF over Europe. *J. Geophys. Res-Atmos.* 125(18), 1-21 DOI: 10.1029/2019JD031989

4.1 Overview

As LULCCs modify the energy and moisture exchange between the land surface and the atmosphere, they also impact ABL structure and dynamics. Following the rationale of Findell and Eltahir (2003b), the ABL structure in turn determines whether locally triggered convective precipitation can occur. Hence, by changing the ABL structure, LULCC may change the potential L-A coupling strength and the likelihood for local convective precipitation. Three experiments with different land cover were conducted with a regional climate model over Europe to investigate LULCC impacts on the ABL and their influence on the potential L-A coupling strength in conjunction with a statistical assessment of changes in the precipitation patterns. The experiments followed the experimental plan of LUCAS Phase I and involved a scenario where Europe is fully covered by forests. In a second land cover change scenario, Europe was fully covered by grassland. In both the forest and grassland scenarios, ice and desert regions were not covered by vegetation, as this would be biologically implausible. The final scenario applied a realistic land cover distribution and was used to relate the magnitude of LULCC impacts. The simulations were performed with WRF in version 3.8.1 which

was coupled to the Noah land surface model with multi-parameterization options (Noah-MP) and forced with ECMWF ERA-Interim reanalysis data. LULCC induced changes in the ABL structure and the potential L-A coupling strength were analyzed by comparing CTP and HI_{low} , as well as the coupling variables from the classification procedure between the three experiments. This analysis was performed for the summer months of the period 1986-2015, as changes in the ABL structure and the coupling strength mainly occurred during summer. Monthly estimates of the coupling strength are provided in Appendix C, which show that the land surface impact on convection triggering is generally lower in the other seasons (dominant atmospheric control). Additionally, the greatest modifications on the ABL structure occurred in summer. In a next step, differences in soil moisture and surface fluxes were associated with differences in the ABL structure and the L-A coupling strength. Finally, changes in cloud fraction and precipitation were evaluated using simple statistical measures to see whether the greatest impacts indeed occurred in the strong coupling region or not. The analysis showed that both afforestation (forest-evaluation) and transition to grassland (grass-evaluation) modified the ABL structure and thus the preconditioning for strong coupling besides the surface flux partitioning over Europe in summer. However, the atmospheric drivers in favor for inhibiting feedback everywhere else as in the hot spot region in the northeast of Europe (mainly stable layering, and dry air in the early-morning boundary layer) were not modified by the LULCC. This limited the major LULCC impacts on the L-A coupling strength to the strong coupling region which coincides with the region under continental climate in Europe (Peel et al., 2007). Also the cloud occurrence was mainly influenced in the strong coupling region, although soil moisture and the surface fluxes were influenced all over the domain. The evaluation of precipitation indicated a higher likelihood for precipitation occurrence with higher evaporative fractions, but statistically significant changes in the precipitation patterns occurred rather limited in space. Besides mountainous regions, the strongest changes in the precipitation patterns happened over the strong coupling region.

4.2 Publication

This publication titled “Land cover impacts on land-atmosphere coupling strength in climate simulations with WRF over Europe” is an open access article published under the terms of the Creative Commons Attribution-NonCommercial License, which permits use, distribution and reproduction in any medium, provided the original work is properly cited and is not used for commercial purposes.

©2020 The Authors. Journal of Geophysical Research: Atmospheres published by John Wiley and Sons Ltd on behalf of the American Geophysical Union.

JGR Atmospheres



RESEARCH ARTICLE

10.1029/2019JD031989

Land Cover Impacts on Land-Atmosphere Coupling Strength in Climate Simulations With WRF Over Europe

Lisa Jach¹ , Kirsten Warrach-Sagi¹ , Joachim Ingwersen², Eigil Kaas³ , and Volker Wulfmeyer¹ 

¹Institute for Physics and Meteorology, University of Hohenheim, Stuttgart, Germany, ²Institute for Soil Science and Land Evaluation, Department of Biogeophysics, University of Hohenheim, Stuttgart, Germany, ³Niels Bohr Institute, Department of Climate and Computational Geophysics, University of Copenhagen, Copenhagen, Denmark

Key Points:

- A region of strong coupling was identified in the northeast of Europe, and the location was not shifted by land use and land cover changes
- Land-atmosphere feedbacks appear to be mainly positive in Europe, and extreme afforestation and deforestation modify the coupling strength
- Significant impacts on clouds and precipitation occur over mountains and the coupling hot spot; however, the impacts are rather limited

Supporting Information:

- Supporting Information S1

Correspondence to:

L. Jach,
lisa.jach@uni-hohenheim.de

Citation:

Jach, L., Warrach-Sagi, K., Ingwersen, J., Kaas, E., & Wulfmeyer, V. (2020). Land cover impacts on land-atmosphere coupling strength in climate simulations with WRF over Europe. *Journal of Geophysical Research: Atmospheres*, 125, e2019JD031989. <https://doi.org/10.1029/2019JD031989>

Received 6 NOV 2019

Accepted 19 AUG 2020

Accepted article online 31 AUG 2020

Abstract Land use and land cover changes are important human forcings to the Earth's climate. This study examines the land-atmosphere coupling strength and the relationship between surface fluxes and clouds and precipitation for three land cover scenarios in the European summer. The WRF model was used to simulate one scenario with extreme afforestation, one with extreme deforestation, and one with realistic land cover for the time period between 1986 and 2015. The simulations were forced with ERA-Interim reanalysis data. The analysis followed a two-step approach. First, the convective triggering potential–low-level humidity index framework was applied to locate potential coupling hot spots, which were then analyzed with regard to their sensitivity toward land use and land cover changes. Second, actual feedbacks between evaporative fraction, cloud cover, and precipitation were analyzed statistically with focus on sign and location of the feedbacks. The results demonstrate that coupling hot spots, exhibiting predominantly positive feedbacks, were identified over parts of Eastern Europe and Scandinavia. In this strongly coupled region, afforestation and deforestation modified the atmospheric humidity and stability by changing the surface flux partitioning. Afforestation is associated with a net drying of the atmosphere due to a disproportionately strong increase in the sensible heat flux. In contrast, deforestation initiated a moistening of the atmosphere. The total precipitation changed only in limited areas significantly, which are mostly located in mountainous regions and the northeast of the domain. In summary, the results indicate a land surface influence on the atmospheric background conditions, and an impact on the potential strength of land surface-precipitation feedbacks.

1. Introduction

Land-atmosphere (L-A) interactions are key processes in the Earth's climate system. Feedbacks are manifold and strongly interconnected. Thus, modifications on the land surface due to land use and land cover changes (LULCCs) can impact the climate significantly. They affect biogeochemical cycles like carbon storages as well as energy and water fluxes at the land surface (Intergovernmental Panel on Climate Change, 2014, 2019). Variations in the latter appear due to modifications in biogeophysical properties of the land surface such as albedo, roughness length, leaf area index, or stomatal resistance.

Underestimating biogeophysical forcings to the climate in models may lead to significant biases in a number of variables. de Noblet-Ducoudré et al. (2012) find that the regional biogeophysical impacts of LULCC can exceed the magnitude of radiative forcing caused by greenhouse gas emissions, although their assessment is still uncertain in sign and magnitude within climate models (Davin & de Noblet-Ducoudré, 2010). This is because counteracting effects of radiative and nonradiative processes on water and energy exchanges vary in time and space and depend on the type of LULCC (Duveiller, Forzieri, et al., 2018; Duveiller, Hooker, & Cescatti, 2018; Snyder et al., 2004). Deforestation, for example, increases the surface albedo, because cropland or grassland usually have a brighter surface than forests. The resulting loss in available energy cools the surface. The concurrent decrease in leaf area and stomatal resistance reduces transpiration, which leads to a reduction of evaporative cooling and, hence, to a warming. The net effect depends on which of these processes dominates (Davin & de Noblet-Ducoudré, 2010). Different forest types diverge in their biogeophysical and biogeochemical forcings, too. Transitions of boreal forests have the largest biogeophysical effects of all

©2020 The Authors.

This is an open access article under the terms of the Creative Commons Attribution-NonCommercial License, which permits use, distribution and reproduction in any medium, provided the original work is properly cited and is not used for commercial purposes.

vegetation types as they have a lower summertime evaporative fraction (EF) than other forests. Their lower albedo increases the available energy at the surface. The additional energy is partitioned into sensible rather than latent heat (Baldocchi et al., 2000; Bonan, 2008; Snyder et al., 2004). Studies of global climate-vegetation dynamics reveal a significant impact of vegetation on the climate and vice versa (e.g., Kumar et al., 2013). Thus, LULCCs have recently become the focus of studies aiming to assess their role in past temperature trends (e.g., Boisier et al., 2012; Huang et al., 2020; Pitman et al., 2009), extreme events (e.g., Findell et al., 2017; Hirsch et al., 2015), and modification of precipitation patterns (e.g., Bagley et al., 2014; Chen et al., 2017; Chen & Dirmeyer, 2017; Lawrence & Chase, 2010). Mahmood et al. (2014) provide an overview of the most notable LULCC and their effects on the climate, and Snyder et al. (2004) assess the influence of vegetation biomes on the climate.

The L-A coupling strength is an approach to quantify the relationship between the land surface and atmospheric states and fluxes. The coupling strength is subject to regional variability (Findell & Eltahir, 2003b; Koster et al., 2004) and temporal variability (Dirmeyer et al., 2014; Guo & Dirmeyer, 2013; Seneviratne et al., 2006), which raises the question of which factors determine the strength of L-A coupling. The lack of a common definition along with the fact that different studies and metrics address different quantities and processes (Knist et al., 2017) complicates the comparability of studies on L-A coupling strength. Additionally, disparate atmospheric models and resolutions, high land surface complexity, and lack of observations make assessments difficult as well (Santanello et al., 2009). Furthermore, many studies have been performed on a global scale and on rather coarse resolutions. Koster et al. (2004), for example, examine the soil moisture-precipitation coupling using an ensemble of atmospheric general circulation models. They find a weak coupling hot spot in Eastern Europe. However, studies on the continental scale are still rare for Europe. Knist et al. (2017) investigate the coupling between soil moisture and surface fluxes as well as surface fluxes and near-surface air temperature variations. They locate a coupling hot spot in eastern-central Europe and attribute this link to reduced or missing dominant moisture or energy limitations on evapotranspiration. Only a limited number of L-A observational studies are currently available, for example, the Land Atmosphere Feedback Experiment (LAFE; Wulfmeyer et al., 2018, 2020). Therefore, new observations dedicated to measuring L-A interactions are under development in Europe. One example is the Land Atmosphere Feedback Observatory (LAFO; <https://lafo.uni-hohenheim.de/>, Späth et al. (2019).

Until now, few studies have employed regional climate models (RCMs) to investigate LULCC forcings on the climate in Europe (Cherubini et al., 2018; Davin et al., 2014; Tölle et al., 2014). The studies usually apply static land cover maps to investigate biogeophysical impacts of single LULCC such as afforestation (e.g., Gálos et al., 2013; Gao et al., 2014). However, realistic, transient LULCCs have not been included in previous RCM-intercomparison studies in Europe (e.g., Christensen & Christensen, 2007). In 2017, the World Climate Research Program Flagship Pilot Study “Land-Use and Climate Across Scales” (LUCAS) was endorsed to investigate the effects of implementing LULCC in RCMs in a coordinated initiative. LUCAS is part of the European branch of the Coordinated Regional Climate Downscaling Experiment (CORDEX, <https://www.cordex.org/>; Giorgi et al. 2009; Gutowski et al. 2016). They aim at examining biogeophysical impacts and their influence on the regional climate on different spatial and temporal scales. The overarching goal is to investigate the potential of the land surface to mitigate climate change and to provide an improved basis for regional climate impact assessments (Rechid et al., 2017). In LUCAS phase I, three land cover scenarios are implemented in an ensemble of RCMs to compare the impacts of (1) extreme afforestation (FOREST) and (2) extreme deforestation (GRASS) with a (3) realistic land cover (CORINE) as baseline in Europe. In the following presented experiments, afforestation refers to a conversion from all nonforest vegetation types to forest. Deforestation refers to the conversion from all vegetation types to grassland in the respective model run.

This study provides an analysis of WRF-NoahMP simulations made by the University of Hohenheim which were included as part of the LUCAS ensemble (Davin et al., 2020). It is a test bed for future coupling strength studies on the LUCAS-ensemble investigating the effects of realistic LULCC. Simulation experiments with idealized extreme LULCC are well suited for assessing the potential sensitivity of atmospheric responses to land surface modifications. The first objective is to locate long-term mean coupling hot spots between surface fluxes and precipitation based on the early-morning atmospheric structure (Findell & Eltahir, 2003a, 2003b) for the European summer. The coupling hot spots and the coupling strength are then analyzed with

Table 1
Choice of Parameterization Schemes of the WRF Configuration

Model physics	Parameterization scheme
Microphysics Scheme	New Thompson scheme (Thompson et al., 2004)
Short-Wave Radiation Scheme	Rapid Radiative Transfer Model (RRTMG) scheme (Iacono et al., 2008)
Long-Wave Radiation Scheme	Rapid Radiative Transfer Model (RRTMG) scheme (Iacono et al., 2008)
Boundary Layer Scheme	MYNN Level 2.5 PBL (Nakanishi & Niino, 2009)
Convection Scheme	Kain-Fritsch scheme (Kain, 2004)
Land Surface Model	NOAH-MP land surface model (Niu et al., 2011)
Surface Layer Scheme	MYNN surface layer scheme (Nakanishi & Niino, 2009)

regard to their sensitivity to extreme LULCC. The second objective is to investigate the relationship between the surface fluxes and clouds and precipitation patterns in dependence of land cover. This work is structured as follows: Section 2 outlines the Materials and Methods, including a model description, the simulation set-up, the land cover scenarios, and the analysis metrics. Section 3 presents the results on L-A coupling strength. Section 4 reports the results on the statistical analysis of the link between surface fluxes, clouds, and total precipitation. The results are discussed in section 5 and summarized in section 6.

2. Experimental Design and Methods

2.1. Model Description

The RCM used in this study is WRF V3.8.1 (Skamarock et al., 2008) coupled to the Noah land surface model with multiparameterization options (NoahMP) (Niu et al., 2011). For the planetary boundary layer (PBL), the MYNN level 2.5 local turbulence parameterization scheme was applied (Nakanishi & Niino, 2009). In line with the WRFb-CLM configuration of the LUCAS ensemble, the number of vertical levels was set to 40 and the model top to a pressure height of 50 hPa (Davin et al., 2020). The cumulus parameterization followed the approach of Kain (2004). Additional parameterization schemes are listed in Table 1. The final physics configuration was based on previous studies from the authors and others (e.g., see Bauer et al., 2015; Kotlarski et al., 2014; Schwitalla et al., 2017; Warrach-Sagi et al., 2013). Soil moisture was initialized on the 1 January 1984 from ERA-Interim reanalysis data (Dee et al., 2011), and the soil texture was derived from a modified version of the Harmonized World Soil Database (HWSD) (Milovac et al., 2014). The vegetation in each grid cell was considered using a dominant approach, and each land cover type was parameterized after the IGBP-MODIS 21-category land use classification used in WRF. The vegetation dynamics were treated through daily interpolation of monthly leaf area index (LAI) values from the MODIS vegetation parameter table. The calculation of stomatal resistance was performed using the Ball-Berry scheme in combination with green vegetation fraction calculated from LAI and the stem area index.

2.2. Simulation Set-Up

Three experiments, which differ in the applied land cover maps, were forced with 6-hourly ERA-Interim reanalysis data on 0.75° resolution from the European Centre for Medium-Range Weather Forecasts. They ran for the years 1984–2015 including 2 years of spin-up, which were excluded from the analyses. All experiments were carried out for the CORDEX domain of Europe (EURO-CORDEX; Jacob et al., 2020) on 0.44° grid spacing. The analyses focused on the summer months of June–August because the sensitivity of convection to land surface influences is expected to be greatest in summer (Dirmeyer et al., 2013; Taylor et al., 2012). Some analyses were carried out for the PRUDENCE subregions (Alps, British Isles, Eastern Europe, France, Iberian Peninsula, Mediterranean, Mid-Europe, and Scandinavia (Christensen & Christensen, 2007)). The original subregions were expanded by two additional ones covering the northeastern and eastern parts of the study domain. The Eastern European Plain extends from 44°N to 70°N and 30°E to the eastern border of the domain (Figure 1c). The Black Sea extends from 25°N to 44°N and 36°E to the eastern border of the domain. The range of climate zones in the domain is heterogeneous. According to the Köppen-Geiger classification (Peel et al., 2007), climates vary from cool continental climates with arctic influence in the high latitudes to Mediterranean climate in southern Europe and from oceanic climate in coastal areas to warm, humid continental climate in Eastern Europe. This variety makes L-A feedback studies quite challenging over Europe.

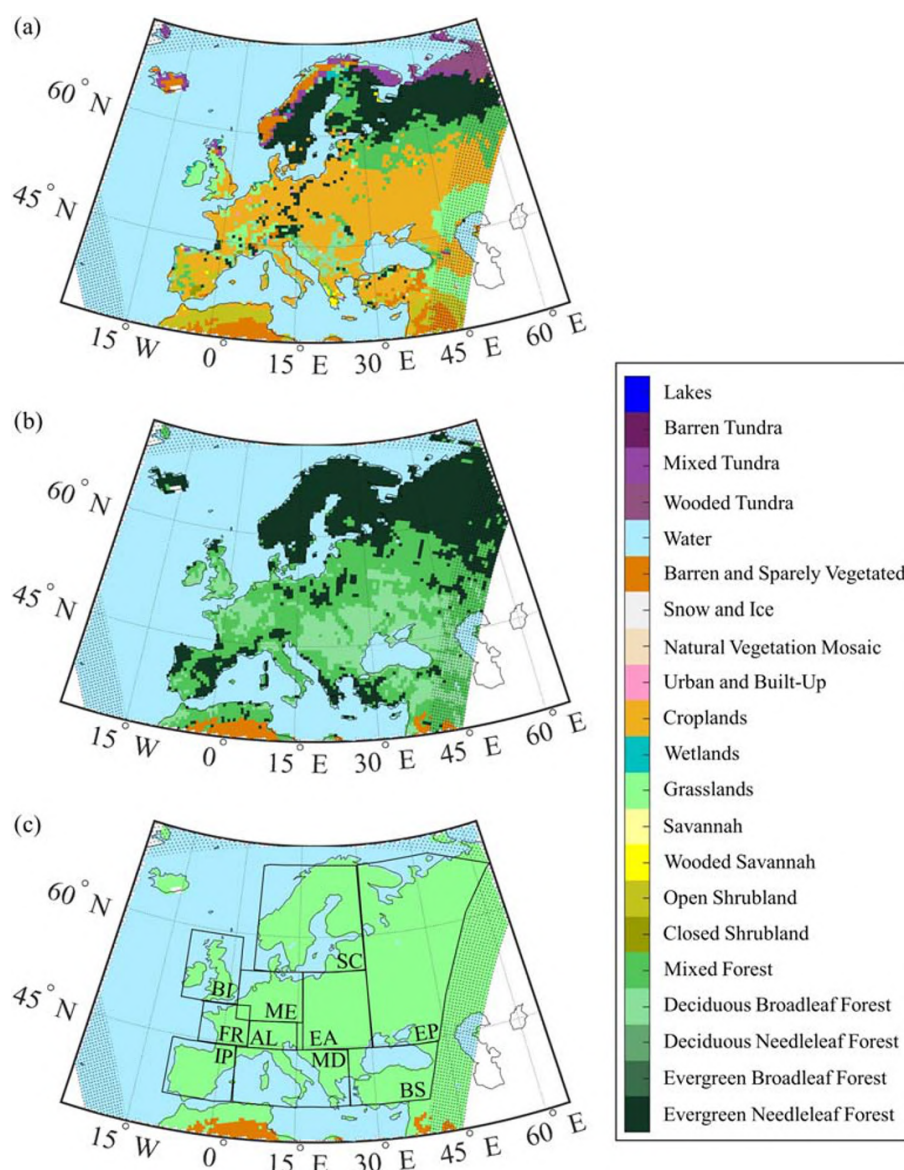


Figure 1. Land use maps of (a) the CORINE, (b) the FOREST, and (c) the GRASS experiments in the EURO-CORDEX EUR-44 domain derived from IGBP-MODIS 21-category land use type classification used in the WRF model. Subplot (c) also contains the boundaries of the expanded PRUDENCE-regions: The Alps (AL), British Isles (BI), Black Sea (BS), Eastern Europe (EA), Eastern European Plain (EP), France (FR), Iberian Peninsula (IP), Mediterranean (MD), Mid-Europe (ME), and Scandinavia (SC).

2.3. Land Cover Scenarios

L-A feedbacks were investigated for three land covers: (1) a realistic real land cover as baseline (CORINE), (2) maximum forest coverage (FOREST), and (3) maximum grassland coverage (GRASS) in Europe. The CORINE 2006 land cover classification (European Environmental Agency, 2013) was implemented for the baseline run (Figure 1a). In the FOREST scenario, a land cover map was used where the total land area is covered by forest where it can realistically grow. This means areas with cold and hot deserts were not covered with vegetation, as it would be biologically implausible. Similarly, all vegetation types were converted to grassland in the GRASS scenario (see Davin et al., 2020, for a detailed description of the maps).

The land cover maps for the FOREST and GRASS experiments were based on a global MODIS-based present-day land cover map at 0.5° resolution with 17 plant functional types (Lawrence & Chase, 2007). Shrub, crop, and grassland types were set to zero in order to produce the FOREST map. The sum of the remaining forest classes was designed to be 100% excluding nonvegetated areas. The proportion of the individual classes was conserved from the original map. Therefore, needleleaf forests mainly cover the high-latitudes and broadleaf forests grow further to the South. The forest plant functional types were converted to C3 and C4 grassland to derive the grass map. Again, the proportion of each type was taken from the original map. The fraction of bare soil was conserved in both experiments (Davin et al., 2020).

The implementation of the derived maps in WRF-NoahMP required a transfer of the plant functional types to the IGBP-MODIS 21-category land use type classification. Plant functional types that are only differing in the climate as well as C3 and C4 grasses were merged. The IGBP-MODIS classification neither represents climates (tropical or temperate forests) nor diverse grassland types (C3 or C4 grasses). In the forest map, cells were classified as Mixed Forests when they had a similar share of different forest types. Finally, cells classified as Ice and Snow in the CORINE 2006 land cover classification were used to mask both the forest and the grass map (Figures 1b and 1c). In the following, afforestation denotes the comparison FOREST-CORINE and deforestation the comparison GRASS-CORINE.

2.4. Land-Atmosphere Coupling Metrics

2.4.1. CTP- HI_{low} Framework

In the past decade, different studies suggested that among other things, the atmospheric conditions in the early morning influence whether the land surface may impact convection triggering throughout the day. While some atmospheric conditions favor convection initiation by increasing the atmospheric moisture (positive feedbacks) (Guillod et al., 2015; Koster et al., 2004), others favor convection initiation by increasing the boundary layer growth through high sensible heat fluxes (negative feedbacks) (Dirmeyer et al., 2014; Taylor et al., 2012). Different regions exhibit a different dominant feedback sign in dependence of the prevailing atmospheric conditions (Findell et al., 2011). The convective triggering potential (CTP)-low-level humidity index (HI_{low}) framework (Findell & Eltahir, 2003a, 2003b) evaluates the potential for the triggering of deep convection in dependence of land surface forcing. It uses the stability and the humidity deficit of the residual layer around the hour of sunrise for this (Dione et al., 2014). It is composed of two atmospheric properties. The CTP is the departure of the modeled temperature profile from the moist adiabatic lapse rate between 100 and 300 hPa above ground. The HI_{low} is the sum of dew-point depressions at 50 and 150 hPa above ground. The variables are fully defined in the Appendix. Further details on data processing are given there, too.

At first, CTP and HI_{low} are used to assess the type of early-morning profile within the CTP- HI_{low} space on each day for every cell (Figure 2a). The threshold values from Findell and Eltahir (2003a) are used to distinguish between days with a wet soil advantage favoring positive feedbacks (1), days with a dry soil advantage favoring negative feedbacks (2), days in a transition zone (3), and atmospherically controlled (AC) days (4). On days with AC conditions, an influence of the surface fluxes on convective precipitation is unlikely. Days are considered AC in three cases. Negative CTP values indicate a temperature inversion in the early-morning atmosphere, which inhibits deep convection. When the humidity deficit is very high ($HI_{low} > 15^{\circ}\text{C}$), precipitation is generally unlikely, and when the humidity deficit is very low ($HI_{low} < 5^{\circ}\text{C}$), precipitation is likely over any surface (Findell & Eltahir, 2003b). Days in the feedback categories (categories 1–3) are jointly referred to as nonatmospherically controlled (nAC) days. The quantity gives an idea of how frequently the land surface may impact convection triggering. The distinction of the different feedback categories enables the assessment of the predominant feedback sign. An atmosphere with a humidity deficit between 5°C and 10°C and unstable conditions ($CTP > 0 \text{ J/kg}$) is associated with a wet soil advantage (Figure 2a). Dryer conditions in the atmosphere ($10^{\circ}\text{C} < HI_{low} < 15^{\circ}\text{C}$) and high instability ($CTP > 200 \text{ J/kg}$) suggest a dry soil advantage (Figure 2a). In the transition zone (Figure 2a), wet or dry soils can both be advantageous. These days are characterized by lower humidity conditions ($10^{\circ}\text{C} < HI_{low} < 15^{\circ}\text{C}$) and low instability ($50 \text{ J/kg} < CTP < 200 \text{ J/kg}$).

In a second step, the relative occurrence of each type of sounding is quantified to evaluate the potential for land surface effects on convection triggering. When a high potential is apparent, the dominant feedback sign is determined for the chosen period (Figure 2b). Each land grid point is classified either as AC, wet

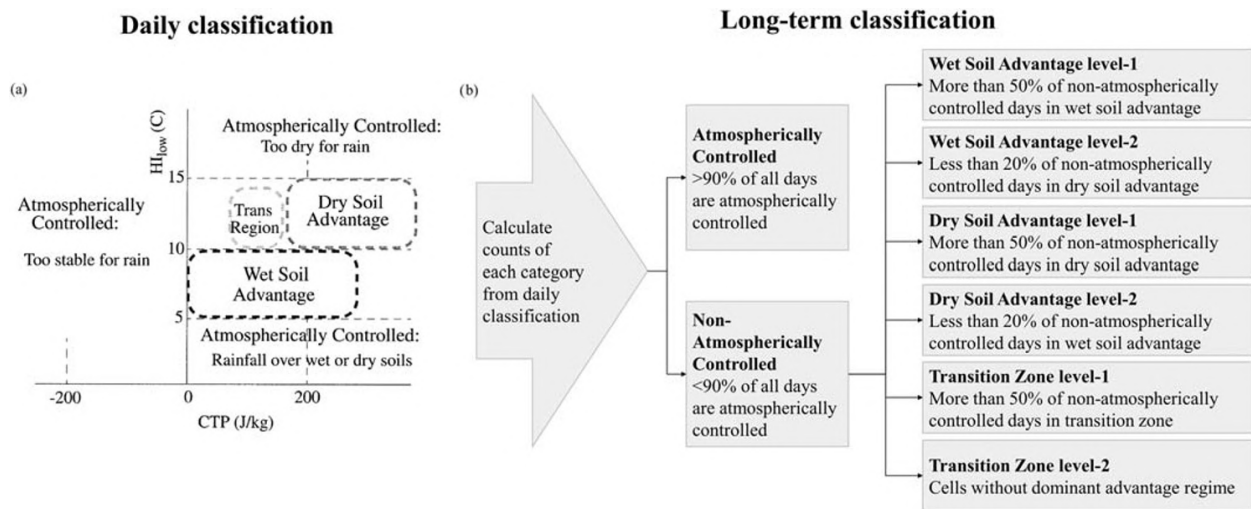


Figure 2. (a) Schematic of the CTP- HI_{low} framework adapted from Findell and Eltahir (2003a) their Figure 15 showing the respective profile types in CTP- HI_{low} space. (b) The long-term classification of a cell is based on the relative frequency of occurrence of each class from (a) in a cell. The schematic displays the descriptions of long-term labeling explained in Findell and Eltahir (2003b).

soil advantage, dry soil advantage, or transition zone with their respective subdivisions (Figure 2b). Furthermore, subcategories of AC are included which indicate the major reason for classifying a cell as AC. AC dry, for example, denotes that HI_{low} is larger than 15°C in the majority of days. Levels 1 and 2 denote the strength of the signal within the feedback categories. The labeling as wet soil advantage level 1 signifies a strong positive signal. This label requires that at least 50% of the nAC days are in wet soil advantage. The same applies for the labeling as transition zone level 1 or dry soil advantage level 1. A cell labeled with level 2 has likely a weaker signal. The labeling as wet soil advantage level 2 requires that less than 20% of the nAC days are in dry soil advantage. For the label dry soil advantage level 2, less than 20% of a cell's nAC days are in wet soil advantage. The label transition zone level 2 includes all remaining cells.

The threshold for determining whether a cell is AC or nAC was lowered from originally 20% to 10% (Figure 2b). A review of the frequency of large-scale weather patterns associated with high potential for convective precipitation events in Europe showed that these occur in about 10% of the summer days (Dittmann & Deutscher Wetterdienst, 1995; Lang, 2010). Local convective precipitation events in summer may cause severe damages and floods also in Central Europe. Therefore, it is of social and economic interest to represent potential feedbacks that could impact these events. Testing threshold values between 5% and 30% showed that the choice of the value only affected the size of the region considered as feedback region. The fraction of nAC days and the prevailing advantage for wet/dry soils within a cell was not affected (not shown).

2.4.2. Statistics on Land-Atmosphere Feedbacks

Statistical analyses were used to explore the relationship between EF, clouds, and total precipitation with diverging land cover. Due to the model grid increment (0.44°), the model data did not permit a reasonable distinction of convective and synoptic clouds and precipitation. The link between EF [latent heat flux/ (sensible + latent heat flux)] and total precipitation, as well as HI_{low} and total precipitation were further explored on the basis of statistical analyses. Daily mean EF, daily early-morning HI_{low} , and daily total precipitation were used for these analyses. Please note that LULCCs are expected also to affect the relationship between soil moisture and EF. This relationship and the influence of EF on precipitation would need to be disentangled. Therefore, EF was used to represent the land surface rather than soil moisture. The cloud statistics in section 4.1 are based on 3-hourly cloud fractions. The significance of differences between the experiments was tested using a Student's t test applying a significance level of 5%.

The dependence of precipitation on either EF or HI_{low} was examined by calculating a regression coefficient and multiplying it by the standard deviation of the respective variable. Combining the regression coefficient as a sensitivity measure with the standard deviation as a variability measure follows the reasoning of the

two-legged metric by Dirmeyer (2011). The coefficients of determination of the regressions were investigated to estimate the share of the variance in precipitation that can be explained by EF or HI_{low} dynamics, respectively.

The probability for precipitation (precipitation > 1 mm) was compared for AC and nAC days. The probability for precipitation was calculated for each bin by first fitting a probability density function for a Gamma distribution. Second, the area under the function was integrated to approximate the probability of precipitation. As the chosen interval size equals 1, the probability density is an approximation for the probability for the chosen interval. Furthermore, the probability for precipitation was analyzed for different ranges of EF. For this purpose, the summer days were subdivided in four equal bins according to their prevailing EF: (1) EF between 0 and 0.25, (2) EF between 0.25 and 0.5, (3) EF between 0.5 and 0.75, and (4) EF between 0.75 and 1 before calculating the probability. The control group contains the total range of EF.

3. Land-Atmosphere Coupling Strength Analysis

3.1. Coupling Hot Spots

The CTP- HI_{low} framework was used to identify potential hot spots for surface moisture-precipitation feedbacks and to determine their dominant sign in Europe. The highest potential for a surface impact on deep convection triggering was found in the northeast of the study area (Figure 3, areas in green or orange), where continental climate prevails (Peel et al., 2007). Typically, continental climate is characterized by pronounced variability in weather patterns because of the missing dampening effect of oceans (Bonan, 2016). Figure 4 displays the components of the CTP- HI_{low} framework. Atmospheric conditions were frequently weakly unstable and intermediately humid (Figures 4a and 4d) in the Northeast. This led to a potential nAC in up to 42.2% (CORINE, Figure 4g) of the summer days over the Eastern European Plain (FOREST: 37.2% and GRASS: 37.8%; not shown).

Feedbacks were predominantly positive in the strong coupling region in each experiment. The share of wet soil advantage days in summer was particularly high in the high-latitudes and decreased southward (Figure S2 in the supporting information). The shares of transition zone and dry soil advantage days both increased toward the south, which was due to a higher humidity deficit and, in case of the dry soil advantage days, higher instability in the residual layer. Dry soil advantage days represented the lowest share all over the domain. The north-south gradient in the frequency distribution of the feedback categories appeared independently of the land cover (Figures S1 and S2).

In southern Europe and at the Atlantic coast, the summer days were almost entirely AC (Figures 3 and 4g) in all experiments. Over the British Isles and at the Scandinavian coast, most early-morning soundings were stable (CTP < 0 J kg⁻¹) and rather humid (HI_{low} < 5°C) (Figures 4a and 4d). This indicated that convection was regularly inhibited by a stable layer, and the surface fluxes hardly initiated any precipitation event (Findell & Eltahir, 2003a; van den Hurk & van Meijgaard, 2010). Summers were typically dry in southern and southwestern Europe, because the subtropical high extends to up to 40°N. Therefore, the probability for precipitation was low, and along with that, the humidity deficit was on average too large to permit a land surface impact on precipitation (Figure 4d). In other words, the moisture flux into the atmosphere was too small to produce clouds and develop precipitation locally. Findell and Eltahir (2003b) applied similar reasoning within their explanations of atmospheric controls in the United States. Similar to the European high latitudes, soundings at the northwestern US Pacific coast were almost entirely stable and humid, while soundings at the southwestern Pacific coast were very dry. The reasoning for atmospheric controls was valid in all experiments, and the location of potentially strong feedbacks appeared rather insensitive to LULCC (Figure 3). The robustness of the location was further tested by perturbing the initial temperature and moisture profiles before classifying the feedback regions (see supporting information). A shift to a completely different region only occurred with extreme and unrealistic moisture increases combined with considerable decreases in temperature (Figure S4).

3.2. Land Surface Impact on Coupling Strength

Although the location of the potential coupling hot spot appeared to be robust, modifications of the surface flux partitioning could influence the local L-A coupling strength (Figures 4h and 4i) and the predominance of the feedback sign.

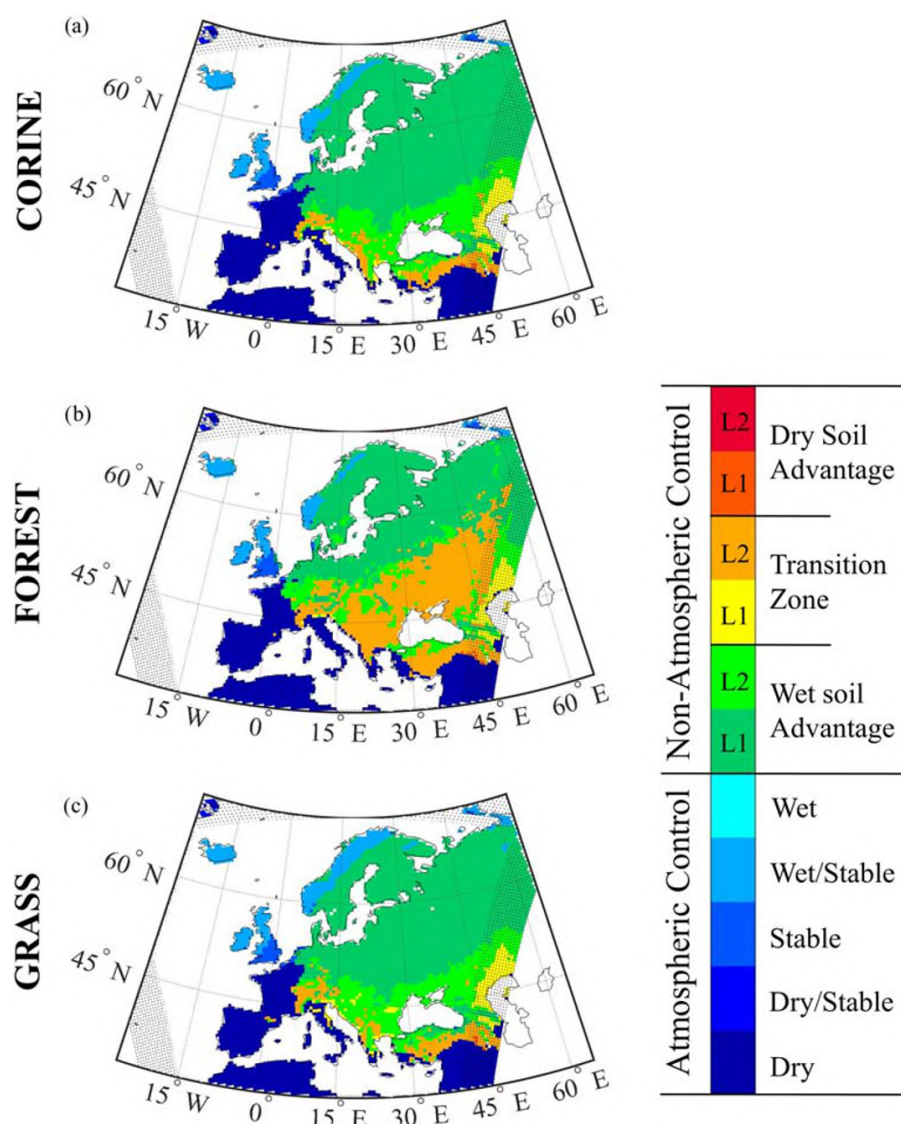


Figure 3. Long-term feedback regimes classified after the CTP-Hilow framework for (a) the CORINE run, (b) the FOREST scenario, and (c) the GRASS scenario. Atmospheric control is indicated in blue and the shadings depict the probable cause for atmospheric control. The nonatmospherically controlled feedback regime wet soil advantage is represented in green, the transition zone in yellow/orange, and the dry soil advantage in red. Levels 1 (L1) and 2 (L2) depict the strength of the signal. Level 1 cells have a strong signal, whereas the signal in level 2 cells is weaker.

In this RCM configuration, afforestation caused a decrease in EF (Figure 5b) everywhere except for western Europe and south of the Black Sea. An albedo decrease led to an increase in available energy, which was predominantly partitioned into sensible heat flux. The resulting significant destabilization and drying of the atmosphere at a significance level of 5% (Figures 4b and 4e) decreased the nAC days per summer. Thus, the feedback strength declined. The strongest impact of afforestation on the atmosphere appeared north of the Black Sea, where increases in CTP and HI_{low} caused a significant loss of nAC days of up to 9.75%. The contrary effect was observed in western Europe, where EF increased by 0.03 and HI_{low} decreased by -0.35°C . In consequence of these changes in western Europe, the fraction of nAC days increased significantly by up to 6.5% in some cells over the Alps.

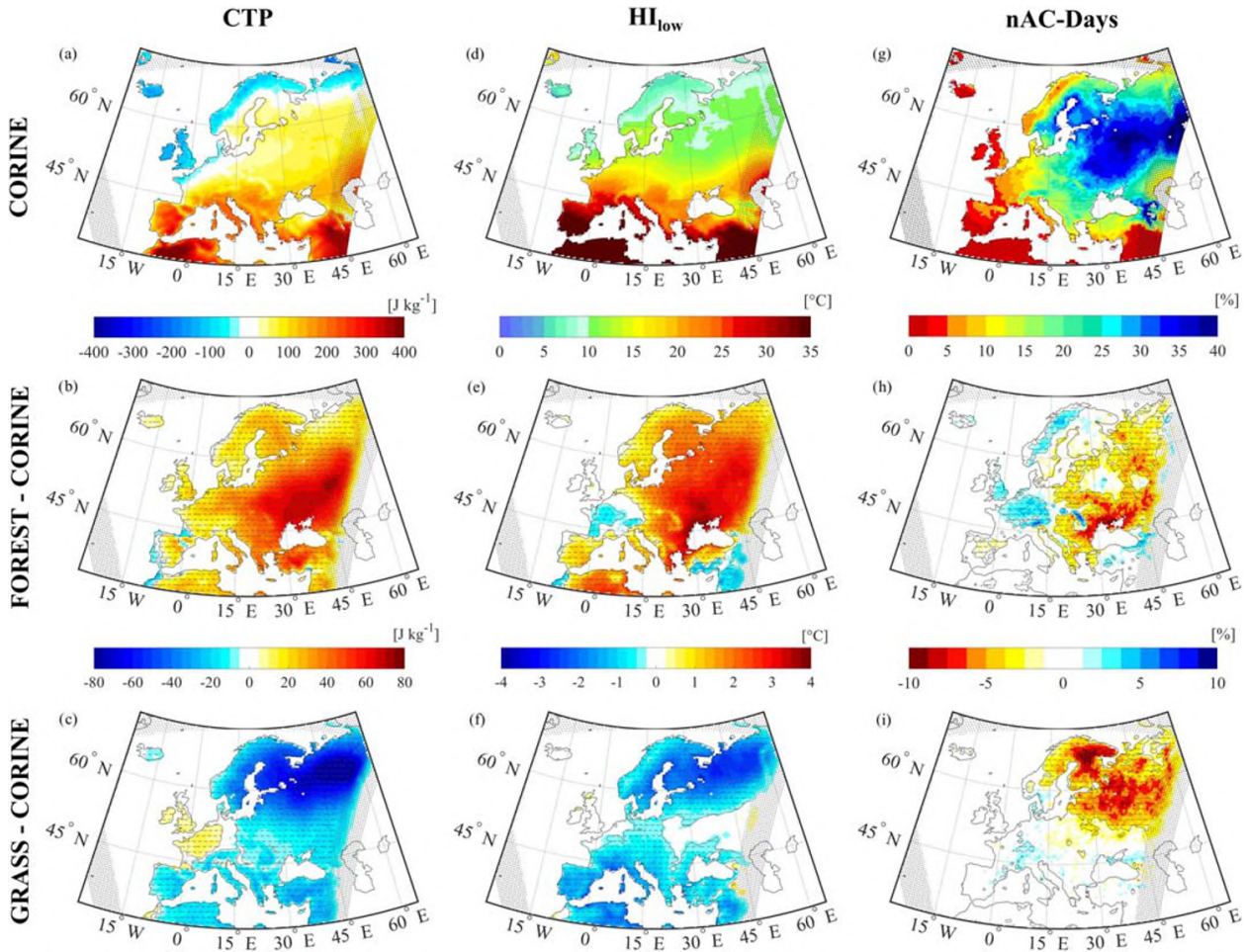


Figure 4. (a) Mean convective triggering potential (CTP) (J kg^{-1}) of the CORINE run, (b) the FOREST-CORINE difference in CTP, and (c) the GRASS-CORINE difference. (d) Mean summertime low-level humidity index (HI_{low}) ($^{\circ}\text{C}$) of the CORINE run, (e) FOREST-CORINE difference in the HI_{low} , and (f) the GRASS-CORINE difference in HI_{low} . (g) The share of nonatmospherically controlled (nAC) days in summer (%), and (h and i) the corresponding differences between FOREST and CORINE and GRASS and CORINE, respectively. Dashed areas indicate statistical significance at the 5% level tested with a Student's t test.

In the FOREST run, the northern part of the feedback region was in wet soil advantage similarly to the baseline run. In the southeastern part of the feedback region, a transition occurred from wet soil advantage to transition zone level 2 (Figure 3b). Afforestation decreased the share of wet soil advantage days both relative to the nAC days in summer (Figure S1b) and relative to all summer days (Figure S2b) in most of the domain. The largest decrease appeared in eastern Europe. Simultaneously, afforestation increased the share of nAC days in transition zone and dry soil advantage (Figures S1e and S1h) leading to a weakening in the predominance of positive feedbacks and a change in the classification. Therefore, afforestation decreased not just the frequency of occurrence of nAC days (Figure 4h) in eastern Europe but also weakened the potential for positive feedbacks all over the domain. The combined effect is expected to result in a lower impact of the latent heat flux on local precipitation in comparison with the conditions of the baseline run.

The major impacts of deforestation on the summer L-A coupling strength occurred in the higher latitudes (Figures 4i, S2c, S2f, and S2i). The higher albedo of grassland generally initiated a decrease in net radiation (not shown) in Europe. In the high latitudes, the conversion of needleleaf forest to grassland caused a considerable increase in EF in GRASS (Figure 5c). This resulted from minor reductions in the latent heat

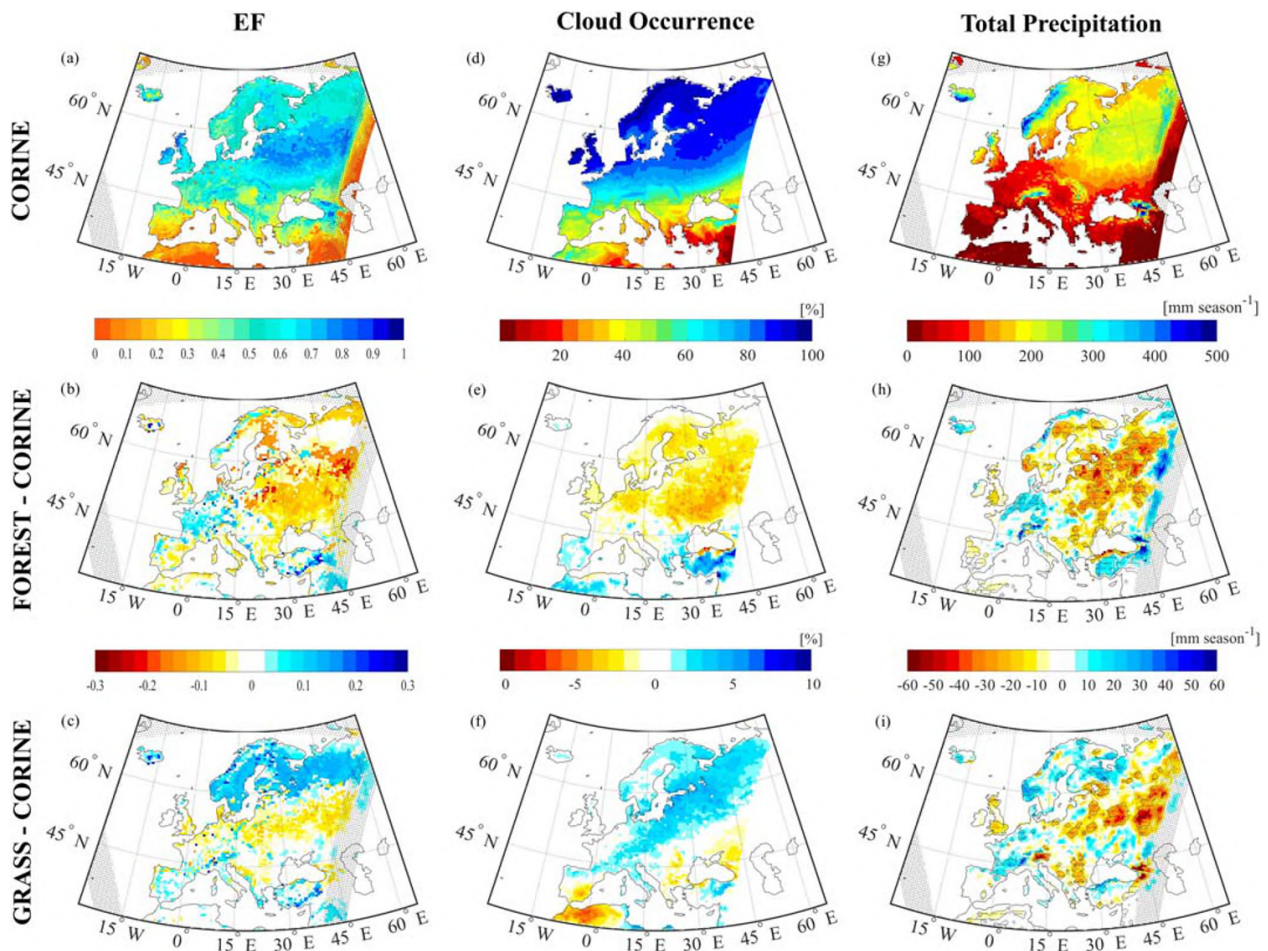


Figure 5. Results from CORINE and their differences due to afforestation (FOREST-CORINE) and deforestation (GRASS-CORINE) in summer. (a) Average evaporative fraction (EF), (b) difference in EF due to afforestation, (c) difference in EF due to deforestation, (d) frequency of occurrence of cloud coverage >3%, (e) difference in the occurrence of clouds due to afforestation, (f) difference in the occurrence of clouds due to deforestation, (g) mean seasonally accumulated total precipitation, (h) difference of precipitation due to afforestation, and (i) difference of precipitation due to deforestation. All values correspond to the June–August average of the period 1986–2015.

flux and strong decreases in the sensible heat flux (not shown). The impacts of decreasing both the atmospheric instability and humidity deficit on the coupling were contradicting (Figure 4c and 4f). On the one hand, the cooling and moistening of the atmosphere indicates that relative humidity approaches saturation more frequently. Occasionally, up to 10% less summer days were in nAC compared to CORINE in the high-latitudes (Figure 4i), and wet AC days occurred more frequently. On the other hand, the predominance of the wet soil advantage was considerably strengthened in the nAC day partitioning (Figure S1c). Transition zone as well as dry soil advantage days occurred less frequently (Figures S1f and S1i). This means when a feedback was probable, wet surface conditions were very likely in favor for triggering precipitation rather than dry surface conditions. Consequently, the feedback region was mostly in levels 1 or 2 wet soil advantage in the GRASS run. In the rest of the domain, LULCC caused a net decrease in EF. This resulted from a reduction in the latent heat flux and minor reductions (cropland) or increases (mixed/deciduous forests) in the sensible heat flux. The changes in both the share of nAC days (average $\pm 0.3\%$) in summer (Figure 4i), and the share of summer days in wet or dry soil advantage or transition zone (Figures S2c, S2f, and S2i) were patchy and insignificant.

4. Effects on Clouds and Precipitation

Given the information about a potential coupling hot spot and a predominance of positive feedbacks, the question arises whether modifications in the surface flux partitioning from LULCC can be associated with changed cloud cover and total precipitation patterns in the predicted manner. Therefore, the aim of this chapter is to assess whether the sign of the response of cloud occurrence and precipitation distribution to afforestation and deforestation match the sign of EF differences.

4.1. Clouds

First, this chapter deals with modifications in the spatial distribution of cloud occurrence induced by LULCC. Second, differences in the frequency of occurrence of clouds in summer on different model heights are explored (Figure 5d). Coverage or occurrence of clouds was assumed, when the degree of coverage in an atmospheric layer exceeded 3% (threshold from Görsdorf & Seifert 2011).

In all experiments, clouds occurred most frequently in the high latitudes. The frequency (Figure 5d) and also the degree of coverage (not shown) decreased southward with the lowest frequencies south of the Black Sea. Besides the regional variance of cloud distribution, clouds also appeared in different altitudes depending on the region (Figure 6) in all experiments. In the high latitudes, lower-level clouds appeared with a higher frequency (Figures 6e and 6f) than in southern Europe (Figures 6i and 6j). Please note that by far most clouds appeared with a degree of coverage of 1 (meaning 100% of coverage) in most layers and in all subregions and experiments (Figures 6a and 6e; values of the CORINE run). In the highest model levels, cirrus clouds appeared with a maximum cloud coverage of 0.2.

Afforestation and deforestation had contrasting effects on clouds in Europe. While the atmospheric drying from afforestation (Figure 5e) coincided with fewer (Figure 5e) and less thick clouds (not shown), the atmospheric moistening from deforestation (Figure 5f) coincided with an increase in the frequency of cloud occurrence there (Figure 5f). The sign of the response to the respective LULCC scenario was consistent in the domain apart from southern Europe (Figures 5e and 5f). In the southern part of the domain, the response in cloud occurrence switched sign in both scenarios. Though the sign of differences was largely consistent, the magnitude of differences from both afforestation and deforestation varied, and the strongest effects from both LULCC scenarios appeared over the Eastern European Plain (Figures 5e and 5f).

Figure 6 shows the frequency distribution of cloud occurrence on model levels. The first row shows the frequency distribution of the whole domain, and the second row shows the results for the Eastern European Plain as an example for a relatively strong influence. The results for the Iberian Peninsula are shown as an example for a southern and rather dry region with weak potential surface influence. Similarly to the spatial averages, the changes in cloud coverage on different model levels were strongest over the Eastern European Plain relative to the rest of the domain (Figures 6g and 6h). Low-level clouds occurred less frequently in FOREST with a maximum loss of 6.5%. Midlevel clouds were slightly increased by 1.9%. Similarly, deforestation mostly impacted the occurrence of low-level clouds, which increased by +5% over the Eastern European Plain (Figure 6h). Both afforestation and deforestation barely influenced the occurrence of clouds over the Iberian Peninsula (Figures 5e and 5f). This is also reflected in the changes of cloud occurrence across different atmospheric heights (Figures 6k and 6l). In general, LULCC predominantly influenced the occurrence of low-level clouds in the whole domain.

4.2. Precipitation

This subsection examines the impacts of LULCC on total precipitation and precipitation probability. Further, it aims to estimate the connections of both EF and HI_{low} changes with the magnitude of changes in precipitation and the probability for precipitation in dependence of the previously identified coupling regimes. The EF-precipitation and HI_{low} -precipitation connections were analyzed by applying an extended regression analysis (denoted as “Coupling Index” in Figures 7a and 7b) and looking at the coefficient of determination of the regression. These were introduced in section 2.4.2.

4.2.1. Precipitation Distribution

All experiments showed a similar spatial distribution of total precipitation (Figure 5g; CORINE run exemplarily). Maxima in precipitation were mostly found in mountainous regions like the Alps, the Scandinavian Mountains, the Carpathians, and the Caucasus in all experiments.

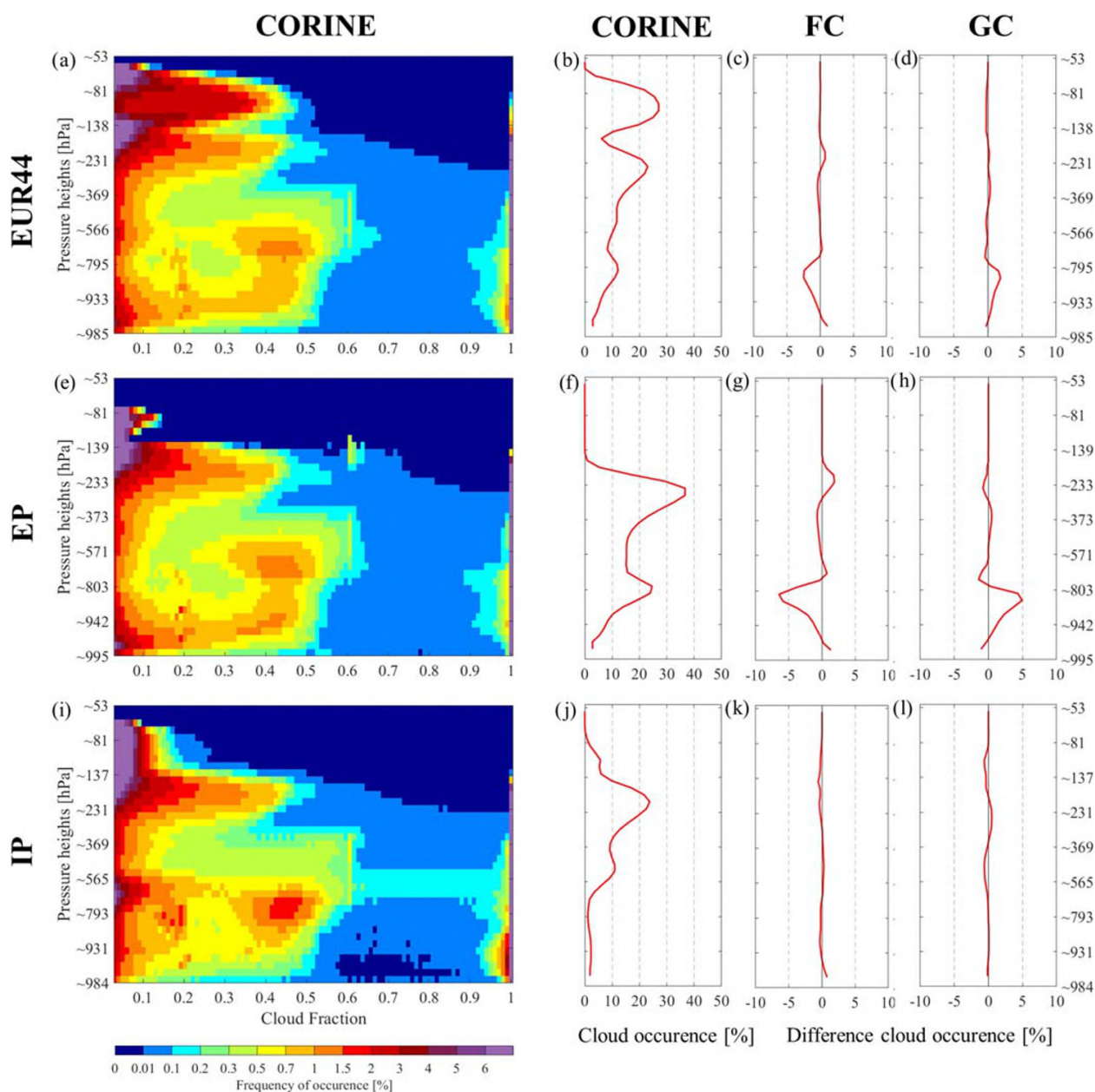


Figure 6. Cloud statistics (a) frequency distribution of different cloud fractions for each atmospheric layer (%) for the EURO-CORDEX domain (EUR44), taken into consideration are only cases with more than 3% cloud coverage, (b) the frequency of occurrence of clouds (degree of coverage >3%) regardless of the cloud fraction for EUR44, (c) the FOREST-CORINE (FC) difference in cloud occurrence on all model levels for EUR44, and (d) the respective difference for the difference GRASS-CORINE (GC) for EUR44. Similarly, (e–h) the results for the Eastern European Plain (EP) as an example for a rather wet region and (i–l) the results for the Iberian Peninsula (IP) as an example for a rather dry region.

Afforestation and deforestation initiated small but statistically significant differences in the total precipitation in summer. The impact on precipitation varied spatially in sign and magnitude (Figures 5h and 5i) in both scenarios. On the one hand, the LULCC impacted the day-to-day potential for local triggering of precipitation by modifying the flux partitioning (Figures 4h and 4i). On the other hand, an enhanced or

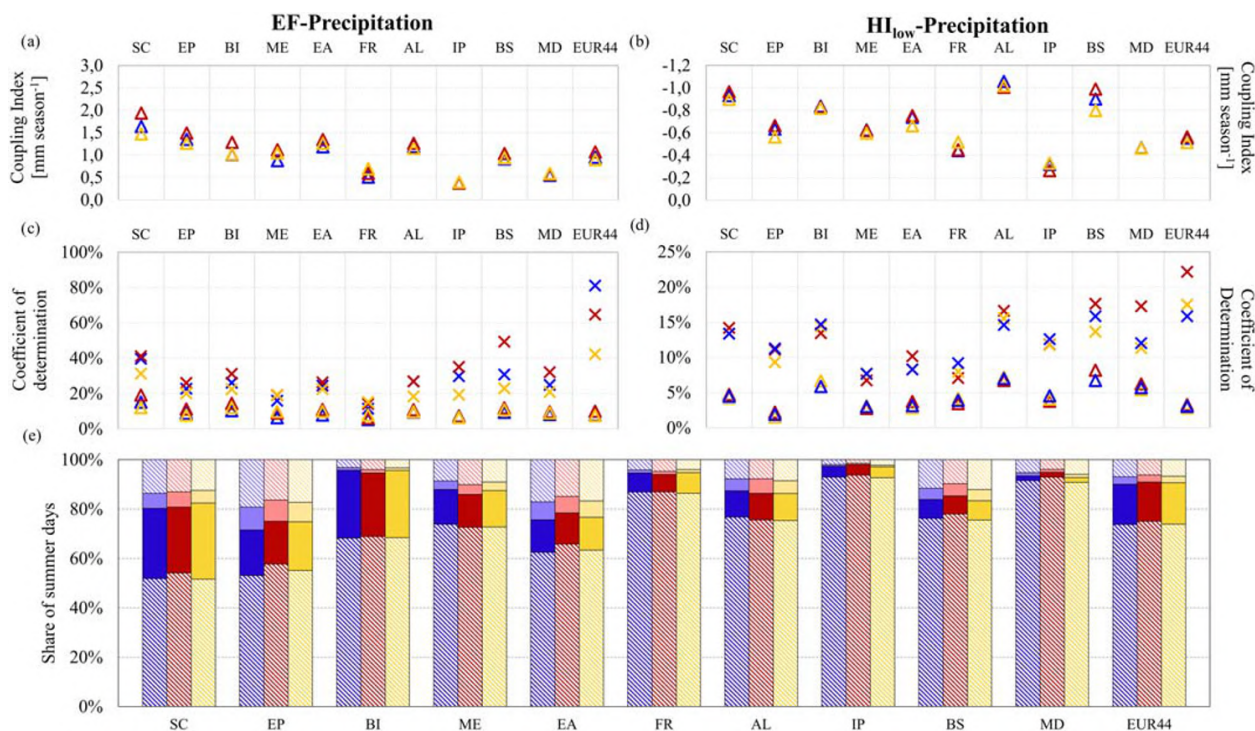


Figure 7. Subregion wise (a) coupling index between the evaporative fraction (EF) and daily total precipitation, (b) coupling index between the low-level humidity index (HI_{low}) and daily total precipitation, (c) coefficient of determination of regressions between EF and precipitation, and (d) coefficients of determination of regressions between HI_{low} and precipitation. Triangles denote regional means and crosses denote regional maxima. (e) Fractions of summer days in atmospheric control (dark colors), with and without precipitation and nonatmospheric control (nAC; light colors). Fractions of AC and nAC days without precipitation are striped. Colors are blue: CORINE, red: FOREST, and yellow: GRASS.

decreased transport of moisture and heat into the atmosphere modified the average atmospheric conditions (Figures 4b, 4c, 4e, and 4f). This modifies the probability for total precipitation and the preconditioning for convection triggering in the atmosphere. In eastern and northeastern Europe, both LULCC resulted in significant decreases in precipitation (significance level: 5%). With afforestation, lower EF and higher humidity deficits in the low-level atmosphere supported the reduction in precipitation (Figures 7a and 7b). The maximum decrease in precipitation occurred over the Eastern European Plain with -63.8 mm per season (Figure 5h). The local connections of precipitation with EF and HI_{low} are further explored in section 4.2.2. In GRASS, the transition from cropland to grassland resulted in a lower EF (Figure 5c), which coincided with less precipitation in this region.

In western Europe, both LULCCs initiated a small increase in precipitation (Figures 5h and 5i). The increase in FOREST may be related with an increase in the latent heat flux, raising the moisture transport into the atmosphere. The additional moisture increased the relative humidity (HI_{low}) and considerably increased CAPE (not shown). Both quantities are expected to favor the occurrence of precipitation in the model, especially, as the Kain-Fritsch convection scheme is known to react sensitively to CAPE. The effect of deforestation was not as straightforward. The local connection between surface moisture and precipitation was particularly weak in France and impacts on atmospheric quantities like CAPE were small.

In the remaining regions, the impact of afforestation on precipitation diverged from the impact of deforestation. Afforestation caused an increase in rainfall over the Alps ($+6.1$ mm/season) and the Black Sea ($+3.0$ mm/season), while deforestation caused a decrease over the Alps (-2.1 mm/season) and the Black Sea (-2.6 mm/season). Both regions have a complex orography which possibly shapes the connection between surface moisture and precipitation (see section 4.2.2). In the high latitudes, the local connection

of the surface moisture appeared to be strong in all scenarios (Figures 7a and 7b). Thus, the surface drying from afforestation was expected to support a decrease in precipitation, whereas the moistening from deforestation rather supported an increase (Figures 5c and 5i).

4.2.2. Surface Flux-Precipitation Connection

The strength of local connections of precipitation with EF and HI_{low} was varying regionally. Please note that local refers to the connection between variables in a certain cell, here. Modifications in surface moisture and low-level humidity are likely to affect also the precipitation of neighboring cells, but these nonlocal influences are difficult to disentangle and they were not quantified within this study.

The coupling index of EF and precipitation was positive in all subregions and experiments (Figure 7a). This confirmed the conclusion drawn from the CTP- HI_{low} framework, that surface moisture-precipitation feedbacks are generally more likely to be positive in the study area. A relatively strong connection between EF and precipitation emerged in the domain's Northeast as well as in regions with complex orography (Alps, Black Sea) in all experiments. In the rest of the domain, total precipitation was less correlated with EF (Figure 7a). The weakest coupling indices were found over southern Europe and France in each experiment (Figure 7a), which was characterized by rather dry conditions. Since the coupling index was low, differences in the precipitation of the different scenarios (Figures 5h and 5i) were not locally attributable to changes in the surface flux partitioning there. However, the modifications in the surface flux partitioning impacted the humidity deficit (Figures 4e and 4f), and hence, they changed the preconditioning for convection triggering and for precipitation development in general (Figure 7b) during the 30-year period.

Though the Black Sea region also faced comparably dry conditions (Figure 4d), the coupling index was considerably higher than in the rest of southern Europe. The presence of mountains was expected to support the vertical motion of air through orographic lifting. Since orography supported the lifting of moist air, more moist surface and low-level atmospheric conditions presumably foster the probability for local precipitation. This is reflected in the EF-precipitation and the HI_{low} -precipitation connections (Figure 7). Both the coupling indices and the coefficients of determination were high in relation to the rest of the domain. All of the maximum values (crosses in Figures 7c and 7d) were observed over mountains. This effect was also observable over the Alps and the Scandinavian mountains.

The share of variance in precipitation explainable by EF amounted to 7.8%, averaged over the domain (FOREST: 10.0% and GRASS: 7.5%) with strong variance between subregions (Figure 7c). While the lowest share of explained variance was found in Central Europe, the largest share was apparent in the high latitudes in all scenarios. In individual cells, up to 40% of the variance in precipitation is explainable by EF over needleleaf forest, there (Figure 7c). However, the pattern of the coefficient of determination did not follow the distribution of the share of nAC days (Figure 4g). Rather, it reflected features of the respective vegetation map. Especially over needleleaf forest, the fraction of explained variance was high, whereas over cropland it was clearly lower (data not shown). Afforestation generally tended to enhance the share of variance in precipitation explainable by the EF—everywhere except for the Alps. Deforestation initiated a mixed response in the EF-precipitation relationship (Figure 7c). On the one hand, in the high latitudes and over the Iberian Peninsula, the share of variance in precipitation explainable by EF decreased due to the conversion from needleleaf forest to grassland. On the other hand, in central and southeastern Europe, converting forests and croplands to grassland increased the variance explained by EF. These findings confirm the conclusion that LULCC has an impact on coupling strength itself. It also highlights the importance of considering the concrete type of vegetation transition.

4.2.3. Atmospherically Versus Nonatmospherically Controlled Days

This subsection describes the difference in precipitation probability between AC and nAC days for the subregions. Table 2 depicts the probability for precipitation on AC and nAC days, as well as the proportion of the total precipitation that fell on nAC days. Please note that precipitation on nAC days is not equated with convective precipitation which was triggered by the land surface.

Although the majority of summer days were AC in every grid cell and most precipitation fell on AC days in absolute terms in each subregion (Figure 7e), the probability for precipitation was clearly higher on nAC days than on AC days. This applied for every subregion except for Scandinavia and the British Isles in all experiments (Table 2). In southern Europe, where precipitation occurrence was rare, the probability for precipitation was considerably higher on nAC days than on AC days (Table 2). In the Mediterranean, the share

Table 2
Average Evaporative Fraction (EF) and Probability for Precipitation for Atmospherically Controlled (AC) and Nonatmospherically Controlled (nAC) Days in Each PRUDENCE-Region and the Percentage of Total Precipitation Actually Falling on nAC Days, for Each Scenario

	CORINE						FOREST						GRASS					
	AC		nAC		Share of P on nAC days		AC		nAC		Share of P on nAC days		AC		nAC		Share of P on nAC days	
	EF	Probability for P ^a	EF	Probability for P ^a	EF	Probability for P ^a	EF	Probability for P ^a	EF	Probability for P ^a	EF	Probability for P ^a	EF	Probability for P ^a	EF	Probability for P ^a	EF	Probability for P ^a
SC	0.58	0.46 (0.26; 0.77)	0.57	0.41 (0.22; 0.67)	19.7%	0.55	0.42 (0.19; 0.84)	0.53	0.41 (0.13; 0.80)	21.6%	0.65	0.47 (0.41; 0.74)	0.64	0.39 (0.27; 0.63)	14.9%			
EP	0.60	0.34 (0.06; 0.59)	0.65	0.40 (0.09; 0.55)	34.9%	0.54	0.30 (0.06; 0.66)	0.60	0.41 (0.10; 0.69)	34.7%	0.65	0.34 (0.07; 0.59)	0.67	0.39 (0.08; 0.55)	30.2%			
BI	0.67	0.36 (0.14; 0.65)	0.62	0.35 (0.11; 0.63)	4.9%	0.63	0.34 (0.24; 0.74)	0.59	0.35 (0.08; 0.77)	6.4%	0.65	0.36 (0.14; 0.69)	0.60	0.33 (0.05; 0.68)	4.6%			
ME	0.55	0.17 (0.05; 0.37)	0.58	0.29 (0.12; 0.48)	23.3%	0.58	0.17 (0.03; 0.49)	0.60	0.33 (0.09; 0.67)	25.8%	0.54	0.18 (0.05; 0.55)	0.57	0.31 (0.07; 0.64)	22.6%			
EA	0.53	0.19 (0.04; 0.44)	0.60	0.33 (0.10; 0.51)	36.3%	0.48	0.19 (0.03; 0.57)	0.57	0.35 (0.09; 0.68)	34.9%	0.51	0.20 (0.03; 0.54)	0.56	0.32 (0.07; 0.60)	33.6%			
FR	0.47	0.10 (0.03; 0.33)	0.52	0.30 (0.09; 0.62)	21.8%	0.51	0.09 (0.02; 0.39)	0.56	0.26 (0.11; 0.60)	24.3%	0.46	0.10 (0.03; 0.48)	0.51	0.30 (0.05; 0.72)	20.8%			
AL	0.47	0.15 (0.03; 0.48)	0.55	0.47 (0.11; 0.80)	33.1%	0.49	0.16 (0.02; 0.55)	0.60	0.51 (0.13; 0.83)	37.0%	0.50	0.16 (0.02; 0.56)	0.60	0.45 (0.06; 0.77)	33.7%			
IP	0.27	0.05 (0.01; 0.43)	0.43	0.34 (0.07; 0.81)	19.5%	0.25	0.05 (0.01; 0.52)	0.38	0.34 (0.05; 0.91)	17.8%	0.28	0.05 (0.01; 0.49)	0.43	0.31 (0.09; 0.78)	20.2%			
BS	0.33	0.10 (0.02; 0.58)	0.47	0.35 (0.12; 0.74)	34.7%	0.35	0.09 (0.01; 0.67)	0.50	0.42 (0.10; 0.87)	36.2%	0.36	0.10 (0.01; 0.67)	0.47	0.34 (0.07; 0.82)	33.4%			
MD	0.27	0.06 (0.01; 0.51)	0.46	0.35 (0.10; 0.77)	41.4%	0.25	0.06 (0.01; 0.61)	0.46	0.39 (0.11; 0.82)	38.4%	0.28	0.05 (0.01; 0.62)	0.43	0.32 (0.06; 0.82)	40.8%			
EUR44	0.29	0.17 (0.01; 0.58)	0.59	0.38 (0.10; 0.57)	28.1%	0.28	0.16 (0.01; 0.67)	0.56	0.40 (0.09; 0.71)	28.6%	0.31	0.18 (0.01; 0.62)	0.60	0.36 (0.07; 0.59)	24.0%			

Note. SC = Scandinavia, EP = Eastern European Plain, BI = British Isles, ME = Mid-Europe, EA = Eastern Europe, FR = France, AL = Alps, IP = Iberian Peninsula, BS = Black Sea, MD = Mediterranean, and EUR44 = EURO-CORDEX domain.
^aThe probability for precipitation (fraction ranging from 0 to 1) is given for all days, and the values in brackets denote the probability on days only with low (0–0.25) and high (0.75–1) values of EF.

of total summer precipitation falling on nAC days corresponded to about 40% in all experiments, even though the occurrence of nAC days was rare in summer. However, the total amount of precipitation was low and so was the net effect of the surface on precipitation. In central and eastern Europe, nAC days had a higher probability for precipitation than AC days, as well, but the differences between AC and nAC days were smaller than in the dry-regions. Between 20% and 33% of the total precipitation per season fell on nAC days (Table 2).

In Scandinavia and over the British Isles, the probability for precipitation was generally high and did not differ considerably between AC and nAC days. Over these two regions, the majority of AC days were wet and stable, and more than 80% or 95%, respectively, of their total precipitation amounts occurred on AC days in all experiments (Figure 7e). A very high relative humidity (low HI_{low}) fostered precipitation on the wet AC days and explained why the probability is similar on AC and the wet soil advantage dominated nAC days. Presumably, the surface flux partitioning was not decisive for the triggering of precipitation on these days. However, investigating the probability for precipitation for different EF bins showed a divergence in the probability of precipitation for different ranges of EF on both AC and nAC days (not shown). The same applied for the daily amount of precipitation. Both increased gradually from very low (probability: 0.01–0.26) to very high EF values (probability: 0.37–0.75) throughout the domain. This did not apply for Scandinavia and the British Isles. In these regions, the probability for precipitation and the amount of rainfall were both higher with a clearly dominating sensible heat flux ($EF < 0.25$) than with a slightly dominating to equal share of sensible heat ($0.25 < EF < 0.5$). This indicated that the surface flux partitioning could still support or inhibit precipitation from large-scale systems, even though they are not decisive for its occurrence.

5. Discussion

Strong, positive, local surface moisture-precipitation feedbacks were identified under continental climate in northeastern Europe by using the CTP- HI_{low} framework in all experiments (section 3.1). Under oceanic, Mediterranean or arctic climate, large-scale atmospheric forcings predominantly inhibit local feedbacks—in accordance with the argumentation of Findell and Eltahir (2003b). The region of potentially strong coupling roughly coincided with the hot spot region of soil moisture-precipitation coupling that Koster et al. (2004) found in their global L-A coupling strength ensemble study in Europe. The robustness of the feedback region's location and the predominant sign of potential feedbacks were further examined with a sensitivity test (description in supporting information). In the summer of 1986, the initial temperature and moisture profiles of the baseline run were perturbed before calculating CTP and HI_{low} and performing the classification. The degrees of temperature and moisture perturbation were chosen to mimic a realistic model spread in moisture and temperature variance for the current climate in Europe. Extreme modifications were tested, as well. Perturbations within the realistic range slightly shifted the coupling hot spot, though it was not moved to a different European region (Figures S3 and S5). Therefore, the location of the coupling hot spot and also the predominance of positive feedbacks are considered robust under current climatic conditions.

The L-A coupling strength is generally a rather model specific quantity (Pitman et al., 2009), whose results may be influenced by the choice of PBL and convection parameterization (Hirsch et al., 2015; Milovac et al., 2016). In section 3.2, it was shown that both LULCC scenarios modified the potential feedback strength by changing the relative humidity and the instability in the early-morning boundary layer. In the presented model configuration, the frequency of potential nAC days decreased in both scenarios. Thus, the probability for a surface influence on precipitation is estimated to decrease from both afforestation and deforestation. Furthermore, the LULCC changed nAC day partitioning between the feedback categories (Figures S1 and S2). Afforestation decreased EF as a result of a dominant albedo effect, and a disproportionately strong increase in the sensible heat flux in most European regions. This finally led to a weakened wet soil advantage in the domain (Figure S1). In GRASS, most transitions to grassland caused a net decrease in the EF. The only exception was the transition from evergreen needleleaf forest to grassland, which mostly occurs in the high latitudes. It caused a loss in available energy as well as an increase in EF which originated from a stronger decrease in the sensible heat flux than in the latent heat flux. The transition from needleleaf forest to grassland also caused the largest impact on the coupling strength due to deforestation in the high

latitudes. On the one hand, feedback days occurred less frequently in summer. On the other hand, it strengthened the predominance of the wet soil advantage on nAC days (Figure S1c). The LULCC responses in surface flux partitioning mostly coincided with the findings of Duveiller, Forzieri, et al. (2018) who examined the effects of a suite of vegetation transitions on the radiation and energy balances at the land surface.

Nevertheless, Davin et al. (2020) demonstrated a divergence in the temperature response to afforestation between the models of the LUCAS ensemble, in which these simulations were included (their WRFb-NoahMP). They showed that the temperature response is directly linked to how afforestation modified the surface flux partitioning in the models. They attributed this inconsistency to a lack of agreement in the calculation of evapotranspiration between models (de Noblet-Ducoudré et al., 2012; Lejeune et al., 2017). Simulations with, for example, the RCA model rather simulated an increase in EF and a concurrent decrease in temperature in response to afforestation in Europe, caused by a net evaporative cooling effect (e.g., Belušić et al., 2019; Davin et al., 2020; Strandberg & Kjellström, 2019). The disagreement in the temperature response to afforestation has implications for the conclusions drawn on the LULCC effects on the coupling strength. The sensitivity test showed that the average temperature and moisture conditions impacted the coupling strength (Figures S5 and S6) and the occurrence of the feedback categories (Figures S3 and S4). While warming and drying enhanced the number of days in dry AC and transition zone (Figure S3i), cooling and moistening enhanced the wet and stable AC (Figure S3a). Hence, the temperature response of a model to LULCC (and likely also the moisture response) is expected to determine how these LULCC modify the coupling. Therefore, the conclusions drawn on the afforestation and deforestation effects on the coupling strength are specific for this model configuration. Further analysis would benefit from the use of an ensemble.

Both LULCC scenarios yielded differences in cloud occurrence and precipitation. The predominating decrease in EF from afforestation was accompanied by a significant decrease in relative humidity in the lower PBL and a concurrent reduction in low-level cloud occurrence and cloud coverage in northeastern and central Europe (section 4.1). Concomitantly, the total precipitation was significantly lower in confined areas within the hot spot region and over mountains (section 4.2.1). In western Europe, afforestation considerably increased relative humidity and CAPE what could be an explanation for the additional precipitation in this region. Although the low-level relative humidity and the occurrence of low-level clouds were significantly increased in the Northeast in GRASS, the total precipitation was lower compared to the baseline run in that area. One possible explanation could be that less CAPE is available for convection triggering over grassland. The higher albedo of grassland reduces the amount of available energy for flux partitioning, wherefore less precipitation is triggered.

Over the study period, the surface fluxes could influence the probability and amount of total precipitation in three different ways. First, moisture and energy enter into the atmosphere throughout the day and either trigger deep convection by increasing the atmospheric humidity through the input of latent heat (e.g., Dirmeyer, 2011) or support PBL growth by adding sensible heat (Dirmeyer et al., 2014; Taylor et al., 2012) (section 4.2.1). Second, the surface fluxes impact the humidity and stability in the residual layer in the seasonal average of June–August in 1986–2015 (section 4.2.1). Hence, the preconditioning changes to more or less favorable conditions for convection and for precipitation in general. Nonlocal effects of the background climate are likely (Winckler et al., 2017), but further research is necessary to identify and quantify remote effects. Third, the surface fluxes may enhance or suppress precipitation from large-scale circulations on days with very humid atmospheric conditions, which mainly occur in Scandinavia and over the British Isles (section 4.2.3). Precipitation is known to dominantly occur there due to either large-scale circulations or cyclones (Belušić et al., 2019; Pfahl & Wernli, 2012) rather than due to local triggering of convection. However, the prevailing EF on a certain day still influences the occurrence and to a minor extent the intensity of precipitation in summer (not shown). It is notable that very low ($EF < 0.25$) values of EF were observed to favor the occurrence of precipitation and rather than intermediate ($0.25 < EF < 0.5$) ones in the wet regions.

Altogether, an increase in the EF coincides with an increase in precipitation, pointing toward reinforcing interactions between surface fluxes and precipitation in the whole study area. The strongest changes in precipitation were predominantly located over mountains and within the strong coupling area which was previously identified with the CTP-HI_{low} framework. Nevertheless, the change in EF distribution from both

LULCC scenarios was small and significant impacts on precipitation occurred only in confined areas. This finding coincides with previous LULCC studies targeting precipitation in Europe, who also found that extreme afforestation had only minor impacts on precipitation (e.g., Seneviratne et al., 2013).

6. Summary

In this study, we investigated the potential L-A coupling strength in connection with actually modeled feedbacks between the turbulent surface fluxes and both clouds and precipitation patterns for the European summer. The study aimed at identifying land surface-precipitation coupling hot spots in dependence on land cover. Further, the intention was to test whether the strongest impacts of LULCC on clouds and precipitation were observed in regions where strong coupling is to be expected. The results give a range of hypothetical maximum impacts of LULCC by comparing the outcome of an extreme afforestation and deforestation scenario with a realistic baseline. To the knowledge of the authors, this is the first study for Europe that addresses L-A coupling strength in terms of surface flux-precipitation feedbacks on the regional scale and in dependence of land cover.

A coupling hot spot was identified in the northeast of the simulation domain mostly covering the Eastern European Plain and parts of Scandinavia and Eastern Europe. Feedbacks were predicted to be predominantly positive in all experiments. The scenarios mainly diverge in the fraction of potential feedback days and, hence, the likelihood of convection initiation by the land surface. With this model configuration, complete afforestation reduced the likelihood of land surface contribution to the triggering of convection in the east of the domain and slightly enhanced it in the west. Conversely, deforestation caused a significant reduction in the likelihood for a land surface impact in the high latitudes. Modeled impacts of the LULCC on clouds and total precipitation confirmed a predominance of reinforcing interactions, and a decrease in EF tended to be accompanied by a decrease in low-level clouds and total precipitation in all European subregions. This is on one hand attributable to local impacts of the surface fluxes during the day and, on the other hand, also to modifications of the boundary layer conditions in the 30 year average.

The presented analyses serve as a test bed for future studies on the impacts of realistic LULCC on the climate, keeping the focus on the impacts of L-A feedbacks and their modifications to climate change. Since studies based on a single RCM have limited generalizability, a possible extension of this work is a multimodel ensemble analysis of the L-A coupling strength to improve the robustness of the obtained results. Besides impacts of PBL and convection parameterization (Chen et al., 2017; Hirsch et al., 2015; Milovac et al., 2016) on estimating the L-A coupling strength, further dependencies, for example, on increasing the model resolution, and, hence, also the resolution of the land surface, to convection-permitting scale, or dynamic vegetation development (Ingwersen et al., 2018), are conceivable. Davin et al. (2020) highlight the need to understand the discrepancies in modeling the evapotranspiration. This is a prerequisite to understanding how and why feedbacks are spatially and temporally variable and how clouds and precipitation are impacted by LULCC. Additional variables, which characterize the boundary layer structure, need to be included in the analysis in order to improve the understanding of different links between the land surface and precipitation. Further studies targeting the understanding of biogeophysical impacts of land cover changes on the climate will be conducted in the scope of LUCAS. The sensitivity of the feedback strength and the sign of feedbacks to differences in atmospheric temperature and moisture will be further explored in a comprehensive sensitivity study. These findings as well as findings from further studies within LUCAS have provided a springboard for future L-A feedback analyses in Europe and improved our understanding about implications of LULCC on the climate.

Appendix A: Definitions of CTP and HI_{low}

Convective Triggering Potential. The CTP ($J kg^{-1}$) is a measure of the atmospheric instability. It represents the deviation of the modeled temperature profile (T_{env}) from the moist adiabatic lapse rate between 100 and 300 hPa above ground (formula from Ferguson & Wood 2011).

$$CTP = \int_{z_{p_{sfc}-100}}^{z_{p_{sfc}-300}} g \left(\frac{T_{parcel} - T_{env}}{T_{env}} \right) dz,$$

with $z_{p_{sfc}-300}$ and $z_{p_{sfc}-100}$ representing the height at surface pressure $p_{sfc} - 300$ hPa and $p_{sfc} - 100$ hPa,

respectively. T_{parcel} represents the temperature of an air parcel, which is lifted along the moist adiabatic lapse rate originating from 100 hPa above the surface and g is the gravitational acceleration.

Low-Level Humidity Index. The HI_{low} (°C) measures the humidity deficit in low-level air. It corresponds to the sum of dew point depressions at 50 and 150 hPa above ground.

$$HI_{low} = (T_{sfc-50} - T_{d,sfc-50}) + (T_{sfc-150} - T_{d,sfc-150})$$

Data. CTP and HI_{low} are calculated from daily early morning atmospheric profiles of temperature and humidity. Early morning profiles represent the state of the atmosphere within the hour of sunrise. Here this is defined as the time step of each day, where incoming shortwave radiation is first larger than zero. It is used as index to extract the temperature and humidity profiles of the local hour of sunrise from hourly model output for each cell and each day.

Data Availability Statement

The alternative land cover maps and the NCL scripts used for the computation of the CTP- HI_{low} framework as well as the name lists can be downloaded from the repository link (<http://doi.org/10.5281/zenodo.3722520>).

References

- Bagley, J. E., Desai, A. R., Harding, K. J., Snyder, P. K., & Foley, J. A. (2014). Drought and deforestation: Has land cover change influenced recent precipitation extremes in the Amazon? *Journal of Climate*, 27(1), 345–361. <https://doi.org/10.1175/JCLI-D-12-00369.1>
- Baldocchi, D., Kelliher, F. M., Black, T. A., & Jarvis, P. (2000). Climate and vegetation controls on boreal zone energy exchange. *Global Change Biology*, 6(S1), 69–83. <https://doi.org/10.1046/j.1365-2486.2000.06014.x>
- Bauer, H.-S., Schwitalla, T., Wulfmeyer, V., Bakhshaii, A., Ehret, U., Neuper, M., & Caumont, O. (2015). Quantitative precipitation estimation based on high-resolution numerical weather prediction and data assimilation with WRF—A performance test. *Tellus A: Dynamic Meteorology and Oceanography*, 67(1), 25047. <https://doi.org/10.3402/tellusa.v67.25047>
- Belušić, D., Fuentes-Franco, R., Strandberg, G., & Jukimenko, A. (2019). Afforestation reduces cyclone intensity and precipitation extremes over Europe. *Environmental Research Letters*, 14(7), 074009. <https://doi.org/10.1088/1748-9326/ab23b2>
- Boisier, J. P., de Noblet-Ducoudré, N., Pitman, A. J., Cruz, F. T., Delire, C., van den Hurk, B. J. J. M., et al. (2012). Attributing the impacts of land-cover changes in temperate regions on surface temperature and heat fluxes to specific causes: Results from the first LUCID set of simulations: BIOGEOGRAPHICAL IMPACTS OF LULCC. *Journal of Geophysical Research*, 117, D12116. <https://doi.org/10.1029/2011JD017106>
- Bonan, G. (2016). *Ecological Climatology: Concepts and Applications* (3rd ed.). Cambridge: Cambridge University Press. <https://doi.org/10.1017/CBO9781107339200>
- Bonan, G. B. (2008). Forests and climate change: Forcings, feedbacks, and the climate benefits of forests. *Science*, 320(5882), 1444–1449. <https://doi.org/10.1126/science.1155121>
- Chen, L., & Dirmeyer, P. A. (2017). Impacts of land-use/land-cover change on afternoon precipitation over North America. *Journal of Climate*, 30(6), 2121–2140. <https://doi.org/10.1175/JCLI-D-16-0589.1>
- Chen, L., Dirmeyer, P. A., Tawfik, A., & Lawrence, D. M. (2017). Sensitivities of land cover–precipitation feedback to convective triggering. *Journal of Hydrometeorology*, 18(8), 2265–2283. <https://doi.org/10.1175/JHM-D-17-0011.1>
- Cherubini, F., Huang, B., Hu, X., Tölle, M. H., & Strömman, A. H. (2018). Quantifying the climate response to extreme land cover changes in Europe with a regional model. *Environmental Research Letters*, 13(7), 074002. <https://doi.org/10.1088/1748-9326/aac794>
- Christensen, J. H., & Christensen, O. B. (2007). *A Summary of the PRUDENCE Model Projections of Changes in European Climate by the End of This Century*. Copenhagen, Denmark: Danish Meteorological Institute.
- Davin, E. L., & de Noblet-Ducoudré, N. (2010). Climatic impact of global-scale deforestation: Radiative versus nonradiative processes. *Journal of Climate*, 23(1), 97–112. <https://doi.org/10.1175/2009JCLI3102.1>
- Davin, E. L., Rechid, D., Breil, M., Cardoso, R. M., Coppola, E., Hoffmann, P., et al. (2020). Biogeophysical impacts of forestation in Europe: First results from the LUCAS (land use and climate across scales) regional climate model intercomparison. *Earth System Dynamics*, 11(1), 183–200. <https://doi.org/10.5194/esd-11-183-2020>
- Davin, E. L., Seneviratne, S. I., Ciais, P., Olliso, A., & Wang, T. (2014). Preferential cooling of hot extremes from cropland albedo management. *Proceedings of the National Academy of Sciences*, 111(27), 9757–9761. <https://doi.org/10.1073/pnas.1317323111>
- de Noblet-Ducoudré, N., Boisier, J.-P., Pitman, A., Bonan, G. B., Brovkin, V., Cruz, F., et al. (2012). Determining robust impacts of land-use-induced land cover changes on surface climate over North America and Eurasia: Results from the first set of LUCID experiments. *Journal of Climate*, 25(9), 3261–3281. <https://doi.org/10.1175/JCLI-D-11-00338.1>
- Dee, D. P., Uppala, S. M., Simmons, A. J., Berrisford, P., Poli, P., Kobayashi, S., et al. (2011). The ERA-Interim reanalysis: Configuration and performance of the data assimilation system. *Quarterly Journal of the Royal Meteorological Society*, 137(656), 553–597. <https://doi.org/10.1002/qj.828>
- Dione, C., Lothon, M., Badiane, D., Campistron, B., Couvreux, F., Guichard, F., & Sall, S. M. (2014). Phenomenology of Sahelian convection observed in Niamey during the early monsoon: Sahelian convection during the early monsoon. *Quarterly Journal of the Royal Meteorological Society*, 140(679), 500–516. <https://doi.org/10.1002/qj.2149>
- Dirmeyer, P. A. (2011). The terrestrial segment of soil moisture-climate coupling: Soil moisture-climate coupling. *Geophysical Research Letters*, 38, L16702. <https://doi.org/10.1029/2011GL048268>
- Dirmeyer, P. A., Jin, Y., Singh, B., & Yan, X. (2013). Evolving land–atmosphere interactions over North America from CMIP5 simulations. *Journal of Climate*, 26(19), 7313–7327. <https://doi.org/10.1175/JCLI-D-12-00454.1>

- Dirmeyer, P. A., Wang, Z., Mbul, M. J., & Norton, H. E. (2014). Intensified land surface control on boundary layer growth in a changing climate: Dirmeyer et al.: Land-PBL feedback in a changing climate. *Geophysical Research Letters*, *41*, 1290–1294. <https://doi.org/10.1002/2013GL058826>
- Dittmann, E., & Deutscher Wetterdienst (Eds.) (1995). *Objektive Wetterlagenklassifikation*. Dt. Wetterdienst, Zentralamt: Offenbach am Main.
- Duveiller, G., Forzieri, G., Robertson, E., Li, W., Georgievski, G., Lawrence, P., et al. (2018). Biophysics and vegetation cover change: A process-based evaluation framework for confronting land surface models with satellite observations. *Earth System Science Data*, *10*(3), 1265–1279. <https://doi.org/10.5194/essd-10-1265-2018>
- Duveiller, G., Hooker, J., & Cescaati, A. (2018). The mark of vegetation change on Earth's surface energy balance. *Nature Communications*, *9*(1), 679. <https://doi.org/10.1038/s41467-017-02810-8>
- European Environmental Agency (2013). CORINE Land Cover (CLC) 2006, CRC/TR32 Database (TR32DB). Version 17. Copenhagen, Denmark: Copernicus Land Monitoring Service. Retrieved from <https://www.eea.europa.eu/data-and-maps/data/clc-2006-raster-3>
- Ferguson, C. R., & Wood, E. F. (2011). Observed land-atmosphere coupling from satellite remote sensing and reanalysis. *Journal of Hydrometeorology*, *12*(6), 1221–1254. <https://doi.org/10.1175/2011JHM1380.1>
- Findell, K. L., Berg, A., Gentine, P., Krasting, J. P., Lintner, B. R., Malyshev, S., et al. (2017). The impact of anthropogenic land use and land cover change on regional climate extremes. *Nature Communications*, *8*(1), 989. <https://doi.org/10.1038/s41467-017-01038-w>
- Findell, K. L., & Eltahir, E. A. B. (2003a). Atmospheric controls on soil moisture-boundary layer interactions. Part I: Framework development. *Journal of Hydrometeorology*, *4*(3), 552–569. [https://doi.org/10.1175/1525-7541\(2003\)004<0552:ACOSML>2.0.CO;2](https://doi.org/10.1175/1525-7541(2003)004<0552:ACOSML>2.0.CO;2)
- Findell, K. L., & Eltahir, E. A. B. (2003b). Atmospheric controls on soil moisture-boundary layer interactions. Part II: Feedbacks within the continental United States. *Journal of Hydrometeorology*, *4*(3), 570–583. [https://doi.org/10.1175/1525-7541\(2003\)004<0570:ACOSML>2.0.CO;2](https://doi.org/10.1175/1525-7541(2003)004<0570:ACOSML>2.0.CO;2)
- Findell, K. L., Gentine, P., Lintner, B. R., & Kerr, C. (2011). Probability of afternoon precipitation in eastern United States and Mexico enhanced by high evaporation. *Nature Geoscience*, *4*(7), 434–439. <https://doi.org/10.1038/ngeo1174>
- Gálos, B., Hagemann, S., Hänsler, A., Kindermann, G., Rechid, D., Sieck, K., et al. (2013). Case study for the assessment of the biogeophysical effects of a potential afforestation in Europe. *Carbon Balance and Management*, *8*(1), 3. <https://doi.org/10.1186/1750-0680-8-3>
- Gao, Y., Markkanen, T., Backman, L., Henttonen, H. M., Pietikäinen, J.-P., Mäkelä, H. M., & Laaksonen, A. (2014). Biogeophysical impacts of peatland forestation on regional climate changes in Finland. *Biogeosciences*, *11*(24), 7251–7267. <https://doi.org/10.5194/bg-11-7251-2014>
- Giorgi, F., Jones, C., & Asrar, G. R. (2009). Addressing climate information needs at the regional level: The CORDEX framework. *WMO Bulletin*, *58*(3).
- Görsdorf, U., & Seifert, A. (2011). *Wolkenstatistik und Modellvalidierung auf der Basis kontinuierlicher Messungen eines 35 GHz-Radars (MOL-RAO Aktuell No. 1/2011)* (p. 2). Offenbach: DWD, Meteorologisches Observatorium Lindenberg - Richard-Aßmann-Observatorium. Retrieved from https://www.dwd.de/DE/forschung/atmosphaerenbeob/lindenbergsaeule/rao_download/aktuell_2011_01.pdf?jsessionid=138D9E89AD7372994E70DA92858AB197.live11041?__blob=publicationFile&v=5
- Guillod, B. P., Orłowsky, B., Miralles, D. G., Teuling, A. J., & Seneviratne, S. I. (2015). Reconciling spatial and temporal soil moisture effects on afternoon rainfall. *Nature Communications*, *6*, 6443. <https://doi.org/10.1038/ncomms7443>
- Guo, Z., & Dirmeyer, P. A. (2013). Interannual variability of land-atmosphere coupling strength. *Journal of Hydrometeorology*, *14*(5), 1636–1646. <https://doi.org/10.1175/JHM-D-12-0171.1>
- Gutowski, W. J. Jr., Giorgi, F., Timbal, B., Frigon, A., Jacob, D., Kang, H.-S., et al. (2016). WCRP COordinated Regional Downscaling EXperiment (CORDEX): A diagnostic MIP for CMIP6. *Geoscientific Model Development*, *9*(11), 4087–4095. <https://doi.org/10.5194/gmd-9-4087-2016>
- Hirsch, A. L., Pitman, A. J., Kala, J., Lorenz, R., & Donat, M. G. (2015). Modulation of land-use change impacts on temperature extremes via land-atmosphere coupling over Australia. *Earth Interactions*, *19*(12), 1–24. <https://doi.org/10.1175/EI-D-15-0011.1>
- Huang, B., Hu, X., Fuglstad, G.-A., Zhou, X., Zhao, W., & Cherubini, F. (2020). Predominant regional biophysical cooling from recent land cover changes in Europe. *Nature Communications*, *11*(1), 1066. <https://doi.org/10.1038/s41467-020-14890-0>
- Iacono, M. J., Delamere, J. S., Mlawer, E. J., Shephard, M. W., Clough, S. A., & Collins, W. D. (2008). Radiative forcing by long-lived greenhouse gases: Calculations with the AER radiative transfer models. *Journal of Geophysical Research*, *113*, D13103. <https://doi.org/10.1029/2008JD009944>
- Ingwersen, J., Högy, P., Wizemann, H. D., Warrach-Sagi, K., & Streck, T. (2018). Coupling the land surface model Noah-MP with the generic crop growth model Gecros: Model description, calibration and validation. *Agricultural and Forest Meteorology*, *262*, 322–339. <https://doi.org/10.1016/j.agrformet.2018.06.023>
- Intergovernmental Panel on Climate Change (Ed.) (2014). Anthropogenic and natural radiative forcing. In *Climate Change 2013 - the Physical Science Basis* (pp. 659–740). Cambridge: Cambridge University Press. <https://doi.org/10.1017/CBO9781107415324.018>
- Intergovernmental Panel on Climate Change (2019). Climate Change and Land. Retrieved October 11, 2019, from <https://www.ipcc.ch/report/srcl/>
- Jacob, D., Teichmann, C., Sobolowski, S., Katragkou, E., Anders, I., Belda, M., et al. (2020). Regional climate downscaling over Europe: Perspectives from the EURO-CORDEX community. *Regional Climate Change*, *20*(2), 1–20. <https://doi.org/10.1007/s10113-020-01606-9>
- Kain, J. S. (2004). The Kain-Fritsch convective parameterization: An update. *Journal of Applied Meteorology*, *43*(1), 170–181. [https://doi.org/10.1175/1520-0450\(2004\)043<0170:TKCPAU>2.0.CO;2](https://doi.org/10.1175/1520-0450(2004)043<0170:TKCPAU>2.0.CO;2)
- Knist, S., Goergen, K., Buonomo, E., Christensen, O. B., Colette, A., Cardoso, R. M., et al. (2017). Land-atmosphere coupling in EURO-CORDEX evaluation experiments: Land-atmosphere coupling in EURO-CORDEX. *Journal of Geophysical Research: Atmospheres*, *122*, 79–103. <https://doi.org/10.1002/2016JD025476>
- Koster, R. D., Dirmeyer, P., Guo, Z., Bonan, G., Chan, E., Cox, P., et al. (2004). Regions of strong coupling between soil moisture and precipitation. *Science*, *305*(5687), 1138–1140. <https://doi.org/10.1126/science.1100217>
- Kotlarski, S., Keuler, K., Christensen, O. B., Colette, A., Déqué, M., Gobiet, A., et al. (2014). Regional climate modeling on European scales: A joint standard evaluation of the EURO-CORDEX RCM ensemble. *Geoscientific Model Development*, *7*(4), 1297–1333. <https://doi.org/10.5194/gmd-7-1297-2014>
- Kumar, S., Dirmeyer, P. A., Merwade, V., DelSole, T., Adams, J. M., & Niyogi, D. (2013). Land use/cover change impacts in CMIP5 climate simulations: A new methodology and 21st century challenges: LU CHANGE IMPACTS IN CMIP5. *Journal of Geophysical Research: Atmospheres*, *118*, 6337–6353. <https://doi.org/10.1002/jgrd.50463>
- Lang, J. (2010). *Bericht zur Untersuchung konvektiver Wetterlagen in Nordrhein-Westfalen (Dokumentation des Projektes "konvektive Wetterlagen (KonWet)" No. 1* (p. 25). Darmstadt, Germany: Landesamt für Natur, Umwelt und Verbraucherschutz Nordrhein-Westfalen.

- Lawrence, P. J., & Chase, T. N. (2007). Representing a new MODIS consistent land surface in the Community Land Model (CLM 3.0). *Journal of Geophysical Research*, *112*, G01023. <https://doi.org/10.1029/2006JG000168>
- Lawrence, P. J., & Chase, T. N. (2010). Investigating the climate impacts of global land cover change in the community climate system model. *International Journal of Climatology*, *30*(13), 2066–2087. <https://doi.org/10.1002/joc.2061>
- Lejeune, Q., Seneviratne, S. I., & Davin, E. L. (2017). Historical land-cover change impacts on climate: Comparative assessment of LUCID and CMIP5 multimodel experiments. *Journal of Climate*, *30*(4), 1439–1459. <https://doi.org/10.1175/JCLI-D-16-0213.1>
- Mahmood, R., Pielke, R. A., Hubbard, K. G., Niyogi, D., Dirmeyer, P. A., McAlpine, C., et al. (2014). Land cover changes and their biogeophysical effects on climate: Land cover changes and their biogeophysical effects on climate. *International Journal of Climatology*, *34*(4), 929–953. <https://doi.org/10.1002/joc.3736>
- Milovac, J., Ingwersen, J., & Warrach-Sagi, K. (2014). *Soil texture forcing data for the whole world for the weather research and forecasting (WRF) model of the University of Hohenheim (UHOH) based on the harmonized world soil database (HWSD) at 30 arc-second horizontal resolution [data set]*. DKRZ, Hamburg, Germany: World Data Center for Climate (WDCC). https://doi.org/10.1594/WDCC/WRF_NOAH_HWSD_world_TOP_SOILTYP
- Milovac, J., Warrach-Sagi, K., Behrendt, A., Späth, F., Ingwersen, J., & Wulfmeyer, V. (2016). Investigation of PBL schemes combining the WRF model simulations with scanning water vapor differential absorption lidar measurements: WRF sensitivity to PBL schemes and LSMs. *Journal of Geophysical Research: Atmospheres*, *121*, 624–649. <https://doi.org/10.1002/2015JD023927>
- Nakanishi, M., & Niino, H. (2009). Development of an improved turbulence closure model for the atmospheric boundary layer. *Journal of the Meteorological Society of Japan*, *87*(5), 895–912. <https://doi.org/10.2151/jmsj.87.895>
- Niu, G.-Y., Yang, Z.-L., Mitchell, K. E., Chen, F., Ek, M. B., Barlage, M., et al. (2011). The community Noah land surface model with multiparameterization options (Noah-MP): 1. Model description and evaluation with local-scale measurements. *Journal of Geophysical Research*, *116*, D12109. <https://doi.org/10.1029/2010JD015139>
- Peel, M. C., Finlayson, B. L., & McMahon, T. A. (2007). Updated world map of the Köppen-Geiger climate classification. *Hydrology and Earth System Sciences*, *11*(5), 1633–1644. <https://doi.org/10.5194/hess-11-1633-2007>
- Pfahl, S., & Wernli, H. (2012). Quantifying the relevance of cyclones for precipitation extremes. *Journal of Climate*, *25*(19), 6770–6780. <https://doi.org/10.1175/JCLI-D-11-00705.1>
- Pitman, A. J., de Noblet-Ducoudré, N., Cruz, F. T., Davin, E. L., Bonan, G. B., Brovkin, V., et al. (2009). Uncertainties in climate responses to past land cover change: First results from the LUCID intercomparison study. *Geophysical Research Letters*, *36*, L14814. <https://doi.org/10.1029/2009GL039076>
- Rechid, D., Davin, E. L., de Noblet-Ducoudré, N., Katragkou, E., & LUCAS-Team (2017). CORDEX Flagship Pilot Study LUCAS—Land Use & Climate Across Scales—A new initiative on coordinated regional land use change and climate experiments for Europe. In *Presented at the 19th EGU General Assembly, EGU2017* (Vol. 19, p. 13172). Vienna, Austria: Geophysical Research Abstracts.
- Santanello, J. A., Peters-Lidard, C. D., Kumar, S. V., Alonge, C., & Tao, W.-K. (2009). A modeling and observational framework for diagnosing local land-atmosphere coupling on diurnal time scales. *Journal of Hydrometeorology*, *10*(3), 577–599. <https://doi.org/10.1175/2009JHM1066.1>
- Schwitalla, T., Bauer, H.-S., Wulfmeyer, V., & Warrach-Sagi, K. (2017). Continuous high-resolution midlatitude-belt simulations for July–August 2013 with WRF. *Geoscientific Model Development*, *10*(5), 2031–2055. <https://doi.org/10.5194/gmd-10-2031-2017>
- Seneviratne, S. I., Lüthi, D., Litschi, M., & Schär, C. (2006). Land-atmosphere coupling and climate change in Europe. *Nature*, *443*(7108), 205–209. <https://doi.org/10.1038/nature05095>
- Seneviratne, S. I., Wilhelm, M., Stanelle, T., Hurk, B., Hagemann, S., Berg, A., et al. (2013). Impact of soil moisture-climate feedbacks on CMIP5 projections: First results from the GLACE-CMIP5 experiment. *Geophysical Research Letters*, *40*(19), 5212–5217. <https://doi.org/10.1002/grl.50956>
- Skamarock, W., Klemp, J., Dudhia, J., Gill, D., Barker, D., Wang, W., et al. (2008). *A description of the advanced research WRF version 3*. Boulder, CO: UCAR/NCAR. <https://doi.org/10.5065/D68S4MVH>
- Snyder, P. K., Delire, C., & Foley, J. A. (2004). Evaluating the influence of different vegetation biomes on the global climate. *Climate Dynamics*, *23*(3–4), 279–302. <https://doi.org/10.1007/s00382-004-0430-0>
- Späth, F., Wulfmeyer, V., Streck, T., & Behrendt, A. (2019). *The Land-Atmosphere Feedback Observatory (LAFO): A Novel Sensor Network to Improve Weather Forecasting and Climate Models*. Presented at the EGU General Assembly. Vienna, Austria: Geophysical Research Abstracts.
- Strandberg, G., & Kjellström, E. (2019). Climate impacts from afforestation and deforestation in Europe. *Earth Interactions*, *23*(1), 1–27. <https://doi.org/10.1175/EI-D-17-0033.1>
- Taylor, C. M., de Jeu, R. A. M., Guichard, F., Harris, P. P., & Dorigo, W. A. (2012). Afternoon rain more likely over drier soils. *Nature*, *489*(7416), 423–426. <https://doi.org/10.1038/nature11377>
- Thompson, G., Rasmussen, R. M., & Manning, K. (2004). Explicit forecasts of winter precipitation using an improved bulk microphysics scheme. Part I: Description and sensitivity analysis. *Monthly Weather Review*, *132*(2), 519–542. [https://doi.org/10.1175/1520-0493\(2004\)132<0519:EFOWPU>2.0.CO;2](https://doi.org/10.1175/1520-0493(2004)132<0519:EFOWPU>2.0.CO;2)
- Tölle, M. H., Gutjahr, O., Busch, G., & Thiele, J. C. (2014). Increasing bioenergy production on arable land: Does the regional and local climate respond? Germany as a case study. *Journal of Geophysical Research: Atmospheres*, *119*, 2711–2724. <https://doi.org/10.1002/2013JD020877>
- van den Hurk, B. J. J. M., & van Meijgaard, E. (2010). Diagnosing land-atmosphere interaction from a regional climate model simulation over West Africa. *Journal of Hydrometeorology*, *11*(2), 467–481. <https://doi.org/10.1175/2009JHM1173.1>
- Warrach-Sagi, K., Schwitalla, T., Wulfmeyer, V., & Bauer, H.-S. (2013). Evaluation of a climate simulation in Europe based on the WRF–NOAH model system: Precipitation in Germany. *Climate Dynamics*, *41*(3–4), 755–774. <https://doi.org/10.1007/s00382-013-1727-7>
- Winckler, J., Reick, C. H., & Pongratz, J. (2017). Robust identification of local biogeophysical effects of land-cover change in a global climate model. *Journal of Climate*, *30*(3), 1159–1176. <https://doi.org/10.1175/JCLI-D-16-0067.1>
- Wulfmeyer, V., Späth, F., Behrendt, A., Jach, L., Warrach-Sagi, K., Ek, M., et al. (2020). The GEWEX Land-Atmosphere Feedback Observatory (GLAFO). *GEWEX Quarterly Newsletter*, *30*(1/2020), 16. https://www.gewex.org/gewex-content/files_mf/1583952472Feb2020.pdf
- Wulfmeyer, V., Turner, D. D., Baker, B., Banta, R., Behrendt, A., Bonin, T., et al. (2018). A new research approach for observing and characterizing land-atmosphere feedback. *Bulletin of the American Meteorological Society*, *99*(8), 1639–1667. <https://doi.org/10.1175/BAMS-D-17-0009.1>

Chapter 5

Impacts of changing atmospheric temperature and moisture on L-A coupling strength

Publication II: Jach, L.L., T. Schwitalla, O. Branch, K. Warrach-Sagi, V. Wulfmeyer, 2022: Sensitivity of land-atmosphere coupling strength to changing temperature and moisture over Europe. *Earth Syst. Dynam.*, 13, 109-132, DOI: 10.5194/esd-13-109-2022.

5.1 Overview

LULCCs are not the only factor causing differences in the ABL structure. Brogli et al. (2019) for instance projected changes in the temperature lapse rates over Europe with climate change, which will also influence the atmospheric stability. Dirmeyer et al. (2013b) and Seneviratne et al. (2006) already showed that the coupling strength exhibits a strengthening trend with climate change. Dirmeyer et al. (2013b) attribute changes to an acceleration of the global water cycle due to soil moisture except during winter, which enhances the land-driven controls on surface fluxes and a growing impact on the boundary layer properties. Seneviratne et al. (2006) link the strengthening to enhance greenhouse gas concentrations, causing warming, increased temperature variability and through this the formation of a new strong coupling zone in Central Europe. In this second paper, the influence of differences in the temperature and moisture profiles on L-A coupling strength was investigated in a comprehensive manner. As the quantification of L-A coupling strength is still challenging, the

analyses aimed at assessing uncertainties in the coupling strength assessment in dependence of atmospheric temperature and moisture. This was done by implementing a posteriori modifications to the modeled thermodynamic profiles of the evaluation run as presented in Jach et al. (2020) and evaluate their effects on the coupling strength. This work expands the work by Jach et al. (2020) in the sense that all possible combinations of temperature and moisture changes in the atmosphere were considered in the analysis. Thus, besides warming and relative drying (forest-evaluation), as well as cooling and relative moistening in the atmosphere (grass-evaluation), also warming and relative moistening as well as cooling and relative drying and isolated changes in temperature and moisture were examined. Additionally, the effects of differences in the vertical distribution of temperature and moisture modifications were considered. The findings indicate reliability of the hot spot location in Northeastern Europe as well as predominance of positive feedback in the northern part of the hot spot, as they were only modified under extreme changes in relative humidity. These would have pushed the northern European climate to semi-arid conditions, and thus are considered unrealistic. At the same time, the dry conditions over the Iberian Peninsula and the Mediterranean inhibited local feedback in all cases. However, variability of more than 10 percent between the modification cases with regard to the occurrence of potential coupling days that uncertainty remains in the accurate quantification of L-A coupling strength. In the southern part of the hot spot, additionally the predominant coupling pathway switched between wet soil advantage (positive coupling) and transition zone (shallow convection only) on a frequent basis, which also indicates uncertainty in the dominant atmospheric response to varying surface conditions. There occurs a north-south dipole in the sensitivity of L-A coupling strength to temperature and moisture changes with a stronger temperature impact in the north and dominant moisture control in the south. Modifications in temperature gradients appear as important as the change in the mean. An increasing temperature gradient usually increases the number of non-atmospherically controlled (nAC)-days while a decreasing gradient indicates a stabilization of the atmosphere which reduces the number of nAC days.

5.2 Publication

This publication titled “Sensitivity of land-atmosphere coupling strength to changing atmospheric temperature and moisture over Europe” is an open access article published under the terms of the Creative Commons Attribution 4.0 License, which permits use, distribution and reproduction in any

medium, provided the original work is properly cited. ©2022 The Authors. Earth System Dynamics published by Copernicus Publications.



Sensitivity of land–atmosphere coupling strength to changing atmospheric temperature and moisture over Europe

Lisa Jach, Thomas Schwitalla, Oliver Branch, Kirsten Warrach-Sagi, and Volker Wulfmeyer

Institute of Physics and Meteorology, University of Hohenheim, Stuttgart, Germany

Correspondence: Lisa Jach (lisa.jach@uni-hohenheim.de)

Received: 21 June 2021 – Discussion started: 6 July 2021

Revised: 20 November 2021 – Accepted: 14 December 2021 – Published: 24 January 2022

Abstract. The quantification of land–atmosphere coupling strength is still challenging, particularly in the atmospheric segment of the local coupling process chain. This is in part caused by a lack of spatially comprehensive observations of atmospheric temperature and specific humidity which form the verification basis for the common process-based coupling metrics. In this study, we aim at investigating where uncertainty in the atmospheric temperature and moisture affects the land–atmosphere coupling strength over Europe, and how changes in the mean temperature and moisture, as well as their vertical gradients, influence the coupling. For this purpose, we implemented systematic a posteriori modifications to the temperature and moisture fields from a regional climate simulation to create a spread in the atmospheric conditions. Afterwards, the process-based coupling metric convective triggering potential – low-level humidity index framework was applied to each modification case.

Comparing all modification cases to the unmodified control case revealed that a strong coupling hotspot region in northeastern Europe was insensitive to temperature and moisture changes, although the number of potential coupling days varied by up to 20 d per summer season. The predominance of positive feedbacks remained unchanged in the northern part of the hotspot, and none of the modifications changed the frequent inhibition of feedbacks due to dry conditions in the atmosphere over the Mediterranean and the Iberian Peninsula. However, in the southern hotspot region in the north of the Black Sea, the dominant coupling class frequently switched between wet soil advantage and transition zone. Thus, both the coupling strength and the predominant sign of feedbacks were sensitive to changes in temperature and moisture in this region. This implies not only uncertainty in the quantification of land–atmosphere coupling strength but also the potential that climate-change-induced temperature and moisture changes considerably impact the climate there, because they also change the predominant atmospheric response to land surface wetness.

1 Introduction

Land–atmosphere (L–A) coupling describes the covariability between the land and atmospheric states, and plays a key role for understanding states in the climate system such as the evolution of the atmospheric boundary layer (ABL) temperatures and humidities. It shapes, e.g., the atmospheric water and energy cycles, and through this influences the intensity and duration of extreme events such as heat waves (Ukkola et al., 2018; Jaeger and Seneviratne, 2011; van Heerwaarden and Teuling, 2014; Schumacher et al., 2019), drought peri-

ods (Miralles et al., 2019) or the occurrence of heavy rainfall events. Furthermore, the feedback processes influence the climate response to land surface modifications (Hirsch et al., 2014; Laguë et al., 2019) suggesting the importance of the processes' accurate representation in climate models to improve projections.

The local coupling (LoCo) process chain outlines the connection between soil moisture and precipitation through the turbulent surface fluxes modifying the evolution of the ABL, and finally, leading to different conditions for cloud and precipitation formation (Santanello et al., 2009, 2011). Various

coupling metrics have been developed to investigate the nature and intensity of this and other relationships in the climate system (Santanello et al., 2018). Individual processes in the chain exhibit different intensities and the feedback sign can diverge in dependence of the region (e.g., Findell et al., 2011; Findell and Eltahir, 2003a, b; Knist et al., 2017; Koster et al., 2004) and the period of time investigated. Coupling hotspots mainly occur in transition regions between dry and wet climates (e.g., Gentine et al., 2013; Koster et al., 2004; Taylor et al., 2012). Temporal variability is apparent at interannual scales (Guo and Dirmeyer, 2013; Lorenz et al., 2015) and in trends of the coupling strength (Dirmeyer et al., 2012, 2013; Seneviratne et al., 2006).

Uncertainty remains in the accurate quantification of the coupling strength along the LoCo process chain, especially in the atmospheric segment. From the physical perspective, the strength is influenced by both the prevailing land surface and the atmospheric state. Jach et al. (2020) showed that extreme afforestation led to weaker coupling between surface moisture and convection triggering, and a less pronounced favor for convection triggering over wet soils in the European summer. The conversion of current vegetation to grassland had the opposite effect. However, Davin et al. (2020) showed that the same land use and land cover change scenarios as used in Jach et al. (2020) initiated different responses in near-surface temperature within the ensemble of regional climate models from the flagship pilot study “Land-Use and Climate Across Scales” (LUCAS) due to deficiencies in the computation of evapotranspiration. Understanding potential implications of these uncertainties for impacts of land use and land cover changes on L–A coupling strength and climate variability was one motivation of our study.

From the technical perspective, the coupling strength is influenced by the choice of the dataset used for the investigation (Dirmeyer et al., 2018; Ferguson and Wood, 2011) and, in the case of models, their configuration such as parameterization schemes (Chen et al., 2017; Milovac et al., 2016; Pitman et al., 2009), initialization (Santanello et al., 2019) or model resolution (Hohenegger et al., 2009; Knist et al., 2020; Sun and Pritchard, 2016, 2018; Taylor et al., 2013). Studies on the regional scale over Europe often use a single model (Baur et al., 2018; Jach et al., 2020; Lorenz et al., 2012) or target only the terrestrial segment (soil moisture–surface flux coupling) of the local coupling process chain (Knist et al., 2017). Coordinated model intercomparison studies such as the Global Land–Atmosphere Coupling Experiment (GLACE) initiative apply general circulation or earth system models (Guo et al., 2006; Koster et al., 2006, 2011; Comer and Best, 2012). On the one hand, this circumvents the need to use lateral boundary layer forcing. On the other hand, the horizontal resolution of these model runs is usually on the order of 1 to 2° grid spacing. This reduces the models’ ability to represent detailed surface characteristics. These, in turn, play a key role for triggering convection, e.g., due to differential heating.

The “convective triggering potential – low-level humidity index” (CTP-HI_{low}) framework (Findell and Eltahir, 2003a, b) is a commonly used process-based coupling metric to investigate the link between surface moisture and convection triggering. It is based on the hypothesis that the structure of the early morning ABL (atmospheric pre-conditioning) gives an indication about the likelihood for locally triggered afternoon precipitation over differently wet soils. Later works added soil moisture (Roundy et al., 2013) or the evaporative fraction (Findell et al., 2011; Berg et al., 2013) as a third dimension. Efforts have been made to test the global applicability of the framework, which made use of climatologies of the metrics (Ferguson and Wood, 2011; Wakefield et al., 2019).

Analyzing the atmospheric segment on a process-based level requires information about the vertical structure of the atmosphere. The data requirements for studying the atmospheric segment of L–A coupling on the process level and in a spatially explicit way can be summarized as follows: vertical temperature and moisture profiles are needed (1) with a sufficiently long data record (period of at least 12 summers for metrics targeting convection triggering), to comply to the data length requirements for robust results (Findell et al., 2015), (2) with a high-enough temporal resolution to be able to extract the time step close to the local sunrise and (3) increasing vertical resolutions improve the estimate (Wakefield et al., 2021). These high requirements limit the datasets available for a study on the continental scale for Europe. Observations of early morning vertical temperature and moisture profiles are rare and usually point measurements. The typical radiosonde launch times (00:00 and 12:00 UTC) do not cover the early morning hours over Europe. Other observational products such as satellite-based profile data have been successfully used to apply the CTP-HI_{low} framework on Roundy and Santanello (2017), although they often have coarse vertical resolutions (Wulfmeyer et al., 2015). The lack of suitable observations challenges the validation of results, which provides the incentive for building up a network of coordinated measurement sites like the Land-Atmosphere Feedback Observatory (LAFO) of the University of Hohenheim (Wulfmeyer et al., 2020; Späth et al., 2019).

To study how sensitive the atmospheric segment of L–A coupling strength responds to differences in the atmospheric pre-conditioning, we developed an approach with which the temperature and moisture output fields from a regional climate model run were modified after the simulation and before applying the CTP-HI_{low} framework. The modifications are expected to change the pre-conditioning and thus potentially the coupling classification. First of all, frequent changes in the classification show that it lies at the boundaries of different classes. However, assuming that the classification framework is accurate enough, frequent changes also reveal that the expectable coupling signal remains uncertain. This is shown as changes in the atmospheric conditions in a presumably realistic range for the current climate could initi-

ate different atmospheric responses such as triggering deep, shallow or no convection in different cases in the same region. Furthermore, it indicates a sensitivity of the coupling to changes in the atmosphere, e.g., arising from climate change or changes at the land surface.

The approach is based on our hypothesis that the temperature and moisture fields can diverge in their mean, as well as their vertical, temporal and horizontal distributions, and the framework only recognizes the differences regardless of their origin. Hence, besides identifying regions with a high sensitivity to differences in the atmospheric conditions, we are able to approximate a range in coupling strength of the atmospheric segment. Here, we focus on the impacts of differences in the mean states and the vertical gradients of temperature and specific humidity in the posterior modification cases compared to the CTRL. For this purpose, we have set up two sets of cases: one targeting the analysis of differences in the mean state and one the analysis of differences in the vertical gradients. Temperature modifications at the surface range between ± 2 K, which is derived from an acceptable range of near-surface temperature biases occurring in climate simulations as defined by Kotlarski et al. (2014), and decrease over height. The a posteriori modifications of moisture were implemented under consideration of the close relationship between temperature and water vapor in the atmosphere, thus taking into account the respective temperature modification (e.g., Willett et al., 2010; Bastin et al., 2019).

With this approach we focus on two research questions:

1. How sensitive is the L–A coupling strength to modification of temperature and moisture profiles during the European summer months (JJA)?
2. Where can we identify reliable L–A coupling hotspots over Europe?

The paper is structured as follows: Sect. 2 describes the dataset analysis methods applied. This is followed by the analysis of the impacts of temperature and moisture modifications on estimates of L–A coupling strength over Europe in Sect. 3. The discussion of the results follows in Sect. 4, and finally, in Sect. 5, we summarize our findings and provide potential implications and an outlook on future research.

2 Materials and methods

2.1 Data

2.1.1 Model data

The database for the following analysis is a model simulation of Jach et al. (2020) hereafter named CTRL. It is a regional climate simulation on a 0.44° grid increment conducted with the Weather Research and Forecasting (WRF) model version 3.8.1 (Skamarock et al., 2008; Powers et al., 2017) coupled to the Noah-MP land surface model (Niu et al., 2011). The applied parameterizations are summarized in

Table 1. The simulation was forced with ERA-Interim re-analysis data from the European Centre for Medium-Range Weather Forecasts (ECMWF) (Dee et al., 2011) for the period 1986–2015 over the EURO-CORDEX domain (Jacob et al., 2020). The vegetation map is based on the CORINE land cover classification from 2006 (European Environmental Agency, 2013), and the soil texture was derived from the Harmonized World Soil Database at 30 arcsec grid spacing (Milovac et al., 2014). The simulation is part of the model ensemble of the regional model intercomparison project LUCAS. LUCAS investigates impacts of the implementation of land use and land cover changes in regional climate simulations.

2.2 CTP- HI_{low} framework

The coupling metric CTP- HI_{low} framework (Findell and Eltahir, 2003a, b) was used to estimate the coupling strength between land surface moisture and convection triggering. It utilizes vertical temperature and moisture profiles around sunrise to calculate an atmospheric stability (CTP) and humidity deficit (HI_{low}) measures.

CTP depicts the divergence of the temperature profile from the moist adiabatic lapse rate integrated between 100 and 300 hPa a.g.l. (above ground level) and is given in the unit $J kg^{-1}$. Its calculation is analogous to that of CAPE for the predefined layer using modeled air temperature. Analyzing this specific layer follows the hypothesis that the ABL top is almost always incorporated, and hence differences in the atmospheric structure may reveal differences in the likelihood for convection triggering. The pressure height estimates are valid for Europe but may limit the investigation of preconditioning in hot and arid regions, where the ABL usually grows to higher altitudes throughout the day. However, the variables CTP and HI_{low} have been used in combination with wind shear before within arid regions with good predictive skill for convection initiation triggered by differential surface heating (e.g., Branch and Wulfmeyer, 2019). Large CTP values denote strong divergence of the temperature profiles from the moist adiabat and hence greater instability. Small but positive values indicate temperature profiles that are close to the moist adiabat, i.e., conditionally unstable, and negative CTP values indicate a temperature inversion in the layer between 100 and 300 hPa above ground, which would inhibit deep convection and the formation of precipitation throughout the subsequent day.

The HI_{low} measures the dew-point depression at 50 and 150 hPa a.g.l. and has the unit $^\circ C$:

$$HI_{low} = (T_{p_{sfc}-50\text{hPa}} - T_{d,p_{sfc}-50\text{hPa}}) + (T_{p_{sfc}-150\text{hPa}} - T_{d,p_{sfc}-150\text{hPa}}), \quad (1)$$

where $T_{p_{sfc}-50\text{hPa}}$ is the temperature at 50 hPa a.g.l. and $T_{d,p_{sfc}-50\text{hPa}}$ the dew-point temperature at 50 hPa a.g.l. Equivalently, $T_{p_{sfc}-150\text{hPa}}$ and $T_{d,p_{sfc}-150\text{hPa}}$ are the temperature and dew-point temperature, respectively, at 150 hPa a.g.l.

Table 1. Applied parameterizations of the simulations from Jach et al. (2020).

Model physics	Parameterization scheme
Microphysics scheme	New Thompson scheme (Thompson et al., 2004)
Shortwave radiation scheme	Rapid Radiative Transfer Model (RRTMG) scheme (Iacono et al., 2008)
Longwave radiation scheme	Rapid Radiative Transfer Model (RRTMG) scheme (Iacono et al., 2008; Mlawer et al., 1997)
Boundary layer scheme	MYNN level 2.5 PBL (Nakanishi and Niino, 2009)
Convection scheme	Kain–Fritsch scheme (Kain, 2004)
Land surface model	Noah-MP land surface model (Niu et al., 2011)
Surface layer scheme	MYNN surface layer scheme (Nakanishi and Niino, 2009)

CTP and HI_{low} form the basis for categorizing early morning ABL conditions on a daily basis in (1) prone-to-triggering convection over wet or (2) dry soils, (3) a transition zone between wet and dry advantages, or (4) conditions inhibiting a contribution of the land surface to the triggering of deep convection. In the latter case, the occurrence of precipitation is purely atmospherically controlled (AC). This can have three causes: either the ABL is very humid ($HI_{low} < 5^{\circ}\text{C}$) and rainfall is just as likely to occur over any surface, or the ABL is very dry ($HI_{low} > 15^{\circ}\text{C}$) and moist convection and precipitation rarely occur in general. Finally, when the ABL is stable ($CTP < 0\text{J kg}^{-1}$), deep convection is inhibited by an inversion. Only shallow clouds can occur. The first three defined classes (1–3) are jointly considered as non-atmospherically controlled (nAC). These indicate the percentage of days within the study period with high potential for feedbacks of any kind. Triggering convection over wet soils (1) follows the hydrological pathway meaning positive soil moisture–evapotranspiration–precipitation feedbacks. Hence, greater soil moisture leads to a moistening of the ABL through evapotranspiration and more precipitation. Conversely, triggering convection over dry soils (2) occurs along the thermal triggering pathway during which a high sensible heat flux leads to boundary layer growth and upward mixing of moist air to heights where condensation and formation of rainfall can occur (Dirmeyer et al., 2014). In the transition zone, convection can be triggered over wet or dry soils, though no convection is the most likely outcome. Here, we apply the original threshold values from Findell and Eltahir (2003a), which are shown in Fig. 1a.

The daily coupling classes are then used to derive a long-term coupling regime for each grid cell, based on the relative occurrence of each class during the study period (Fig. 1b). At first, a cell with more than 90 % of the days in the study period under atmospheric control is defined as AC. If this is not the case, the partitioning of the nAC days in wet and dry soil advantage, as well as transition zone days, is used to determine the dominant coupling class. A level-1 coupling regime denotes that > 50 % of the nAC days in the cell are in the respective coupling class. Level-2 wet or dry soil advantage means that less than 20 % of the respective other class occurs

in the cell during the study period, while level-2 transition zone covers all cells remaining unlabeled.

2.3 Modification approach

Early morning profiles of temperature and moisture are required to compute the CTP- HI_{low} framework investigating the pre-conditioning for convection triggering during the day. Due to the large expansion of the domain covering several time zones, the ABL evolution on the eastern edge of the domain is in a different stage as that of the western edge at the same UTC time step, which can lead to substantial differences in the results of the coupling metric (Wakefield et al., 2021). Hence, the accurate UTC time step to depict the pre-convective ABL for the coupling assessment cannot be unified throughout the domain. To ensure this comparability between eastern and western Europe, we determined the sunrise hour in the model using shortwave downward radiation. The profiles were extracted for the UTC time step in which shortwave downward radiation exceeded a value of zero the first time for each day and cell. The profiles from model output around local time sunrise of each day serve as the basis for the sensitivity analysis. In the following section, we describe how the profiles were modified. The approach is based on our hypothesis that the temperature and moisture fields can vary in terms of their mean, and their horizontal, vertical and temporal distributions. In this study, we investigate the impact of modifying the mean and the vertical distribution. The temporal and horizontal distributions were not modified, although, e.g., warming is known to widen and flatten the distribution of temperature over time and therefore slightly change the shape of the distribution. The processes and mechanisms leading to a change in the temporal distribution are complex and non-linear, meaning that they cannot be reproduced easily by the modifications. Differences in the spatial distribution (such as warmer conditions in France with colder conditions over eastern Europe) were not specifically depicted. The CTP- HI_{low} framework utilizes single columns and does not recognize horizontal connections.

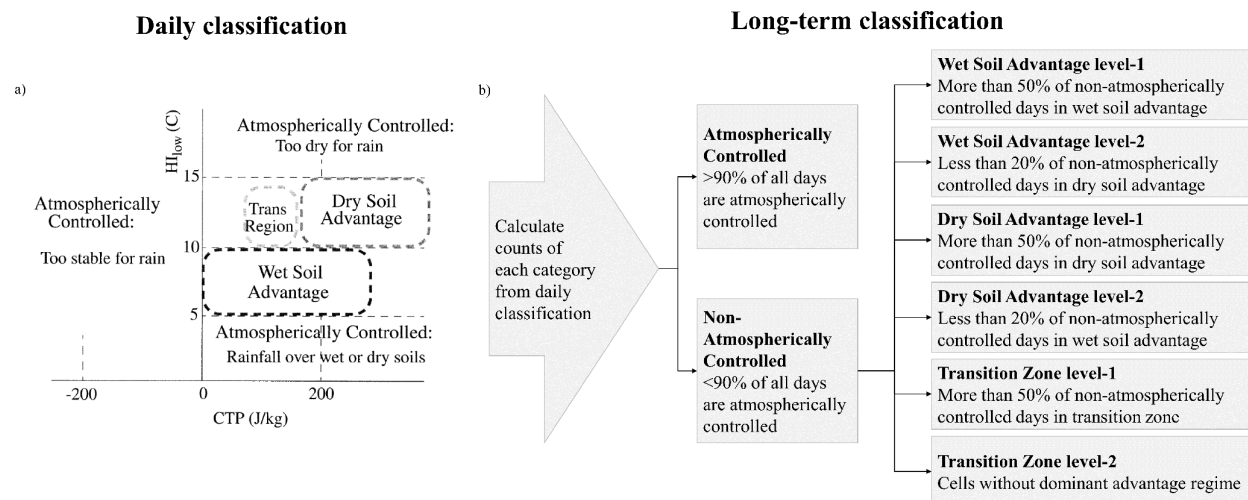


Figure 1. Schematic depicting the coupling strength classification with the convective triggering potential – low-level humidity (CTP- HI_{low}) framework by Findell and Eltahir (2003a, b) (adopted from Jach et al., 2020). Panel (a) shows the threshold values from Findell and Eltahir (2003a); their Fig. 15. Panel (b) summarizes the approach for the long-term classification as explained in Findell and Eltahir (2003b).

2.3.1 Temperature modifications

The temperature profiles were modified by adding a constant temperature (T) factor in Kelvin to the daily profiles. The factor is fixed in time, homogeneous over the domain and decreases with altitude. Decreasing the impact over height follows the hypothesis that a surface temperature change does not propagate evenly throughout the atmospheric column. The T factor for each atmospheric layer was derived using a simple linear regression model and calculating the mean coefficient of determination for each atmospheric layer. Therefore, it corresponds to the fraction of variance in temperature for each atmospheric layer explainable by the temperature variance at the surface.

The first set of temperature modifications (hereafter called the core set) captures differences in the mean air temperature near the surface and in the vertical by applying the temperature factor. In this case, the modification amounts to ± 2 K at the surface ($= 2 \times T$ factor). This range was derived from the acceptable range of biases in temperatures in Kotlarski et al. (2014). Plots with stronger modifications of ± 5 K covering the full range of the model bias of this particular run are provided in the Supplement. A second set of modifications served to investigate the effect of differences in the shape of the profiles (e.g., greater or smaller inversions) leading to differences in the gradients. For this purpose, we determined the divergence of the mean temperature profiles of summers with the highest near-surface temperature or near-surface moisture anomalies from the mean temperature profile of all 30 years to produce five divergence T factors. Chosen were the summers with (1) minimum (cold) and (2) maximum (hot) near-surface temperature, as well as the summers with the (3) minimum (dry) and (4) maximum (wet) near-surface relative hu-

midity, as well as (5) maximum near-surface specific humidity (wet_abs). The year with the minimum near-surface specific humidity corresponds to the cold summer. Table 2 summarizes the years chosen for the divergence T factors and the sign of their surface temperature and moisture anomalies, respectively. These were added to the temperature profiles from the CTRL run on a daily basis. In a second step, the divergence cases were further modified by adding the same factor used for the core set in order to investigate the effect of differences in the gradient with additional surface warming or cooling on the coupling strength. Larger modification factors up to ± 5 K led to similar patterns of differences and diverged in the magnitude of the impact in most cases.

2.3.2 Moisture modifications

Besides the temperature, also the moisture content in the atmosphere is expected to have an impact on the coupling strength. Willett et al. (2010) investigated the scaling of concurrent temperature and moisture changes for different regions around the globe based on observations and models. For the Northern Hemisphere, they found that temperature and moisture are strongly positively correlated and that 1 K temperature changes corresponds to on average 8.81 % change in moisture. The factors for northern ($9.66 \% K^{-1}$) and southern ($7.74 \% K^{-1}$) Europe slightly deviate. Under the assumption that the scaling is valid through the entire atmospheric column, the Northern Hemisphere factor was used for the moisture modifications. Hence, the magnitude of the change is dependent on the respective temperature modification and the moisture present in the atmosphere in the CTRL. This ensures two things: first, the relation of temperature and moisture is maintained, and second, the higher atmospheric

Table 2. Anomalies from the JJA mean of the CTRL run in temperature and moisture in years chosen as basis for the alternative factors; * indicates that the cold and dry_abs are the same year.

	Negative T anomaly		Positive T anomaly		
Negative q anomaly	cold/dry_abs* (1986)	dry (1994)	–	–	–
Positive q anomaly	–	–	hot (2003)	wet_abs (2010)	wet (2013)

layers do not experience unrealistic increases in moisture, which could have occurred using fixed factors. As for the temperature modifications, the mean moisture and the shape of the profiles were modified but the temporal and spatial variances were not.

To further prevent the development of unrealistically high moisture content in the atmosphere in humid regions, the saturation vapor pressure was determined for the temperature after modification and used to cap the moisture increase. Negative moisture content was prevented by setting a lower boundary of 0 g kg^{-1} . Thus, the relative humidity (in terms of specific humidity divided by saturation specific humidity) is designed to remain between 0 % and 100 % in all atmospheric layers.

2.4 Statistical sensitivity assessment

A sensitivity index was used to achieve a grid wise estimate whether temperature modifications or moisture modifications have a higher impact on the corresponding variable. The index compares the magnitude of differences in a variable x caused by modifying moisture or temperature only from the CTRL. The approach is described using the following formula:

$$x_{\text{sens}} = \frac{\sum \left((x_{Q_{\text{low}}} - x_{\text{ref}})^2 + (x_{Q_{\text{hi}}} - x_{\text{ref}})^2 \right) - \sum \left((x_{T_{\text{low}}} - x_{\text{ref}})^2 + (x_{T_{\text{hi}}} - x_{\text{ref}})^2 \right)}{\sum \left((x_{Q_{\text{low}}} - x_{\text{ref}})^2 + (x_{Q_{\text{hi}}} - x_{\text{ref}})^2 \right) + \sum \left((x_{T_{\text{low}}} - x_{\text{ref}})^2 + (x_{T_{\text{hi}}} - x_{\text{ref}})^2 \right)}, \quad (2)$$

where x_{ref} is the value of the unmodified case, $x_{Q_{\text{low}}}$ is the value of the modification case of isolated decrease in moisture, $x_{Q_{\text{hi}}}$ is the case with an isolated increase in moisture, $x_{T_{\text{low}}}$ is the case with an isolated decrease in temperature, and $x_{T_{\text{hi}}}$ is the case with an isolated increase in temperature, respectively. Thus, the modification cases with isolated temperature or moisture modifications were used for this analysis. The index was then normalized to a value between -1 and 1 by dividing the squared sum of differences induced by moisture changes minus the squared sum of differences induced by temperature changes by the total squared sum of differences from the CTRL in all cases. A sensitivity index close to -1 indicates a strong temperature control on the variable, while a sensitivity index close to 1 indicates a strong mois-

ture control. With a sensitivity index around 0 , moisture and temperature variations have an equal impact on changes in x .

In this study, we used the temperature modification of $\pm 2 \text{ K}$, and the cases with the corresponding moisture modifications of $\pm 2 \cdot 8.81 \% \text{ K}^{-1}$, from the core modifications set to estimate the relative importance of temperature versus moisture changes for CTP, HI_{low} and the occurrence of nAC days, wet and dry soil advantage as well as transition zone days. We limited the analysis to regions where on average at least 2 d per summer ($\sim 2.5 \%$ of the summer days) are in the respective category.

2.5 Uncertainty of hotspot location and feedback sign

Two measures were used to depict the sensitivity of the long-term coupling regimes in the modification cases. The first metric I_{feed} measures the degree of agreement of the long-term classification based on the CTP- HI_{low} framework among the modification cases with that of the CTRL case. A value close to 1 indicates that nearly all modifications had the same long-term coupling regime no matter which modification factors were applied. A value close to 0 indicates an overall disagreement in the long-term coupling regimes with the CTRL case indicating that the classification is sensitive to differences in the temperature and moisture profiles.

$$I_{\text{feed}} = 1 - \frac{\sum_1^n (\text{cat}_n \neq \text{cat}_{\text{CTRL}})}{n}, \quad (3)$$

with $\sum_1^n (\text{cat}_n \neq \text{cat}_{\text{CTRL}})$ denoting the sum of modification cases in which the long-term coupling regimes disagree with that of the CTRL case, and n being the number of all modification cases tested. A second metric I_{cat} was used to quantify the share of modification cases in which each of the coupling classes occurred. It was determined for nAC days, and days in wet soil advantage, dry soil advantage or transition zone. Level-1 and level-2 cells of the coupling classes were grouped together before deriving the metric.

$$I_{\text{cat}} = \frac{\sum n_{\text{cat}}}{n}, \quad (4)$$

with n_{cat} being the number of modification cases in the respective regime. A value of 0 denotes that the class was never

dominant and a value of 1 denotes that the class was always dominant.

3 Results

3.1 Comparison model and reanalysis

This section provides a statistical comparison of the mean and temporal distribution of near-surface temperature and specific humidity from the CTRL run with an ERA5-based bias-corrected reanalysis dataset (C3S, 2020) to quantify uncertainty originating from climatological inconsistencies of the model as compared to the reanalysis data. The statistical analyses comprise of the bias and two measures to compare the temporal distributions: a statistical z test and the probability density function (PDF) skill score after Perkins et al. (2007).

The model has a dry bias over the Mediterranean, France and the British Isles, and the z test showed that the temperature distribution is shifted towards warmer conditions (Fig. 2a and b). Over the eastern part of the domain, the model has a cold bias and overestimates the frequency of cooler days. The z value, which remained consistently below 2 throughout the domain, indicated that the differences in the temporal distribution are statistically insignificant. The PDF skill score drew a similar picture (Fig. 2c). The distributions strongly resemble with values > 0.8 over most of central and eastern Europe as well as over the high latitudes. The skill is weaker in the southern part of the domain. The model particularly misrepresents the temperature distribution over the Alpine region, in the south of the Black Sea and the northern African desert.

The moisture bias is presented in terms of the specific humidity. The model has a dry bias of up to -2 g kg^{-1} over the Mediterranean and southeastern Europe (Fig. 2d), which corresponds to maximally 20 % difference from the climatological mean of the reanalysis data in summer. The specific humidity is slightly overestimated by up to 0.5 g kg^{-1} over Scandinavia and the British Isles and slightly underestimated in central and eastern Europe in the same range. The differences in specific humidity correspond to less than 10 % difference from the climatological mean (not shown). The z statistic showed that the temporal distribution of specific humidity was shifted to dryer or more humid conditions correspondingly (Fig. 2e). However, the z value remained consistently below 1, indicating that the differences in the temporal distributions between model and reanalysis data are insignificant. Again, the PDF skill score matched the findings from the z statistic (Fig. 2e and f). The skill of the model to represent the distribution of specific humidity is particularly high over the East European Plain and central Europe with scores mostly > 0.9 . The skill is lower over the Mediterranean, dropping to a range between 0.4–0.6.

3.2 Sensitivity analysis

In this section, we describe how differences in the mean temperature and moisture profiles impact the frequency of favorable conditions for local land-surface-triggered deep convection, how the likelihood for convection triggered over wet versus dry soils changes and how these influences are represented in classifications of long-term coupling regimes with the CTP-HI_{low} framework.

3.2.1 Regional differences introduced by modifications

In the core set, the modifications reach to approximately 500 hPa a.g.l. The cases cover a range of different combinations of temperature and moisture modifications to estimate (1) modifications with the same sign that represent changes following the observed positive correlations between T and q in Europe. Additionally, examining (2) the isolated effects of temperature and moisture allows for the disentanglement of their impacts on the coupling strength as well as (3) modifications with opposing signs. The core set aimed at covering four possible combinations of differences in the climate conditions, namely, cooler and moister conditions, cooler and dryer conditions, warmer and moister conditions, as well as warmer and dryer conditions.

Previous observational and global model studies suggested that temperature and moisture are considerably positively correlated in most regions around the globe and trends lie around 7 % change in moisture per Kelvin change in temperature, reflecting the Clausius–Clapeyron rate for increases in moisture, which maintains a quasi-constant relative humidity (Bastin et al., 2019; Willett et al., 2010). In Europe, the scaling of moisture to temperature was slightly higher (Sect. 2.3.2). In addition to the rates described before, a rate of $5 \% \text{ K}^{-1}$ was tested to represent a change in moisture per Kelvin change in temperature below the Clausius–Clapeyron rate. Figure 3 depicts the divergence in frequency of nAC days from the CTRL run with 2 K warmer and cooler conditions for all land points. Impacts on the coupling strength and the pre-conditioning for the different coupling regimes have the same sign for each tested rate. A higher scaling of moisture with temperature – as observed in northern Europe – enhanced the effects on the coupling.

For the following analysis, we combined the rate of the Northern Hemisphere ($8.81 \% \text{ K}^{-1}$) with 2 K temperature changes at the land surface. Figure 4 shows the coefficient of determination used as basis for the modification over height as well as the temperature and dew-point temperature profiles after modification. CTP and HI_{low} changes were uniform throughout the domain. Their spatial patterns were largely maintained from the CTRL run, which were considered reasonable (Jach et al., 2020). When temperature and moisture modifications had the same sign (e.g., warmer and moister), the sign of differences in nAC days was uniform throughout the domain (Fig. 5a and i). Cooler and dryer conditions re-

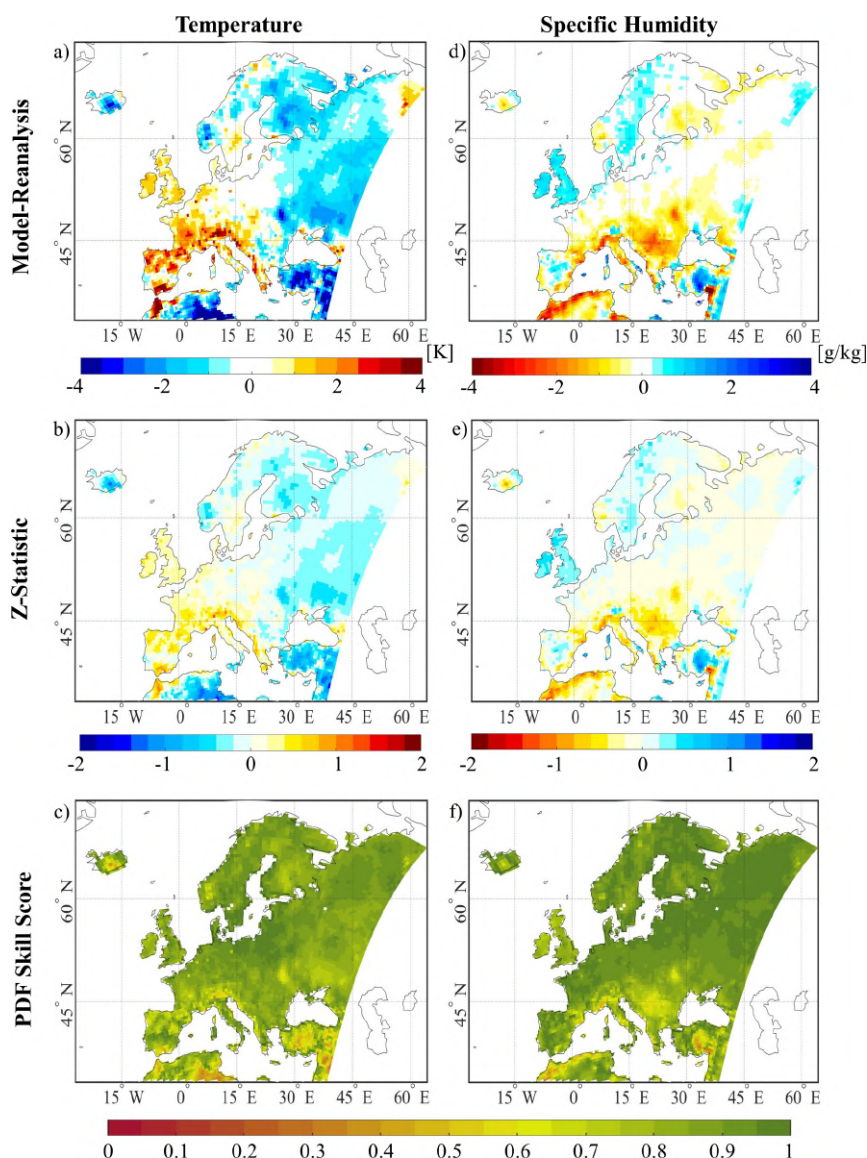


Figure 2. Statistical metrics for comparison of modeled temperature and specific humidity from CTRL with bias-corrected ERA5 reanalysis data (C3S, 2020). Panel (a) shows the value of a Z statistic comparing the temporal distribution of modeled temperature with reanalysis; panel (b) shows the PDF skill score as a second measure to compare the temporal distribution of modeled temperature with reanalysis. Panels (c, d) are the same as (a, b) but for specific humidity.

duced potential coupling days by about 5 %, whereas warmer and moister conditions increased the frequency of nAC days by 3 %–5 %.

Analyzing the cases with individual modifications in temperature and moisture was used to disentangle their respective impacts on different coupling variables. Isolated temperature changes primarily influenced the coupling strength in northern Europe, where lower temperatures weaken the coupling over energy-limited regions – such as Scandinavia and over the East European Plain. This happened as a conse-

quence of more early morning profiles showing stable conditions. Conversely, a warming initiated a strengthening of the coupling (Fig. 5h). The impact was smaller in southern Europe, and it switched sign. Lower temperatures reduced the humidity deficit, and thus decreased the amount of days during which a low atmospheric moisture content inhibited convective precipitation. Moisture modifications had a larger impact in the south of the domain. While dryer conditions were favorable for the occurrence of coupling days in the north, moister conditions were favorable in the south. The

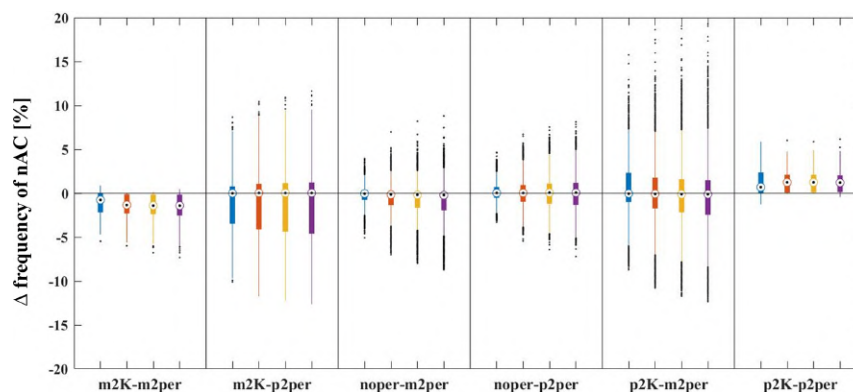


Figure 3. Changes in frequency of non-atmospherically controlled (nAC) days in response to different combinations of temperature and moisture changes in the core modification set. m2K denotes a cooling by 2 K at the surface, p2K a warming of 2 K at the surface, m2per denotes a drying of 2 times the scaling factor, and p2per denotes a moistening of 2 times the respective scaling factor in the domain for different $T - q$ scaling factors. Blue: $5 \% \text{ K}^{-1}$, orange: $7.74 \% \text{ K}^{-1}$, yellow: $8.81 \% \text{ K}^{-1}$, purple: $9.66 \% \text{ K}^{-1}$.

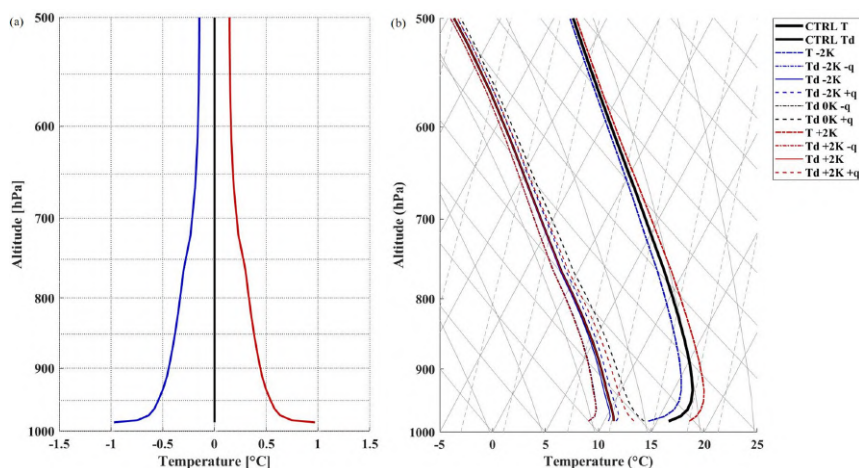


Figure 4. Temperature modification factor derived using a simple linear regression model and extracting the coefficient of determination for each atmospheric layer (a). Profiles of temperature (T) and dew-point temperature (T_d) after modification (b). Red indicates warmer temperature and blue cooler temperatures, and unchanged temperature is denoted in black. Dash-dotted lines indicate a reduction in moisture, solid lines unchanged moisture and dashed lines an increase in moisture.

same spatial patterns occurred when the implemented modifications differed in sign (Fig. 5c and g). Spatial patterns of impacts on the coupling variables were similar, and therefore differences added up, leading to relatively high differences in the frequency of nAC days (Fig. 5c and g) and their partitioning in wet and dry advantages (Fig. 6). Differences in the frequency of nAC days reached up to 10% of the summer days. Nevertheless, following the argument that moisture scales positively with temperature, real-world temperature and moisture impacts are expected to counteract each other, leading to weak net effects.

The partitioning of nAC days experienced some small shifts of up to $\pm 10\%$ between the categories (Fig. 6). The predominance of the wet soil advantage in the north and

of the transition zone around the Black Sea remained unaffected. The spatial patterns of changes in wet soil advantage days closely followed that in nAC days in most modification cases. A change in the partitioning predominantly occurred between wet soil advantage and transition zone days. Drier and warmer conditions increased the frequency of transition zone days relative to the CTRL case, vice versa for moister and cooler conditions. Any modification case initiated a dominant dry soil advantage.

The impact on the long-term classification of coupling regimes did not reflect the changes in nAC days and their partitioning in wet and dry advantages for convection (Fig. 7). Differences to the CTRL case mainly occurred over eastern Europe at the edges of the coupling region, and the predomi-

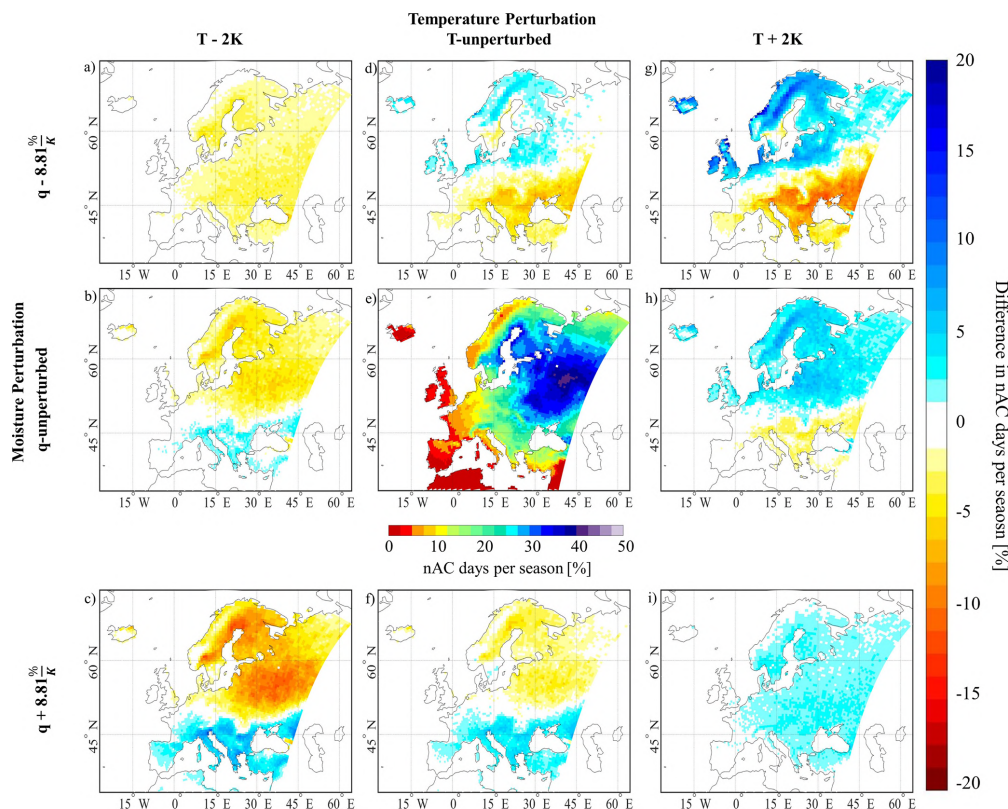


Figure 5. Difference in the seasonal share of non-atmospherically controlled (nAC) days [%] from CTRL for each modification case of the core set. The center image is the CTRL case modified after Jach et al. (2020) (their Fig. 4g). The columns denote the temperature change and the rows the relative change in moisture.

nance for positive feedbacks remained unchanged also in the cases with strong changes in relative humidity. The modifications initiated changes between wet soil advantage levels 1 and 2, as well as transition zone levels 1 and 2. None of the modification cases experienced a considerable shift in location or a change in the predominant sign of feedbacks compared to the CTRL (Figs. 6 and 7).

3.2.2 Sensitivity of the coupling to separated changes in temperature and moisture

This section further examines the relative importance of temperature versus moisture modifications for the variables CTP, HI_{low} , as well as the share of nAC days, wet soil advantage, transition zone and dry soil advantage days in Europe. The sensitivity index as described in Sect. 2.4 was used to estimate the magnitude of the control of temperature and moisture relative to each other for each variable throughout the domain.

The temperature and moisture modifications changed CTP and HI_{low} linearly. Differences in CTP, the stability of the atmospheric layering, were almost solely controlled by modifications of the temperature, as indicated by a sensitivity in-

dex of -1 throughout the domain (not shown). In the case of HI_{low} , the impacts of temperature and moisture modifications were of similar magnitude, though, moisture had a slightly higher impact, indicated by small but positive values. The magnitude of temperature and moisture controls on HI_{low} became more equal in mountainous regions.

The sensitivity index for the share of nAC days in summer showed a clear dipole pattern (Fig. 8a). In northern Europe, the coupling is rather impacted by temperature variations. Temperature controls the coupling by determining the stability of the atmosphere.

In southern Europe, moisture was the controlling factor, and little relative humidity in the low-level ABL limits the occurrence of feedbacks in consequence of limited moisture availability for deep moist convection. The sensitivity index computed for the wet soil advantage showed a similar pattern. Hence, sensitivity of the coupling exhibited a regional dependency to temperature and moisture changes, which hints at humidity- and energy-limited regimes controlling the coupling. The dry soil advantage rarely occurred, but its occurrence is rather controlled by temperature variations in northeastern Europe (Fig. 8d) and by moisture in

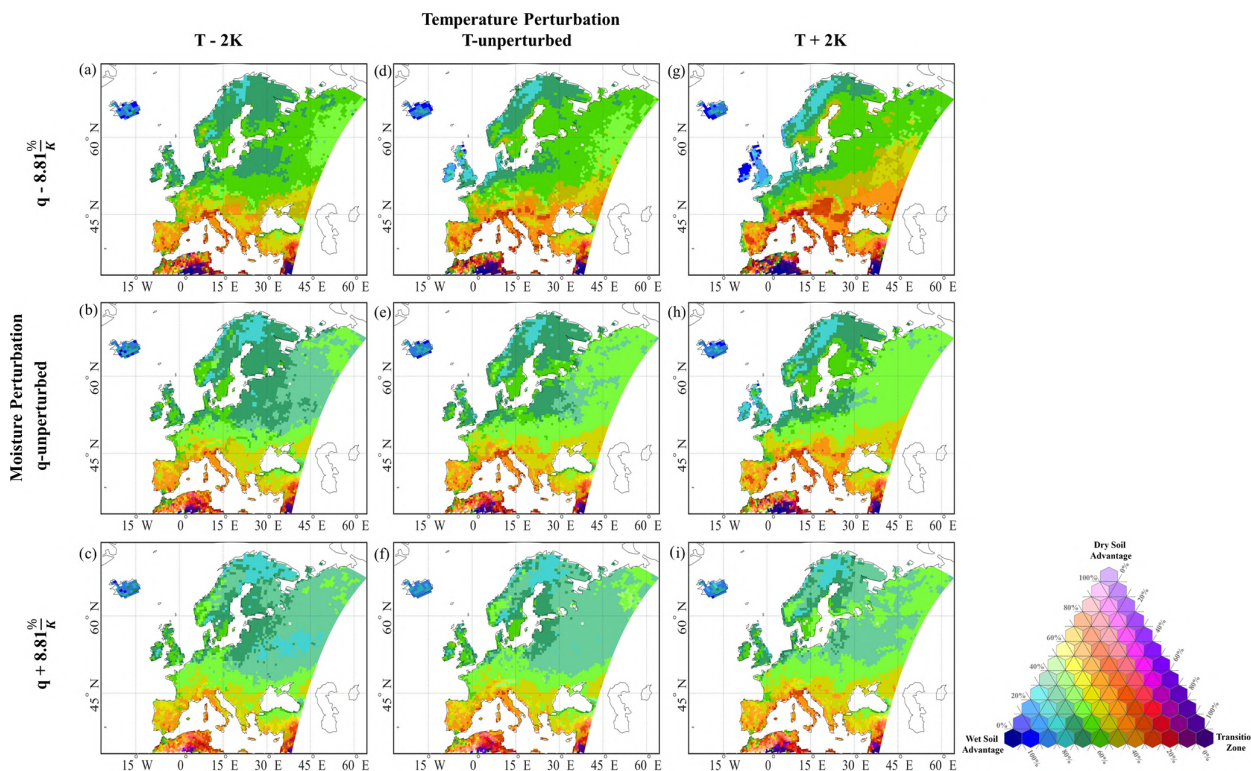


Figure 6. Composition of the non-atmospherically controlled days comprising wet soil advantage, dry soil advantage and transition zone days for all core modification cases. The columns denote the temperature change and the rows the relative change in moisture.

southeastern Europe. The sensitivity of the transition zone shows a complete different pattern. The moisture modifications caused higher differences in the occurrence of transition zone days in the coupling hotspot, while temperature modifications only had a higher impact towards the southwest (Fig. 8c).

3.2.3 Effects of changing temperature and moisture gradients

The following section deals with the analysis of how changes to steeper or less steep temperature and moisture gradients can influence the coupling classification and to compare how such differences can impact the result of the coupling metric. Figure 9 shows the divergence factors for each case which were derived from the temperature difference of the corresponding summer (Table 2) from the climatological mean temperature averaged over the domain. The other subplots show the resulting temperature and dew-point temperature profiles in the lower ABL. For the cases chosen because of their moisture anomaly – namely the dry and the wet cases – the moisture factor was derived by multiplying the T factor with -1 to derive moister conditions in the wet and dryer conditions in the dry case. This was done to circumvent that, in the dry case, a higher temperature would be associated

with an increase in moisture (thus a moistening) of the ABL with positive temperature–moisture relationship. As CTP is almost entirely controlled by the air temperature, this practice only affected HI_{low} .

We first investigated the impact of shifting the temperature and moisture gradients from the CTRL case using the divergence factors of the extreme years (see Sect. 2.3.1). The main impact concerned changes in CTP, since this is an integrated variable. Changes in the temperature gradient moved the lapse rate more toward the dry or moist adiabats, and hence influence the atmospheric stability. The hot and the dry divergence factors increased the early morning temperature gradients between 100–300 hPa above ground, shifting them closer to the dry adiabat, but also enhanced the surface inversion (Fig. 9). This caused an increase in CTP, while the enhancement of the surface inversion, which is likely resulting in a higher convective inhibition, is not accounted for in the framework. In the other three cases (cold, wet, wet_abs), the temperature gradient was decreased between 100–300 hPa a.g.l., consequently decreasing CTP (Fig. 10). The cases diverge in the mean temperature change among each other. Likewise, the temperature inversion decreased in the lower atmospheric layers (Fig. 9). Differences in HI_{low} resulted from both temperature and moisture changes. However, HI_{low} changes were small in most cases (Fig. 10),

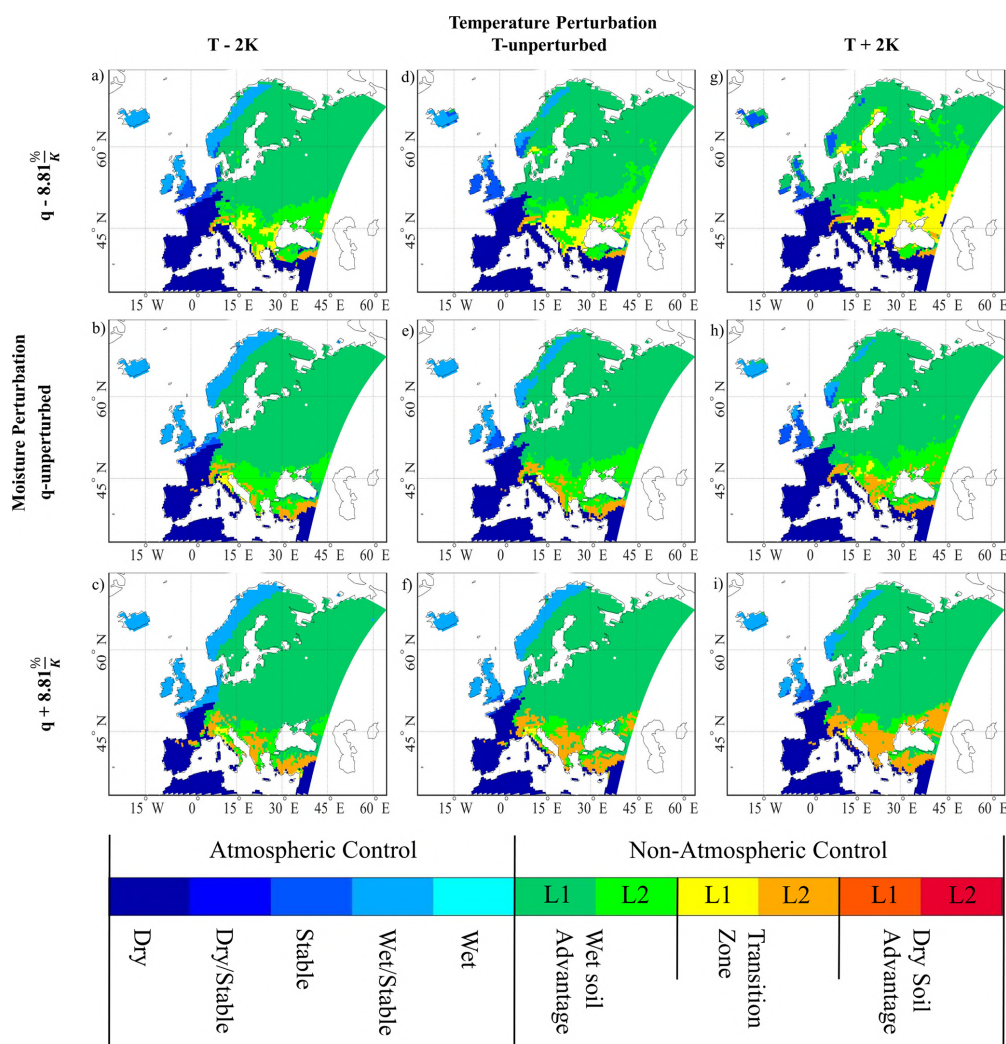


Figure 7. Long-term classification of coupling regimes for the core set modification cases. The columns denote a temperature change and the rows a change in moisture. The center image is the CTRL case and modified after Jach et al. (2020) (their Fig. 3a). The columns denote the temperature change and the rows the relative change in moisture.

because temperature and moisture change simultaneously, which led to small changes in relative humidity. The only considerable exception was the dry case, where the T factor was multiplied by -1 . In this case, HI_{low} increased by about 1°C .

The combination of temperature and moisture changes in each case determines the difference for the share of nAC days (Fig. 11a). The effects are summarized in the following points:

- In the hot case, a higher temperature and temperature gradient between 100–300 hPa a.g.l. was caused with corresponding changes in moisture. These led to greater instability with a constant humidity deficit, which in-

creased the expansion of the hotspot and the fraction of nAC days within the L–A coupling hotspot.

- The dry case involved a larger temperature gradient but less moisture in the atmosphere. A greater instability was combined with a higher humidity deficit, which jointly caused an increase in the fraction of nAC days in summer in the hotspot, but the area of the domain included in the hotspot remained unchanged. Higher humidity deficits reduced the coupling of land surface and convection around the Black Sea but increased the likelihood for convection triggering over wet soils in the north.

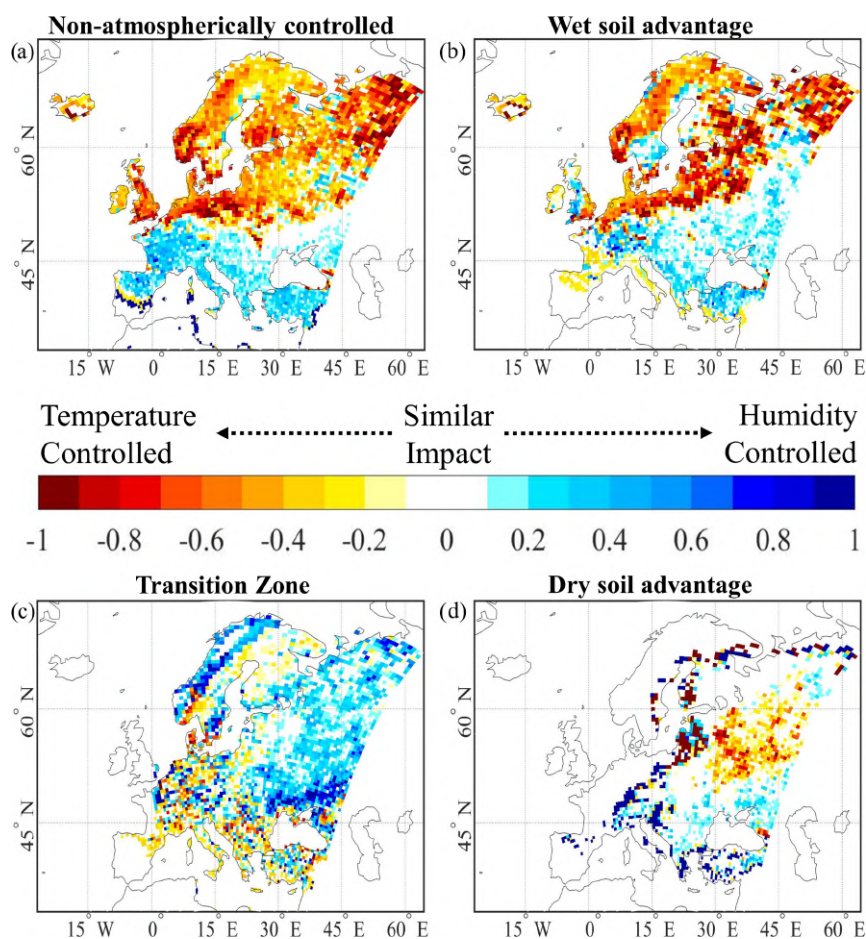


Figure 8. Sensitivity score of (a) non-atmospherically controlled days per summer season, (b) wet soil advantage days per summer season, (c) transition zone days per summer season and (d) dry soil advantage days per summer season to changes individual modifications in the air temperature profile (−1 indicates totally temperature controlled) and specific humidity profiles (1 indicates totally humidity controlled).

- The cold case resulted in a combination of lower temperature, a decrease in the temperature gradient between 100–300 hPa a.g.l. and moisture changes corresponding to $8.81\% \text{ K}^{-1}$, which led to a reduction in the expansion of the hotspot region in the study area and a loss of nAC days.
- The wet_abs and wet cases showed temperature increases but shallower temperature gradients with corresponding changes in moisture, which resulted in minor impacts on the coupling.

Further examination of the differences in the share of the coupling categories shows that the area in wet soil advantage shrinks in all divergence cases (Fig. 11b). Warmer temperatures strengthened the frequency of the wet soil advantage in the hotspot and cooling weakened it. Days in the transition zone experienced the opposite effect (Fig. 11c). However, all combinations of changes in the gradients led to an expan-

sion of the transition-zone-labeled region over land. Though the dry soil advantage never became dominant, which can be seen in the unchanged expansion over land (Fig. 11d), temperature changes still influenced the frequency of days during which negative feedbacks could occur. Similar to the wet soil advantage, higher temperatures increased the frequency of days in dry soil advantage during summer.

3.3 Uncertainty of the coupling regimes

Here, we examine changes in the occurrence of the coupling classes during summer which is based on the daily classification (comp. Fig. 1a), and to which extent the long-term classification, indicating the dominance of a coupling class in a cell, reflects these changes. Under the assumption that the modification cases cover a reasonable spread in atmospheric temperature and moisture for the prevailing climate, it aims at understanding how sensitively the coupling strength and

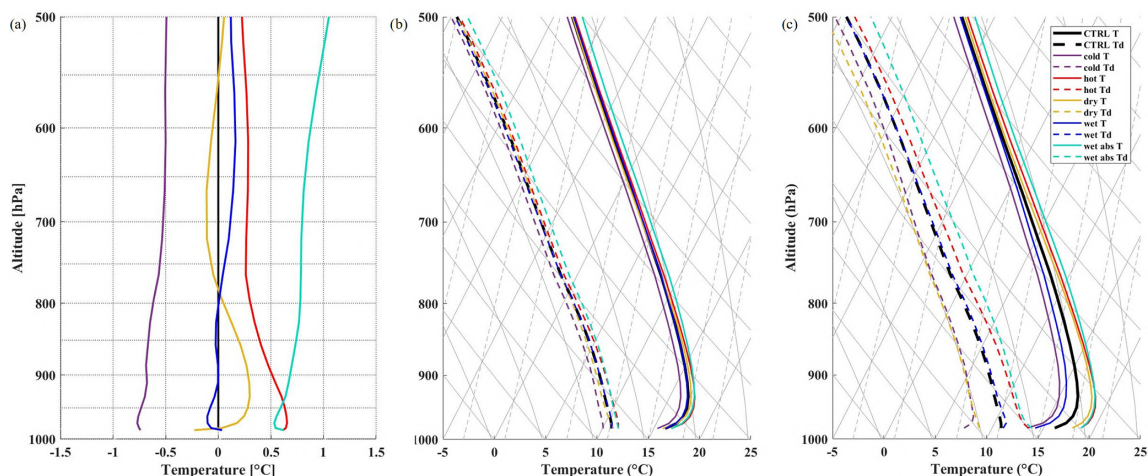


Figure 9. (a) Divergence temperature (T) factors derived from differences of the domain average temperature profiles of the corresponding summers to the 30-year mean (Table 2) which were used to modify daily model output, (b) domain average of T and T_d profiles for the divergence T factors, and (c) their additional modifications with the core T factor. Purple: cold, red: hot, yellow: dry, blue: wet, turquoise: wet abs; solid lines represent temperature and dashed lines represent dew-point temperature.

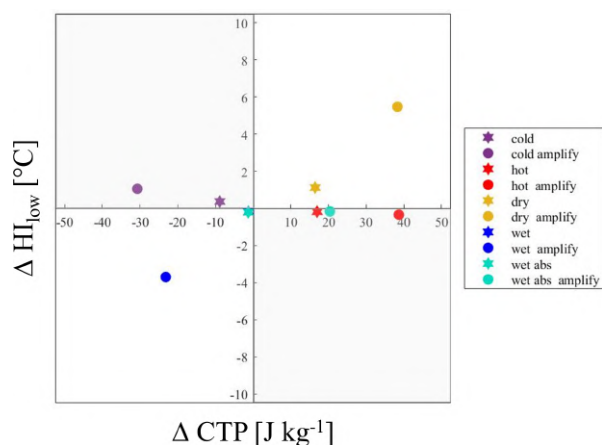


Figure 10. Changes in convective triggering potential (CTP) and low-level humidity index (HI_{low}) due to the divergence factors.

the pre-dominant coupling class respond to temperature and moisture differences within this spread. For this purpose, we first looked at the sensitivity of the long-term regime classification by determining the share of modification cases in which the coupling classification coincided with that of the CTRL case (Fig. 12). A high share as assessed with Eq. (3) indicated high agreement in the classified coupling regimes of the modification cases (red areas), and therefore low sensitivity, while green-to-blue colors indicate weak or no agreement of the modified coupling regimes with that of the CTRL case and therefore high sensitivity. Please note that no agreement also involves changes between a coupling regime in level 1 and level 2. We further quantified the frequency of

occurrence of each coupling regime in the modification cases using Eq. (4) to explore which coupling regimes occurred in the different cases. The Iberian Peninsula, northern Africa and the northeast of Europe showed high agreement in the regime classification of all modification cases and thus low sensitivity to temperature and moisture changes. Over the Iberian Peninsula and over northern Africa, the dry atmospheric controlled regime reliably predominated in all cases, whereas over northeastern Europe, it was reliably classified in one of the nAC coupling regimes (Fig. 13a). In the transition between these two regions there was a belt, where the coupling regime changed on a regular basis. Thus, it appeared to be sensitive to temperature and moisture changes. The absence of several coupling regimes suggests that over Scandinavia, the British Isles and central Europe, the question is whether or not feedbacks occur. When feedbacks occurred, wet soils were in favor (Fig. 13a and b). In southeastern Europe, from the Alps to around the Black Sea, summers were reliably in non-atmospherical control (Fig. 13a), but the dominant coupling regime switched between wet soil advantage and transition zone (Fig. 13b and c). Some cells had an equal share of modification cases in wet soil advantage and transition zone. A dominant dry soil advantage occurred only in single cells and cases over Turkey.

Secondly, we explored differences regarding the occurrence of the different coupling classes within all summer days between the modification cases. This is based on the daily classification of the profiles in CTP- HI_{low} space. The analysis of sensitivity in the long-term coupling regimes allows to distinguish five regions used for a spatial aggregation: (1) pure nAC, where less than two modification cases changed the coupling regime maintaining nAC in nearly

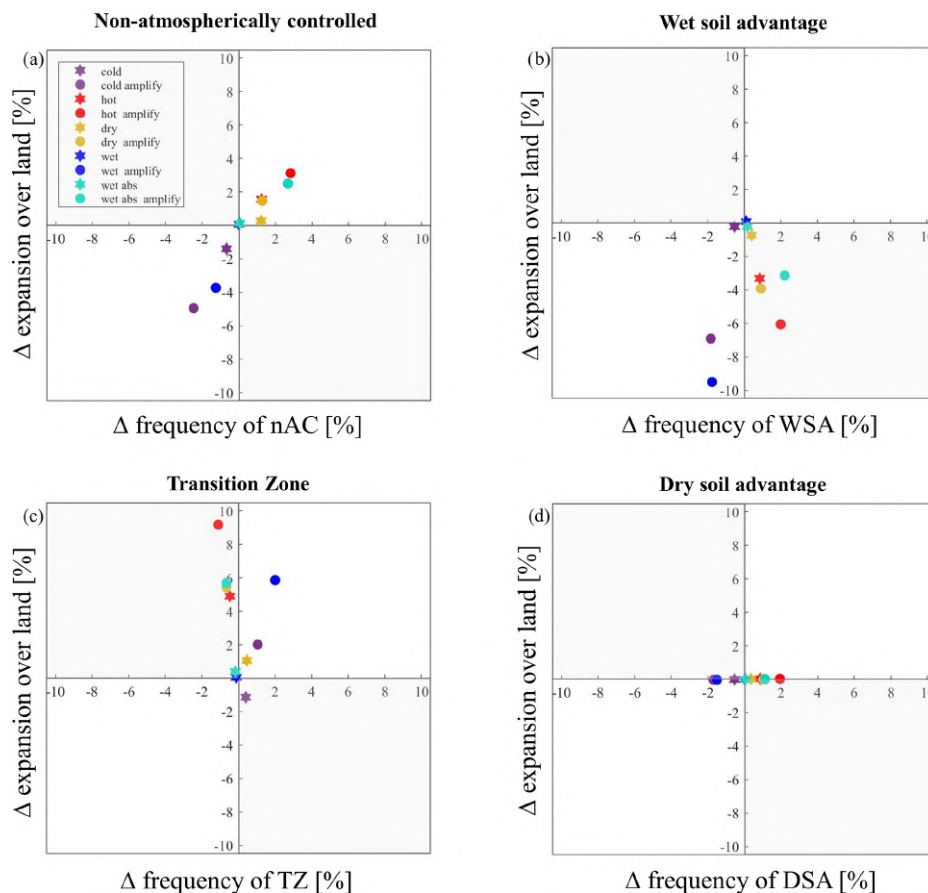


Figure 11. Impacts of the divergence cases on the spatial expansion and the occurrence of the coupling classes in summer for (a) non-atmospherically controlled (nAC) days, (b) wet soil advantage (WSA), (c) transition zone (TZ) and (d) dry soil advantage (DSA). The x axis depicts the changes in the average frequency of occurrence during summer and the y axis shows changes in the fraction of land area covered by the respective coupling regime.

all cases, and (2) pure AC, where less than two modification cases changed the coupling regime maintaining AC in nearly all cases. Further, there are three regions with frequent switches (at least two cases) in the coupling regime. In region (3), the coupling regime changed between any AC class and the wet soil advantage, in region (4) the changes were between AC classes, the wet soil advantage and the transition zone, and in region (5) the changes were between the wet soil advantage and the transition zone. The cell remained in nAC in any of the modification cases. Figure 14 shows the distribution of summer days in the coupling classes for these regions and all cases. Figure 15 further adds sensitivity maps depicting the average dominance of each coupling regime relative to the other coupling classes and their occurrence (given in days) in summer. Hatched areas denote that the number of days in the respective coupling regime varied considerably by more than 10 % of the summer days between the modification cases.

In the pure AC region, the modification cases' impact on the distribution was negligible. Dry AC days dominated, and modifications of temperature and moisture barely influenced the atmospheric pre-conditioning. Considerable variance in the occurrence of coupling days of in part more than 20 % of the summer days occurred mainly in the hotspot region (Figs. 14 and 15d). In the pure nAC region, the number of nAC days ranged on spatial average between 19.2 and 28.5 d per season. The number of wet soil advantage days was relatively stable (ranged between 12.4 and 17.7 d), but the number of transition zone days varied in part considerably (between 4.3 and 11.8 d) with cases showing warming and great relative drying (p2K–m2per, dry amplification) having the most days in transition zone (Figs. 14a and 15b).

As indicated before, the classification was most variable in the WSA–TZ transition region. Similar to the pure nAC region, the number of nAC days varied in spatial average between 15 and 26.1 d between the modification cases (Fig. 15d), but in contrast to the pure nAC region, the num-

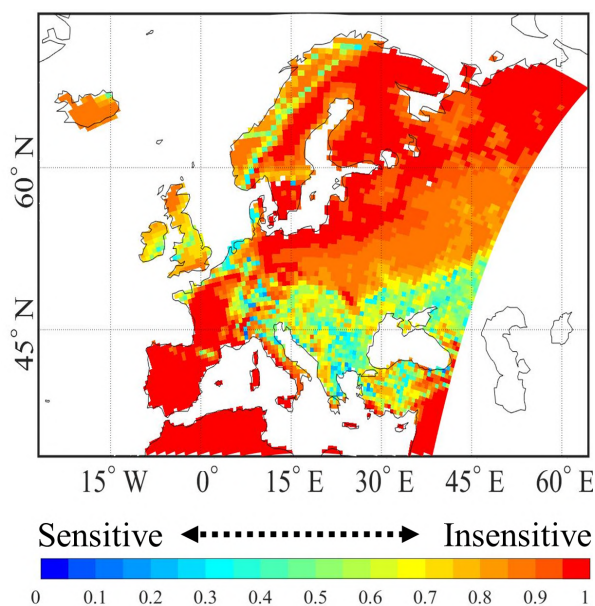


Figure 12. Comparison of modification cases with CTRL from no modification case as CTRL. Red colors indicate that the coupling classification is sensitive to modifications in temperature and moisture, and greenish colors indicate that the coupling classification is insensitive to modifications in temperature and moisture.

ber of days in the transition zone was relatively stable, and the number of days in wet soil advantage varied considerably (between 5.2 and 13.3 d) (Fig. 15a and b). The cases experiencing a strong reduction in relative humidity again showed the strongest shifts in the average occurrence of coupling classes throughout the season, which can be seen in clearly less nAC days and wet soil advantage days compared to the rest of the modification cases. In the AC–WSA transition region, the number of nAC days was at about the threshold of 10 % distinguishing AC and nAC (compare Fig. 1b), and differences in the distribution of coupling classes were usually small. Only the cases experiencing warming combined with great reductions in relative humidity exhibited a considerable impact. These cases experienced a clear increase in wet soil advantage days.

The same analyses were also performed for modification cases with higher temperature modifications between ± 5 K and all combinations of moisture changes, as done in the core modification set (not shown). This slightly enlarged the transition belt between AC and nAC, and increased the region where dominant wet soil advantage or transition zone can occur. Apart from that, the patterns for sensitive regions (Fig. 12) were substantially similar, and the absence of cells in dominant dry soil advantage remained unaffected.

4 Discussion

We modified daily temperature and moisture profiles around local sunrise of 30 summers from a regional climate simulation to examine the sensitivity of land–convection coupling strength to differences in the thermodynamic structure over Europe. The CTP- HI_{low} framework was applied to each of 18 modification cases grouped into two sets, on the one hand, to understand implications of warmer, cooler, moister or dryer atmospheric conditions for the coupling strength, and on the other hand, to investigate the sensitivity of the strong coupling region’s location and the predominant sign of feedbacks within the domain. Analyses of the latter base on the idea that regions lying at the boundaries of two or more categories are particularly sensitive to changes in the atmosphere, as small changes in the pre-conditioning could initiate a different atmospheric response to surface wetness conditions.

Comparing the model’s mean near-surface temperature and moisture as well as their temporal distributions with reanalysis data showed that the model has a dry, warm bias over the southern part of the domain and rather a cold bias with small differences in moisture over the northern part. The differences between the temperature and moisture distributions of model and reanalysis data were statistically insignificant (Ferguson and Wood, 2011). Therefore, the relative frequencies of wet soil advantage, dry soil advantage, transition zone and AC days from the model in summer are assumed to be represented in a realistic range and relation to each other.

Nevertheless, uncertainty in the quantification of the coupling classes’ occurrence arising from model specific biases has to be acknowledged. The cold bias over eastern Europe results from an overestimation of cooler days at the expense of warmer ones, while the tails of the distribution are represented well in the model (not shown). Assuming that cooler days have a more stable atmospheric layering, the cold bias suggests an underestimation of CTP, and, given that the moisture bias in the same region is small, also an underestimation of the humidity deficit. This could hint at an underestimation of the modeled dry soil advantage days but also an overestimation of wet and stable AC days in the corresponding region. In the southern, mostly atmospherically controlled part of the domain, the warm and dry bias suggests an underestimation of the relative humidity and thus and overestimation of HI_{low} . The dry atmospheric conditions were one of the major inhibiting factors for coupling events in the model, which hints at an overestimation of dry AC days in the model. However, the distributions of temperature and moisture diverge more in the southern part; the quantification of potential coupling days has to be treated with caution over the Iberian Peninsula and the Mediterranean.

Studying spatial differences in the impacts of temperature and moisture changes reveals a north–south dipole in the coupling strength’s sensitivity to changes in both variables indicated by a switch in the sign between the northern and the southern parts of the domain. Furthermore, temperature

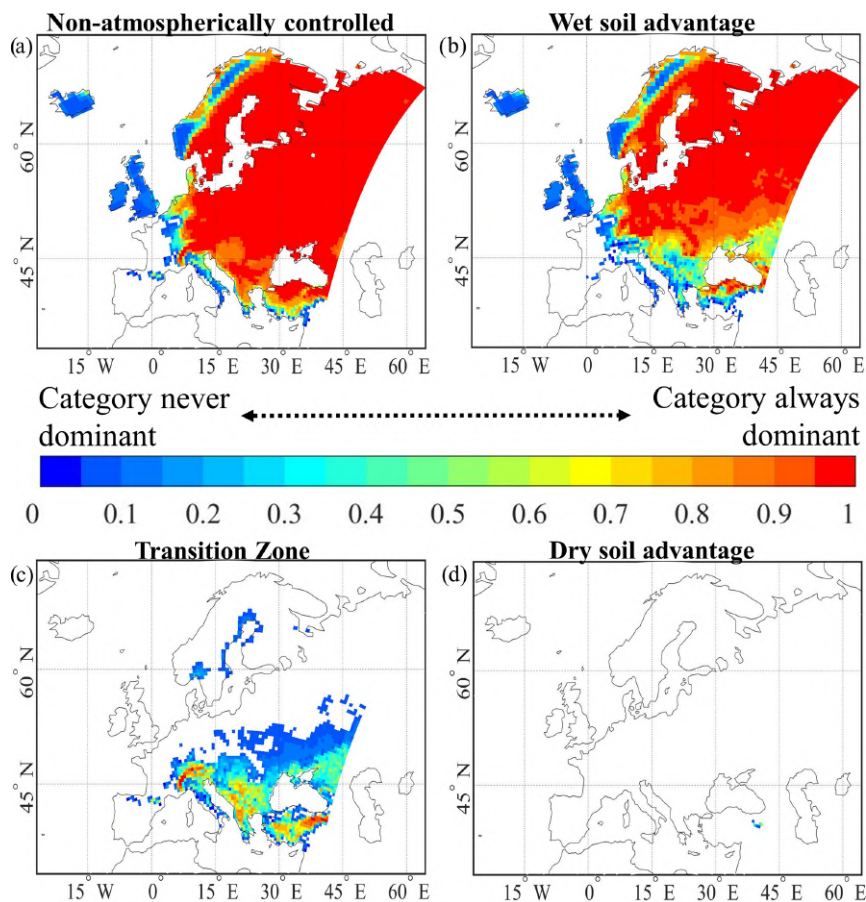


Figure 13. Sensitivity of coupling classes of (a) any coupling class, (b) classified as wet soil advantage level 1 or level 2, (c) classified as transition zone level 1 or level 2, and (d) classified as dry soil advantage level 1 or level 2.

and moisture changes have contrary effects on the coupling strength throughout the domain. This means that simultaneous increases or decreases, respectively, in temperature and moisture have small net effects, and given that atmospheric temperature and moisture are strongly positively correlated in the Northern Hemisphere (e.g., Willett et al., 2010; Bastin et al., 2019), simultaneous changes of the same sign are considered most realistic. A strengthening of the coupling as a result of atmospheric warming is in line with the trend of stronger coupling in consequence of climate change over Europe. Seneviratne et al. (2006) showed the formation and expansion of a transitional region between wet and dry climates over central and eastern Europe in which strong L–A interactions can be expected. Dirmeyer et al. (2013) showed the trend of increasing coupling strength from a global perspective for both the land and the atmospheric segment.

Analyzing the relative importance of temperature versus moisture changes for the coupling strength within the domain suggests that the temperature control on the coupling strength is stronger in northern Europe, in particular that of

coupling days in wet soil advantage (Fig. 8a and b), while moisture variations rather control the coupling strength in southern Europe. Please note that the sign of changes in nAC days and the coupling classes is not sensitive to the choice of the temperature–moisture scaling rate within a tested range of about $\pm 2\% \text{ K}^{-1}$ around the Clausius–Clapeyron rate of $7\% \text{ K}^{-1}$ (Fig. 3). However, the rate does impact the magnitude of changes. In the event of a rate below $7\% \text{ K}^{-1}$, the impact of the respective modification cancels out in the more moisture-controlled south. The areas of temperature and moisture control for nAC days coincide with the energy- and moisture-limited regimes for evapotranspiration over Europe (Knist et al., 2017; Denissen et al., 2020; Seneviratne et al., 2006). Our findings suggest that the energy and moisture limitations further propagate from the land segment of the coupling (connection between soil moisture and surface fluxes) to the atmospheric segment (connection between surface fluxes and boundary layer properties) along the local coupling process chain (Santanello et al., 2018).

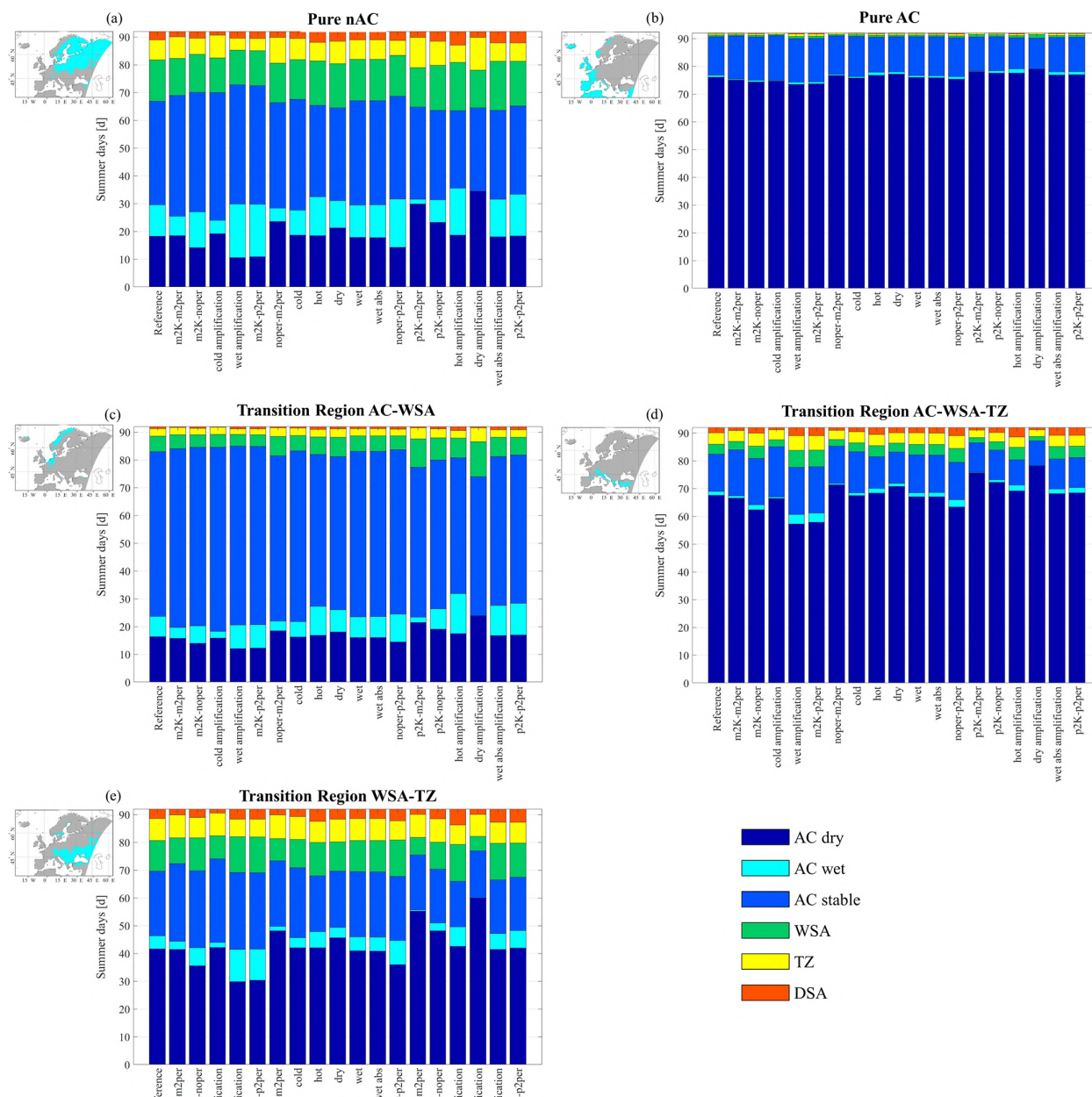


Figure 14. Average distribution of the classes in the daily classification for all modification cases spatially aggregated in (a) cells always in nAC, (b) cells always in AC, (c) cells in which the long-term classification frequently switched between AC and nAC, (d) cells in which the long-term classification frequently switched between wet soil advantage (WSA) and transition zone (TZ).

Differences in the impacts of modified temperature and moisture gradients showed that the consideration of changes in the gradients can be as important for understanding differences in land–convection coupling as the temperature or moisture change itself. Please note that the vertical resolution of the model (40 levels) limits the representation of details in the profiles, and a higher vertical resolution would provide a more accurate estimate of the temperature and moisture gra-

dients (Wakefield et al., 2021). However, while they, on the one hand, showed that lower vertical resolution introduces uncertainty, they also showed that data with limited resolution still provide reasonable results. Thus, the effects of altered gradients are expected to remain substantially similar also with a higher vertical resolution model output. It shows that increasing the temperature gradient, and hence destabilizing the atmosphere, usually increases the number of

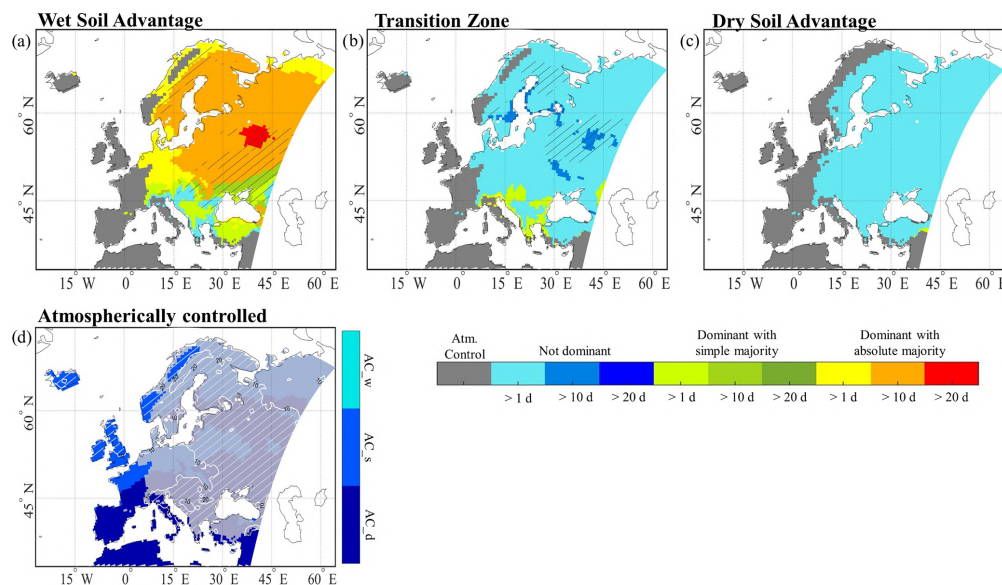


Figure 15. Uncertainty maps of the non-atmospherically controlled classes: (a) wet soil advantage, (b) transition zone and (c) dry soil advantage. The colors indicate whether a class is on average dominant in absolute or simple majority, or whether another class is dominant. The color gradation denotes the average number of days. The hatching indicates that in these regions the variance in the number of days in this class is larger than 10%. Panel (d) shows which atmospherically controlled class dominated in all cases. The hatched area marks the region in which the spread between the modification cases in occurrence of atmospherically controlled days per season is larger than 10%.

nAC days, whereas shallower gradients reduce them. Thus, a warming signal propagating deeply through the atmospheric column (e.g., *wet_abs*, Figs. 10 and 11) leads to a smaller increase in the coupling strength than one that warms only the lower atmospheric levels, resulting in a greater temperature gradient between 100–300 hPa a.g.l. (hot). However, in the latter case, a stronger surface temperature inversion needs to be dissolved by surface lifting, heating or moistening to enable buoyant lifting and deep convection. Inversions potentially reduce ABL growth during mixed layer development and thus inhibit the triggering of deep convection during the subsequent day and hence weaken the coupling again. This effect cannot be represented in the framework, as it does not resolve inversions in about the lowest 1000 m of the ABL. Further, including the energy partitioning at the land surface in the analysis would inform about ABL moistening and heating during the day and in particular the period of mixed layer development. Brogli et al. (2019) projected lapse-rate decreases in consequence of stronger upper-tropospheric than surface warming over Europe by the end of the 21st century, and that the decreases are stronger over northern Europe than over the Mediterranean. Warming and decreasing lapse rates are assumed to have contrary effects on the coupling strength, showing that further research is necessary to understand and quantify impacts of future warming on the L–A coupling strength.

Finally, the reliability of the coupling hotspot as suggested by Jach et al. (2020) was analyzed, at first, by testing the

sensitivity of the daily classification of atmospheric preconditioning in consequence of the modifications, and secondly, by checking whether and how frequently the dominance of a feedback advantage was changed over the 30-year period. We have shown that modifications of temperature and moisture cause considerable differences in both the occurrence of nAC days and their partitioning in the different coupling classes over the strong coupling region throughout the summer season. However, this does not necessarily imply a change in the dominance of a coupling class. There are two regions in which the dominant coupling class is insensitive to changes in the atmospheric structure, wherefore a consistent regime can be expected. On the one hand, the atmospherically controlled southwest and Atlantic coastal areas of Europe remain in atmospheric control in every modification case. Even considerable increases in low-level atmospheric relative humidity did not decrease the humidity deficit to a level in which local surface triggered deep convection can occur on a frequent basis. On the other hand, none of the modification cases reduced the coupling so that the strong positively coupled region over the East European Plain disappeared. Thus, this region is considered a reliable hotspot region for positive feedbacks. Evidence for the location of the hotspot is also found in Koster et al. (2004) or Seneviratne et al. (2006), who investigated hotspots of soil moisture–precipitation coupling in a global model ensemble.

Frequent changes in the coupling regime occur over parts of Scandinavia, Germany and from the Alps to around the

Black Sea. Regime changes are related to two effects or a combination of those. Firstly, the modifications frequently increase the number of nAC days above the threshold to be considered nAC and hence expand the size of the hotspot. This happens at the border between the reliable AC and the strong coupling region. Differences among the modification cases are usually small, which suggests that the effect in reality is small. Secondly, the region from the Alps to around the Black Sea has always enough nAC days to be considered nAC, but the dominant coupling class regularly shifts between the wet soil advantage and transition zone depending on the atmospheric temperature and moisture. The number of wet soil advantage and transition zone days is fairly equal in this region. Differences in temperature and moisture control which class dominates, and hence, following their definition, whether deep convection or shallow convection is more likely. This makes the region particularly interesting for future research on L–A feedback.

It has to be noted that the analysis focused on analyzing differences in the mean and vertical gradients of temperature and moisture to approximate a potentially realistic spread in the atmospheric segment of L–A coupling strength for Europe. The horizontal and temporal distributions were maintained, as the modification factors cannot cover changes in variability which would change the shape of the distributions. However, differences in the temporal distribution are to be expected in consequence of non-linear feedback processes, when a change in the mean temperature and moisture occurs, which can also impact the L–A coupling (Hirsch et al., 2014). Yet, a prediction of changes in the temporal distribution is complex and beyond what can be done with a modification factor. This suggests that further investigation is necessary to understand differences in the temporal distribution of temperature and moisture in the atmosphere and link them to L–A coupling to improve the understanding of modification in the coupling under changing climatic conditions.

5 Summary

By studying the sensitivity of the atmospheric segment of L–A coupling strength to modifications in vertical temperature and moisture during 30 summers over Europe, we have shown that the atmospheric pre-conditioning and the coupling are indeed sensitive to changes in temperature and moisture. However, no combination of temperature and moisture changes relocated or reshaped the coupling hotspot strongly over northeastern and eastern Europe. Differences in the frequency of occurrence of advantageous atmospheric conditions for feedbacks of any kind suggest that uncertainty remains in the accuracy of the coupling strength itself, but stronger coupling relative to the rest of the domain is considered reliable there. Further research including the development of datasets usable for validation or the analy-

sis of L–A coupling in the most recent reanalysis datasets is required for refined approximations of the L–A coupling strength. Furthermore, the predominance of positive feedbacks, meaning convection is preferably triggered over wet soils, was preserved in all cases over the northern part of the coupling hotspot. Therefore, it is predestined for future studies on the impacts of natural and deliberate land surface modifications on the local and regional climate as options for climate change mitigation, as an influence can be expected and the dominant response is certain. This is particularly interesting in light of rising temperatures and the related trend of strengthened L–A coupling under global warming (Dirmeyer et al., 2013; Seneviratne et al., 2006). In the southern part, the coupling classes wet soil advantage and transition zone have an equal share throughout summer, and temperature and moisture modifications cause a switch in the regime in several cases, implying uncertainty in the dominant coupling regime. This makes the region particularly interesting for further studies on L–A coupling, because small changes in the atmospheric conditions may lead to a different atmospheric response. Additionally, the understanding and improved representation of these feedback processes in regional climate models are expected to reduce uncertainties in summer precipitation predictions in climate projections. Especially, the parameterization of convective precipitation has been shown to introduce uncertainties and more advanced triggering mechanisms for convection may lead to an improvement of precipitation predictions (Chen et al., 2017).

Finally, process-based coupling studies still face a substantial lack of spatially comprehensive data covering the vertical structure of the ABL on the regional scale and hence the reliance on model data. Efforts of creating a network of coordinated continuous long-term measurements such as the GLAFO initiative (Wulfmeyer et al., 2020) are required to close the gap and provide a validation basis for modeling-based studies. The modeling-based studies, in turn, are confronted with data storage and computation limitations, which currently leads to the practice of storing 3-D fields only with a limited number of vertical levels. The trend of increasing complexity of atmospheric models, higher temporal and spatial resolutions, as well as spatial and temporal coverage of simulations strongly exacerbates storage limitations. Though single model studies are limited in their generalizability as, e.g., the choice of parameterizations or lateral boundary conditions cause uncertainty in coupling assessments, it is unlikely that comprehensive model ensemble studies will become feasible on the regional scale in the short and medium terms. Therefore, we consider this modification approach as a valuable alternative to study the sensitivity of the atmospheric segment of L–A coupling providing evidence for the location of a L–A coupling hotspot and a range for potential coupling strength under current climatic conditions.

Data availability. The model results are available on the CERA database of the DKRZ (http://cera-www.dkrz.de/WDCC/ui/Compact.jsp?acronym=DKRZ_LTA_1140_ds00005; Jach et al. 2021). The bias-corrected reanalysis data are available through the C3S platform and were downloaded in October 2020 (<https://doi.org/10.24381/CDS.20D54E34>; C3S, 2020).

Supplement. The supplement related to this article is available online at: <https://doi.org/10.5194/esd-13-109-2022-supplement>.

Author contributions. LJ performed the simulations and did the analysis. LJ and TS designed the analysis. LJ prepared the manuscript with contributions from all co-authors.

Competing interests. The contact author has declared that neither they nor their co-authors have any competing interests.

Disclaimer. Publisher’s note: Copernicus Publications remains neutral with regard to jurisdictional claims in published maps and institutional affiliations.

Acknowledgements. We thank two anonymous reviewers for their comments and helpful remarks on the manuscript. This work was completed in part with the CSL High-Performance Storage System provided by Computational Science Lab at the University of Hohenheim, and we acknowledge support by the state of Baden-Württemberg through bwHPC.

Financial support. The research of this study was funded by the Anton and Petra Ehrmann-Stiftung Research Training Group “Water-People-Agriculture”.

Review statement. This paper was edited by Gabriele Messori and reviewed by two anonymous referees.

References

- Bastin, S., Drobinski, P., Chiriaco, M., Bock, O., Roehrig, R., Gallardo, C., Conte, D., Domínguez Alonso, M., Li, L., Lionello, P., and Parracho, A. C.: Impact of humidity biases on light precipitation occurrence: observations versus simulations, *Atmos. Chem. Phys.*, 19, 1471–1490, <https://doi.org/10.5194/acp-19-1471-2019>, 2019.
- Baur, F., Keil, C., and Craig, G. C.: Soil moisture–precipitation coupling over Central Europe: Interactions between surface anomalies at different scales and the dynamical implication, *Q. J. Roy. Meteorol. Soc.*, 144, 2863–2875, <https://doi.org/10.1002/qj.3415>, 2018.
- Berg, A., Findell, K., Lintner, B. R., Gentine, P., and Kerr, C.: Precipitation Sensitivity to Surface Heat Fluxes over North America in Reanalysis and Model Data, *J. Hydrometeorol.*, 14, 722–743, <https://doi.org/10.1175/JHM-D-12-0111.1>, 2013.
- Branch, O. and Wulfmeyer, V.: Deliberate enhancement of rainfall using desert plantations, *P. Natl. Acad. Sci. USA*, 116, 201904754, <https://doi.org/10.1073/pnas.1904754116>, 2019.
- Brogli, R., Kröner, N., Sørland, S. L., Lüthi, D., and Schär, C.: The Role of Hadley Circulation and Lapse-Rate Changes for the Future European Summer Climate, *J. Climate*, 32, 385–404, <https://doi.org/10.1175/JCLI-D-18-0431.1>, 2019.
- Chen, L., Dirmeyer, P. A., Tawfik, A., and Lawrence, D. M.: Sensitivities of Land Cover–Precipitation Feedback to Convective Triggering, *J. Hydrometeorol.*, 18, 2265–2283, <https://doi.org/10.1175/JHM-D-17-0011.1>, 2017.
- Comer, R. E. and Best, M. J.: Revisiting GLACE: Understanding the Role of the Land Surface in Land–Atmosphere Coupling, *J. Hydrometeorol.*, 13, 1704–1718, <https://doi.org/10.1175/JHM-D-11-0146.1>, 2012.
- C3S: Near surface meteorological variables from 1979 to 2018 derived from bias-corrected reanalysis, C3S [data set], <https://doi.org/10.24381/CDS.20D54E34>, 2020.
- Davin, E. L., Rechid, D., Breil, M., Cardoso, R. M., Coppola, E., Hoffmann, P., Jach, L. L., Katragkou, E., de Noblet-Ducoudré, N., Radtke, K., Raffa, M., Soares, P. M. M., Sofiadis, G., Strada, S., Strandberg, G., Tölle, M. H., Warrach-Sagi, K., and Wulfmeyer, V.: Biogeophysical impacts of forestation in Europe: first results from the LUCAS (Land Use and Climate Across Scales) regional climate model intercomparison, *Earth Syst. Dynam.*, 11, 183–200, <https://doi.org/10.5194/esd-11-183-2020>, 2020.
- Dee, D. P., Uppala, S. M., Simmons, A. J., Berrisford, P., Poli, P., Kobayashi, S., Andrae, U., Balmaseda, M. A., Balsamo, G., Bauer, P., Bechtold, P., Beljaars, A. C. M., van de Berg, L., Bidlot, J., Bormann, N., Delsol, C., Dragani, R., Fuentes, M., Geer, A. J., Haimberger, L., Healy, S. B., Hersbach, H., Hólm, E. V., Isaksen, I., Kållberg, P., Köhler, M., Matricardi, M., McNally, A. P., Monge-Sanz, B. M., Morcrette, J.-J., Park, B.-K., Peubey, C., de Rosnay, P., Tavolato, C., Thépaut, J.-N., and Vitart, F.: The ERA-Interim reanalysis: configuration and performance of the data assimilation system, *Q. J. Roy. Meteorol. Soc.*, 137, 553–597, <https://doi.org/10.1002/qj.828>, 2011.
- Denissen, J. M. C., Teuling, A. J., Reichstein, M., and Orth, R.: Critical Soil Moisture Derived From Satellite Observations Over Europe, *J. Geophys. Res.-Atmos.*, 125, e2019JD031672, <https://doi.org/10.1029/2019JD031672>, 2020.
- Dirmeyer, P. A., Cash, B. A., Kinter, J. L., Stan, C., Jung, T., Marx, L., Towers, P., Wedi, N., Adams, J. M., Altshuler, E. L., Huang, B., Jin, E. K., and Manganello, J.: Evidence for Enhanced Land–Atmosphere Feedback in a Warming Climate, *J. Hydrometeorol.*, 13, 981–995, <https://doi.org/10.1175/JHM-D-11-0104.1>, 2012.
- Dirmeyer, P. A., Jin, Y., Singh, B., and Yan, X.: Trends in Land–Atmosphere Interactions from CMIP5 Simulations, *J. Hydrometeorol.*, 14, 829–849, <https://doi.org/10.1175/JHM-D-12-0107.1>, 2013.
- Dirmeyer, P. A., Wang, Z., Mbuhi, M. J., and Norton, H. E.: Intensified land surface control on boundary layer growth in a changing climate: Dirmeyer et al.: Land-PBL feedback in a changing climate, *Geophys. Res. Lett.*, 41, 1290–1294, <https://doi.org/10.1002/2013GL058826>, 2014.

- Dirmeyer, P. A., Chen, L., Wu, J., Shin, C.-S., Huang, B., Cash, B. A., Bosilovich, M. G., Mahanama, S., Koster, R. D., Santanello, J. A., Ek, M. B., Balsamo, G., Dutra, E., and Lawrence, D. M.: Verification of Land–Atmosphere Coupling in Forecast Models, Reanalyses, and Land Surface Models Using Flux Site Observations, *J. Hydrometeorol.*, 19, 375–392, <https://doi.org/10.1175/JHM-D-17-0152.1>, 2018.
- European Environmental Agency: CORINE Land Cover (CLC) 2006, CRC/TR32 Database (TR32DB), Version 17, Copernicus Land Monitoring Service, Copenhagen, available at: <https://www.eea.europa.eu/data-and-maps/data/clc-2006-raster-3> (last access: 21 January 2022), 2013.
- Ferguson, C. R. and Wood, E. F.: Observed Land–Atmosphere Coupling from Satellite Remote Sensing and Reanalysis, *J. Hydrometeorol.*, 12, 1221–1254, <https://doi.org/10.1175/2011JHM1380.1>, 2011.
- Findell, K. L. and Eltahir, E. A. B.: Atmospheric Controls on Soil Moisture–Boundary Layer Interactions. Part I: Framework Development, *J. Hydrometeorol.*, 4, 552–569, [https://doi.org/10.1175/1525-7541\(2003\)004<0552:ACOSML>2.0.CO;2](https://doi.org/10.1175/1525-7541(2003)004<0552:ACOSML>2.0.CO;2), 2003a.
- Findell, K. L. and Eltahir, E. A. B.: Atmospheric Controls on Soil Moisture–Boundary Layer Interactions. Part II: Feedbacks within the Continental United States, *J. Hydrometeorol.*, 4, 570–583, [https://doi.org/10.1175/1525-7541\(2003\)004<0570:ACOSML>2.0.CO;2](https://doi.org/10.1175/1525-7541(2003)004<0570:ACOSML>2.0.CO;2), 2003b.
- Findell, K. L., Gentine, P., Lintner, B. R., and Kerr, C.: Probability of afternoon precipitation in eastern United States and Mexico enhanced by high evaporation, *Nat. Geosci.*, 4, 434–439, <https://doi.org/10.1038/ngeo1174>, 2011.
- Findell, K. L., Gentine, P., Lintner, B. R., and Guillod, B. P.: Data Length Requirements for Observational Estimates of Land–Atmosphere Coupling Strength, *J. Hydrometeorol.*, 16, 1615–1635, <https://doi.org/10.1175/JHM-D-14-0131.1>, 2015.
- Gentine, P., Holtslag, A. A. M., D’Andrea, F., and Ek, M.: Surface and Atmospheric Controls on the Onset of Moist Convection over Land, *J. Hydrometeorol.*, 14, 1443–1462, <https://doi.org/10.1175/JHM-D-12-0137.1>, 2013.
- Guo, Z. and Dirmeyer, P. A.: Interannual Variability of Land–Atmosphere Coupling Strength, *J. Hydrometeorol.*, 14, 1636–1646, <https://doi.org/10.1175/JHM-D-12-0171.1>, 2013.
- Guo, Z., Dirmeyer, P. A., Koster, R. D., Sud, Y. C., Bonan, G., Oleson, K. W., Chan, E., Versegny, D., Cox, P., Gordon, C. T., McGregor, J. L., Kanae, S., Kowalczyk, E., Lawrence, D., Liu, P., Mocko, D., Lu, C.-H., Mitchell, K., Malyshev, S., McAvaney, B., Oki, T., Yamada, T., Pitman, A., Taylor, C. M., Vasic, R., and Xue, Y.: GLACE: The Global Land–Atmosphere Coupling Experiment. Part II: Analysis, *J. Hydrometeorol.*, 7, 611–625, <https://doi.org/10.1175/JHM511.1>, 2006.
- Hirsch, A. L., Pitman, A. J., and Kala, J.: The role of land cover change in modulating the soil moisture–temperature land–atmosphere coupling strength over Australia, *Geophys. Res. Lett.*, 41, 5883–5890, <https://doi.org/10.1002/2014GL061179>, 2014.
- Hohenegger, C., Brockhaus, P., Bretherton, C. S., and Schär, C.: The Soil Moisture–Precipitation Feedback in Simulations with Explicit and Parameterized Convection, *J. Climate*, 22, 5003–5020, <https://doi.org/10.1175/2009JCLI2604.1>, 2009.
- Iacono, M. J., Delamere, J. S., Mlawer, E. J., Shephard, M. W., Clough, S. A., and Collins, W. D.: Radiative forcing by long-lived greenhouse gases: Calculations with the AER radiative transfer models, *J. Geophys. Res.-Atmos.*, 113, D13103, <https://doi.org/10.1029/2008JD009944>, 2008.
- Jach, L., Warrach-Sagi, K., Ingwersen, J., Kaas, E., and Wulfmeyer, V.: Land Cover Impacts on Land–Atmosphere Coupling Strength in Climate Simulations With WRF Over Europe, *J. Geophys. Res.-Atmos.*, 125, e2019JD031989, <https://doi.org/10.1029/2019JD031989>, 2020.
- Jach, L., Warrach-Sagi, K., and Wulfmeyer, V.: FPS LUCAS EUR-44 UHOH ECMWF-ERAINT WRF381, DOKU at DKRZ [data set], available at: http://cera-www.dkrz.de/WDCC/ui/Compact.jsp?acronym=DKRZ_LTA_1140_ds00005 (last access: 21 January 2022), 2021.
- Jacob, D., Teichmann, C., Sobolowski, S., Katragkou, E., Anders, I., Belda, M., Benestad, R., Boberg, F., Buonomo, E., Cardoso, R. M., Casanueva, A., Christensen, O. B., Christensen, J. H., Coppola, E., De Cruz, L., Davin, E. L., Dobler, A., Domingues, M., Fealy, R., Fernandez, J., Gaertner, M. A., García-Díez, M., Giorgi, F., Gobiet, A., Goergen, K., Gómez-Navarro, J. J., González Alemán, J. J., Gutiérrez, C., Gutiérrez, J. M., Güttler, I., Haensler, A., Halenka, T., Jerez, S., Jiménez-Guerrero, P., Jones, R. G., Keuler, K., Kjellström, E., Knist, S., Kotlarski, S., Maraun, D., van Meijgaard, E., Mercogliano, P., Montávez, J. P., Navarra, A., Nikulin, G., de Noblet-Decoudré, N., Panitz, H.-J., Pfeifer, S., Piazza, M., Pichelli, E., Pietikäinen, J.-P., Prein, A. F., Preuschmann, S., Rechid, D., Rockel, B., Romera, R., Sánchez, E., Sieck, K., Soares, P. M. M., Somot, S., Snec, L., Sørland, S. L., Termonia, P., Truhetz, H., Vaudard, R., Warrach-Sagi, K., and Wulfmeyer, V.: Regional climate downscaling over Europe: perspectives from the EURO-CORDEX community, *Reg. Clim. Change*, 20, 51, <https://doi.org/10.1007/s10113-020-01606-9>, 2020.
- Jaeger, E. B. and Seneviratne, S. I.: Impact of soil moisture–atmosphere coupling on European climate extremes and trends in a regional climate model, *Clim. Dynam.*, 36, 1919–1939, <https://doi.org/10.1007/s00382-010-0780-8>, 2011.
- Kain, J. S.: The Kain–Fritsch Convective Parameterization: An Update, *J. Appl. Meteorol. Clim.*, 43, 170–181, [https://doi.org/10.1175/1520-0450\(2004\)043<0170:TKCPAU>2.0.CO;2](https://doi.org/10.1175/1520-0450(2004)043<0170:TKCPAU>2.0.CO;2), 2004.
- Knist, S., Goergen, K., Buonomo, E., Christensen, O. B., Colette, A., Cardoso, R. M., Fealy, R., Fernández, J., García-Díez, M., Jacob, D., Kartsios, S., Katragkou, E., Keuler, K., Mayer, S., van Meijgaard, E., Nikulin, G., Soares, P. M. M., Sobolowski, S., Szepszo, G., Teichmann, C., Vautard, R., Warrach-Sagi, K., Wulfmeyer, V., and Simmer, C.: Land–atmosphere coupling in EURO-CORDEX evaluation experiments: Land–Atmosphere Coupling in EURO-CORDEX, *J. Geophys. Res.-Atmos.*, 122, 79–103, <https://doi.org/10.1002/2016JD025476>, 2017.
- Knist, S., Goergen, K., and Simmer, C.: Effects of land surface inhomogeneity on convection-permitting WRF simulations over central Europe, *Meteorol. Atmos. Phys.*, 132, 53–69, <https://doi.org/10.1007/s00703-019-00671-y>, 2020.
- Koster, R. D., Dirmeyer, P., Guo, Z., Bonan, G., Chan, E., Cox, P., Gordon, C. T., Kanae, S., Kowalczyk, E., Lawrence, D., Liu, P., Lu, C.-H., Malyshev, S., McAvaney, B., Mitchell, K., Mocko, D., Oki, T., Oleson, K., Pitman, A., Sud, Y. C., Taylor, C. M.,

- Verseghy, D., Vasic, R., Xue, Y., and Yamada, T.: Regions of Strong Coupling Between Soil Moisture and Precipitation, *Science*, 305, 1138–1140, <https://doi.org/10.1126/science.1100217>, 2004.
- Koster, R. D., Sud, Y. C., Guo, Z., Dirmeyer, P. A., Bonan, G., Oleson, K. W., Chan, E., Verseghy, D., Cox, P., Davies, H., Kowalczyk, E., Gordon, C. T., Kanae, S., Lawrence, D., Liu, P., Mocko, D., Lu, C.-H., Mitchell, K., Malyshev, S., McAvaney, B., Oki, T., Yamada, T., Pitman, A., Taylor, C. M., Vasic, R., and Xue, Y.: GLACE: The Global Land-Atmosphere Coupling Experiment. Part I: Overview, *J. Hydrometeorol.*, 7, 590–610, <https://doi.org/10.1175/JHM510.1>, 2006.
- Koster, R. D., Mahanama, S. P. P., Yamada, T. J., Balsamo, G., Berg, A. A., Boisserie, C., Dirmeyer, P. A., Doblas-Reyes, F. J., Drewwitt, G., Gordon, C. T., Guo, Z., Jeong, J.-H., Lee, W.-S., Li, Z., Luo, L., Malyshev, S., Merryfield, W. J., Seneviratne, S. I., Stanelle, T., van den Hurk, B. J. J. M., Vitart, F., and Wood, E. F.: The Second Phase of the Global Land-Atmosphere Coupling Experiment: Soil Moisture Contributions to Subseasonal Forecast Skill, *J. Hydrometeorol.*, 12, 805–822, <https://doi.org/10.1175/1175JHM1365.1>, 2011.
- Kotlarski, S., Keuler, K., Christensen, O. B., Colette, A., Déqué, M., Gobiet, A., Goergen, K., Jacob, D., Lüthi, D., van Meijgaard, E., Nikulin, G., Schär, C., Teichmann, C., Vautard, R., Warrach-Sagi, K., and Wulfmeyer, V.: Regional climate modeling on European scales: a joint standard evaluation of the EURO-CORDEX RCM ensemble, *Geosci. Model Dev.*, 7, 1297–1333, <https://doi.org/10.5194/gmd-7-1297-2014>, 2014.
- Laguë, M. M., Bonan, G. B., and Swann, A. L. S.: Separating the Impact of Individual Land Surface Properties on the Terrestrial Surface Energy Budget in both the Coupled and Uncoupled Land-Atmosphere System, *J. Climate*, 32, 5725–5744, <https://doi.org/10.1175/JCLI-D-18-0812.1>, 2019.
- Lorenz, R., Davin, E. L., and Seneviratne, S. I.: Modeling land-climate coupling in Europe: Impact of land surface representation on climate variability and extremes: Land-Climate Coupling In Europe, *J. Geophys. Res.*, 117, D20109, <https://doi.org/10.1029/2012JD017755>, 2012.
- Lorenz, R., Pitman, A. J., Hirsch, A. L., and Sribnovsky, J.: Intraseasonal versus Interannual Measures of Land-Atmosphere Coupling Strength in a Global Climate Model: GLACE-1 versus GLACE-CMIP5 Experiments in ACCESS1.3b, *J. Hydrometeorol.*, 16, 2276–2295, <https://doi.org/10.1175/JHM-D-14-0206.1>, 2015.
- Milovac, J., Ingwersen, J., and Warrach-Sagi, K.: Soil texture forcing data for the whole world for the Weather Research and Forecasting (WRF) Model of the University of Hohenheim (UHOH) based on the Harmonized World Soil Database (HWSD) at 30 arc-second horizontal resolution, WDC Climate, https://doi.org/10.1594/WDC/WRF_NOAH_HWSD_world_TOP_SOILTYP, 2014.
- Milovac, J., Warrach-Sagi, K., Behrendt, A., Späth, F., Ingwersen, J., and Wulfmeyer, V.: Investigation of PBL schemes combining the WRF model simulations with scanning water vapor differential absorption lidar measurements: WRF Sensitivity to PBL Schemes and LSMs, *J. Geophys. Res.-Atmos.*, 121, 624–649, <https://doi.org/10.1002/2015JD023927>, 2016.
- Miralles, D. G., Gentile, P., Seneviratne, S. I., and Teuling, A. J.: Land-atmospheric feedbacks during droughts and heatwaves: state of the science and current challenges: Land feedbacks during droughts and heatwaves, *Ann. N. Y. Acad. Sci.*, 1436, 19–35, <https://doi.org/10.1111/nyas.13912>, 2019.
- Mlawer, E. J., Taubman, S. J., Brown, P. D., Iacono, M. J., and Clough, S. A.: Radiative transfer for inhomogeneous atmospheres: RRTM, a validated correlated-*k* model for the longwave, *J. Geophys. Res.*, 102, 16663–16682, <https://doi.org/10.1029/97JD00237>, 1997.
- Nakanishi, M. and Niino, H.: Development of an Improved Turbulence Closure Model for the Atmospheric Boundary Layer, *J. Meteorol. Soc. Jpn. Ser. II*, 87, 895–912, <https://doi.org/10.2151/jmsj.87.895>, 2009.
- Niu, G.-Y., Yang, Z.-L., Mitchell, K. E., Chen, F., Ek, M. B., Barlage, M., Kumar, A., Manning, K., Niyogi, D., Rosero, E., Tewari, M., and Xia, Y.: The community Noah land surface model with multiparameterization options (Noah-MP): 1. Model description and evaluation with local-scale measurements, *J. Geophys. Res.-Atmos.*, 116, D12109, <https://doi.org/10.1029/2010JD015139>, 2011.
- Perkins, S. E., Pitman, A. J., Holbrook, N. J., and McAneney, J.: Evaluation of the AR4 Climate Models' Simulated Daily Maximum Temperature, Minimum Temperature, and Precipitation over Australia Using Probability Density Functions, *J. Climate*, 20, 4356–4376, <https://doi.org/10.1175/JCLI4253.1>, 2007.
- Pitman, A. J., de Noblet-Ducoudré, N., Cruz, F. T., Davin, E. L., Bonan, G. B., Brovkin, V., Claussen, M., Delire, C., Ganzeveld, L., Gayler, V., van den Hurk, B. J. J. M., Lawrence, P. J., van der Molen, M. K., Müller, C., Reick, C. H., Seneviratne, S. I., Strengers, B. J., and Voldoire, A.: Uncertainties in climate responses to past land cover change: First results from the LUCID intercomparison study, *Geophys. Res. Lett.*, 36, L14814, <https://doi.org/10.1029/2009GL039076>, 2009.
- Powers, J. G., Klemp, J. B., Skamarock, W. C., Davis, C. A., Dudhia, J., Gill, D. O., Coen, J. L., Gochis, D. J., Ahmadov, R., Peckham, S. E., Grell, G. A., Michalakes, J., Trahan, S., Benjamin, S. G., Alexander, C. R., Dimego, G. J., Wang, W., Schwartz, C. S., Romine, G. S., Liu, Z., Snyder, C., Chen, F., Barlage, M. J., Yu, W., and Duda, M. G.: The Weather Research and Forecasting Model: Overview, System Efforts, and Future Directions, *B. Am. Meteorol. Soc.*, 98, 1717–1737, <https://doi.org/10.1175/BAMS-D-15-00308.1>, 2017.
- Roundy, J. K. and Santanello, J. A.: Utility of Satellite Remote Sensing for Land-Atmosphere Coupling and Drought Metrics, *J. Hydrometeorol.*, 18, 863–877, <https://doi.org/10.1175/JHM-D-16-0171.1>, 2017.
- Roundy, J. K., Ferguson, C. R., and Wood, E. F.: Temporal Variability of Land-Atmosphere Coupling and Its Implications for Drought over the Southeast United States, *J. Hydrometeorol.*, 14, 622–635, <https://doi.org/10.1175/JHM-D-12-090.1>, 2013.
- Santanello, J. A., Peters-Lidard, C. D., Kumar, S. V., Alonge, C., and Tao, W.-K.: A Modeling and Observational Framework for Diagnosing Local Land-Atmosphere Coupling on Diurnal Time Scales, *J. Hydrometeorol.*, 10, 577–599, <https://doi.org/10.1175/2009JHM1066.1>, 2009.
- Santanello, J. A., Peters-Lidard, C. D., and Kumar, S. V.: Diagnosing the Sensitivity of Local Land-Atmosphere Coupling via the Soil Moisture-Boundary Layer Interaction, *J. Hydrometeorol.*, 12, 766–786, <https://doi.org/10.1175/JHM-D-10-05014.1>, 2011.

- Santanello, J. A., Dirmeyer, P. A., Ferguson, C. R., Findell, K. L., Tawfik, A. B., Berg, A., Ek, M., Gentine, P., Guillod, B. P., van Heerwaarden, C., Roundy, J., and Wulfmeyer, V.: Land–Atmosphere Interactions: The LoCo Perspective, *B. Am. Meteorol. Soc.*, 99, 1253–1272, <https://doi.org/10.1175/BAMS-D-17-0001.1>, 2018.
- Santanello Jr., J. A., Lawston, P., Kumar, S., and Dennis, E.: Understanding the Impacts of Soil Moisture Initial Conditions on NWP in the Context of Land–Atmosphere Coupling, *J. Hydrometeorol.*, 20, 793–819, <https://doi.org/10.1175/JHM-D-18-0186.1>, 2019.
- Schumacher, D. L., Keune, J., van Heerwaarden, C. C., Vilà-Guerau de Arellano, J., Teuling, A. J., and Miralles, D. G.: Amplification of mega-heatwaves through heat torrents fuelled by upwind drought, *Nat. Geosci.*, 12, 712–717, <https://doi.org/10.1038/s41561-019-0431-6>, 2019.
- Seneviratne, S. I., Lüthi, D., Litschi, M., and Schär, C.: Land–atmosphere coupling and climate change in Europe, *Nature*, 443, 205–209, <https://doi.org/10.1038/nature05095>, 2006.
- Skamarock, W., Klemp, J., Dudhia, J., Gill, D., Barker, D., Wang, W., Huang, X.-Y., and Duda, M.: A Description of the Advanced Research WRF Version 3, UCAR/NCAR, <https://doi.org/10.5065/D68S4MVH>, 2008.
- Späth, F., Wulfmeyer, V., Streck, T., and Behrendt, A.: The Land–Atmosphere Feedback Observatory (LAFO): A novel sensor network to improve weather forecasting and climate models, in: EGU General Assembly, 7–12 April 2019, Vienna, Austria, 2019.
- Sun, J. and Pritchard, M. S.: Effects of explicit convection on global land–atmosphere coupling in the superparameterized CAM: Explicit Convection On Global Land–Atmosphere Coupling, *J. Adv. Model. Earth Syst.*, 8, 1248–1269, <https://doi.org/10.1002/2016MS000689>, 2016.
- Sun, J. and Pritchard, M. S.: Effects of Explicit Convection on Land Surface Air Temperature and Land–Atmosphere Coupling in the Thermal Feedback Pathway, *J. Adv. Model. Earth Syst.*, 10, 2376–2392, <https://doi.org/10.1029/2018MS001301>, 2018.
- Taylor, C. M., de Jeu, R. A. M., Guichard, F., Harris, P. P., and Dorigo, W. A.: Afternoon rain more likely over drier soils, *Nature*, 489, 423–426, <https://doi.org/10.1038/nature11377>, 2012.
- Taylor, C. M., Birch, C. E., Parker, D. J., Dixon, N., Guichard, F., Nikulin, G., and Lister, G. M. S.: Modeling soil moisture–precipitation feedback in the Sahel: Importance of spatial scale versus convective parameterization, *Geophys. Res. Lett.*, 40, 6213–6218, <https://doi.org/10.1002/2013GL058511>, 2013.
- Thompson, G., Rasmussen, R. M., and Manning, K.: Explicit Forecasts of Winter Precipitation Using an Improved Bulk Microphysics Scheme. Part I: Description and Sensitivity Analysis, *Mon. Weather Rev.*, 132, 519–542, [https://doi.org/10.1175/1520-0493\(2004\)132<0519:EFOWPU>2.0.CO;2](https://doi.org/10.1175/1520-0493(2004)132<0519:EFOWPU>2.0.CO;2), 2004.
- van Heerwaarden, C. C. and Teuling, A. J.: Disentangling the response of forest and grassland energy exchange to heatwaves under idealized land–atmosphere coupling, *Biogeosciences*, 11, 6159–6171, <https://doi.org/10.5194/bg-11-6159-2014>, 2014.
- Ukkola, A. M., Pitman, A. J., Donat, M. G., De Kauwe, M. G., and Angélic, O.: Evaluating the Contribution of Land–Atmosphere Coupling to Heat Extremes in CMIP5 Models, *Geophys. Res. Lett.*, 45, 9003–9012, <https://doi.org/10.1029/2018GL079102>, 2018.
- Wakefield, R. A., Basara, J. B., Furtado, J. C., Illston, B. G., Ferguson, Craig, R., and Klein, P. M.: A Modified Framework for Quantifying Land–Atmosphere Covariability during Hydrometeorological and Soil Wetness Extremes in Oklahoma, *J. Appl. Meteorol. Clim.*, 58, 1465–1483, <https://doi.org/10.1175/JAMC-D-18-0230.1>, 2019.
- Wakefield, R. A., Turner, D. D., and Basara, J. B.: Evaluation of a land–atmosphere coupling metric computed from a ground-based infrared interferometer, *J. Hydrometeorol.*, 22, 2073–2087, <https://doi.org/10.1175/JHM-D-20-0303.1>, 2021.
- Willett, K. M., Jones, P. D., Thorne, P. W., and Gillett, N. P.: A comparison of large scale changes in surface humidity over land in observations and CMIP3 general circulation models, *Environ. Res. Lett.*, 5, 025210, <https://doi.org/10.1088/1748-9326/5/2/025210>, 2010.
- Wulfmeyer, V., Hardesty, R. M., Turner, D. D., Behrendt, A., Cadeddu, M. P., Di Girolamo, P., Schlüssel, P., Van Baelen, J., and Zus, F.: A review of the remote sensing of lower tropospheric thermodynamic profiles and its indispensable role for the understanding and the simulation of water and energy cycles: Remote Sensing Of Thermodynamic Profiles, *Rev. Geophys.*, 53, 819–895, <https://doi.org/10.1002/2014RG000476>, 2015.
- Wulfmeyer, V., Späth, F., Behrendt, A., Jach, L., Warrach-Sagi, K., Ek, M., Turner, D. D., Senff, C., Ferguson, C. R., Santanello, J., Lee, T. R., Buban, M., and Verhoef, A.: The GEWEX Land–Atmosphere Feedback Observatory (GLAFO), *GEWEX Quarterly*, 30, 6–11, 2020.

Chapter 6

Summary

Coupling between land surface conditions and convectively triggered local precipitation is complex and variable in space and time, which makes it hard to depict in models. The coupling happens on various temporal and spatial scales, and is dependent on the land state in combination with the prevailing thermodynamic and dynamic characteristics of the atmosphere. Land state and spatial heterogeneity thereof determine the rates of surface moistening and heating of the ABL from the surface, and can cause differential heating to trigger local updrafts, respectively. The atmospheric conditions determine on the one hand, the moisture or heat demand of the atmosphere required to reach saturation, and the atmospheric stability. On the other hand, the strength of horizontal and vertical transport in form of wind can dampen or allow local updrafts to occur.

In this dissertation, a combination of sensitivity RCM experiments and a posteriori modifications of the model output were combined with the application of a process-based coupling metric to investigate the long-term mean coupling signal between land surface wetness and the potential to trigger deep convection during the European summer. LULCCs and large-scale changes in the atmospheric thermodynamic characteristics were investigated regarding their potential to modify the long-term coupling strength and the predominant sign of feedbacks. The analyses focused on the summers between 1986-2015. The analyses of the papers were complemented by assessing whether the influence of the pre-conditioning on convection triggering was reflected in the modeled precipitation frequency (Appendix A).

Objective 1: Investigate the influence of extreme LULCC on the coupling between the land surface and convection triggering by comparing the L-A coupling strength of regional climate simulations with different vegetation cover over Europe.

Each vegetation type has characteristic radiative and non-radiative properties which determine the available energy and the turbulent flux partitioning at the land surface in conjunction with the prevailing background climate (Duveiller et al., 2018b). It follows that LULCC change these characteristics, which in consequence, impacts the air temperature, cloud cover, and can modify the circulation (section 2.3.1). However, the impacts of LULCC on L-A coupling strength and local convection triggering are not well understood, yet.

Therefore, the first part of this dissertation (section 4) focused on analyzing the impact of LULCCs on the coupling between surface wetness and convection triggering by conducting sensitivity experiments with extreme LULCCs and comparing the potential coupling strength of the simulations against a reference simulation with realistic land cover. The sensitivity experiments were conducted with the WRF model in version 3.8.1 coupled to the NoahMP land surface model for the period 1986-2015 over the Euro-CORDEX domain and forced with ERA-Interim reanalysis data. The sensitivity cases comprised of a run with entirely afforested land surface, meaning that all vegetation types which were not forest, bare land or ice were set to zero and the forest types were scaled to cover the entire vegetated area. In the second sensitivity case, the vegetated area was converted to grassland. The analyses followed a two-step approach. First, a coupling hot spot was identified applying the CTP- HI_{low} framework and the potential coupling strength was analyzed regarding its magnitude and the changes imposed by modifying the land cover. Second, changes in the cloud cover and covariance of EF and precipitation were analyzed statistically.

The reference simulation showed a potential coupling hot spot over Northeastern Europe, which denotes the greatest frequency of favorable conditions for convection triggering due to surface moistening or heating the ABL. Both afforestation and the transition to grassland initiated considerable modifications of the atmospheric conditions due to the changes in the energy balance, which caused statistically significant differences in the share of nAC-days per season. Using the presented model configuration, afforestation caused warmer conditions and a decrease in the relative humidity, which led to higher instability and an increase in the humidity deficit. The changes of the ABL structure caused a decrease of the coupling strength with greatest impacts over Eastern Europe and the Black

Sea region. Conversely, the transition to grassland initiated a cooling and more moist atmospheric conditions over most of the European continent. The consequent decrease in coupling strength mostly concentrated on Scandinavia and the North of the Eastern European Plain, where the atmosphere was already stable and humid most of the time. The results from both sensitivity experiments point out the LULCC's potential to influence the degree to which the land state is important for locally triggered deep moist convection. Since Davin et al. (2020) and Breil et al. (2020) indicated disagreement in the models' responses in temperature and EF within the LUCAS ensemble, which was already found in other ensemble exercises (e.g. Pitman et al., 2009), the concrete impacts of afforestation or the transition to grassland on the L-A coupling strength are limited in their generalizability. However, despite uncertainty in the exact LULCC impact on coupling strength, which depends on the respective temperature and humidity response of the model, it appears certain that changes in the energy balance coming from LULCCs influence L-A coupling strength by changing the ratio of ABL moistening and heating on a day-to-day basis and by modifying the average ABL structure. These changes occurred predominantly in the hot spot region.

Objective 2: Quantify the impacts of modifying atmospheric temperature and moisture profiles for L-A coupling strength and analyze regional differences in the sign and magnitude of impacts on L-A coupling strength during the European summer months.

Disagreement in the models' temperature responses and the changes in the energy balance within the LUCAS ensemble motivated a more comprehensive and holistic assessment of how modifications of the atmospheric temperature and moisture fields impact L-A coupling over Europe. Additionally, besides LULCC, the climate system contains also other causes for changes in the atmospheric thermodynamic characteristics of the lower ABL. Climate change e.g. causes surface warming, but also warming in the upper troposphere to another degree, which changes the temperature profiles and thus the stability of the atmosphere (Brogli et al., 2019). The analysis of their impacts detached from the cause of temperature and moisture changes allows for a more generalized picture.

For this purpose, a posteriori modifications of the atmospheric temperature and moisture were used to change the respective output fields from the evaluation simulation with WRF-NoahMP before assessing the L-A coupling strength. This approach followed the rationale that temperature and moisture fields can diverge in their mean and variability, and the coupling metric can only assess

these differences without recognizing their cause. The modification cases were set up in two groups. One had the focus on changes in the temperature and moisture means, and the second targeted on the influence of changes in the vertical gradients.

Temperature modifications dominated the impacts on coupling strength over Northern Europe, where stable condition regularly inhibit local coupling. A temperature increase which also increased the gradient, caused a destabilization of the atmosphere and through this an increase in coupling strength. The importance of atmospheric moisture for the strength of L-A interactions increases toward the South, where temperature and moisture jointly control the relative humidity of the lower ABL. The frequency of days with low relative humidity increases, wherefore stronger ABL moistening from the surface (or moistening from advection of moist air which was not studied explicitly here) would be required to trigger convection. Comparing the relative frequency of days with favorable pre-conditioning (nAC-days) between the modification cases revealed that the coupling hot spot with predominantly positive coupling over Eastern Europe appeared insensitive to the modifications, despite considerable variance (> 10% of all summer days) in the frequency of nAC-days. In the South of the hot spot region, the modifications caused changes in the dominant coupling pathway on a frequent basis implying uncertainty in the response of the atmosphere to differently wet surfaces initiated by differences in the atmospheric conditions themselves. Though strong coupling over Eastern Europe appears certain relative to the rest of the continent, uncertainty remains over Central Europe. This was suggested on the one hand, by the variability in coupling strength initiated by temperature and moisture changes, and on the other hand, by the model's warm and dry bias in this region indicating that it underestimates the atmospheric relative humidity, which was the major inhibiting factor for coupling on a frequent basis. Over Iberia and most of Africa, locally triggered deep convection remained limited by the atmospheric (and surface) dryness in all modification cases.

Final Concluding Remarks. The results of this dissertation demonstrate that the strongest local L-A coupling with convection triggering and potentially local precipitation occurs over Eastern and Northeastern Europe, which is in line with previous global scale assessments applying coarser grid increments (Koster et al., 2004; Ferguson and Wood, 2011). The atmospheric conditions inhibiting local coupling were not outweighed in any of the sensitivity tests providing evidence for physical reasoning of a coupling hot spot over Eastern and Northeastern Europe. This conclusion is further supported by the fact that the strongest impacts from LULCC on ABL properties and cloud cover

were imposed in this region, which additionally led to the greatest LULCC influence on variability in coupling strength itself. The finding that temperature and moisture modifications of the same magnitude introduced the largest variability in the frequency of favorable pre-conditioning for convection triggering over Eastern and Northeastern Europe further undermines this conclusion. However, though stronger coupling is a solid feature relative to the rest of the domain, the presented findings also highlight the remaining uncertainty in the exact quantification of the magnitude of coupling strength as it depends on both the implemented land cover and the temperature and moisture fields. Both underlie data set specific inconsistencies which likely influence the magnitude of the coupling. This also implies uncertainty in the spatial extent of the coupling hot spot over Central Europe, as well as in the coupling pathway around the Black Sea shown by the variability in the dominant coupling class found in the sensitivity tests. Furthermore, comparing the patterns of favorable thermodynamic pre-conditioning against that of the relative frequency of weak synoptic forcing (Figure A.1) suggests that the favorable pre-conditioning does not necessarily assert due to dampening wind effects. Thus, further research is warranted which considers the effects of atmospheric dynamics in addition to the thermodynamic characteristics and the land surface wetness. Especially, with regard to analyzing atmospheric dynamics in conjunction with L-A coupling strength or including convective precipitation directly in the analyses, future research would benefit from increasing the model resolution to convection-permitting scale (<4 km grid increment). Higher model resolutions imply a more detailed representation of the land surface including soil moisture distribution, land cover and orographic features (Knist et al., 2020). Additionally, the large-scale flow patterns in the atmosphere can be represented with more detail, which are influenced by the refined representation of the orography (Knist et al., 2020). Convective precipitation events can be treated explicitly, rendering the use of convection parameterizations unnecessary, which was found to be one of the major sources of uncertainty for precipitation (e.g. Warrach-Sagi et al., 2013). The importance of discussing the model resolution in L-A coupling studies was shown e.g by Hohenegger et al. (2009), who found a switch in the feedback sign in their statistical assessment of soil moisture-precipitation feedback between a convection-permitting and non convection-permitting simulation over the Alpine region. However, as Wakefield et al. (2021) demonstrated that lower resolution thermodynamic profiles provide reasonable results for the CTP-HI_{low} framework, and this dissertation focuses on the thermodynamic pre-conditioning for convection triggering excluding the effects of atmospheric dynamics,

the presented findings are assumed to be relatively insensitive to the model resolution. Despite the advantages of an improved representation of the L-A system, raising the model resolution together with the increasing demand for larger ensemble sizes in model intercomparison studies exacerbates the demand for computational resources and data storage space. This pushes against boundaries of current technical feasibility, when analyzing 3D-fields of the atmosphere over a climate period, which is required to receive statistical robustness in the quantification. Thus, careful planning is important not only scientifically, but also with regard to the efficient use of resources.

This dissertation offers advances in understanding the role of vegetation to influence precipitation occurrence and how variability in the atmospheric temperature and moisture fields impact the role of the land surface to trigger deep moist convection locally. The sensitivity experiments with LULCC demonstrate that besides soil moisture, the vegetation cover is a key factor for L-A interactions, and hence, also for a more precise quantification of L-A coupling strength. LULCCs impact whether the land surface predominantly heats or moistens the ABL, wherefore, they can modify the thermodynamic characteristics on the long-term and influence in which ratio the atmosphere is fueled by moisture or heat during each day. This highlights again the importance of an accurate representation of the land cover in models to improve precipitation patterns in seasonal forecasts and climate projections. Together with the connection of the energy balance with the thermodynamic characteristics, disagreements in the LUCAS models' responses in the energy flux partitioning to LULCC suggest also a model dependence in the response of L-A coupling strength. It depends on each models' respective change in the energy balance and how it feeds back to atmospheric temperature and moisture. The a posteriori modifications served to estimate the effects of other combinations of changes in the thermodynamic structure on the coupling strength than simulated with the WRF-NoahMP configuration detached from a concrete LULCC forcing. Further, they covered a realistic range of temperature and moisture conditions for the recent climate over Europe to account for the disagreement in the model responses. These sensitivity assessments revealed a dominant impact from changes in the temperature gradient over Northern Europe, with warmer conditions and stronger gradients increasing the coupling strength, and moisture impacts overweight in controlling the coupling strength over Southern Europe. The areas of predominant temperature and moisture controls on the coupling roughly resemble with the energy- and moisture-limited regimes for ET as identified e.g. by Seneviratne et al. (2010) or Knist et al. (2017). In a nutshell, the findings

advance our understanding on how physical influencing factors in the climate system contribute to the development of local L-A coupling with precipitation considering the thermodynamic aspects of convection triggering, and provides inside into causes for spatial and temporal variability in L-A coupling strength.

Chapter 7

Outlook

This dissertation concentrated on differences in the long-term coupling signal as well as spatial variability therein over a historical climate period. Future analyses could target the investigation of temporal variability in coupling strength from sub-seasonal to interannual time-scales over Europe. This includes analyzing whether links exist between different characteristics of large-scale weather patterns (apart from the strength of synoptic forcing) and systematic anomalies in L-A coupling strength in relation to the long-term mean. The responses of L-A coupling strength to differences in the thermodynamic characteristics (Jach et al., 2022) likely also evolve in the comparison of different summers, which would suggest interannual variability in L-A coupling strength. The analysis could be based on RCM simulations on convection-permitting scale, as they allow for an improved representation of land surface heterogeneities, large-scale flow patterns and precipitation patterns. However, switching to convection-permitting scale necessitates evaluating the effect of different the model resolutions on L-A coupling strength estimates calculated with process-level coupling metrics, beforehand.

Another interesting perspective is the evaluation of impacts from vegetation dynamics on coupling strength in regional climate simulations, which would also benefit from increasing the model resolution as compared to the simulations analyzed here. Warrach-Sagi et al. (2022) showed that the representation of dynamic crop growth and its impact on LAI and root growth leads to enhanced coupling strength between soil moisture, surface fluxes, and ABL conditions as well as more favorable preconditioning for convection compared to a fixed climatology. Simultaneously, its representation reduces the model's temperature bias. Additionally, climate conditions such as moisture availability, temperature or incoming radiation influence vegetation growth in different years. Variability in

the climatic conditions causes differences in LAI, thus impacting ET and the degree of evaporative cooling on an interannual time scale. This in turn influences the atmospheric thermodynamic structure (e.g. Jach et al., 2020) and thus is supposed to impact the development of convective precipitation events. Seneviratne et al. (2006) investigated the impact of dynamic soil moisture against prescribed soil moisture climatologies in regional climate simulations. They showed an increase in coupling strength in the fully coupled model system, compared to runs applying a soil moisture climatology. Almost all state-of-the-art regional climate models use static climatologies for the vegetation variables, neglecting the aforementioned vegetation-climate dynamics. However, it has to be acknowledged that most land surface models cannot represent fully coupled dynamics for the various vegetation types included, yet. Despite that, the results of Warrach-Sagi et al. (2022) suggest a similar response in the coupling strength to that of Seneviratne et al. (2006) when allowing the vegetation to dynamically respond to the climate conditions. This complements with the activities planned for LUCAS phase 2, in which annual LULCCs will be implemented in transient regional climate simulations to investigate their influence on climate.

Appendix A

Excursus: Potential Coupling Strength and Modeled Precipitation Frequency

Following the statement of Dirmeyer et al., [2018b](#), there is

"[...] a robust propagation of useful signal through land surface fluxes, near-surface meteorological states, and boundary layer properties, but largely disappearing at precipitation, implying problems with the convective parameterization."

Feedback mechanisms are usually not explicitly prescribed or parameterized in models, but result implicitly from the complex interactions of processes in parameterization schemes (Koster et al., [2006](#)). Hence, the strength of different relationships can be overestimated or underestimated in models (Dirmeyer et al., [2018a](#)), and as precipitation results from of a complex chain of processes and is calculated in different parameterization schemes influenced by the grid increment, it is particularly likely to suffer from an insufficient representation of L-A feedback processes.

Analyses of the surface influence on convective precipitation over Europe usually either evaluate single convective cases using convection permitting models (Baur et al., [2018](#); Keil et al., [2019](#); Koukoulou et al., [2019](#)) or observations (Wulfmeyer et al., [2011](#)), or applying sensitivity simulations to assess the response of precipitation amount, frequency or intensity to different perturbations of soil moisture (Hohenegger et al., [2009](#); Leutwyler et al., [2021](#)). However, it has rarely been explored which conditions are necessary so that cumulus schemes trigger precipitation, and in which manner surface wetness feedback with triggering convective precipitation are actually represented or not. Thus, the following analyses make use of the information on atmospheric pre-conditioning for local

convection as well as the surface flux partitioning to explore the occurrence of precipitation triggering in the WRF-NoahMP simulation. It examines whether precipitation is triggered under the L-A conditions anticipated with most favorable conditions for convection triggering in the Kain-Fritsch (KF) cumulus scheme (Kain, 2004) which applies a thermodynamically based-trigger function and a CAPE-based convective mass flux closure. The vertical mass-flux is known to react sensitive to relative humidity, particularly with low amounts of CAPE available (Kain and Fritsch, 1990).

To evaluate the model's precipitation representation, firstly, the modeled wet-day frequency was compared to the wet-day frequency from E-OBS (Cornes et al., 2018, version 25.0e). As the coupling metric focuses on the triggering of convection, the analyses were limited to the frequency of precipitation events and leaves out other attributes such as the precipitation amount, its intensity, timing of precipitation occurrence during the day, and the duration. An event was defined as daily accumulated precipitation > 1 mm. This is followed by investigating the frequency of occurrence of precipitation for different combinations of EF and atmospheric pre-conditioning under the aspect of whether the behavior of precipitation meets the assumed behavior of each coupling class with different surface wetness (e.g. more frequent precipitation on wet soil advantage days with high EF than with low EF).

A.1 Wet-day frequency

The modeled frequency of precipitation days was evaluated against that of E-OBS for all summers between 1986-2015 in order to assess whether precipitation occurrence is over- or underestimated in the model. The number of wet-days per season represents the frequency of precipitation occurrences in both datasets. All data were regridded to 0.44° on a regular lat-lon grid using the bilinear interpolation algorithm of the Climate Data Operators (CDO).

Three types of precipitation were compared against each other of which only the total precipitation was compared against E-OBS. The other two served to analyze under which conditions the model triggers precipitation. The three types were: wet-days based on total precipitation, those based on precipitation from the KF cumulus scheme only, and wet-days occurring under high pressure conditions with low pressure gradients (HPA, high pressure area), thus filtering for favorable dynamic conditions. The identification of HPA-precipitation events follows the attribution method

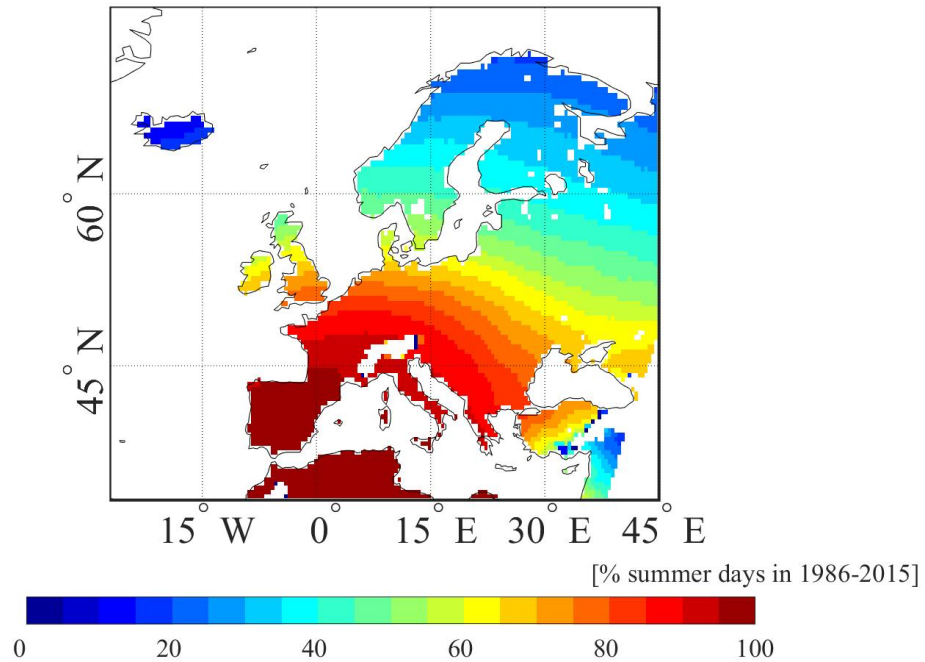


FIGURE A.1: Fraction of summer days under high-pressure conditions with low pressure gradients in the WRF-NoahMP simulation.

of Rüdüsühli et al. (2020) under the premise that convective summer precipitation events typically occur during a high pressure system under weak synoptic forcing. The attribution method uses the geopotential at 850 hPa to filter the total precipitation on an hourly basis before accumulating over each day. A geopotential $> 14500 \text{ m}^2/\text{s}^2$ denotes high-pressure conditions and a pressure gradient below 0.02 m/m denotes weak synoptic forcing. Cells with an average surface pressure below 850 hPa have been masked out, because the criteria from Rüdüsühli et al., 2020 would have required an extrapolation of the geopotential below model topography. HPA-conditions predominantly occurred over Southwestern (up to 100%) and Central Europe (70-90%), and decrease towards the Northeast of Europe (Figure A.1). Precipitation from the cumulus scheme is assumed to include the convective precipitation in its physical sense, but broadly speaking rather represents small-scale precipitation events and thus includes all local precipitation events independent of their trigger. For interpreting the results it is worth to recall that the simulation was conducted on 0.44° resolution. Therefore, on the one hand, precipitation from the cumulus scheme typically constitutes the major share of the total precipitation. On the other hand, horizontal pressure gradients are assumed to be too weak in the model because of the resolution, which can bias the filtering of precipitation events. Please note that the precipitation types are not independent from each other as total precipitation is the sum of

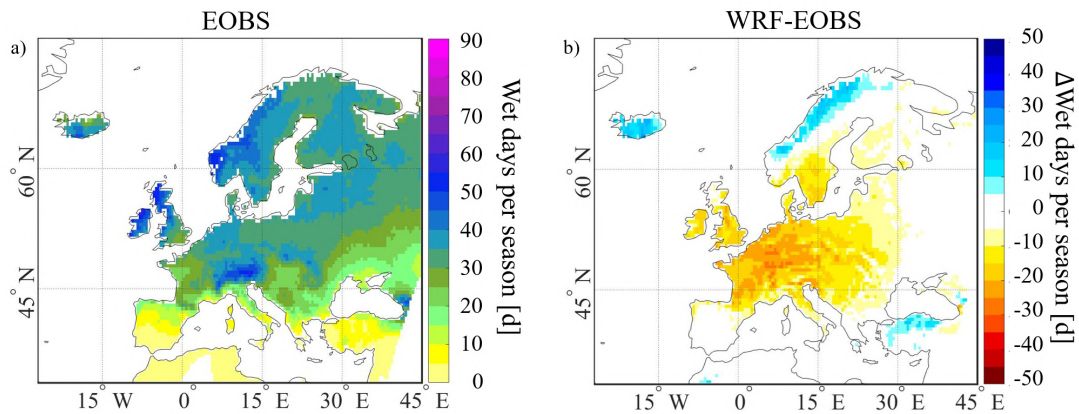


FIGURE A.2: Wet-day frequency per season from a) E-OBS over the period 1986-2015 and b) the bias in wet-day frequency of the WRF-NoahMP evaluation simulation.

precipitation from the convection scheme and the microphysics scheme, and the HPA-precipitation is filtered from the total precipitation. Therefore, issues in the convection scheme will be visible in all types.

The comparison of wet-days from total precipitation between E-OBS and WRF showed an underestimation of the wet-day frequency in the model, particularly over Central Europe (Figure A.2). Most precipitation events in the cumulus scheme occurred over the Northeastern European Plain (Figure A.3) resembling with the patterns of nAC-days (see Jach et al., 2022, their Figure 5e). The share of cumulus scheme precipitation is highest in southern Europe, where it comprises 70-100% of the precipitation events in the study period, while over France, Scandinavia and the coastal regions the fraction decreased to 10-40%.

HPA-precipitation mainly occurred over Central Europe around the Alps and the Carpathian Mountain range (Figure A.3c), matching the patterns from Rüdüsühli et al. (2020) though suggesting a lower share of total precipitation falling under HPA-conditions (Figure A.3d). The lack of precipitation events over Central Europe in all three types of precipitation likely originated from the cumulus parameterization. The area coincided with the region in which the model has a dry and warm bias (see Jach et al., 2022 their Figure 2) and the KF scheme is known to be sensitive to RH at the surface.

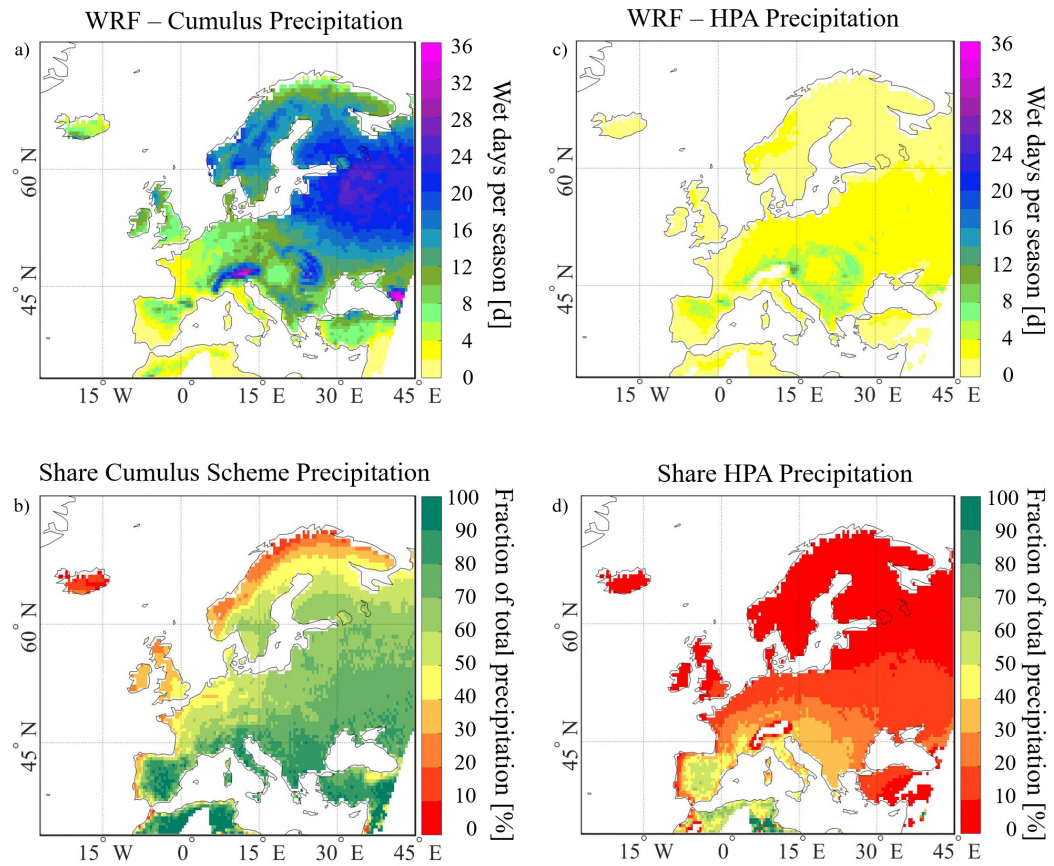


FIGURE A.3: Wet-day frequency per season from a) the Kain-Fritsch cumulus parameterization and b) the fraction of total precipitation originating from the cumulus scheme. c) and d) show the same for the high-pressure area (HPA) precipitation.

A.2 Implications of Precipitation Occurrence on Feedback Representation

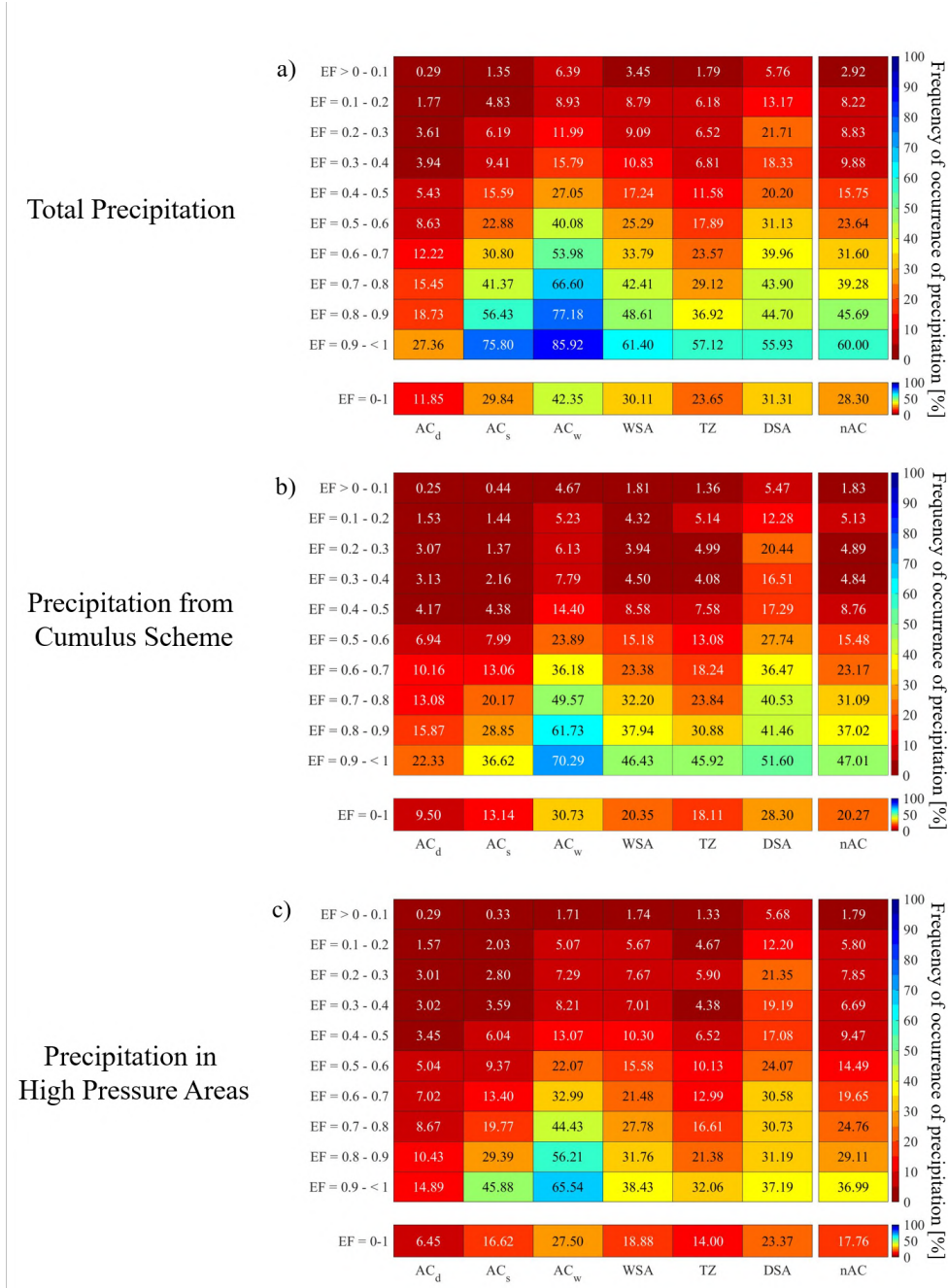


FIGURE A.4: Frequency of precipitation occurrence per evaporative fraction (EF)-pre-conditioning bin for a) the total precipitation b) the cumulus scheme precipitation, and c) high pressure area precipitation. The rows indicate the EF-bins, while the columns depict the different coupling classes. The lowest row contains the frequency of occurrence for each coupling class without considering differences in the EF. The right-most column shows the frequency of occurrence of precipitation for nAC-days, which is the sum of the columns for wet soil advantage, dry soil advantage and transition zones days.

Finally, EF and atmospheric pre-conditioning for convection triggering were used to bin the precipitation events according to the conditions under which they occurred. The aim was to examine under which combination of surface wetness and atmospheric pre-conditioning precipitation occurs most frequently, with and without filtering events under weak synoptic forcing as well as examining cumulus scheme precipitation alone. The triggering mechanism implemented in the KF scheme is based on the thermodynamic characteristics of the atmosphere, wherefore the convective precipitation and the pre-conditioning of convection triggering depend on the same quantities. This has the advantage that one can investigate under which conditions the scheme actually triggers precipitation. Taking into account the anticipated regimes for convective precipitation from the framework gives an indication about the plausibility of the conditions under which convective precipitation occurs in the model.

Binning precipitation data according to the prevailing surface wetness was based on daily mean evaporative fraction. The data were grouped into ten bins with equally sized intervals of 0.1. The daily CTP- HI_{low} classification was used to bin the precipitation events according to the atmospheric pre-conditioning for convection triggering, whereby the atmospherically controlled days were divided into dry AC (CTP > 0 J/kg, HI_{low} > 15°C), wet AC (CTP > 0 J/kg, HI_{low} < 5°C) and stable AC (CTP < 0 J/kg, any HI_{low}).

Figure A.4 depicts the relative frequency of occurrence of precipitation per bin for total precipitation, cumulus scheme precipitation and HPA-precipitation. The bins showed a clear disparity between low and high evaporative fractions, and thus between dry and wet surface conditions. Furthermore, comparing e.g. dry and wet AC-days, which clearly diverge in their humidity deficit, additionally showed the precipitation occurrence's dependence on the atmospheric humidity, as considerably more precipitation occurs with a wet than with a dry atmosphere. The influence of atmospheric stability is not clearly visible in the selected depiction of the frequency of occurrence of precipitation. The difference between total and cumulus scheme precipitation under stable AC conditions suggests that a considerable share of precipitation comes from the microphysics scheme. However, the results also indicate that stable initial conditions do not entirely inhibit cumulus scheme precipitation.

Generally, there occurs a growing frequency of occurrence of precipitation with increasing humidity of land surface and atmosphere irrespective of the pre-conditioning suggesting a generally positive surface wetness-precipitation feedback in the model. This behavior was also found by Cioni and

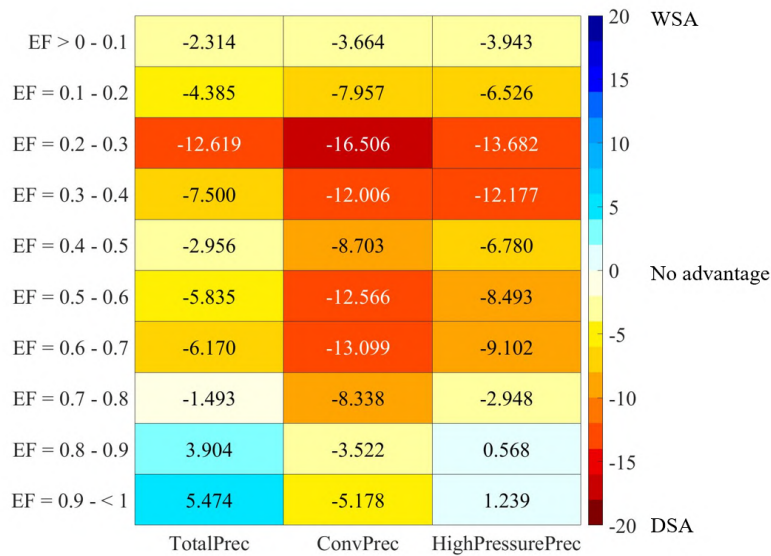


FIGURE A.5: Difference of precipitation occurrence between the wet soil advantage (WSA) and the dry soil advantage (DSA) for all ranges of the evaporative fraction (EF) and all precipitation types.

Hohenegger (2017), who showed a general increase in precipitation frequency and precipitation amount over wetter soils using idealized large-eddy model (LEM) simulations. The simulation were initialized using the original soundings from Findell and Eltahir (2003b). They further showed that deep convection was indeed initialized earlier during wet soil advantage days with wet soils and dry soil advantage days over dry soil, respectively, suggesting wet and dry soil advantages respectively in the timing of precipitation triggering. However, their LEM simulations did not require a cumulus parameterization such as simulations with a grid increment of several ten-kilometers do. The parameterization mainly determines the timing of triggering convection on this scale. Generally positive (spatial) soil moisture-precipitation feedback was also found by Leutwyler et al. (2021) and by Guillod et al. (2015).

Of the nAC-days, transition zone days show fewer precipitation occurrences than days pre-conditioned to favor either wet or dry surface conditions, which matches the definition of transition zone days. This definition says that shallow convection and thus no precipitation is the most likely outcome. Nevertheless, the frequency of occurrence of precipitation increases with higher EF, also for the transition zone days indicating an overall wet soil advantage. Similarly for dry soil advantage days which appears to contradict the rationale of dry soil advantage days from Findell and Eltahir (2003b)

at the first glance.

However, comparing the frequency of occurrence of precipitation of wet soil advantage against that of dry soil advantage for a given range of EF reveals another aspect of the coupling (Figure A.5). For an EF ranging between 0.1 and 0.6, more precipitation occurs with dry soil advantage relative to an atmosphere in wet soil advantage. Only with very high EF (> 0.8), precipitation occurs more frequency with an atmosphere in wet soil advantage than dry soil advantage. This dry soil advantage in the frequency of occurrence of precipitation is visible in total precipitation and even more pronounced in HPA-precipitation, but not in the cumulus precipitation. Differences in the frequency of occurrence of precipitation between wet soil advantage and dry soil advantage remain negative throughout all EF bins, but is most pronounced in the low to intermediate EF-range.

A.3 Discussion

This section aimed at investigating under which combination of L-A conditions precipitation occurred in the WRF-NoahMP simulation. It was examined whether the model reasonably represents a dependence of the precipitation occurrence on the atmospheric pre-conditioning as assessed with the CTP-HI_{low} framework under consideration of the prevailing surface wetness.

The model considerably underestimated the precipitation frequency over Central Europe, where it also has a warm and dry bias in the near-surface meteorological variables. The precipitation bias is weak in other regions. As typically the largest share of precipitation comes from the cumulus parameterization in summer with the applied model resolution, the precipitation bias likely originates there. This theory is also supported by the fact that the KF scheme is known to react sensitive to RH and CAPE (Kain and Fritsch, 1990). It applies a triggering mechanism (activation of the scheme) based on the thermodynamic characteristics of the ABL up to 300 hPA above ground level, and the simulated precipitation amount is the net effect of condensation in the updraft and evaporation of condensate in the downdraft. As the evaporation rate of condensate presumably increases under dry atmospheric condition, which decreases the moisture reaching the ground (becoming visible as precipitation), both the triggering mechanism and the final amount of condensate reaching the surface depend on the prevailing RH in the ABL.

Analyzing the occurrence of precipitation under different surface wetness and initial atmospheric

conditions confirmed that the modeled precipitation frequency is associated with the surface wetness and atmospheric humidity, as most precipitation occurred under wet conditions. However, it has to be noted that this is not enough to establish a physical causal relationship of the surface wetness initiating precipitation, as e.g. morning precipitation would increase EF during the day, but it suggests a dependence in the model system. Furthermore, a high spatial resemblance of the cumulus scheme precipitation and the frequency of favorable conditions for surface triggered precipitation (nAC-days) is rather associated with a co-dependency of nAC-days and cumulus precipitation on the thermodynamic characteristics of the low-level atmosphere. Nevertheless, Cioni and Hohenegger (2017) showed a similar increase in precipitation frequency with higher surface wetness on wet as well as dry soil advantage days in their LEM simulations. Thus, further research in this direction can be promising to advance the understanding of mid-latitude convective precipitation occurrence and its dependence on land surface conditions.

A direct comparison of the wet and dry soil advantage categories (implying intermediate wetness in the atmosphere for all EF-ranges) also reveals a dry soil advantage for low EF ranges and a wet soil advantage for high EF values. The generally higher frequency of cumulus scheme precipitation with dry soil advantage than as wet soil advantage suggests that this behavior arises from the microphysics parameterization. Williams (2019) and Chen et al. (2017) showed that other, more physically based triggering mechanisms lead to an improvement in the representation of surface wetness feedback with precipitation.

Finally, the KF scheme seems to be mostly sensitive to surface wetness and the humidity in the low-level atmosphere, which is largely in line with other studies on soil moisture-precipitation feedback over Europe. However, the scheme does not easily reflect the behavior of wet versus dry soil advantage as anticipated by the framework. In general, the binning allowed for a useful insight in the behavior of the convection scheme and the conditions under which it triggers precipitation. In this regard, it seems a promising next step to examine which coupling behavior is represented in more advanced convection schemes such as the scale-aware Grell-Freitas scheme or the new Tiedke scheme, which is used in the modeling system underlying the ECMWF reanalysis datasets.

Appendix B

Annual Cycle of Land-Convection Coupling Strength

This section provides monthly coupling classifications based on the CTP-HI_{low} framework, as well as the frequency of potential coupling days (nAC-days) assessed for the period 1986-2015. The classification was done for the simulation with realistic land cover, as well as for both LULCC simulations. To achieve a clear arrangement was achieved by aggregating the months seasonally. Each panel shows the long-term coupling classification in the first row (subplots a-c) and the nAC fields in the second row (subplots d-f). Deviations in nAC-days originating from the LULCC are shown the lower two rows (subplots g-l) of each panel.

The winter months (Appendix Figure B.1 a)-f)) are almost entirely AC over the European continental areas. Some days with favorable pre-conditioning for coupling occur in coastal regions. These conditions prevail until March. The preceding months show a strengthening of the coupling along with an eastward and northward migration of the coupling hot spot during the growing period (Appendix Figure B.2 a)-f), Appendix Figure B.3a)-f)). The north-eastward shift stops in July, which is when also the strengthening maximizes. Afterwards, the hot spot starts to move southward and weaken again during autumn (Appendix Figure B.4 a)-f)) and it shifts back westward. A similar development and spatial shift of the atmospheric coupling leg, which is also included in the complete coupling chain, was shown in a global animation by Paul Dirmeyer (http://cola.gmu.edu/dirmeyer/nasa_map_12.html).

Shifting now the focus to differences between FOREST and CORINE (third row) as well as between GRASS and CORINE (forth row) reveals another interesting aspect. The differences in nAC-day

frequency originating from both vegetation transitions also increase during the growing period and maximize in July (Appendix Figures B.1-B.4, subplots g)-l)). As the frequency of nAC-days is based on assessing the ABL structure, the differences in nAC-days imply impacts on the ABL structure from LULCC, in the first place. Even without inferring on convection triggering, this effect in itself suggests coupling between land surface and atmosphere.

In closing, the annual cycle of land-convection coupling strength showed a considerable increase in LULCC impacts on the ABL structure resulting in differences in the atmospheric preconditioning for convection triggering during the growing period. As LULCC impacts were considerably weaker between autumn and spring, all analyses conducted in the context of this dissertation focused on the summer months.

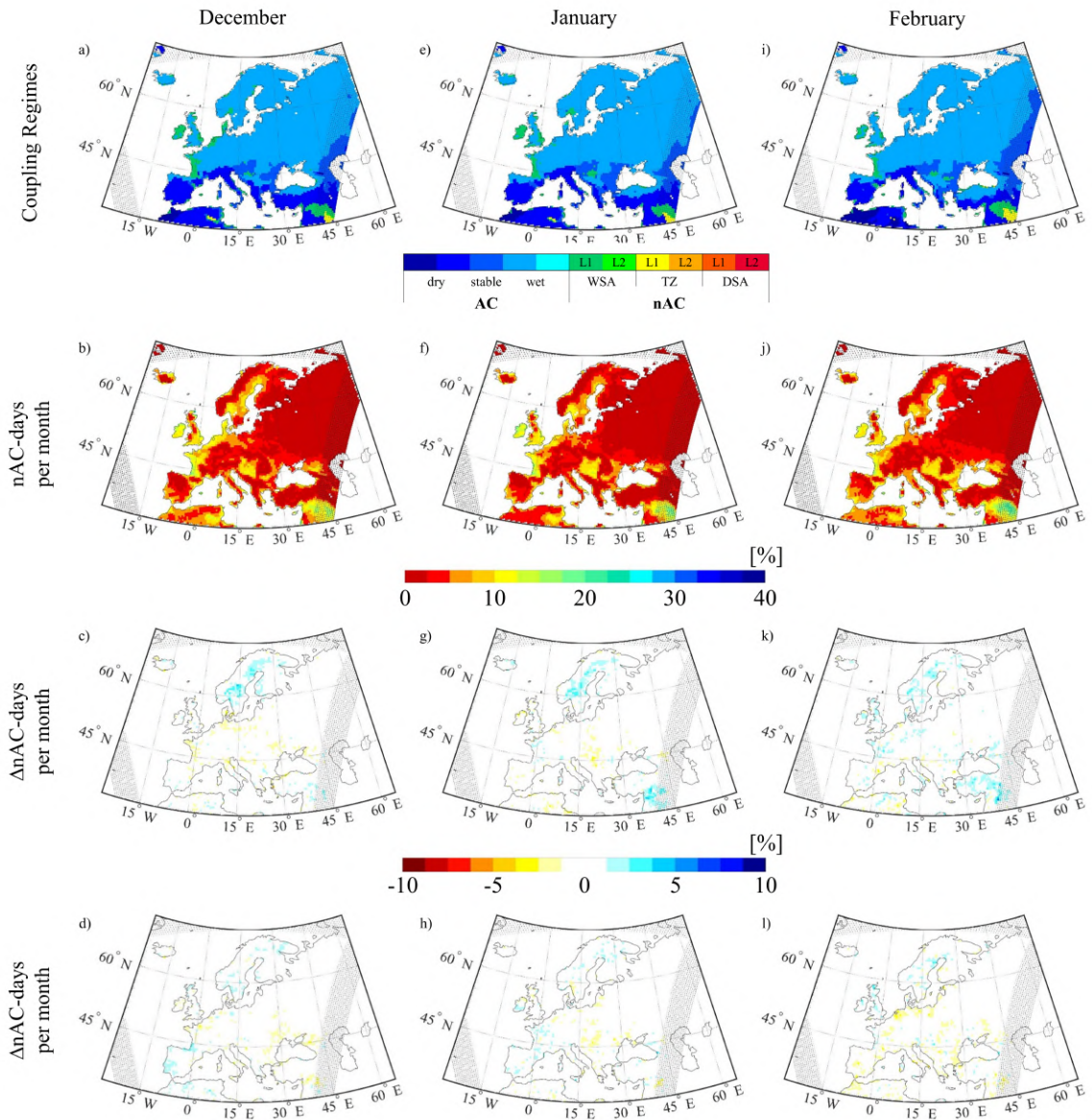


FIGURE B.1: Monthly long-term coupling signals based on the ‘Convective Triggering Potential – low-level Humidity Index’ framework (a-c) for the winter months December, January, and February between 1986-2015. Subplots d-f show the fraction of non-atmospherically controlled (nAC) days per month, subplots g-i show the difference in the fraction of nAC-days when realistic land cover (from 2006) is changed to forest over the entire European continent (FOREST-CORINE), and subplots j-l show the differences in the fraction of nAC-days when the land cover is changed to grassland over the entire European continent (GRASS-CORINE).

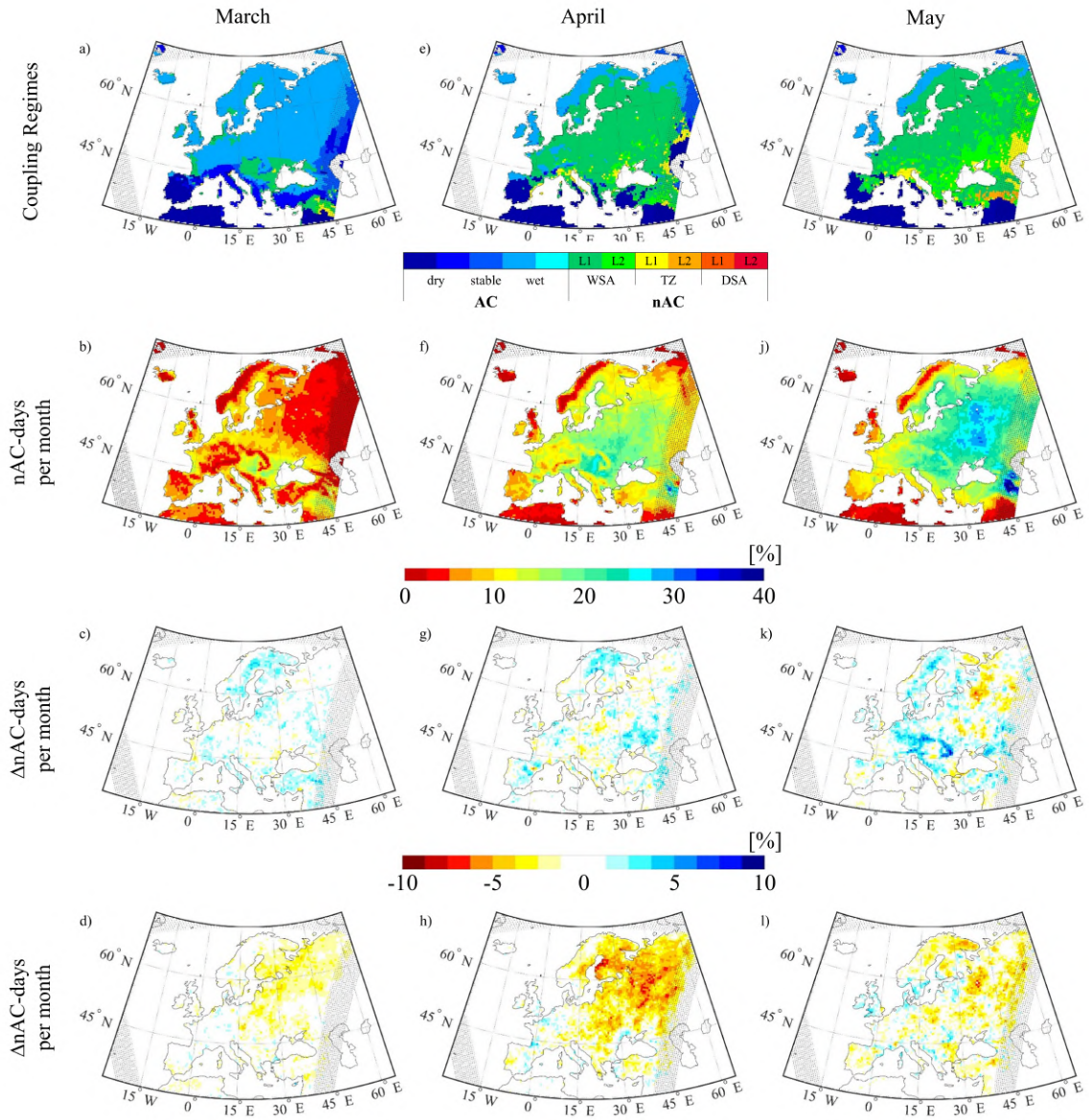


FIGURE B.2: As Appendix Figure B.1 but for March, April and May.

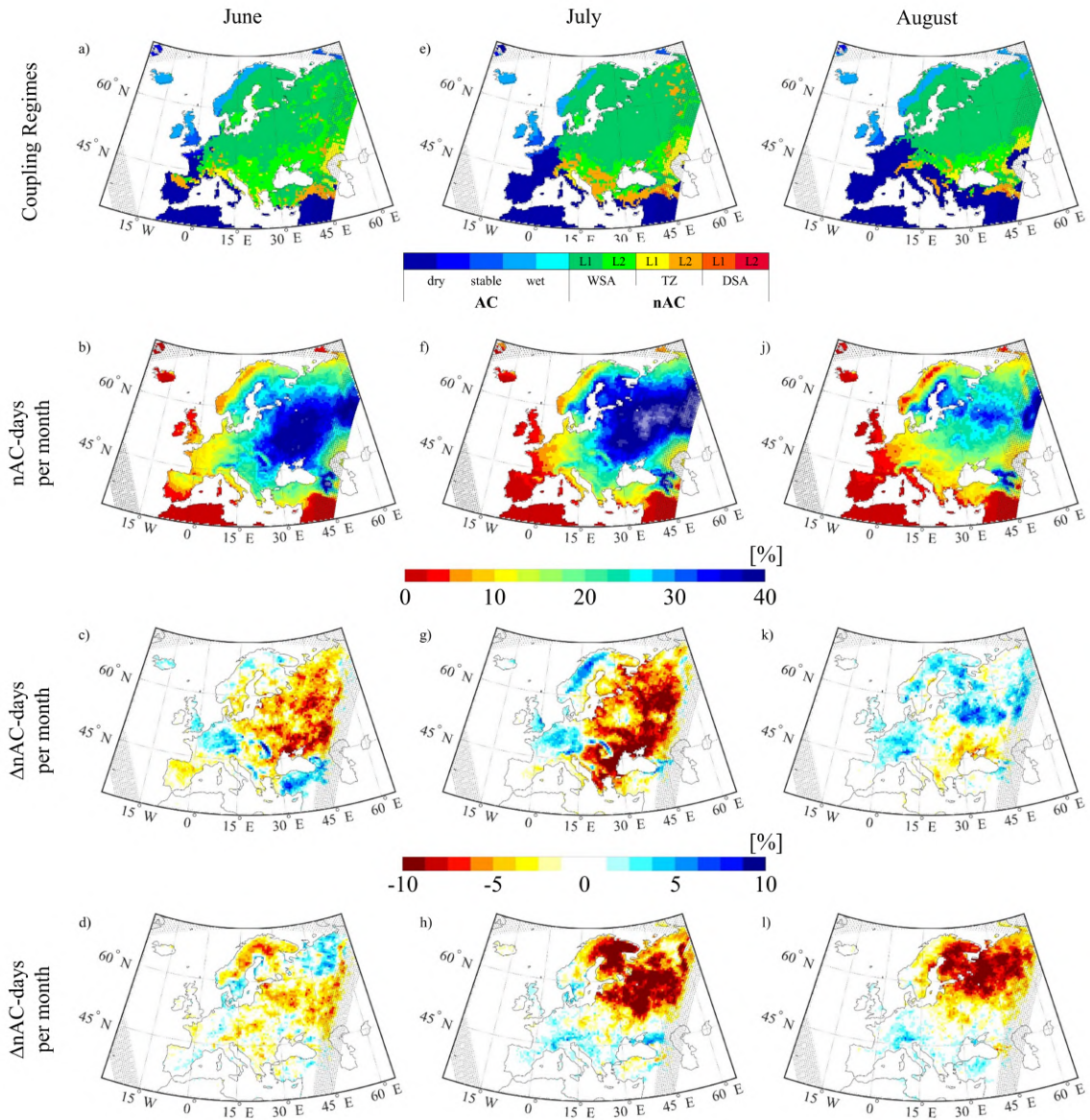


FIGURE B.3: As Appendix Figure B.1 but for June, July and August.

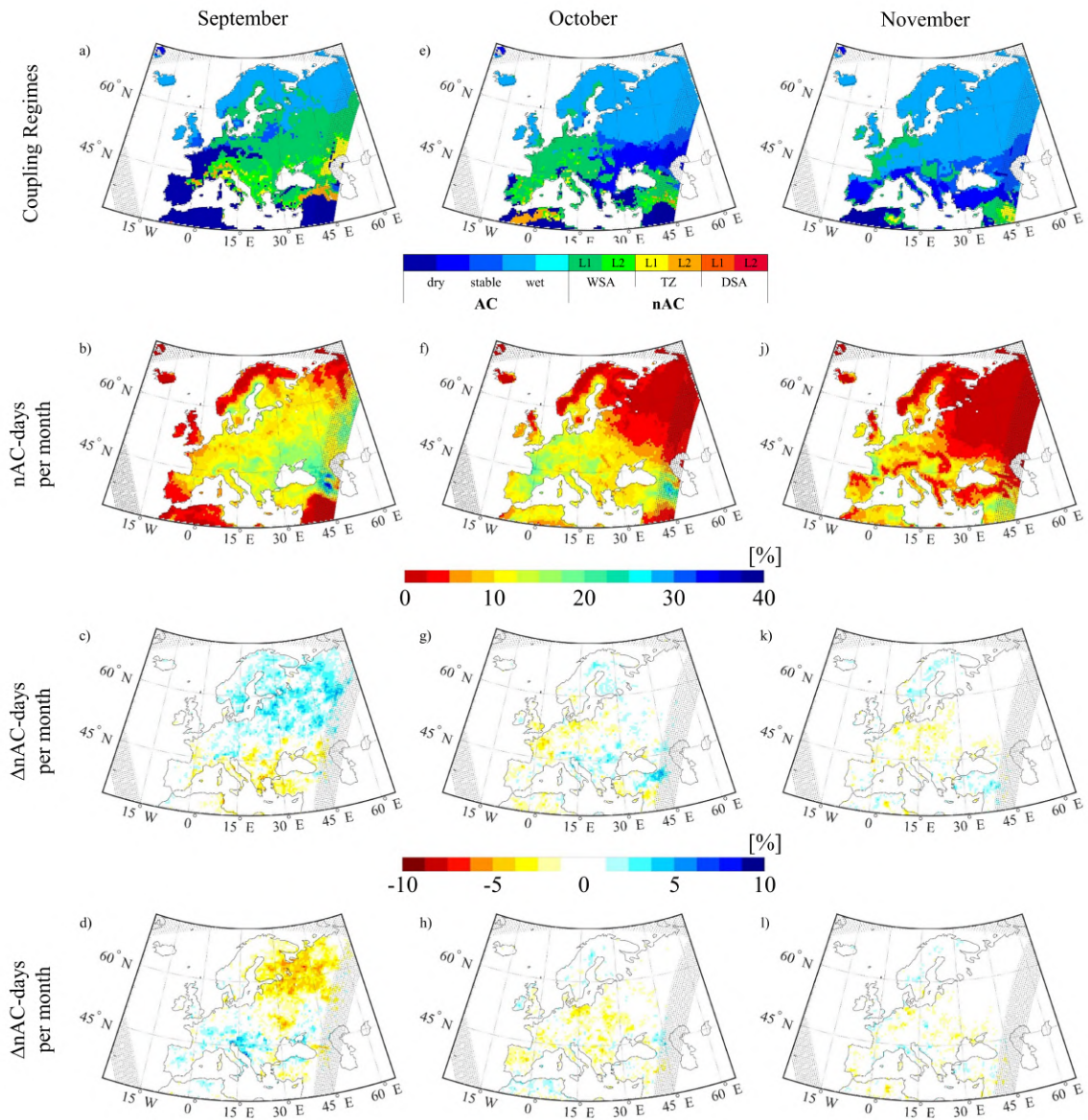


FIGURE B.4: As Appendix Figure B.1 but for September, October and November.

Appendix C

Supplementary Material Publication I



Journal of Geophysical Research: Atmospheres

Supporting Information for

Land Cover Impacts on Land-Atmosphere Coupling Strength in Climate Simulations with WRF over Europe

Lisa Jach¹, Kirsten Warrach-Sagi¹, Joachim Ingwersen², Eigil Kaas³, Volker Wulfmeyer¹

¹Institute for Physics and Meteorology, University of Hohenheim, Stuttgart, Germany

²Institute for Soil Science and Land Evaluation, Department of Biogeophysics, University of Hohenheim, Stuttgart, Germany

³Niels Bohr Institute, Department of Climate and Computational Geophysics, University of Copenhagen, Copenhagen, Denmark

Contents of this file

Text S1 and S2
Figures S1 to S6

Introduction

This file contains additional information about the share of the feedback categories in all land cover scenarios (Text S1 and Figures S1, S2). Additionally, text S2 describes the methodology of a complementary sensitivity test of the CTP-HI_{low} classification (Figures S3-S6). It was performed to estimate the robustness of the findings with regard to location of regions with strong coupling, and the predominant feedback sign, as presented in the main manuscript. Perturbations were applied to all initial temperature and moisture profiles of the summer 1986. The test was based on the data from the baseline run, and the classification was performed as described in section 2.4.1 of the main manuscript.

Text S1 Relative share of feedback regimes

The Figures S1 and S2 show the share of wet soil advantage, transition zone and dry soil advantage days. Figure S1 depicts the share in relation to the non-atmospherically controlled (nAC) days in summer. A share of 100% in, e.g., wet soil advantage means that all nAC days in summer are in wet soil advantage, irrespective of the nAC-days' frequency of occurrence. The long-term CTP-HI_{low} classification builds upon this. However, this representation does not provide information about the actual frequency of occurrence of a feedback advantage within summer, which complicates the interpretation. Therefore, Figure S2 additionally depicts the occurrence of each feedback category in relation to all summer days.

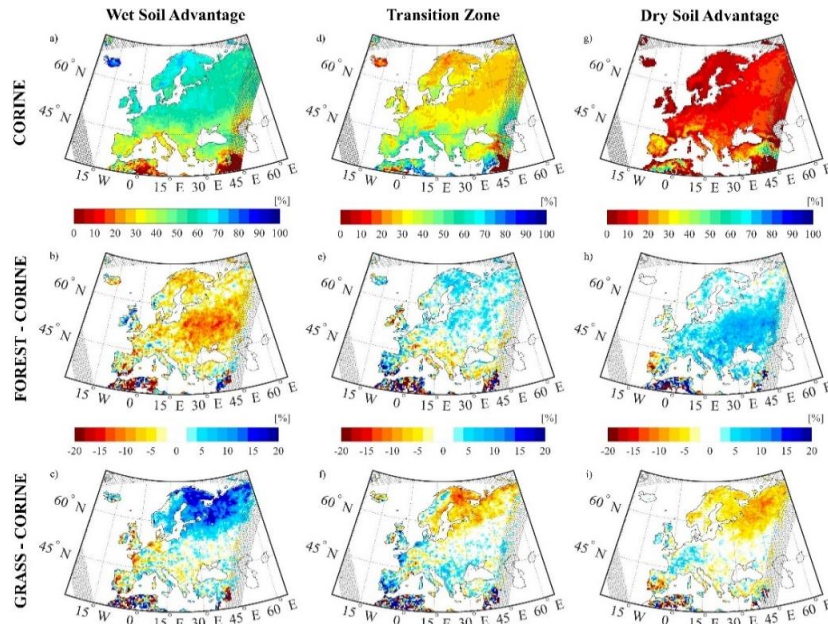


Figure S1: a) Average share of wet soil advantage days of the non-atmospherically controlled days of the CORINE run in summers of the period 1986-2000, b) difference in wet soil advantage days due to afforestation, and c) due to deforestation. d)-f) Same as for a)-c) but for days in transition zone, g)-i) same as a)-c) but for days in dry soil advantage.

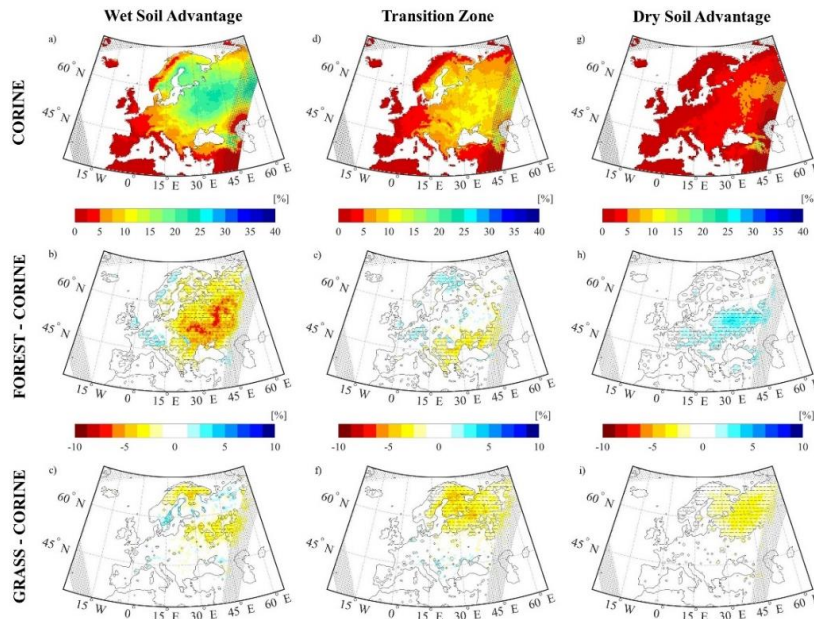


Figure S2: Average seasonal share of the feedback categories. a) Average share of summer days in wet soil advantage in the CORINE run in the period 1986-2015, b) difference in the share of wet soil advantage day due to afforestation, and c) for deforestation. d)-f) Same as for a)-c) but for days in transition zone, g)-i) same as a)-c) due for days in dry soil advantage.

Text S2 Sensitivity of CTP- HI_{low} framework classification to perturbations of the initial temperature and moisture profiles in summer 1986

Purpose and approach

Different model configurations and parameterization schemes are expected to generate differences in simulated temperature and moisture profiles. These profiles form the basis for calculating CTP and HI_{low} , and ultimately for classifying the land-atmosphere coupling regimes. Systematic perturbations of the early-morning temperature and moisture profiles were expected to approximate the spread in modelled temperature and moisture, and hence the differences in feedback classifications between models – at least to some extent. The purpose of this sensitivity test was to assess the robustness of the identification of strong coupling region and dominating feedback sign by an a priori perturbation of the initial temperature and moisture fields. The test was conducted based on the data of the CORINE simulation of the summer 1986.

Individual and combined perturbations of different intensities were applied to the daily initial temperature and moisture profiles at sunrise over the entire column. A variety of perturbation intensities were tested and the resulting intensities were selected with reference to literature, as described next. For the perturbation of temperature, 2K (or 4K) were added or subtracted over the whole column. The range of +/- 2K covers the range of reasonable temperature biases as seen in a EURO-CORDEX ensemble with 0.44° and 0.11° resolution (Kotlarski et al. 2014). The +/- 4K perturbations were applied to represent larger biases that are regionally existent in some models. The mixing ratio was perturbed in terms of units of standard deviation (USD) over the whole column to account for differences in the variance of moisture between low and high altitudes. Unlike temperature, specific humidity was not evaluated in detail in the EURO-CORDEX ensemble, yet. Therefore, the choice of the different intensities of humidity perturbations was based on the range of HI_{low} values computed within a global analysis of CTP and HI_{low} based on the ERA5 reanalysis data set (Branch and Wulfmeyer 2019). HI_{low} values larger than 30°C occurred only in arid and semi-arid regions in this classification. Following this, atmospheric drying, which results in an average $HI_{low} > 30^\circ\text{C}$, is not reasonable in Central and Northern Europe in the current climate. Similarly, atmospheric moistening that leads to saturation in the low-level atmospheric humidity on a regular basis, seems unrealistic in the European summer. Following these boundaries, moisture perturbations between +/- 0.5 USD intended to represent a rather realistic spread in moisture distribution. The +/- 1.5 USD cases were chosen to explore the effect of extreme moisture changes on the classification.

Figure S3 shows the CTP- HI_{low} classifications for the realistic range of temperature and moisture perturbations, and Figure S4 depicts the CTP- HI_{low} classifications for the extreme perturbation range. Complementary, Figure S5 and Figure S6 show the fractions of non-atmospherically controlled days for the realistic and extreme perturbation range, respectively. The results are discussed in the section 5 of the main manuscript.

Limitations of the sensitivity analysis

The approach for perturbing the temperature and moisture profiles cannot fully represent the spread between models that would be observable in a multi-model ensemble. Since, the temperature perturbations were applied linearly with height, the shape of the profiles is maintained. Differences in the shape may lead to stronger changes in the spatial distribution of CTP which cannot be captured with the applied approach. Similarly, differences in the shape of moisture profiles cannot be captured.

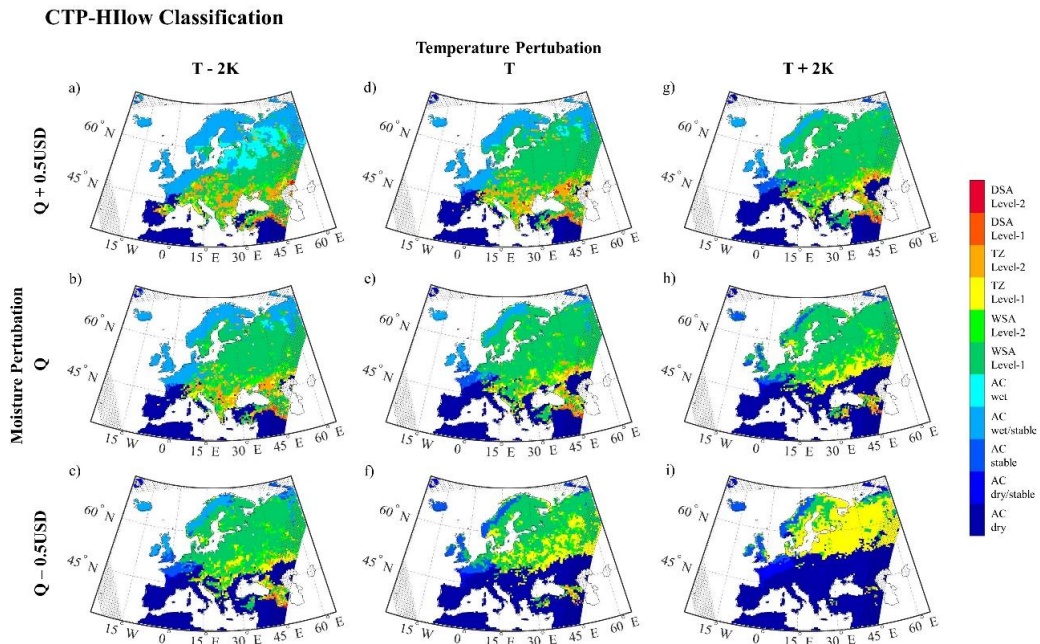


Figure S3: Long-term feedback regime classification after the CTP-HI_{low} framework for the summer months of 1986. Columns indicate the temperature perturbations (+2K, unperturbed and -2K) and rows indicate the moisture perturbations (+0.5 USD, unperturbed, and -0.5 USD).

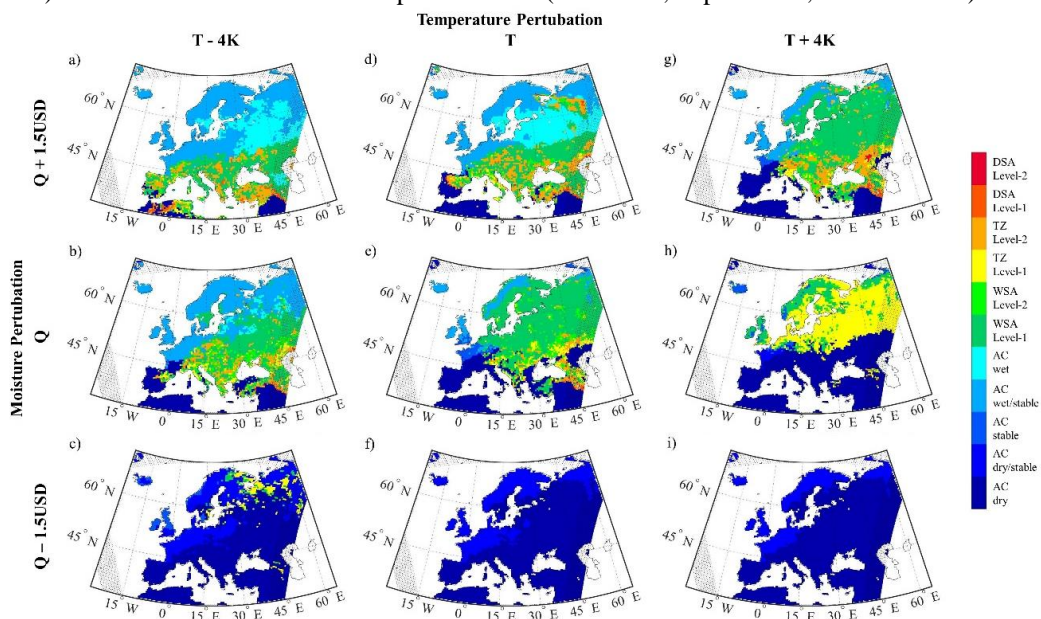


Figure S4: Same as Figure S3 but for temperature perturbations of +/- 4K and moisture perturbations of +/- 1.5 USD.

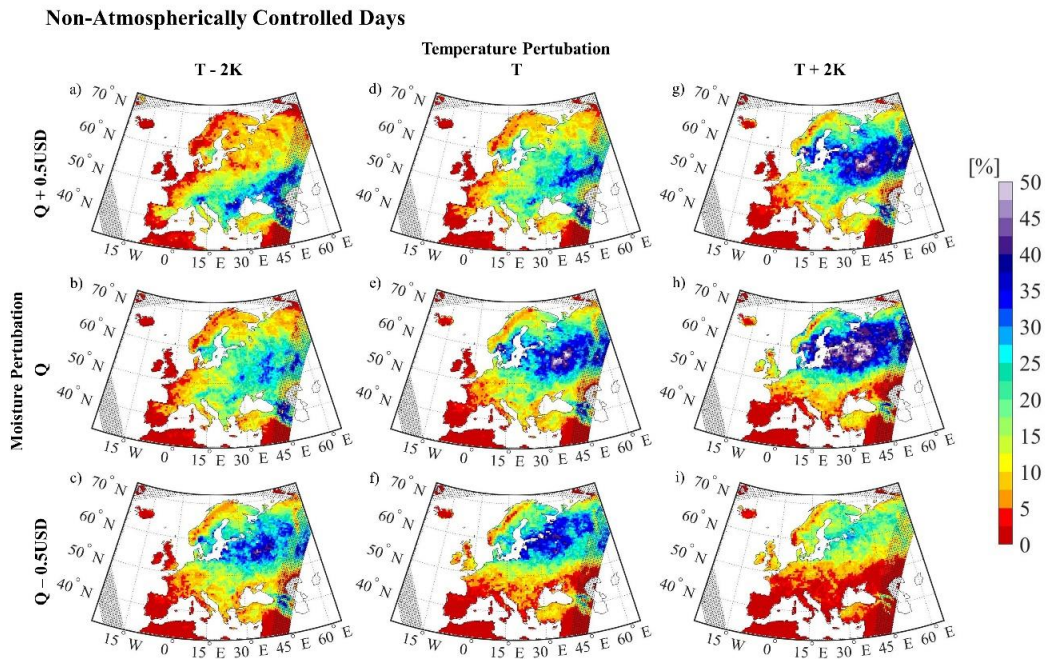


Figure S5: Share of non-atmospherically controlled days [%] in the summer months of 1986. Columns indicate the temperature perturbations (+2K, unperturbed and -2K) and rows indicate the moisture perturbations (+0.5 USD, unperturbed, and -0.5 USD).

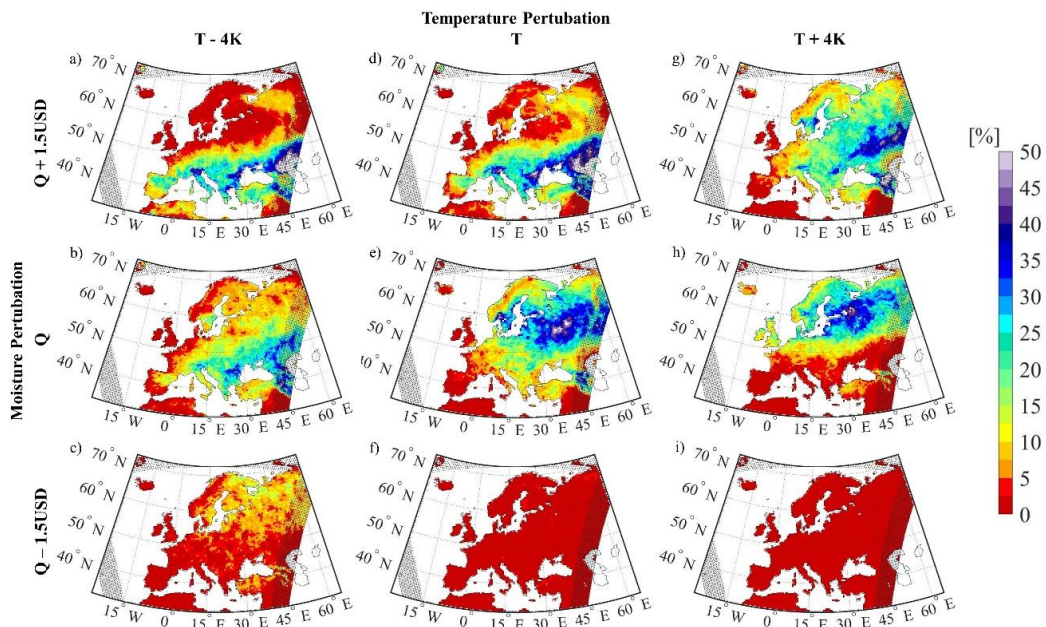


Figure S6: Same as Figure S5 but for temperature perturbations of +/- 4K and moisture perturbations of +/- 1.5 USD.

Appendix D

Supplementary Material Publication II

Supplement of Earth Syst. Dynam., 13, 109–132, 2022
<https://doi.org/10.5194/esd-13-109-2022-supplement>
© Author(s) 2022. CC BY 4.0 License.



Supplement of

Sensitivity of land–atmosphere coupling strength to changing atmospheric temperature and moisture over Europe

Lisa Jach et al.

Correspondence to: Lisa Jach (lisa.jach@uni-hohenheim.de)

The copyright of individual parts of the supplement might differ from the article licence.

Supplementary Material

1 Non-atmospherically controlled days after a-posteriori model output modification of $\pm 5K$

We applied the same methodology as in the core modifications set with higher modification factors corresponding to $\pm 5K$ and with 8.81%/K change in the specific humidity.

- 5 Figure S 1 shows the changes in average fraction of nAC-days in the summer months introduced by the corresponding modification factors. The signal of the change signal, as well as the patterns remained similar to that with $\pm 2K$ modifications in all cases apart from the cases with moisture decrease and either temperatures unchanged (d) or increasing temperatures (g). In the latter case, the relative humidity and thus the humidity deficit were severely decreased by more than 40% over the high-latitudes which reduced the frequency of nAC-days by more than 20% of the summer days and thus reduced the size of the
- 10 hotspot tremendously. Furthermore, all nAC-days were pushed in the transition zone category shown in Figure S 2g. However, an average relative humidity in summer of 60% rather occurs in the Mediterranean region, which is why such an extreme change in the classification over the historical period 1986-2015 is considered unrealistic.

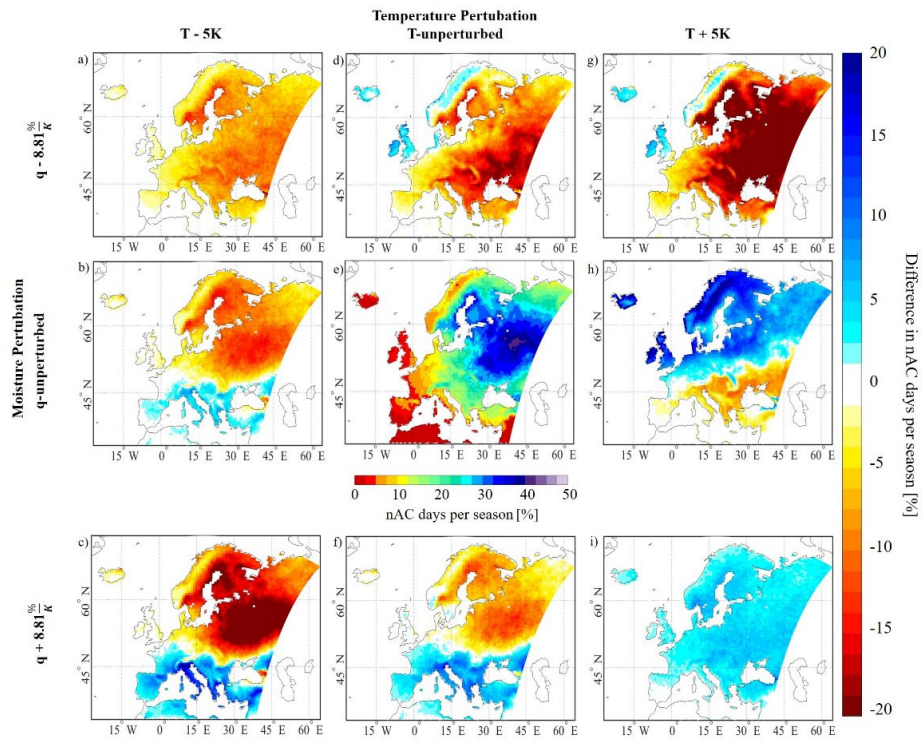


Figure S 1: Cases of $\pm 5K$ of posterior modification and corresponding modifications of the specific humidity.

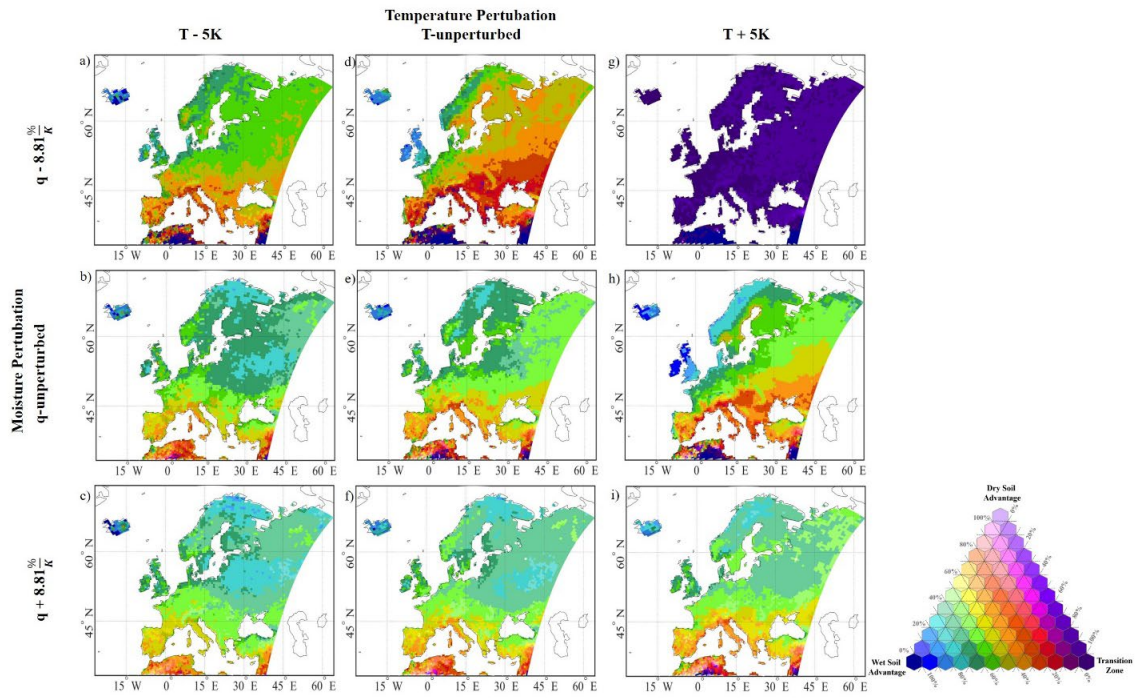


Figure S 2: nAC-day partitioning of the $\pm 5K$ posterior output modification cases.

Bibliography

- Alessandri, A. and A. Navarra, 2008: On the coupling between vegetation and rainfall inter-annual anomalies: Possible contributions to seasonal rainfall predictability over land areas. in: *Geophysical Research Letters* 35.2, DOI: [10.1029/2007GL032415](https://doi.org/10.1029/2007GL032415).
- Asselin, O., M. Leduc, D. Paquin, K. Winger, A. Di Luca, M. Bukovsky, B. Music, and M. Giguère, 2022: *Climate Response to Severe Forestation: A Regional Climate Model Intercomparison Study*, preprint, Earth system interactions with the biosphere: landuse, DOI: [10.5194/egusphere-2022-291](https://doi.org/10.5194/egusphere-2022-291).
- Barthlott, C., R. Burton, D. Kirshbaum, K. Hanley, E. Richard, J.-P. Chaboureau, J. Trentmann, B. Kern, H.-S. Bauer, T. Schwitalla, C. Keil, Y. Seity, A. Gadian, A. Blyth, S. Mobbs, C. Flamant, and J. Handwerker, 2011: Initiation of deep convection at marginal instability in an ensemble of mesoscale models: a case-study from COPS: COPS Mesoscale Model Intercomparison for IOP 8b. in: *Quarterly Journal of the Royal Meteorological Society* 137 S1, pp. 118–136, DOI: [10.1002/qj.707](https://doi.org/10.1002/qj.707).
- Basara, J. B., J. I. Christian, R. A. Wakefield, J. A. Otkin, E. H. Hunt, and D. P. Brown, 2019: The evolution, propagation, and spread of flash drought in the Central United States during 2012. in: *Environmental Research Letters* 14.8, p. 084025, DOI: [10.1088/1748-9326/ab2cc0](https://doi.org/10.1088/1748-9326/ab2cc0).
- Baur, F., C. Keil, and G. C. Craig, 2018: Soil moisture–precipitation coupling over Central Europe: Interactions between surface anomalies at different scales and the dynamical implication. in: *Quarterly Journal of the Royal Meteorological Society* 144.717, pp. 2863–2875, DOI: [10.1002/qj.3415](https://doi.org/10.1002/qj.3415).
- Baur, F., C. Keil, and C. Barthlott, 2022: Combined effects of soil moisture and microphysical perturbations on convective clouds and precipitation for a locally forced case over Central Europe. in: *Quarterly Journal of the Royal Meteorological Society*, qj.4295, DOI: [10.1002/qj.4295](https://doi.org/10.1002/qj.4295).

- Berg, A., K. Findell, B. R. Lintner, P. Gentine, and C. Kerr, 2013: Precipitation Sensitivity to Surface Heat Fluxes over North America in Reanalysis and Model Data. in: *Journal of Hydrometeorology* 14.3, pp. 722–743, DOI: [10.1175/JHM-D-12-0111.1](https://doi.org/10.1175/JHM-D-12-0111.1).
- Berg, A. and J. Sheffield, 2018: Soil Moisture–Evapotranspiration Coupling in CMIP5 Models: Relationship with Simulated Climate and Projections. in: *Journal of Climate* 31.12, pp. 4865–4878, DOI: [10.1175/JCLI-D-17-0757.1](https://doi.org/10.1175/JCLI-D-17-0757.1).
- Branch, O. and V. Wulfmeyer, 2019: Deliberate enhancement of rainfall using desert plantations. in: *Proceedings of the National Academy of Sciences*, p. 201904754, DOI: [10.1073/pnas.1904754116](https://doi.org/10.1073/pnas.1904754116).
- Breil, M., D. Rechid, E. L. Davin, N. de Noblet-Ducoudré, E. Katragkou, R. M. Cardoso, P. Hoffmann, L. L. Jach, P. M. M. Soares, G. Sofiadis, S. Strada, G. Strandberg, M. H. Tölle, and K. Warrach-Sagi, 2020: The Opposing Effects of Reforestation and Afforestation on the Diurnal Temperature Cycle at the Surface and in the Lowest Atmospheric Model Level in the European Summer. in: *Journal of Climate* 33.21, pp. 9159–9179, DOI: [10.1175/JCLI-D-19-0624.1](https://doi.org/10.1175/JCLI-D-19-0624.1).
- Breil, M., E. L. Davin, and D. Rechid, 2021: What determines the sign of the evapotranspiration response to afforestation in European summer? In: *Biogeosciences* 18.4, pp. 1499–1510, DOI: [10.5194/bg-18-1499-2021](https://doi.org/10.5194/bg-18-1499-2021).
- Brogli, R., N. Kröner, S. L. Sørland, D. Lüthi, and C. Schär, 2019: The Role of Hadley Circulation and Lapse-Rate Changes for the Future European Summer Climate. in: *Journal of Climate* 32.2, pp. 385–404, DOI: [10.1175/JCLI-D-18-0431.1](https://doi.org/10.1175/JCLI-D-18-0431.1).
- Catalano, F., A. Alessandri, M. De Felice, Z. Zhu, and R. B. Myneni, 2016: Observationally based analysis of land–atmosphere coupling. in: *Earth System Dynamics* 7.1, pp. 251–266, DOI: [10.5194/esd-7-251-2016](https://doi.org/10.5194/esd-7-251-2016).
- Chen, L. and P. A. Dirmeyer, 2017: Impacts of Land-Use/Land-Cover Change on Afternoon Precipitation over North America. in: *Journal of Climate* 30.6, pp. 2121–2140, DOI: [10.1175/JCLI-D-16-0589.1](https://doi.org/10.1175/JCLI-D-16-0589.1).
- Chen, L., P. A. Dirmeyer, A. Tawfik, and D. M. Lawrence, 2017: Sensitivities of Land Cover–Precipitation Feedback to Convective Triggering. in: *Journal of Hydrometeorology* 18.8, pp. 2265–2283, DOI: [10.1175/JHM-D-17-0011.1](https://doi.org/10.1175/JHM-D-17-0011.1).

-
- Chen, C., D. Li, Y. Li, S. Piao, X. Wang, M. Huang, P. Gentine, R. R. Nemani, and R. B. Myneni, 2020: Biophysical impacts of Earth greening largely controlled by aerodynamic resistance. in: *Science Advances* 6.47, eabb1981, DOI: [10.1126/sciadv.abb1981](https://doi.org/10.1126/sciadv.abb1981).
- Chen, L. and P. A. Dirmeyer, 2020a: Distinct Impacts of Land Use and Land Management on Summer Temperatures. in: *Frontiers in Earth Science* 8, p. 245, DOI: [10.3389/feart.2020.00245](https://doi.org/10.3389/feart.2020.00245).
- 2020b: Reconciling the disagreement between observed and simulated temperature responses to deforestation. in: *Nature Communications* 11.1, DOI: [10.1038/s41467-019-14017-0](https://doi.org/10.1038/s41467-019-14017-0).
- Cioni, G. and C. Hohenegger, 2017: Effect of Soil Moisture on Diurnal Convection and Precipitation in Large-Eddy Simulations. in: *Journal of Hydrometeorology* 18.7, pp. 1885–1903, DOI: [10.1175/JHM-D-16-0241.1](https://doi.org/10.1175/JHM-D-16-0241.1).
- Coppola, E., S. Sobolowski, E. Pichelli, F. Raffaele, B. Ahrens, I. Anders, N. Ban, S. Bastin, M. Belda, D. Belusic, A. Caldas-Alvarez, R. M. Cardoso, S. Davolio, A. Dobler, J. Fernandez, L. Fita, Q. Fumiere, F. Giorgi, K. Goergen, I. Güttler, T. Halenka, D. Heinzeller, Ø. Hodnebrog, D. Jacob, S. Kartsios, E. Katragkou, E. Kendon, S. Khodayar, H. Kunstmann, S. Knist, A. Lavín-Gullón, P. Lind, T. Lorenz, D. Maraun, L. Marelle, E. van Meijgaard, J. Milovac, G. Myhre, H.-J. Panitz, M. Piazza, M. Raffa, T. Raub, B. Rockel, C. Schär, K. Sieck, P. M. M. Soares, S. Somot, L. Srnec, P. Stocchi, M. H. Tölle, H. Truhetz, R. Vautard, H. de Vries, and K. Warrach-Sagi, 2018: A first-of-its-kind multi-model convection permitting ensemble for investigating convective phenomena over Europe and the Mediterranean. in: *Climate Dynamics*, DOI: [10.1007/s00382-018-4521-8](https://doi.org/10.1007/s00382-018-4521-8).
- Cornes, R. C., G. van der Schrier, E. J. M. van den Besselaar, and P. D. Jones, 2018: An Ensemble Version of the E-OBS Temperature and Precipitation Data Sets. in: *Journal of Geophysical Research: Atmospheres* 123.17, pp. 9391–9409, DOI: [10.1029/2017JD028200](https://doi.org/10.1029/2017JD028200).
- Daloz, A. S., C. Schwingshackl, P. Mooney, S. Strada, D. Rechid, E. L. Davin, E. Katragkou, N. de Noblet-Ducoudré, M. Belda, T. Halenka, M. Breil, R. M. Cardoso, P. Hoffmann, D. C. A. Lima, R. Meier, P. M. M. Soares, G. Sofiadis, G. Strandberg, M. H. Toelle, and M. T. Lund, 2022: Land–atmosphere interactions in sub-polar and alpine climates in the CORDEX flagship pilot study Land Use and Climate Across Scales (LUCAS) models – Part 1: Evaluation of the snow-albedo effect. in: *The Cryosphere* 16.6, pp. 2403–2419, DOI: [10.5194/tc-16-2403-2022](https://doi.org/10.5194/tc-16-2403-2022).
-

- Davin, E. L. and N. de Noblet-Ducoudré, 2010: Climatic Impact of Global-Scale Deforestation: Radiative versus Nonradiative Processes. in: *Journal of Climate* 23.1, pp. 97–112, DOI: [10.1175/2009JCLI3102.1](https://doi.org/10.1175/2009JCLI3102.1).
- Davin, E. L., D. Rechid, M. Breil, R. M. Cardoso, E. Coppola, P. Hoffmann, L. L. Jach, E. Karagkou, N. de Noblet-Ducoudré, K. Radtke, M. Raffa, P. M. M. Soares, G. Sofiadis, S. Strada, G. Strandberg, M. H. Tölle, K. Warrach-Sagi, and V. Wulfmeyer, 2020: Biogeophysical impacts of forestation in Europe: first results from the LUCAS (Land Use and Climate Across Scales) regional climate model intercomparison. in: *Earth System Dynamics* 11.1, pp. 183–200, DOI: [10.5194/esd-11-183-2020](https://doi.org/10.5194/esd-11-183-2020).
- DelSole, T. and M. K. Tippett, 2007: Predictability: Recent insights from information theory: PREDICTABILITY. in: *Reviews of Geophysics* 45.4, DOI: [10.1029/2006RG000202](https://doi.org/10.1029/2006RG000202).
- Devanand, A., M. Huang, D. M. Lawrence, C. M. Zarzycki, Z. Feng, P. J. Lawrence, Y. Qian, and Z. Yang, 2020: Land Use and Land Cover Change Strongly Modulates Land-Atmosphere Coupling and Warm-Season Precipitation Over the Central United States in CESM2-VR. in: *Journal of Advances in Modeling Earth Systems* 12.9, DOI: [10.1029/2019MS001925](https://doi.org/10.1029/2019MS001925).
- Dione, C., M. Lothon, D. Badiane, B. Campistron, F. Couvreux, F. Guichard, and S. M. Sall, 2014: Phenomenology of Sahelian convection observed in Niamey during the early monsoon: Sahelian convection during the early monsoon. in: *Quarterly Journal of the Royal Meteorological Society* 140.679, pp. 500–516, DOI: [10.1002/qj.2149](https://doi.org/10.1002/qj.2149).
- Dirmeyer, P. A., 2006: The Hydrologic Feedback Pathway for Land–Climate Coupling. in: *Journal of Hydrometeorology* 7.5, pp. 857–867, DOI: [10.1175/JHM526.1](https://doi.org/10.1175/JHM526.1).
- 2011: The terrestrial segment of soil moisture-climate coupling: SOIL MOISTURE-CLIMATE COUPLING. in: *Geophysical Research Letters* 38.16, n/a–n/a, DOI: [10.1029/2011GL048268](https://doi.org/10.1029/2011GL048268).
- Dirmeyer, P. A., B. A. Cash, J. L. Kinter, C. Stan, T. Jung, L. Marx, P. Towers, N. Wedi, J. M. Adams, E. L. Altshuler, B. Huang, E. K. Jin, and J. Manganello, 2012: Evidence for Enhanced Land–Atmosphere Feedback in a Warming Climate. in: *Journal of Hydrometeorology* 13.3, pp. 981–995, DOI: [10.1175/JHM-D-11-0104.1](https://doi.org/10.1175/JHM-D-11-0104.1).
- Dirmeyer, P. A., Y. Jin, B. Singh, and X. Yan, 2013a: Evolving Land–Atmosphere Interactions over North America from CMIP5 Simulations. in: *Journal of Climate* 26.19, pp. 7313–7327, DOI: [10.1175/JCLI-D-12-00454.1](https://doi.org/10.1175/JCLI-D-12-00454.1).

-
- 2013b: Trends in Land–Atmosphere Interactions from CMIP5 Simulations. in: *Journal of Hydrometeorology* 14.3, pp. 829–849, DOI: [10.1175/JHM-D-12-0107.1](https://doi.org/10.1175/JHM-D-12-0107.1).
- Dirmeyer, P. A., Z. Wang, M. J. Mbuh, and H. E. Norton, 2014: Intensified land surface control on boundary layer growth in a changing climate: Dirmeyer et al.: Land-PBL feedback in a changing climate. in: *Geophysical Research Letters* 41.4, pp. 1290–1294, DOI: [10.1002/2013GL058826](https://doi.org/10.1002/2013GL058826).
- Dirmeyer, P. A., L. Chen, J. Wu, C.-S. Shin, B. Huang, B. A. Cash, M. G. Bosilovich, S. Mahanama, R. D. Koster, J. A. Santanello, M. B. Ek, G. Balsamo, E. Dutra, and D. M. Lawrence, 2018a: Verification of Land–Atmosphere Coupling in Forecast Models, Reanalyses, and Land Surface Models Using Flux Site Observations. in: *Journal of Hydrometeorology* 19.2, pp. 375–392, DOI: [10.1175/JHM-D-17-0152.1](https://doi.org/10.1175/JHM-D-17-0152.1).
- Dirmeyer, P. A., S. Halder, and R. Bombardi, 2018b: On the Harvest of Predictability From Land States in a Global Forecast Model. in: *Journal of Geophysical Research: Atmospheres* 123.23, DOI: [10.1029/2018JD029103](https://doi.org/10.1029/2018JD029103).
- Dirmeyer, P. A., G. Balsamo, E. M. Blyth, R. Morrison, and H. M. Cooper, 2021: Land-Atmosphere Interactions Exacerbated the Drought and Heatwave Over Northern Europe During Summer 2018. in: *AGU Advances* 2.2, DOI: [10.1029/2020AV000283](https://doi.org/10.1029/2020AV000283).
- Doyle, M. E., J. Tomasella, D. A. Rodriguez, and S. C. Chou, 2013: Experiments using new initial soil moisture conditions and soil map in the Eta model over La Plata Basin. in: *Meteorology and Atmospheric Physics* 121.3, pp. 119–136, DOI: [10.1007/s00703-013-0265-5](https://doi.org/10.1007/s00703-013-0265-5).
- Duveiller, G., G. Forzieri, E. Robertson, W. Li, G. Georgievski, P. Lawrence, A. Wiltshire, P. Ciais, J. Pongratz, S. Sitch, A. Arneth, and A. Cescatti, 2018a: *Biophysics and vegetation cover change: a process-based evaluation framework for confronting land surface models with satellite observations*, preprint, Biosphere – Biogeosciences, DOI: [10.5194/essd-2018-24](https://doi.org/10.5194/essd-2018-24).
- Duveiller, G., J. Hooker, and A. Cescatti, 2018b: The mark of vegetation change on Earth’s surface energy balance. in: *Nature Communications* 9.1, DOI: [10.1038/s41467-017-02810-8](https://doi.org/10.1038/s41467-017-02810-8).
- Ebell, K., S. Bachner, A. Kapala, and C. Simmer, 2008: Sensitivity of summer precipitation simulated by the CLM with respect to initial and boundary conditions. in: *Meteorologische Zeitschrift* 17.4, pp. 421–431, DOI: [10.1127/0941-2948/2008/0305](https://doi.org/10.1127/0941-2948/2008/0305).
-

- Ek, M. B. and A. A. M. Holtslag, 2004: Influence of Soil Moisture on Boundary Layer Cloud Development. in: *Journal of Hydrometeorology* 5.1, pp. 86–99, DOI: [10.1175/1525-7541\(2004\)005<0086:IOSMOB>2.0.CO;2](https://doi.org/10.1175/1525-7541(2004)005<0086:IOSMOB>2.0.CO;2).
- Ek, M. B., 2016: *On the nature of local land-atmosphere coupling strength for vegetated surfaces*.
- Ek, M. B. and L. Mahrt, 1994: Daytime Evolution of Relative Humidity at the Boundary Layer Top. in: *Monthly Weather Review* 122.12, pp. 2709–2721, DOI: [10.1175/1520-0493\(1994\)122<2709:DEORHA>2.0.CO;2](https://doi.org/10.1175/1520-0493(1994)122<2709:DEORHA>2.0.CO;2).
- Feldman, A. F., D. J. Short Gianotti, I. F. Trigo, G. D. Salvucci, and D. Entekhabi, 2019: Satellite-Based Assessment of Land Surface Energy Partitioning–Soil Moisture Relationships and Effects of Confounding Variables. in: *Water Resources Research* 55.12, pp. 10657–10677, DOI: [10.1029/2019WR025874](https://doi.org/10.1029/2019WR025874).
- Ferguson, C. R. and E. F. Wood, 2011: Observed Land–Atmosphere Coupling from Satellite Remote Sensing and Reanalysis. in: *Journal of Hydrometeorology* 12.6, pp. 1221–1254, DOI: [10.1175/2011JHM1380.1](https://doi.org/10.1175/2011JHM1380.1).
- Findell, K. L. and E. A. B. Eltahir, 2003a: Atmospheric controls on soil moisture-boundary layer interactions: Three-dimensional wind effects. in: *Journal of Geophysical Research* 108 D8, DOI: [10.1029/2001JD001515](https://doi.org/10.1029/2001JD001515).
- 2003b: Atmospheric Controls on Soil Moisture–Boundary Layer Interactions. Part I: Framework Development. in: *Journal of Hydrometeorology* 4.3, pp. 552–569, DOI: [10.1175/1525-7541\(2003\)004<0552:ACOSML>2.0.CO;2](https://doi.org/10.1175/1525-7541(2003)004<0552:ACOSML>2.0.CO;2).
- 2003c: Atmospheric Controls on Soil Moisture–Boundary Layer Interactions. Part II: Feedbacks within the Continental United States. in: *Journal of Hydrometeorology* 4.3, pp. 570–583, DOI: [10.1175/1525-7541\(2003\)004<0570:ACOSML>2.0.CO;2](https://doi.org/10.1175/1525-7541(2003)004<0570:ACOSML>2.0.CO;2).
- Findell, K. L., P. Gentine, B. R. Lintner, and C. Kerr, 2011: Probability of afternoon precipitation in eastern United States and Mexico enhanced by high evaporation. in: *Nature Geoscience* 4.7, pp. 434–439, DOI: [10.1038/ngeo1174](https://doi.org/10.1038/ngeo1174).
- Findell, K. L., P. Gentine, B. R. Lintner, and B. P. Guillod, 2015: Data Length Requirements for Observational Estimates of Land–Atmosphere Coupling Strength. in: *Journal of Hydrometeorology* 16.4, pp. 1615–1635, DOI: [10.1175/JHM-D-14-0131.1](https://doi.org/10.1175/JHM-D-14-0131.1).

- Findell, K. L., A. Berg, P. Gentine, J. P. Krasting, B. R. Lintner, S. Malyshev, J. A. Santanello, and E. Shevliakova, 2017: The impact of anthropogenic land use and land cover change on regional climate extremes. in: *Nature Communications* 8.1, DOI: [10.1038/s41467-017-01038-w](https://doi.org/10.1038/s41467-017-01038-w).
- Froidevaux, P., L. Schlemmer, J. Schmidli, W. Langhans, and C. Schär, 2014: Influence of the Background Wind on the Local Soil Moisture–Precipitation Feedback. in: *Journal of the Atmospheric Sciences* 71.2, pp. 782–799, DOI: [10.1175/JAS-D-13-0180.1](https://doi.org/10.1175/JAS-D-13-0180.1).
- Frye, J. D. and T. L. Mote, 2010: The Synergistic Relationship between Soil Moisture and the Low-Level Jet and Its Role on the Prestorm Environment in the Southern Great Plains. in: *Journal of Applied Meteorology and Climatology* 49.4, pp. 775–791, DOI: [10.1175/2009JAMC2146.1](https://doi.org/10.1175/2009JAMC2146.1).
- Gerken, T., G. T. Bromley, B. L. Ruddell, S. Williams, and P. C. Stoy, 2018: Convective suppression before and during the United States Northern Great Plains flash drought of 2017. in: *Hydrology and Earth System Sciences* 22.8, pp. 4155–4163, DOI: [10.5194/hess-22-4155-2018](https://doi.org/10.5194/hess-22-4155-2018).
- Ghate, V. P. and P. Kollias, 2016: On the Controls of Daytime Precipitation in the Amazonian Dry Season. in: *Journal of Hydrometeorology* 17.12, pp. 3079–3097, DOI: [10.1175/JHM-D-16-0101.1](https://doi.org/10.1175/JHM-D-16-0101.1).
- Goodwell, A. E. and P. Kumar, 2017: Temporal information partitioning: Characterizing synergy, uniqueness, and redundancy in interacting environmental variables. in: *Water Resources Research* 53.7, pp. 5920–5942, DOI: [10.1002/2016WR020216](https://doi.org/10.1002/2016WR020216).
- Granger, C. W. J., 1969: Investigating Causal Relations by Econometric Models and Cross-spectral Methods. in: *Econometrica* 37.3, p. 424, DOI: [10.2307/1912791](https://doi.org/10.2307/1912791).
- Grell, G. A. and S. R. Freitas, 2014: A scale and aerosol aware stochastic convective parameterization for weather and air quality modeling. in: *Atmospheric Chemistry and Physics* 14.10, pp. 5233–5250, DOI: [10.5194/acp-14-5233-2014](https://doi.org/10.5194/acp-14-5233-2014).
- Guillod, B. P., B. Orlowsky, D. G. Miralles, A. J. Teuling, and S. I. Seneviratne, 2015: Reconciling spatial and temporal soil moisture effects on afternoon rainfall. in: *Nature Communications* 6, p. 6443, DOI: [10.1038/ncomms7443](https://doi.org/10.1038/ncomms7443).
- Guo, Z., P. A. Dirmeyer, R. D. Koster, Y. C. Sud, G. Bonan, K. W. Oleson, E. Chan, D. Verseghy, P. Cox, C. T. Gordon, J. L. McGregor, S. Kanae, E. Kowalczyk, D. Lawrence, P. Liu, D. Mocko, C.-H. Lu, K. Mitchell, S. Malyshev, B. McAvaney, T. Oki, T. Yamada, A. Pitman, C. M. Taylor,

- R. Vasic, and Y. Xue, 2006: GLACE: The Global Land–Atmosphere Coupling Experiment. Part II: Analysis. in: *Journal of Hydrometeorology* 7.4, pp. 611–625, DOI: [10.1175/JHM511.1](https://doi.org/10.1175/JHM511.1).
- Guo, Z. and P. A. Dirmeyer, 2013: Interannual Variability of Land–Atmosphere Coupling Strength. in: *Journal of Hydrometeorology* 14.5, pp. 1636–1646, DOI: [10.1175/JHM-D-12-0171.1](https://doi.org/10.1175/JHM-D-12-0171.1).
- Heerwaarden, C. C. van, J. Vilà-Guerau de Arellano, A. F. Moene, and A. A. M. Holtslag, 2009: Interactions between dry-air entrainment, surface evaporation and convective boundary-layer development: DRY-AIR ENTRAINMENT, SURFACE EVAPORATION AND CBL DEVELOPMENT. in: *Quarterly Journal of the Royal Meteorological Society* 135.642, pp. 1277–1291, DOI: [10.1002/qj.431](https://doi.org/10.1002/qj.431).
- Heerwaarden, C. C. van, J. Vilà Guerau de Arellano, A. Gounou, F. Guichard, and F. Couvreux, 2010: Understanding the Daily Cycle of Evapotranspiration: A Method to Quantify the Influence of Forcings and Feedbacks. in: *Journal of Hydrometeorology* 11.6, pp. 1405–1422, DOI: [10.1175/2010JHM1272.1](https://doi.org/10.1175/2010JHM1272.1).
- Hohenegger, C., P. Brockhaus, C. S. Bretherton, and C. Schär, 2009: The Soil Moisture–Precipitation Feedback in Simulations with Explicit and Parameterized Convection. in: *Journal of Climate* 22.19, pp. 5003–5020, DOI: [10.1175/2009JCLI2604.1](https://doi.org/10.1175/2009JCLI2604.1).
- Hong, S.-Y., Y. Noh, and J. Dudhia, 2006: A New Vertical Diffusion Package with an Explicit Treatment of Entrainment Processes. in: *Monthly Weather Review* 134.9, pp. 2318–2341, DOI: [10.1175/MWR3199.1](https://doi.org/10.1175/MWR3199.1).
- Hong, S., V. Lakshmi, and E. E. Small, 2007: Relationship between Vegetation Biophysical Properties and Surface Temperature Using Multisensor Satellite Data. in: *Journal of Climate* 20.22, pp. 5593–5606, DOI: [10.1175/2007JCLI1294.1](https://doi.org/10.1175/2007JCLI1294.1).
- Hong, S.-Y., H. Park, H.-B. Cheong, J.-E. E. Kim, M.-S. Koo, J. Jang, S. Ham, S.-O. Hwang, B.-K. Park, E.-C. Chang, and H. Li, 2013: The Global/Regional Integrated Model system (GRIMs). in: *Asia-Pacific Journal of Atmospheric Sciences* 49.2, pp. 219–243, DOI: [10.1007/s13143-013-0023-0](https://doi.org/10.1007/s13143-013-0023-0).
- Hsu, H. and P. A. Dirmeyer, 2021: Nonlinearity and Multivariate Dependencies in the Terrestrial Leg of Land-Atmosphere Coupling. in: *Water Resources Research* 57.2, DOI: [10.1029/2020WR028179](https://doi.org/10.1029/2020WR028179).

-
- Hübener, H., K. Bülow, C. Fooker, B. Früh, P. Hoffmann, S. Höpp, K. Keuler, C. Menz, V. Mohr, K. Radtke, H. Ramthun, A. Spekat, C. Steger, F. Toussaint, K. Warrach-Sagi, and M. Woldt, 2017: ReKliEs-De Ergebnisbericht. in: Publisher: World Data Center for Climate (WDCC), DOI: [10.2312/WDCC/REKLIESDE_ERGEBNISBERICHT](https://doi.org/10.2312/WDCC/REKLIESDE_ERGEBNISBERICHT).
- Huggannavar, V. and J. Indu, 2020: Seasonal variability of soil moisture-precipitation feedbacks over India. in: *Journal of Hydrology* 589, p. 125181, DOI: [10.1016/j.jhydro.2020.125181](https://doi.org/10.1016/j.jhydro.2020.125181).
- Hurk, B. J. J. M. van den and E. van Meijgaard, 2010: Diagnosing Land–Atmosphere Interaction from a Regional Climate Model Simulation over West Africa. in: *Journal of Hydrometeorology* 11.2, pp. 467–481, DOI: [10.1175/2009JHM1173.1](https://doi.org/10.1175/2009JHM1173.1).
- Iacono, M. J., J. S. Delamere, E. J. Mlawer, M. W. Shephard, S. A. Clough, and W. D. Collins, 2008: Radiative forcing by long-lived greenhouse gases: Calculations with the AER radiative transfer models. in: *Journal of Geophysical Research* 113 D13, DOI: [10.1029/2008JD009944](https://doi.org/10.1029/2008JD009944).
- IPCC, 2019: *Climate Change and Land: an IPCC special report on climate change, desertification, land degradation, sustainable land management, food security, and greenhouse gas fluxes in terrestrial ecosystem*.
- 2021: *Climate Change 2021: The Physical Science Basis. Contribution of Working Group I to the Sixth Assessment Report of the Intergovernmental Panel on Climate Change [Masson-Delmotte, V., P. Zhai, A. Pirani, S.L. Connors, C. Péan, S. Berger, N. Caud, Y. Chen, L. Goldfarb, M.I. Gomis, M. Huang, K. Leitzell, E. Lonnoy, J.B.R. Matthews, T.K. Maycock, T. Waterfield, O. Yelekçi, R. Yu, and B. Zhou (eds.)]* 6. Cambridge University Press.
- Jach, L., K. Warrach-Sagi, J. Ingwersen, E. Kaas, and V. Wulfmeyer, 2020: Land Cover Impacts on Land-Atmosphere Coupling Strength in Climate Simulations With WRF Over Europe. in: *Journal of Geophysical Research: Atmospheres* 125.18, DOI: [10.1029/2019JD031989](https://doi.org/10.1029/2019JD031989).
- Jacob, D., C. Teichmann, S. Sobolowski, E. Katragkou, I. Anders, M. Belda, R. Benestad, F. Boberg, E. Buonomo, R. M. Cardoso, A. Casanueva, O. B. Christensen, J. H. Christensen, E. Coppola, L. De Cruz, E. L. Davin, A. Dobler, M. Domingues, R. Fealy, J. Fernandez, M. A. Gaertner, M. García-Díez, F. Giorgi, A. Gobiet, K. Goergen, J. J. Gómez-Navarro, J. J. González Alemán, C. Gutiérrez, J. M. Gutiérrez, I. Güttler, A. Haensler, T. Halenka, S. Jerez, P. Jiménez-Guerrero, R. G. Jones, K. Keuler, E. Kjellström, S. Knist, S. Kotlarski, D. Maraun, E. van Meijgaard, P. Mercurigliano, J. P. Montávez, A. Navarra, G. Nikulin, N. de Noblet-Decoudré, H.-J. Panitz, S. Pfeifer,
-

- M. Piazza, E. Pichelli, J.-P. Pietikäinen, A. F. Prein, S. Preuschmann, D. Rechid, B. Rockel, R. Romera, E. Sánchez, K. Sieck, P. M. Soares, S. Somot, L. Srnec, S. L. Sørland, P. Termonia, H. Truhetz, R. Vaudard, K. Warrach-Sagi, and V. Wulfmeyer, 2020: Regional climate downscaling over Europe: perspectives from the EURO-CORDEX community. in: *Regional Climate Change*, DOI: <https://doi.org/10.1007/s10113-020-01606-9>.
- Jach, L., T. Schwitalla, O. Branch, K. Warrach-Sagi, and V. Wulfmeyer, 2022: Sensitivity of land–atmosphere coupling strength to changing atmospheric temperature and moisture over Europe. in: *Earth System Dynamics* 13.1, pp. 109–132, DOI: [10.5194/esd-13-109-2022](https://doi.org/10.5194/esd-13-109-2022).
- Jaeger, E. B. and S. I. Seneviratne, 2011: Impact of soil moisture–atmosphere coupling on European climate extremes and trends in a regional climate model. in: *Climate Dynamics* 36.9, pp. 1919–1939, DOI: [10.1007/s00382-010-0780-8](https://doi.org/10.1007/s00382-010-0780-8).
- Kain, J. S., 2004: The Kain–Fritsch Convective Parameterization: An Update. in: *Journal of Applied Meteorology* 43.1, pp. 170–181, DOI: [10.1175/1520-0450\(2004\)043<0170:TKCPAU>2.0.CO;2](https://doi.org/10.1175/1520-0450(2004)043<0170:TKCPAU>2.0.CO;2).
- Kain, J. S. and J. M. Fritsch, 1990: A One-Dimensional Entraining/Detraining Plume Model and Its Application in Convective Parameterization. in: *Journal of the Atmospheric Sciences* 47.23, pp. 2784–2802, DOI: [10.1175/1520-0469\(1990\)047<2784:AODEPM>2.0.CO;2](https://doi.org/10.1175/1520-0469(1990)047<2784:AODEPM>2.0.CO;2).
- Kar, S. C., P. Mali, and A. Routray, 2014: Impact of Land Surface Processes on the South Asian Monsoon Simulations Using WRF Modeling System. in: *Pure and Applied Geophysics* 171.9, pp. 2461–2484, DOI: [10.1007/s00024-014-0834-7](https://doi.org/10.1007/s00024-014-0834-7).
- Keil, C., F. Baur, K. Bachmann, S. Rasp, L. Schneider, and C. Barthlott, 2019: Relative contribution of soil moisture, boundary-layer and microphysical perturbations on convective predictability in different weather regimes. in: *Quarterly Journal of the Royal Meteorological Society* 145.724, pp. 3102–3115, DOI: [10.1002/qj.3607](https://doi.org/10.1002/qj.3607).
- Knist, S., K. Goergen, E. Buonomo, O. B. Christensen, A. Colette, R. M. Cardoso, R. Fealy, J. s. Fernández, M. García-Díez, D. Jacob, S. Kartsios, E. Katragkou, K. Keuler, S. Mayer, E. van Meijgaard, G. Nikulin, P. M. M. Soares, S. Sobolowski, G. Szepszo, C. Teichmann, R. Vautard, K. Warrach-Sagi, V. Wulfmeyer, and C. Simmer, 2017: Land-atmosphere coupling in EURO-CORDEX evaluation experiments: Land-Atmosphere Coupling in EURO-CORDEX. in: *Journal of Geophysical Research: Atmospheres* 122.1, pp. 79–103, DOI: [10.1002/2016JD025476](https://doi.org/10.1002/2016JD025476).

-
- Knist, S., K. Goergen, and C. Simmer, 2020: Effects of land surface inhomogeneity on convection-permitting WRF simulations over central Europe. in: *Meteorology and Atmospheric Physics* 132.1, pp. 53–69, DOI: [10.1007/s00703-019-00671-y](https://doi.org/10.1007/s00703-019-00671-y).
- Koster, R. D. and M. J. Suarez, 2001: Soil Moisture Memory in Climate Models. in: *Journal of Hydrometeorology* 2.6, pp. 558–570, DOI: [10.1175/1525-7541\(2001\)002<0558:SMMICM>2.0.CO;2](https://doi.org/10.1175/1525-7541(2001)002<0558:SMMICM>2.0.CO;2).
- Koster, R. D., P. Dirmeyer, Z. Guo, G. Bonan, E. Chan, P. Cox, C. Gordon, S. Kanae, E. Kowalczyk, D. Lawrence, P. Liu, C.-H. Lu, S. Malyshev, B. McAvaney, K. Mitchell, D. Mocko, T. Oki, K. Oleson, A. Pitman, Y. Sud, C. M. Taylor, D. Verseghy, R. Vasic, Y. Xue, and Yamada, 2004: Regions of Strong Coupling Between Soil Moisture and Precipitation. in: *Science* 305.5687, pp. 1138–1140, DOI: [10.1126/science.1100217](https://doi.org/10.1126/science.1100217).
- Koster, R. D., Y. C. Sud, Z. Guo, P. A. Dirmeyer, G. Bonan, K. W. Oleson, E. Chan, D. Verseghy, P. Cox, H. Davies, E. Kowalczyk, C. T. Gordon, S. Kanae, D. Lawrence, P. Liu, D. Mocko, C.-H. Lu, K. Mitchell, S. Malyshev, B. McAvaney, T. Oki, T. Yamada, A. Pitman, C. M. Taylor, R. Vasic, and Y. Xue, 2006: GLACE: The Global Land–Atmosphere Coupling Experiment. Part I: Overview. in: *Journal of Hydrometeorology* 7.4, pp. 590–610, DOI: [10.1175/JHM510.1](https://doi.org/10.1175/JHM510.1).
- Kottmeier, C., N. Kalthoff, C. Barthlott, U. Corsmeier, J. van Baelen, A. Behrendt, R. Behrendt, A. Blyth, R. Coulter, S. Crewell, P. di Girolamo, M. Dorninger, C. Flamant, and Foken, 2008: Mechanisms initiating deep convection over complex terrain during COPS. in: *Meteorologische Zeitschrift* 17.6, pp. 931–948, DOI: [10.1127/0941-2948/2008/0348](https://doi.org/10.1127/0941-2948/2008/0348).
- Koukoula, M., E. I. Nikolopoulos, J. Kushta, N. S. Bartsotas, G. Kallos, and E. N. Anagnostou, 2019: A Numerical Sensitivity Analysis of Soil Moisture Feedback on Convective Precipitation. in: *Journal of Hydrometeorology* 20.1, pp. 23–44, DOI: [10.1175/JHM-D-18-0134.1](https://doi.org/10.1175/JHM-D-18-0134.1).
- Laguë, M. M., G. B. Bonan, and A. L. S. Swann, 2019: Separating the Impact of Individual Land Surface Properties on the Terrestrial Surface Energy Budget in both the Coupled and Uncoupled Land–Atmosphere System. in: *Journal of Climate* 32.18, pp. 5725–5744, DOI: [10.1175/JCLI-D-18-0812.1](https://doi.org/10.1175/JCLI-D-18-0812.1).
- Lang, J., 2010: *Bericht zur Untersuchung konvektiver Wetterlagen in Nordrhein-Westfalen*, Dokumentation des Projektes "konvektive Wetterlagen (KonWet)" 1, Landesamt für Natur, Umwelt und Verbraucherschutz Nordrhein-Westfalen, p. 25.
-

- Lavín-Gullón, Á., J. Fernandez, S. Bastin, R. M. Cardoso, L. Fita, T. M. Giannaros, K. Goergen, J. M. Gutierrez, S. Kartsios, E. Katragkou, T. Lorenz, J. Milovac, P. M. M. Soares, S. Sobolowski, and K. Warrach-Sagi, 2021: Internal variability versus multi-physics uncertainty in a regional climate model. in: *International Journal of Climatology* 41 S1, DOI: [10.1002/joc.6717](https://doi.org/10.1002/joc.6717).
- Lawrence, D. M., G. C. Hurtt, A. Arneth, V. Brovkin, K. V. Calvin, A. D. Jones, C. D. Jones, P. J. Lawrence, N. de Noblet-Ducoudré, J. Pongratz, S. I. Seneviratne, and E. Shevliakova, 2016: The Land Use Model Intercomparison Project (LUMIP) contribution to CMIP6: rationale and experimental design. in: *Geoscientific Model Development* 9.9, pp. 2973–2998, DOI: [10.5194/gmd-9-2973-2016](https://doi.org/10.5194/gmd-9-2973-2016).
- Leutwyler, D., A. Imamovic, and C. Schär, 2021: The Continental-Scale Soil-Moisture Precipitation Feedback in Europe with Parameterized and Explicit Convection. in: *Journal of Climate*, pp. 1–56, DOI: [10.1175/JCLI-D-20-0415.1](https://doi.org/10.1175/JCLI-D-20-0415.1).
- Li, Y., X. Yuan, H. Zhang, R. Wang, C. Wang, X. Meng, Z. Zhang, S. Wang, Y. Yang, B. Han, K. Zhang, X. Wang, H. Zhao, G. Zhou, Q. Zhang, Q. He, N. Guo, W. Hou, C. Zhang, G. Xiao, X. Sun, P. Yue, S. Sha, H. Wang, T. Zhang, J. Wang, and Y. Yao, 2019: Mechanisms and Early Warning of Drought Disasters: Experimental Drought Meteorology Research over China. in: *Bulletin of the American Meteorological Society* 100.4, pp. 673–687, DOI: [10.1175/BAMS-D-17-0029.1](https://doi.org/10.1175/BAMS-D-17-0029.1).
- Lim, K.-S. S. and S.-Y. Hong, 2010: Development of an Effective Double-Moment Cloud Microphysics Scheme with Prognostic Cloud Condensation Nuclei (CCN) for Weather and Climate Models. in: *Monthly Weather Review* 138.5, pp. 1587–1612, DOI: [10.1175/2009MWR2968.1](https://doi.org/10.1175/2009MWR2968.1).
- Lo, M.-H., W.-Y. Wu, L. I. Tang, D. Ryu, M. Rashid, and R.-J. Wu, 2021: Temporal Changes in Land Surface Coupling Strength: An Example in a Semi-Arid Region of Australia. in: *Journal of Climate* 34.4, pp. 1503–1513, DOI: [10.1175/JCLI-D-20-0250.1](https://doi.org/10.1175/JCLI-D-20-0250.1).
- Lorenz, R., E. L. Davin, and S. I. Seneviratne, 2012: Modeling land-climate coupling in Europe: Impact of land surface representation on climate variability and extremes: LAND-CLIMATE COUPLING IN EUROPE. in: *Journal of Geophysical Research: Atmospheres* 117 D20, DOI: [10.1029/2012JD017755](https://doi.org/10.1029/2012JD017755).
- Lorenz, R., A. J. Pitman, A. L. Hirsch, and J. Srbinovsky, 2015: Intraseasonal versus Interannual Measures of Land–Atmosphere Coupling Strength in a Global Climate Model: GLACE-1 versus

-
- GLACE-CMIP5 Experiments in ACCESS1.3b. in: *Journal of Hydrometeorology* 16.5, pp. 2276–2295, DOI: [10.1175/JHM-D-14-0206.1](https://doi.org/10.1175/JHM-D-14-0206.1).
- Ma, Y., X. Meng, Y. Ao, Y. Yu, G. Li, S. Lyu, J. Li, and J. Xu, 2021: Soil Moisture-Boundary Layer Feedbacks on the Loess Plateau in China Using Radiosonde Data with 1-D Atmospheric Boundary Layer Model. in: *Atmosphere* 12.12, p. 1619, DOI: [10.3390/atmos12121619](https://doi.org/10.3390/atmos12121619).
- Markowski, P. and Y. Richardson, 2010: *Mesoscale meteorology in midlatitudes*, Chichester: Wiley-Blackwell, ISBN: 978-0-470-74213-6.
- McDermid, S. S., C. Montes, B. I. Cook, M. J. Puma, N. Y. Kiang, and I. Aleinov, 2019: The Sensitivity of Land–Atmosphere Coupling to Modern Agriculture in the Northern Midlatitudes. in: *Journal of Climate* 32.2, pp. 465–484, DOI: [10.1175/JCLI-D-17-0799.1](https://doi.org/10.1175/JCLI-D-17-0799.1).
- Merrifield, A. L., I. R. Simpson, K. A. McKinnon, S. Sippel, S. Xie, and C. Deser, 2019: Local and Nonlocal Land Surface Influence in European Heatwave Initial Condition Ensembles. in: *Geophysical Research Letters* 46.23, pp. 14082–14092, DOI: [10.1029/2019GL083945](https://doi.org/10.1029/2019GL083945).
- Mooney, P. A., D. Rechid, E. L. Davin, E. Katragkou, N. de Noblet-Ducoudré, M. Breil, R. M. Cardoso, A. S. Daloz, P. Hoffmann, D. C. A. Lima, R. Meier, P. M. M. Soares, G. Sofiadis, S. Strada, G. Strandberg, M. H. Toelle, and M. T. Lund, 2022: Land–atmosphere interactions in sub-polar and alpine climates in the CORDEX Flagship Pilot Study Land Use and Climate Across Scales (LUCAS) models – Part 2: The role of changing vegetation. in: *The Cryosphere* 16.4, pp. 1383–1397, DOI: [10.5194/tc-16-1383-2022](https://doi.org/10.5194/tc-16-1383-2022).
- Nakanishi, M. and H. Niino, 2009: Development of an Improved Turbulence Closure Model for the Atmospheric Boundary Layer. in: *Journal of the Meteorological Society of Japan* 87.5, pp. 895–912, DOI: [10.2151/jmsj.87.895](https://doi.org/10.2151/jmsj.87.895).
- Navarra, A. and J. Tribbia, 2005: The Coupled Manifold*. in: *Journal of the Atmospheric Sciences* 62.2, pp. 310–330, DOI: [10.1175/JAS-3345.1](https://doi.org/10.1175/JAS-3345.1).
- Noblet-Ducoudré, N. de, J.-P. Boisier, A. Pitman, G. B. Bonan, V. Brovkin, F. Cruz, C. Delire, V. Gayler, B. J. J. M. van den Hurk, P. J. Lawrence, M. K. van der Molen, C. Müller, C. H. Reick, B. J. Strengers, and A. Voldoire, 2012: Determining Robust Impacts of Land-Use-Induced Land Cover Changes on Surface Climate over North America and Eurasia: Results from the First Set of LUCID Experiments. in: *Journal of Climate* 25.9, pp. 3261–3281, DOI: [10.1175/JCLI-D-11-00338.1](https://doi.org/10.1175/JCLI-D-11-00338.1).
-

- Pearson, 1895: VII. Note on regression and inheritance in the case of two parents. in: *Proceedings of the Royal Society of London* 58.347, pp. 240–242, DOI: [10.1098/rsp1.1895.0041](https://doi.org/10.1098/rsp1.1895.0041).
- Peel, M. C., B. L. Finlayson, and T. A. McMahon, 2007: Updated world map of the Köppen-Geiger climate classification. in: *Hydrology and Earth System Sciences* 11.5, pp. 1633–1644, DOI: [10.5194/hess-11-1633-2007](https://doi.org/10.5194/hess-11-1633-2007).
- Phillips, T. J., S. A. Klein, H.-Y. Ma, Q. Tang, S. Xie, I. N. Williams, J. A. Santanello, D. R. Cook, and M. S. Torn, 2017: Using ARM Observations to Evaluate Climate Model Simulations of Land–Atmosphere Coupling on the U.S. Southern Great Plains: Model LAC Evaluation by ARM Data. in: *Journal of Geophysical Research: Atmospheres* 122.21, pp. 11,524–11,548, DOI: [10.1002/2017JD027141](https://doi.org/10.1002/2017JD027141).
- Pitman, A. J., N. de Noblet-Ducoudré, F. T. Cruz, E. L. Davin, G. B. Bonan, V. Brovkin, M. Claussen, C. Delire, L. Ganzeveld, V. Gayler, B. J. J. M. van den Hurk, P. J. Lawrence, M. K. van der Molen, C. Müller, C. H. Reick, S. I. Seneviratne, B. J. Strengers, and A. Voltaire, 2009: Uncertainties in climate responses to past land cover change: First results from the LUCID intercomparison study. in: *Geophysical Research Letters* 36.14, DOI: [10.1029/2009GL039076](https://doi.org/10.1029/2009GL039076).
- Rechid, D., E. L. Davin, N. de Noblet-Ducoudré, and E. Katragkou, 2017: CORDEX Flagship Pilot Study LUCAS - Land Use & Climate Across Scales - a new initiative on coordinated regional land use change and climate experiments for Europe. in: 19th EGU General Assembly, EGU2017, vol. Vol. 19 or 13172, Vienna, Austria.
- Roundy, J. K., C. R. Ferguson, and E. F. Wood, 2013: Temporal Variability of Land–Atmosphere Coupling and Its Implications for Drought over the Southeast United States. in: *Journal of Hydrometeorology* 14.2, pp. 622–635, DOI: [10.1175/JHM-D-12-090.1](https://doi.org/10.1175/JHM-D-12-090.1).
- 2014: Impact of land-atmospheric coupling in CFSv2 on drought prediction. in: *Climate Dynamics* 43.1, pp. 421–434, DOI: [10.1007/s00382-013-1982-7](https://doi.org/10.1007/s00382-013-1982-7).
- Roundy, J. K. and E. F. Wood, 2015: The Attribution of Land–Atmosphere Interactions on the Seasonal Predictability of Drought. in: *Journal of Hydrometeorology* 16.2, pp. 793–810, DOI: [10.1175/JHM-D-14-0121.1](https://doi.org/10.1175/JHM-D-14-0121.1).
- Roundy, J. K. and J. A. Santanello, 2017: Utility of Satellite Remote Sensing for Land–Atmosphere Coupling and Drought Metrics. in: *Journal of Hydrometeorology* 18.3, pp. 863–877, DOI: [10.1175/JHM-D-16-0171.1](https://doi.org/10.1175/JHM-D-16-0171.1).

-
- Ruddell, B. L. and P. Kumar, 2009a: Ecohydrologic process networks: 1. Identification: ECOHYDROLOGIC PROCESS NETWORKS, 1. in: *Water Resources Research* 45.3, DOI: [10.1029/2008WR007279](https://doi.org/10.1029/2008WR007279).
- 2009b: Ecohydrologic process networks: 2. Analysis and characterization: ECOHYDROLOGIC PROCESS NETWORKS, 2. in: *Water Resources Research* 45.3, DOI: [10.1029/2008WR007280](https://doi.org/10.1029/2008WR007280).
- Rüdisühli, S., M. Sprenger, D. Leutwyler, C. Schär, and H. Wernli, 2020: Attribution of precipitation to cyclones and fronts over Europe in a kilometer-scale regional climate simulation. in: *Weather and Climate Dynamics* 1.2, pp. 675–699, DOI: [10.5194/wcd-1-675-2020](https://doi.org/10.5194/wcd-1-675-2020).
- Salvucci, G. D., J. A. Saleem, and R. Kaufmann, 2002: Investigating soil moisture feedbacks on precipitation with tests of Granger causality. in: *Advances in Water Resources* 25.8, pp. 1305–1312, DOI: [10.1016/S0309-1708\(02\)00057-X](https://doi.org/10.1016/S0309-1708(02)00057-X).
- Santanello, J. A., C. D. Peters-Lidard, S. V. Kumar, C. Alonge, and W.-K. Tao, 2009: A Modeling and Observational Framework for Diagnosing Local Land–Atmosphere Coupling on Diurnal Time Scales. in: *Journal of Hydrometeorology* 10.3, pp. 577–599, DOI: [10.1175/2009JHM1066.1](https://doi.org/10.1175/2009JHM1066.1).
- Santanello, J. A., C. D. Peters-Lidard, and S. V. Kumar, 2011: Diagnosing the Sensitivity of Local Land–Atmosphere Coupling via the Soil Moisture–Boundary Layer Interaction. in: *Journal of Hydrometeorology* 12.5, pp. 766–786, DOI: [10.1175/JHM-D-10-05014.1](https://doi.org/10.1175/JHM-D-10-05014.1).
- Santanello, J. A., P. A. Dirmeyer, C. R. Ferguson, K. L. Findell, A. B. Tawfik, A. Berg, M. Ek, P. Gentine, B. P. Guillod, C. van Heerwaarden, J. Roundy, and V. Wulfmeyer, 2018: Land–Atmosphere Interactions: The LoCo Perspective. in: *Bulletin of the American Meteorological Society* 99.6, pp. 1253–1272, DOI: [10.1175/BAMS-D-17-0001.1](https://doi.org/10.1175/BAMS-D-17-0001.1).
- Seneviratne, S. I., D. Lüthi, M. Litschi, and C. Schär, 2006: Land–atmosphere coupling and climate change in Europe. in: *Nature* 443.7108, pp. 205–209, DOI: [10.1038/nature05095](https://doi.org/10.1038/nature05095).
- Seneviratne, S. I., T. Corti, E. L. Davin, M. Hirschi, E. B. Jaeger, I. Lehner, B. Orlowsky, and A. J. Teuling, 2010: Investigating soil moisture–climate interactions in a changing climate: A review. in: *Earth-Science Reviews* 99.3, pp. 125–161, DOI: [10.1016/j.earscirev.2010.02.004](https://doi.org/10.1016/j.earscirev.2010.02.004).
- Seneviratne, S. I. and R. D. Koster, 2012: A Revised Framework for Analyzing Soil Moisture Memory in Climate Data: Derivation and Interpretation. in: *Journal of Hydrometeorology* 13.1, pp. 404–412, DOI: [10.1175/JHM-D-11-044.1](https://doi.org/10.1175/JHM-D-11-044.1).
-

- Seneviratne, S. I., M. Wilhelm, T. Stanelle, B. Hurk, S. Hagemann, A. Berg, F. Cheruy, M. E. Higgins, A. Meier, V. Brovkin, M. Claussen, A. Ducharne, J. Dufresne, K. L. Findell, J. Ghattas, D. M. Lawrence, S. Malyshev, M. Rummukainen, and B. Smith, 2013: Impact of soil moisture-climate feedbacks on CMIP5 projections: First results from the GLACE-CMIP5 experiment. in: *Geophysical Research Letters* 40.19, pp. 5212–5217, DOI: [10.1002/gr1.50956](https://doi.org/10.1002/gr1.50956).
- Santanello Jr., J. A., P. Lawston, S. Kumar, and E. Dennis, 2019: Understanding the Impacts of Soil Moisture Initial Conditions on NWP in the Context of Land–Atmosphere Coupling. in: *Journal of Hydrometeorology* 20.5, pp. 793–819, DOI: [10.1175/JHM-D-18-0186.1](https://doi.org/10.1175/JHM-D-18-0186.1).
- Sofiadis, G., E. Katragkou, E. L. Davin, D. Rechid, N. de Noblet-Ducoudre, M. Breil, R. M. Cardoso, P. Hoffmann, L. Jach, R. Meier, P. A. Mooney, P. M. M. Soares, S. Strada, M. H. Tölle, and K. Warrach Sagi, 2022: Afforestation impact on soil temperature in regional climate model simulations over Europe. in: *Geoscientific Model Development* 15.2, pp. 595–616, DOI: [10.5194/gmd-15-595-2022](https://doi.org/10.5194/gmd-15-595-2022).
- Song, H.-J., C. R. Ferguson, and J. K. Roundy, 2016: Land–Atmosphere Coupling at the Southern Great Plains Atmospheric Radiation Measurement (ARM) Field Site and Its Role in Anomalous Afternoon Peak Precipitation. in: *Journal of Hydrometeorology* 17.2, pp. 541–556, DOI: [10.1175/JHM-D-15-0045.1](https://doi.org/10.1175/JHM-D-15-0045.1).
- Spearman, C., 1907: Demonstration of Formulae for True Measurement of Correlation. in: *The American Journal of Psychology* 18.2, p. 161, DOI: [10.2307/1412408](https://doi.org/10.2307/1412408).
- Stap, L. B., B. J. J. M. van den Hurk, C. C. van Heerwaarden, and R. A. J. Neggers, 2014: Modeled Contrast in the Response of the Surface Energy Balance to Heat Waves for Forest and Grassland. in: *Journal of Hydrometeorology* 15.3, pp. 973–989, DOI: [10.1175/JHM-D-13-029.1](https://doi.org/10.1175/JHM-D-13-029.1).
- Tawfik, A. B. and P. A. Dirmeyer, 2014: A process-based framework for quantifying the atmospheric preconditioning of surface-triggered convection: HEATED CONDENSATION FRAMEWORK. in: *Geophysical Research Letters* 41.1, pp. 173–178, DOI: [10.1002/2013GL057984](https://doi.org/10.1002/2013GL057984).
- Tawfik, A. B., P. A. Dirmeyer, and J. A. Santanello, 2015a: The Heated Condensation Framework. Part I: Description and Southern Great Plains Case Study. in: *Journal of Hydrometeorology* 16.5, pp. 1929–1945, DOI: [10.1175/JHM-D-14-0117.1](https://doi.org/10.1175/JHM-D-14-0117.1).

-
- 2015b: The Heated Condensation Framework. Part II: Climatological Behavior of Convective Initiation and Land–Atmosphere Coupling over the Conterminous United States. in: *Journal of Hydrometeorology* 16.5, pp. 1946–1961, DOI: [10.1175/JHM-D-14-0118.1](https://doi.org/10.1175/JHM-D-14-0118.1).
- Taylor, C. M., R. A. M. de Jeu, F. Guichard, P. P. Harris, and W. A. Dorigo, 2012: Afternoon rain more likely over drier soils. in: *Nature* 489.7416, pp. 423–426, DOI: [10.1038/nature11377](https://doi.org/10.1038/nature11377).
- Taylor, C. M., 2015: Detecting soil moisture impacts on convective initiation in Europe. in: *Geophysical Research Letters* 42.11, pp. 4631–4638, DOI: [10.1002/2015GL064030](https://doi.org/10.1002/2015GL064030).
- Tebaldi, C., K. Debeire, V. Eyring, E. Fischer, J. Fyfe, P. Friedlingstein, R. Knutti, J. Lowe, B. O’Neill, B. Sanderson, D. van Vuuren, K. Riahi, M. Meinshausen, Z. Nicholls, K. B. Tokarska, G. Hurtt, E. Kriegler, J.-F. Lamarque, G. Meehl, R. Moss, S. E. Bauer, O. Boucher, V. Brovkin, Y.-H. Byun, M. Dix, S. Gualdi, H. Guo, J. G. John, S. Kharin, Y. Kim, T. Koshiro, L. Ma, D. Olivie, S. Panickal, F. Qiao, X. Rong, N. Rosenbloom, M. Schupfner, R. Sférian, A. Sellar, T. Semmler, X. Shi, Z. Song, C. Steger, R. Stouffer, N. Swart, K. Tachiiri, Q. Tang, H. Tatebe, A. Voldoire, E. Volodin, K. Wyser, X. Xin, S. Yang, Y. Yu, and T. Ziehn, 2021: Climate model projections from the Scenario Model Intercomparison Project (ScenarioMIP) of CMIP6. in: *Earth System Dynamics* 12.1, pp. 253–293, DOI: [10.5194/esd-12-253-2021](https://doi.org/10.5194/esd-12-253-2021).
- Thompson, G., R. M. Rasmussen, and K. Manning, 2004: Explicit Forecasts of Winter Precipitation Using an Improved Bulk Microphysics Scheme. Part I: Description and Sensitivity Analysis. in: *Monthly Weather Review* 132.2, pp. 519–542, DOI: [10.1175/1520-0493\(2004\)132<0519:EFOWPU>2.0.CO;2](https://doi.org/10.1175/1520-0493(2004)132<0519:EFOWPU>2.0.CO;2).
- Tuinenburg, O. A., R. W. A. Hutjes, C. M. J. Jacobs, and P. Kabat, 2011: Diagnosis of Local Land–Atmosphere Feedbacks in India. in: *Journal of Climate* 24.1, pp. 251–266, DOI: [10.1175/2010JCLI3779.1](https://doi.org/10.1175/2010JCLI3779.1).
- Tuttle, S. and G. Salvucci, 2016: Empirical evidence of contrasting soil moisture-precipitation feedbacks across the United States. in: *Science* 352.6287, pp. 825–828, DOI: [10.1126/science.aaa7185](https://doi.org/10.1126/science.aaa7185).
- Tuttle, S. E. and G. D. Salvucci, 2017: Confounding factors in determining causal soil moisture-precipitation feedback: CONFOUNDING FACTORS IN S-P FEEDBACK. in: *Water Resources Research* 53.7, pp. 5531–5544, DOI: [10.1002/2016WR019869](https://doi.org/10.1002/2016WR019869).
-

- Vautard, R., N. Kadyrov, C. Iles, F. Boberg, E. Buonomo, K. Bülow, E. Coppola, L. Corre, E. Meijgaard, R. Nogherotto, M. Sandstad, C. Schwingshackl, S. Somot, E. Aalbers, O. B. Christensen, J. M. Ciarlò, M. Demory, F. Giorgi, D. Jacob, R. G. Jones, K. Keuler, E. Kjellström, G. Lenderink, G. Levvasseur, G. Nikulin, J. Sillmann, C. Solidoro, S. L. Sørland, C. Steger, C. Teichmann, K. Warrach-Sagi, and V. Wulfmeyer, 2020: Evaluation of the large EURO-CORDEX regional climate model ensemble. in: *Journal of Geophysical Research: Atmospheres*, DOI: [10.1029/2019JD032344](https://doi.org/10.1029/2019JD032344).
- Vogel, M. M., R. Orth, F. Cheruy, S. Hagemann, R. Lorenz, B. J. J. M. Hurk, and S. I. Seneviratne, 2017: Regional amplification of projected changes in extreme temperatures strongly controlled by soil moisture-temperature feedbacks. in: *Geophysical Research Letters* 44.3, pp. 1511–1519, DOI: [10.1002/2016GL071235](https://doi.org/10.1002/2016GL071235).
- Wakefield, R. A., J. B. Basara, J. C. Furtado, B. G. Illston, C. R. Ferguson, and P. M. Klein, 2019: A Modified Framework for Quantifying Land–Atmosphere Covariability during Hydrometeorological and Soil Wetness Extremes in Oklahoma. in: *Journal of Applied Meteorology and Climatology* 58.7, pp. 1465–1483, DOI: [10.1175/JAMC-D-18-0230.1](https://doi.org/10.1175/JAMC-D-18-0230.1).
- Wakefield, R. A., D. D. Turner, and J. B. Basara, 2021: Evaluation of a land-atmosphere coupling metric computed from a ground-based infrared interferometer. in: *Journal of Hydrometeorology*, DOI: [10.1175/JHM-D-20-0303.1](https://doi.org/10.1175/JHM-D-20-0303.1).
- Wang, W., B. T. Anderson, N. Phillips, R. K. Kaufmann, C. Potter, and R. B. Myneni, 2006: Feedbacks of Vegetation on Summertime Climate Variability over the North American Grasslands. Part I: Statistical Analysis. in: *Earth Interactions* 10.17, pp. 1–27, DOI: [10.1175/EI196.1](https://doi.org/10.1175/EI196.1).
- Warrach-Sagi, K., J. Ingwersen, T. Schwitalla, C. Troost, J. Aurbacher, L. Jach, T. Berger, T. Streck, and V. Wulfmeyer, 2022: Noah-MP with the generic crop growth model Gecros in the WRF model: Effects of dynamic crop growth on land-atmosphere interaction. in: *Journal of Geophysical Research: Atmospheres*, DOI: [10.1029/2022JD036518](https://doi.org/10.1029/2022JD036518).
- Weckwerth, T. M. and D. B. Parsons, 2006: A Review of Convection Initiation and Motivation for IHOP_2002. in: *Monthly Weather Review* 134.1, pp. 5–22, DOI: [10.1175/MWR3067.1](https://doi.org/10.1175/MWR3067.1).
- Williams, I. N. and M. S. Torn, 2015: Vegetation controls on surface heat flux partitioning, and land-atmosphere coupling: VEGETATION AND LAND-ATMOSPHERE COUPLING. in: *Geophysical Research Letters* 42.21, pp. 9416–9424, DOI: [10.1002/2015GL066305](https://doi.org/10.1002/2015GL066305).

-
- Williams, I. N., 2019: Evaluating Soil Moisture Feedback on Convective Triggering: Roles of Convective and Land-Model Parameterizations. in: *Journal of Geophysical Research: Atmospheres* 124.1, pp. 317–332, DOI: [10.1029/2018JD029326](https://doi.org/10.1029/2018JD029326).
- Warrach-Sagi, K., T. Schwitalla, V. Wulfmeyer, and H.-S. Bauer, 2013: Evaluation of a climate simulation in Europe based on the WRF–NOAH model system: precipitation in Germany. in: *Climate Dynamics* 41.3, pp. 755–774, DOI: [10.1007/s00382-013-1727-7](https://doi.org/10.1007/s00382-013-1727-7).
- Wulfmeyer, V., A. Behrendt, C. Kottmeier, U. Corsmeier, C. Barthlott, G. C. Craig, M. Hagen, D. Althausen, F. Aoshima, M. Arpagaus, H.-S. Bauer, L. Bennett, A. Blyth, C. Brandau, C. Champollion, S. Crewell, G. Dick, P. Di Girolamo, M. Dorninger, Y. Dufournet, R. Eigenmann, R. Engelmann, C. Flamant, T. Foken, T. Gorgas, M. Grzeschik, J. Handwerker, C. Hauck, H. Höller, W. Junkermann, N. Kalthoff, C. Kiemle, S. Klink, M. König, L. Krauss, C. N. Long, F. Madonna, S. Mobbs, B. Neining, S. Pal, G. Peters, G. Pigeon, E. Richard, M. W. Rotach, H. Russchenberg, T. Schwitalla, V. Smith, R. Steinacker, J. Trentmann, D. D. Turner, J. van Baelen, S. Vogt, H. Volkert, T. Weckwerth, H. Wernli, A. Wieser, and M. Wirth, 2011: The Convective and Orographically-induced Precipitation Study (COPS): the scientific strategy, the field phase, and research highlights: COPS strategy, field phase, and highlights. in: *Quarterly Journal of the Royal Meteorological Society* 137 S1, pp. 3–30, DOI: [10.1002/qj.752](https://doi.org/10.1002/qj.752).
- Yin, J., J. D. Albertson, J. R. Rigby, and A. Porporato, 2015: Land and atmospheric controls on initiation and intensity of moist convection: CAPE dynamics and LCL crossings. in: *Water Resources Research* 51.10, pp. 8476–8493, DOI: [10.1002/2015WR017286](https://doi.org/10.1002/2015WR017286).
- Zhang, Q., Z. Yang, X. Hao, and H. Li, 2019: Dynamic response of land–atmosphere-coupling parameters to precipitation in the sparse-vegetated Asian summer monsoon transition zone. in: *Environmental Earth Sciences* 78.16, DOI: [10.1007/s12665-019-8525-4](https://doi.org/10.1007/s12665-019-8525-4).
- Zhao, C., X. Meng, Y. Li, S. Lyu, J. Guo, and H. Liu, 2022: Impact of Soil Moisture on Afternoon Convection Triggering Over the Tibetan Plateau Based on 1-D Boundary Layer Model. in: *Journal of Geophysical Research: Atmospheres* 127.2, DOI: [10.1029/2021JD035591](https://doi.org/10.1029/2021JD035591).

Acknowledgements

This endeavor would not have been possible without the expert guidance of my supervisor Prof. Dr. Volker Wulfmeyer. I would like to thank you for your support and the constructive suggestions and discussions during the course of my doctoral studies. Thank you for sharing your knowledge and for giving me the opportunity to be part of the IPM team and its projects. You encouraged me to leave my comfort zone to reach out and network in the scientific community.

I would like to express my deepest gratitude to Dr. Kirsten Warrach-Sagi. To me you are one of two mentors in my academic life, because by sharing your expertise and vision about regional climate modeling and science in general you supported me already during my Bachelor and Master times, and you substantially helped me to find my way to where I am, now.

Special thanks go to my office partner Dr. Oliver Branch for your open ears, bringing in your expertise in the countless advises, and for regularly raising new perspectives. Special thanks merit also to Dr. Thomas Schwitalla. You always had a helping hand or mind for questions and problems, particularly, when it came to computational issues.

I would like to express my appreciation to the Anton and Petra Ehrmann-foundation Research Training Group "Water-People-Agriculture" for financing this PhD project and for the professional and organizational support during the PhD training. In particular, I would like to thank Dr. Marcus Giese for your support in administrative questions and for always finding uncomplicated solutions.

Thanks also to Rohith Thundathil and Paolo Mori for being my colleagues, for sharing coffee breaks discussing, and for supporting me with your ideas. I would like to thank also Dr. Hans-Stefan Bauer and Dr. Florian Späth for your support while working together. Further, I'd like to acknowledge the support from Elisabeth Ott for all kinds of issues regarding contracts and travel organization.

Finally, I would like to thank my partner Daniel for your emotional support, your help by listening to me in the attempt to sort my thoughts and ideas, and for your belief in me. Further, I would like to thank my family for supporting me already my whole life and of course also during the course of my studies. Last but not least, I would like to thank my high school physics teacher Paul Feltes. You encouraged my interest in learning about climate change during various extracurricular projects, which formed the wish to become an earth system or climate scientist in the first place.

Curriculum vitae

PERSONAL DATA

Name: Lisa Lea Jach
Date of birth: 29. August 1993
Place of birth: Frechen, Germany
Citizenship: German
Email: lisoel.ja@googlemail.com

ACADEMIC BACKGROUND AND EDUCATION

02/2018 - Present **PhD Candidate**
Institute of Physics and Meteorology,
University of Hohenheim, Stuttgart
Key aspects: Land-atmosphere interactions, biogeophysical land
use change impacts, regional climate modeling

08/2015 - 11/2017 **Master of Science**
in “Environmental Science – Soil, Water and Biodiversity”
(EnvEuro) European double-degree master’s program
1st year University of Hohenheim
2nd year University of Copenhagen
Key aspects: climate change, soil resources and
land use, environmental modeling

10/2011 - 11/2015 **Bachelor of Science**
in "Biobased Products and Bioenergy" University of Hohenheim
Key aspects: agricultural engineering, economics of bioenergy
production, impacts of energy production on the global environment

06/2011 **University Entrance Diploma (Abitur)**
Gymnasium Frechen, (Secondary school ISCED Level 3,
Frechen, Germany)

GRANTS

02/2018 - 01/2021 **PhD Scholarship**
from the Anton and Petra Ehrmann foundation research training
group "Water-People-Agriculture" at the University of Hohenheim

03/2017 **Helmut-Aurenz Scholarship**
for research stays in the context of final thesis

MEMBERSHIPS AND VOLUNTARY WORK

05/2022 - 10/2022 **Guest Scientist** at the German Aerospace Center,
Microwaves and Radar Institute, Department of Reconnaissance and
Security, Working Group on Signatures

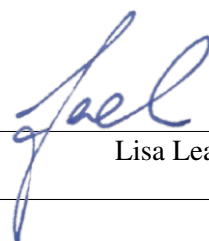
07/2021 - 06/2022 **Elected PhD representative** in the Faculty
Council of the Faculty of Natural Sciences

2020 - present **Member of the LoCo Working Group**
from the GEWEX GLASS-Panel

10/2019 - present **PhD Representative** in the WPA Steering Committee

04/2017 - present **Project Member** in the WCRP FPS-LUCAS community

Stuttgart-Hohenheim, 27.09.2022



Lisa Lea Jach

Publications

PUBLICATIONS IN PEER-REVIEWED JOURNALS

Davin, E.L., D. Rechid, M. Breil, R.M. Cardoso, E. Coppola, P. Hoffman, **L.L. Jach**, E. Katragkou, N. de Noblet-Ducoudré, K. Radke, M. Raffa, P.M.M. Soares, G. Sofiadis, S. Strada, G. Strandberg, M. H. Tölle, K. Warrach-Sagi, and V. Wulfmeyer, 2020: “Biogeophysical impacts of forestation in Europe: First results from the LUCAS Regional Climate Model intercomparison. ”. *Earth Syst. Dyn.*, 11, 183-200. DOI: [10.5194/esd-11-183-2020](https://doi.org/10.5194/esd-11-183-2020)

Breil, M., D. Rechid, E. L. Davin, N. Noblet-Ducoudré, de, E. Katragkou, R. M. Cardoso, P. Hoffmann, textbfL. L. Jach, P. M. Soares, G. Sofiadis, S. Strada, G. Strandberg, M. H. Tölle, and K. Warrach-Sagi, 2020: “The opposing effects of reforestation and afforestation on the diurnal temperature cycle at the surface and in the lowest atmospheric model level in the european summer?”. *J. Climate*, 33(23),9159-9179. DOI: [10.1175/JCLI-D-19-0624.1](https://doi.org/10.1175/JCLI-D-19-0624.1)

Jach, L., K. Warrach-Sagi, J. Ingwersen, E. Kaas, and V. Wulfmeyer, 2020: “Land cover impacts on land-atmosphere coupling strength in climate simulations with WRF over Europe”. *J. Geophys. Res-Atmos*, 125(23), 1-21. DOI: [10.1029/2019JD031989](https://doi.org/10.1029/2019JD031989)

Rousi, E., A.H. Fink, L.S. Andersen, F.N. Becker, G. Beobide-Arsuaga, M. Breil, G. Cozzi, J. Heinke, **L. Jach**, D. Niermann, D. Petrovic, A. Richling, J. Riebold, S. Steidl, L. Suarez-Gutierrez, J. Tradowsky, D. Coumou, A. Düsterhus, F. Ellsäßer, G. Fragkoulidis, D. Gliksman, D. Handorf, K. Haustein, K. Kornhuber, H. Kunstmann, J.G. Pinto, K. Warrach-Sagi, and E. Xoplaki, 2022: “The extremely hot and dry 2018 summer in central and northern Europe from a multi-faceted weather and climate perspective”, EGUsphere [preprint], DOI: [10.5194/egusphere-2022-813](https://doi.org/10.5194/egusphere-2022-813).

Sofiadis, G., E. Katragkou, E.L. Davin, D. Rechid, N. de Noblet-Ducoudre, M. Breil, R.M. Cardoso, P. Hoffmann, **L. Jach**, R. Meier, P.A. Mooney, P.M.M. Soares, S. Strada, M.H. Tölle, and K. Warrach Sagi, 2022: “Afforestation impact on soil temperature in regional climate model simulations over Europe”. *Geosci. Model Dev.*, 15, 595-616. DOI: [10.5194/gmd-15-595-2022](https://doi.org/10.5194/gmd-15-595-2022)

Jach, L., T. Schwitalla, O. Branch, K. Warrach-Sagi, and V. Wulfmeyer, 2022: “Sensitivity of land–atmosphere coupling strength to changing atmospheric temperature and moisture over Europe”. *Earth Syst. Dynam.*, 13, 109-132. DOI: [10.5194/esd-13-109-2022](https://doi.org/10.5194/esd-13-109-2022)

Warrach-Sagi, K., J. Ingwersen, T. Schwitalla, C. Troost, J. Aurbacher, **L. Jach**, T. Berger, T. Streck, and V. Wulfmeyer, 2022: “Noah-MP with the generic crop growth model Gecros in the WRF model: Effects of dynamic crop growth on land-atmosphere interaction”. in: *J. Geophys. Res.-Atmos.*, e2022JD036518, DOI: [10.1029/2022JD036518](https://doi.org/10.1029/2022JD036518) .

NON PEER-REVIEWED PUBLICATIONS

Wulfmeyer, V., F. Späth, A. Behrendt, **L. Jach**, K. Warrach-Sagi, M. Ek, D. D. Turner, C. Senff, C. R. Ferguson, J. Santanello, T. R. Lee, M. Buban, and A. Verhoef, 2020: “The GEWEX Land-Atmosphere Feedback Observatory (GLAFO)”. *GEWEX Quarterly Newsletter*, Vol. 30(1/2020),16.

PRESENTATIONS

Davin E.L., D. Rechid, M. Breil, R.M. Cardoso, E. Coppola, P. Hoffmann, **L.L. Jach**, E. Katragkou, N. de Noblet-Ducoudré, K. Radtke, M. Raffa, P.M.M. Soares, G. Sofiadis, S. Strada, G. Strandberg, M.H. Tölle, K. Warrach-Sagi, V. Wulfmeyer, 2019: “Biogeophysical impacts of forestation in Europe: First results from the LUCAS Regional Climate Model intercomparison”. *Final Conference of the DFG Research Unit 1695 Regional Climate Change*, Germany. April 2019.

Jach, L., K. Warrach-Sagi, V. Wulfmeyer, 2019: “Land-atmosphere coupling strength in dependence of the land-cover in European climate simulations”. *bwHPC Symposium 2019*, Karlsruhe, Germany. September 2019.

Jach, L., K. Warrach-Sagi, V. Wulfmeyer, 2019: “Land-atmosphere coupling strength in dependence of the land-cover in European climate simulations”. *ICRC-CORDEX (International Conference on Regional Climate)*, Beijing, China. October 2019.

Jach, L., T. Schwitalla, K. Warrach-Sagi, and V. Wulfmeyer, 2021: “Study of the sensitivity of land-convection coupling in the European summer”. *vEGU21*, Session CL4.17 – Land–atmosphere interactions and climate extremes, EGU21-8406 vPICO presentations. April 2021.

Rita M. Cardoso, Daniela D. C. A. Lima, Pedro M. M. Soares, Diana Rechid, Marcus Breil, Erika Coppola, Edouard Davin, Peter Hoffmann, **Lisa Jach**, Eleni Katragkou Katragkou, Ronny Meier, Priscilla A. Mooney, Natalie de Noblet-Ducoudré, Hans-Juergen Panitz, Ioannis Sofiadis, Susanna Strada, Gustav Strandberg, Merja Tölle, and Kirsten Warrach-Sagi, 2021: “Land-atmosphere coupling during compound extreme heat and drought events in the LUCAS experiment: a new coupling metric for climate extremes”. *vEGU21*, Session CL3.1.1 – Regional Climate Modeling, EGU21-15797, vPICO presentations. April 2021.

Rousi, E., Fink, A., and Suarez-Gutierrez, L. and the ClimXtreme project (including **L. Jach**), 2022: “A comprehensive study of the extreme heat and drought of the 2018 European summer”. *EGU General Assembly 2022*, Vienna, Austria, 23–27 May 2022, EGU22-9831, DOI: 10.5194/egusphere-egu22-9831.

Ellsäßer, F. and Xoplaki, E. and the climXtreme research network on climate change and extreme events (including **L. Jach**), 2022: Compound events in Germany: drivers and case studies. *EGU General Assembly 2022*, Vienna, Austria, 23–27 May 2022, EGU22-11534, DOI: 10.5194/egusphere-egu22-11534.

POSTER

Warrach-Sagi, K., **L. Jach**, and E. Kaas, 2018: “Land use sensitivity of convection triggering potential in Europe in climate simulations with WRF”. *EGU-General Assembly*. April 2018.

Breil,M., Rechid,D., Davin,E.L., De Noblet-Ducourdré,N., Katragkou,E., Cardoso,R.M., Hoffmann,P., **Jach, L.L.**, Soares,P.M.M., Sofiadis,G., Strandberg,G., Tölle,M.H., Warrach-Sagi,K., 2019: “The impact of afforestation on the diurnal cycles of temperature and turbulent heat fluxes”. *EGU-General Assembly*. April 2019.



Annex 2 to the University of Hohenheim doctoral degree regulations for Dr. rer. nat.

Affidavit according to Sec. 7(7) of the University of Hohenheim doctoral degree regulations for Dr. rer. nat.

1. For the dissertation submitted on the topic

Sensitivity of Land-Atmosphere Coupling Strength in Dependence of Land Cover and Atmospheric Thermodynamics over Europe

I hereby declare that I independently completed the work.

2. I only used the sources and aids documented and only made use of permissible assistance by third parties. In particular, I properly documented any contents which I used - either by directly quoting or paraphrasing - from other works.
3. I did not accept any assistance from a commercial doctoral agency or consulting firm.
4. I am aware of the meaning of this affidavit and the criminal penalties of an incorrect or incomplete affidavit.

I hereby confirm the correctness of the above declaration: I hereby affirm in lieu of oath that I have, to the best of my knowledge, declared nothing but the truth and have not omitted any information.

Stuttgart, 20.07.2023

Place and Date

Signature